Immunociblage du cerveau par des nanocapsules lipidiques

Arnaud Béduneau

UNIVERSITE D'ANGERS **Année 2007**
U.F.R. des Sciences Pharmaceutiques N° 825

IMMUNOCIBLAGE DU CERVEAU PAR DES NANOCAPSULES LIPIDIQUES

THESE DE DOCTORAT

EN PHARMACOLOGIE EXPERIMENTALE

ECOLE DOCTORALE D'ANGERS

Présentée et soutenue publiquement

Le 18 avril 2007

à Angers

par **Arnaud BEDUNEAU**

Devant le jury ci-dessous :

Jean-Pierre BENOIT, Professeur des Universités, Université d'Angers	Directeur de thèse
Didier BETBEDER, Professeur des Universités, Université d'Artois	Rapporteur
Jean-Christophe OLIVIER, Professeur des Universités, Université de Poitiers	Rapporteur
Jacques BARBET, Directeur de Recherche INSERM, Université de Nantes	Examinateur
Patrick SAULNIER, Professeur des Universités, Université d'Angers	Examinateur

INSERM U646, Ingénierie de la Vectorisation Particulaire
IBT, 10 rue André Boquel, 49100 Angers, France

UNIVERSITE D'ANGERS **Année 2007**
U.F.R. des Sciences Pharmaceutiques N° 825

IMMUNOCIBLAGE DU CERVEAU PAR DES NANOCAPSULES LIPIDIQUES

THESE DE DOCTORAT

EN PHARMACOLOGIE EXPERIMENTALE

ECOLE DOCTORALE D'ANGERS

Présentée et soutenue publiquement

Le 18 avril 2007

à Angers

par **Arnaud BEDUNEAU**

Devant le jury ci-dessous :

Jean-Pierre BENOIT, Professeur des Universités, Université d'Angers	Directeur de thèse
Didier BETBEDER, Professeur des Universités, Université d'Artois	Rapporteur
Jean-Christophe OLIVIER, Professeur des Universités, Université de Poitiers	Rapporteur
Jacques BARBET, Directeur de Recherche INSERM, Université de Nantes	Examinateur
Patrick SAULNIER, Professeur des Universités, Université d'Angers	Examinateur

INSERM U646, Ingénierie de la Vectorisation Particulaire
IBT, 10 rue André Boquel, 49100 Angers, France

Je souhaite remercier vivement,

Monsieur Jean-Pierre Benoît, Professeur à l'Université d'Angers et directeur de l'Unité INSERM U646, de m'avoir donné l'opportunité d'effectuer ma thèse au sein de son Laboratoire et pour ses précieux conseils qui m'ont permis de faire avancer ce projet.

Monsieur Patrick Saulnier, Professeur à l'Université d'Angers et co-encadrant de ce travail de thèse. Merci pour ta bonne humeur, ton enthousiasme et la confiance que tu m'as accordée, ces 3 années de travail passées à tes cotés furent très enrichissantes.

Monsieur Didier Betbeder, Professeur à l'Université d'Artois et Monsieur Jean-Christophe Olivier, Professeur à l'Université de Poitiers, de me faire l'honneur de participer à ce jury et pour avoir accepté de consacrer du temps à l'évaluation de ce travail de thèse en qualité de rapporteur.

Monsieur Jacques Barbet, Directeur de recherche à l'Unité INSERM U601 de Nantes, de me faire l'honneur de participer à ce jury.

Je tiens à remercier également,

Christophe Chesné et Catherine Rougier de la société Biopredic International pour m'avoir fourni gracieusement les cellules endothéliales cérébrales de rat.

François Hindré. Merci de t'être impliqué dans la réalisation de ce travail. Tes idées, tes remarques aussi cinglantes que pertinentes, distillées au cours de nos nombreuses pauses enfumées m'ont été d'une précieuse aide.

Anne Clavreul. Je te remercie pour m'avoir initié aux « joies de la biologie ». Merci pour ta disponibilité, tes judicieux conseils mais aussi pour la patience dont tu as su faire preuve à mon égard.

Mimie. Je tenais vraiment à te remercier pour ton aide et ta biodisponibilité. Tu as toujours été présente, armée de ta bonne humeur (quoi que…) et de ta franchise légendaire. Je te souhaite beaucoup de bonheur pour la nouvelle vie qui t'attend à la fin de cette année.

Pierrot. Je te remercie pour ta contribution dans ce travail de thèse. J'ai pu compter sur toi lors des expérimentations animales, aussi bien tôt le matin que tard le soir. Nos discussions endiablées sur le club de foot du Louroux me manqueront.

Frank Boury. Heureusement que tu n'as pas tenu rigueur de notre première rencontre car autrement, je n'aurais pas pu découvrir les joies de la physico-chimie des colloïdes.

Jacques Proust pour m'avoir donné l'occasion de collaborer avec l'équipe de chimie-biophysique d'Yvan Panaiotov.

Yvan Panaïotov, et Tzvetanka. Merci de m'avoir accueilli avec autant d'hospitalité dans votre Laboratoire.

Yvan Minkov. Merci de m'avoir encadré lors de mes séjours à Sofia. J'ai trouvé très intéressant ton regard sur la science et sur la vie en générale.

Nico. Tu m'as accompagné durant mes deux dernières années de thèse pendant et après le travail. Je te souhaite bonne chance pour la suite et notamment un poste de « maître de conf » que tu convoites tant.

Franck L. Radiopharmacien de talent, je tenais absolument à te remercier pour les nombreux cafés que tu m'as offerts.

Alex. Merci de m'avoir supporté pendant ces trois années et demie. Je te suis très reconnaissant d'avoir esquissé un sourire à chacune de mes blagues, même celles que je te répétais pour la quarantième fois. J'espère que l'on réussira à oublier ce dialecte qui est devenu, au fil du temps, incontournable dans notre bureau (vi c'est vrai !). Beaucoup de bonheur pour la suite et continue à exploiter tes talents d'artiste, notamment l'art de la mosaïque…

Mes nouveaux collègues de bureau. Archi, tu es un exemple pour nous de droiture et de savoir-vivre. Maud, tes qualités humaines t'ont permis de t'intégrer très rapidement au sein du Labo. Je tenais à te remercier pour le temps que tu as consacré à corriger l'anglais de mes articles scientifiques et pour ton aide dans ma recherche de « post-doc ».

Anne S. Tu es un modèle d'altruisme et de gentillesse, tu as toujours pris le temps de répondre à mes questions. Je te souhaite beaucoup de bonheur, aussi bien dans ta vie professionnelle que personnelle.

Christina Huber, François-Loïc Pichard, Anne-Caroline Debois-Grollier et Florine Villard, pour votre participation active.

Merci également aux nombreuses personnes que j'ai côtoyées au Laboratoire, Kamel, Sara, Gaétan, Erika, Marie, Thomas P, Pascal, Florence, Nolwenn, Anne AP, Emilie A et Emilie R (pour leur « mythique compagnie », enfin je me comprends…), Mathilde, Emilien, Jacqueline, Gisèle, Laurence, Edith, Nicoletta, Thomas B, Mathieu, Arnaud V, Ali, Pierre, Fred T, Fred L, David, Jérôme…

J'adresse également mes remerciements au Comité Départementale de la Ligue contre le Cancer et à l'Association pour la Recherche sur le Cancer pour les aides financières octroyées.

« *A ma famille,*

A mes amis »

SOMMAIRE

INTRODUCTION GENERALE

Le traitement des maladies cérébrales constitue un des axes majeurs de la recherche pharmaceutique mondiale. Malgré les efforts réalisés depuis des dizaines années, la plupart des médicaments développés à cet effet se sont avérés peu efficaces. La principale raison est liée à la faible accessibilité du système nerveux central (SNC). En effet, la majorité des molécules thérapeutiques administrées par voie intraveineuse, ne peut atteindre les tissus cérébraux du fait de la présence de la barrière hémato-encéphalique (BHE), qui sépare le sang du parenchyme cérébral (figure 1).

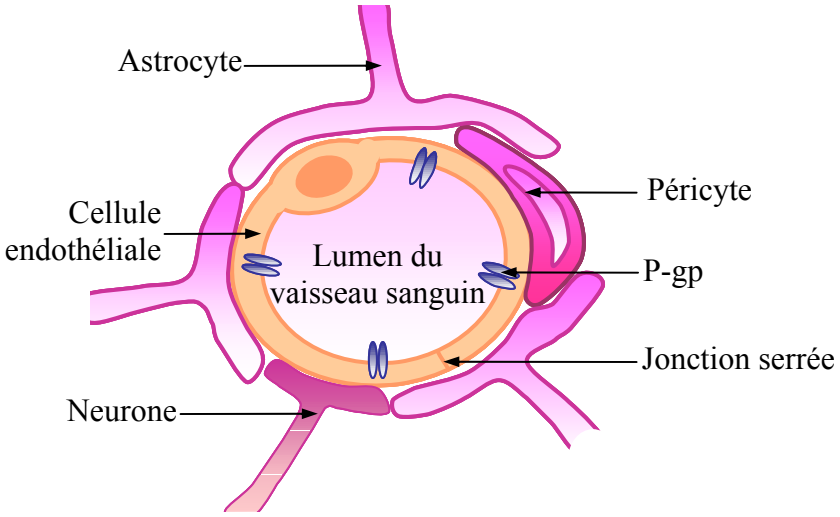

Figure 1. Représentation schématique de la BHE

Cette barrière biologique très complexe, est constituée notamment de cellules endothéliales reliées entre elles par des jonctions serrées, réduisant nettement sa perméabilité [1]. De plus, la P-glycoproteine (P-gp), fortement exprimée sur la BHE, favorise l'efflux des agents thérapeutiques. Seules les molécules présentant des propriétés physico-chimiques particulières, notamment une faible masse moléculaire et un fort caractère lipophile, sont capables de traverser cette barrière biologique. Ainsi, l'acheminement de médicaments au sein

des tissus cérébraux constitue un véritable challenge dans le traitement des maladies cérébrales comme les gliomes malins (astrocytome anaplasique, glioblastome multiforme, etc.) ou les maladies neurodégénératives.

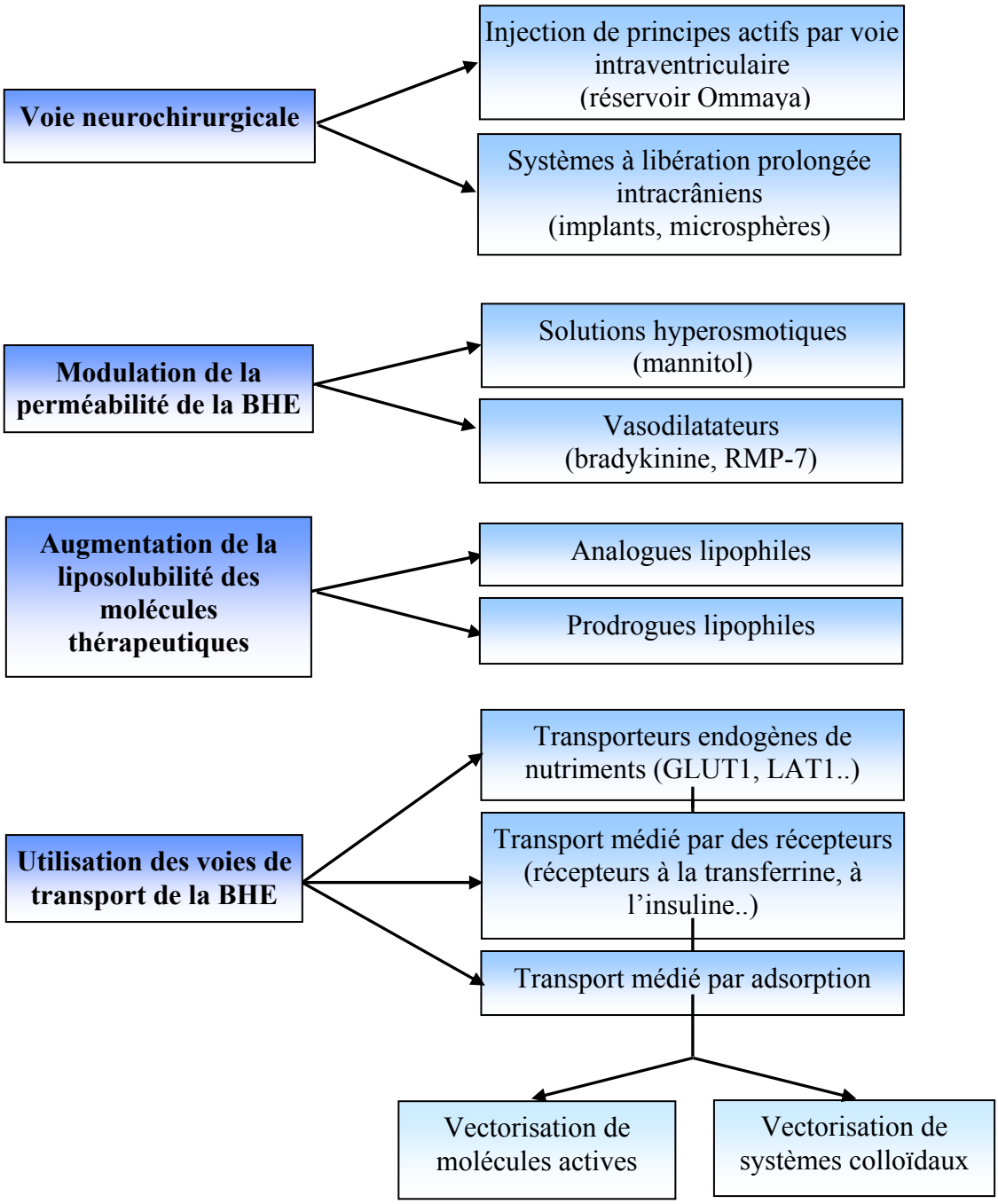

Figure 2. Stratégies pour améliorer la délivrance de molécules actives dans le SNC

Depuis de nombreuses années, différentes stratégies ont été mises en place afin d'administrer des molécules thérapeutiques, notamment des anticancéreux, au sein du cerveau (figure 2). Parmi ces stratégies, la voie neurochirurgicale a été très étudiée. La délivrance par voie intraventriculaire de principes actifs par le biais de pompes reliées à des cathéters (réservoir Ommaya) [2] a montré des résultats encourageants. Cependant, des effets neurotoxiques ont été rencontrés, liés à la concentration élevée de principes actifs dans le parenchyme cérébral et à leur distribution aléatoire. La pose d'implants dans la cavité de résection ou bien l'injection *in situ* de microsphères [3, 4] ont également été réalisées. Le Gliadel®, implant polymérique intracrânien contenant un anticancéreux, la carmustine, a montré une légère augmentation de la médiane de survie des patients atteints de gliomes de haut grade (deux mois) [5]. Il est actuellement indiqué en traitement d'appoint de la chirurgie et de la rathiothérapie, chez les patients atteints d'un glioblastome multiforme récurrent. Malgré les résultats intéressants, l'efficacité thérapeutique de ces systèmes à libération prolongée, est principalement limitée par la faible diffusion des molécules au sein des tissus cérébraux (1-2 mm autour de l'implant).

Des stratégies non-invasives ont également été mises au point. Parmi elles, la modulation de la perméabilité de la BHE combinée à l'administration de molécules thérapeutiques a aussi été envisagée. L'ouverture transitoire de la BHE après l'injection intracarotidienne de solutions hyperosmotiques [6] ou d'agents vasodilatateurs comme la bradykinine ou le RMP-7 [7], a favorisé significativement le passage de principes actifs dans le cerveau. Cependant, le bénéfice apporté était moindre comparé à la toxicité générée par cette méthode. Une seconde approche consistant à augmenter le caractère hydrophile des molécules actives (prodrogues [8] ou analogues lipophiles [9]), a amélioré de façon conséquente, leur transport à travers la BHE. Cependant, malgré une concentration accrue au sein du

parenchyme cérébral, aucune amélioration notoire du traitement n'a été constatée en comparaison avec les anticancéreux classiques [10]. En outre, l' utilisation des voies de transport exprimées au niveau de la BHE, à savoir les transporteurs de nutriments, la transcytose médiée par récepteur et la transcytose médiée par adsorption représente une approche non-invasive très prometteuse (figure 3).

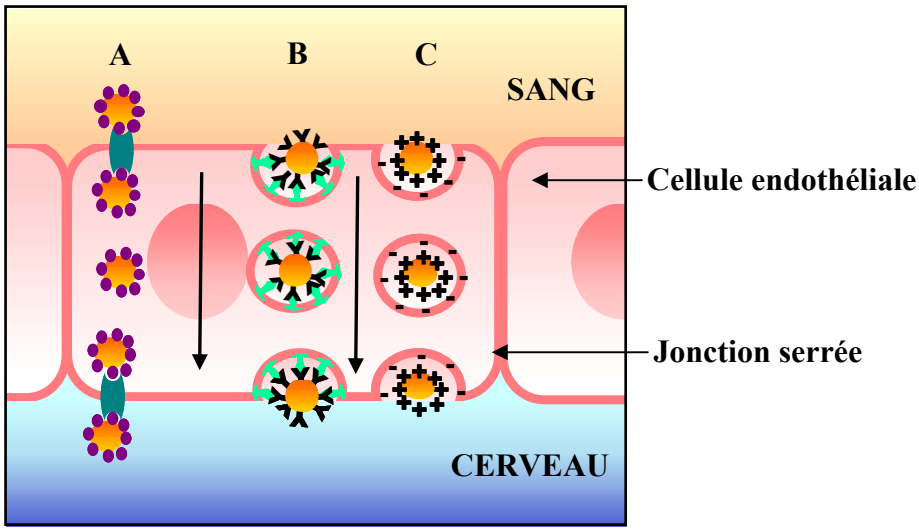

Figure 3. Principales voies de transport au niveau de la BHE:

(A) : Transporteur de nutriments

(B) : Transcytose médiée par récepteur

(C) : Transcytose médiée par adsorption

Cette stratégie dite « de ciblage actif », consiste à utiliser des biomolécules interagissant avec ces différents systèmes, permettant ainsi la reconnaissance spécifique de la BHE et son franchissement. Ces « chevaux de Troie moléculaires » peuvent être conjugués directement aux molécules actives ou bien à des systèmes colloïdaux contenant un principe actif. Cette deuxième solution s'avère plus judicieuse car les systèmes particulaires protègent du milieu

extérieur les molécules actives encapsulées et donc limitent les phénomènes de dégradation par des agents chimiques ou biologiques. De plus, ils diminuent leur toxicité et peuvent prolonger leur temps de résidence vasculaire.

Les études réalisées à partir des transporteurs de nutriments ont montré leur intérêt pour la vectorisation de molécules actives [11] mais très peu de résultats probants ont été obtenus avec des systèmes particulaires. En revanche, l'intérêt de la transcytose médiée par récepteur a été très largement démontré pour le ciblage de molécules actives et de systèmes particulaires au niveau du SNC [12]. Cette voie est plus spécifique au cerveau que la transcytose médiée par adsorption, qui a également une haute activité au niveau du foie et des reins [13]. Les principaux récepteurs présents au niveau de la BHE et capables de médier la transcytose, incluent le récepteur à la transferrine, à l'insuline, aux apolipoprotéines E.. [14-16] Les ligands de reconnaissance peuvent être de nature endogène. Cependant, après leur administration dans la circulation sanguine, des interactions ont lieu avec le milieu environnant. En effet, l'activité biologique de l'insuline peut provoquer l'hypoglycémie et le ciblage via la transferrine est le plus souvent inhibé par la présence d'une forte concentration systémique de transferrine endogène saturant les récepteurs. Afin de limiter ces effets, des anticorps monoclonaux se liant aux récepteurs mentionnés précédemment, ont été développés. En se fixant sur les épitopes externes, ces anticorps monoclonaux n'entrent pas en compétition avec les molécules plasmatiques. Parmi la large gamme d'anticorps monoclonaux synthétisés, l'anticorps monoclonal dirigé contre le récepteur à la transferrine est un candidat idéal pour la vectorisation du cerveau [17]. Le récepteur à la transferrine est très fortement exprimé sur les cellules endothéliales cérébrales et il médie la transcytose. [18] Par ailleurs, il est surexprimé sur les cellules à forte activité mitotique comme les cellules de gliome [19], favorisant aussi le ciblage des tumeurs cérébrales. La conjugaison des ligands de reconnaissance se fait le plus souvent, de façon covalente ou par la technologie avidine / biotine. Contrairement à la liaison

avidine / biotine, la liaison chimique n'est pas immunogène mais elle peut altérer dans certains cas, l'activité de reconnaissance des anticorps.

Les systèmes colloïdaux utilisés dans le cadre de délivrance systémique de molécules actives dans le SNC doivent respecter le cahier des charges suivant :

- biocompatible,
- biodégradable,
- physiquement stable dans le sang,
- taille nanométrique,
- faiblement immunogène (furtif)

Le caractère furtif du vecteur est, en effet, une propriété essentielle pour favoriser son accumulation dans le cerveau. Le recouvrement des particules par des polymères hydrophiles et flexibles comme le poly(éthylène) glycol (PEG) a permis de prolonger significativement le temps de résidence vasculaire des systèmes particulaires [20]. La barrière stérique conférée par le PEG autour de la particule, empêche l'adsorption d'opsonines, impliquées dans les mécanismes de phagocytose.

Les principaux systèmes particulaires (Figure 4) utilisés pour la vectorisation active du cerveau se répartissent en quatre groupes :

- les micelles polymériques : arrangement spontané de polymères amphiphiles [21]
- les liposomes : vésicule unilamellaire ou multilamellaire constituée notamment de phospholipides et de cholestérol [22-24]
- les nanoparticules à cœur lipidique solide [25]
- les nanoparticules polymériques : nanosphères ou nanocapsules constituées de polymères synthétiques (poly(acide lactique-co-glycolique) [26], poly(2-cyanoacrylate de butyle)..) [27] ou naturels (chitosane, gélatine…) [28].

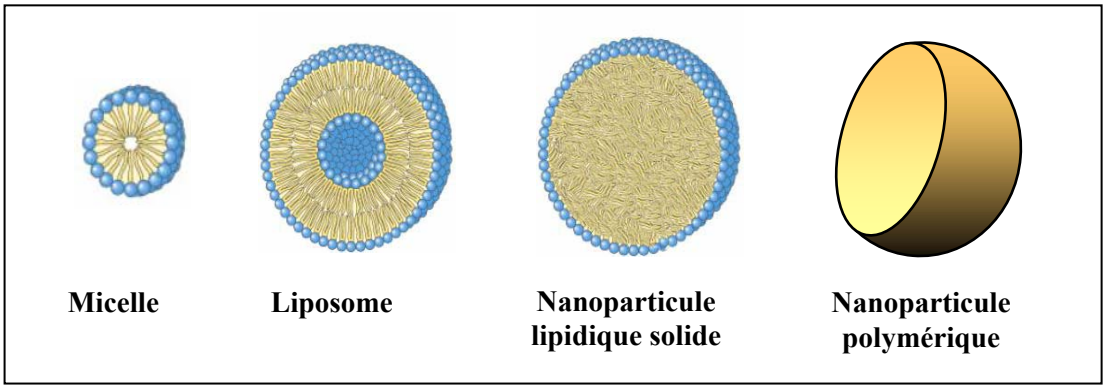

Figure 4. Représentation schématique de différents systèmes colloïdaux utilisés pour le transport de molécules actives au SNC.

Un système colloïdal original, destiné à l'administration de molécules lipophiles, a été développé dans notre laboratoire. Il s'agit de nanocapsules lipidiques (NCL) constituées d'un cœur liquide de triglycérides à chaînes moyennes, entouré de phospholipides (Lipoïd® S75-3) et de polymères hydrophiles (Solutol® HS15). Comme le montre la figure 5, ces nanocapsules lipidiques rassemblent à elles seules, les nombreux avantages des systèmes particulaires mentionnés précédemment. Elles constituent par conséquent, un vecteur de choix pour la délivrance de molécules lipophiles dans le cerveau.

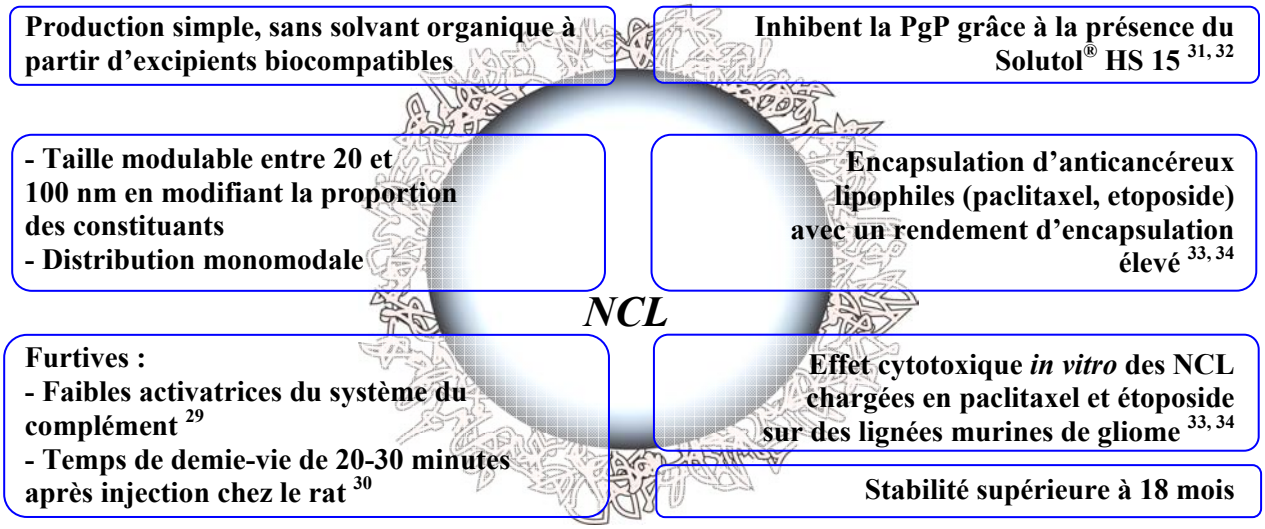

Figure 5. Avantages des NCL

Ce travail de thèse s'inscrit dans cette stratégie de ciblage actif du cerveau. Un système particulaire reconnaissant spécifiquement les tissus cérébraux, a été mis au point à partir des NCL. Afin de cibler activement le cerveau, nous avons greffé des anticorps monoclonaux dirigés contre le récepteur à la transferrine de rat (OX26) sur la surface des NCL conduisant à la formation d'immunonanocapsules. Pour limiter les interactions éventuelles entre la partie Fc de l'anticorps et le système réticuloendothélial, nous avons développé une seconde génération d'immunonanocapsules portant des fragments Fab' en lieu et place des anticorps entiers OX26. Le but est de favoriser la reconnaissance des cellules cibles en prolongeant le temps de résidence vasculaire des NCL.

La première partie de cette thèse est une revue bibliographique s'intéressant aux différents vecteurs colloïdaux qui ont été mis au point pour délivrer, de façon spécifique, des molécules actives au niveau des tumeurs cérébrales.

La seconde partie organisée en quatre chapitres, porte sur le travail expérimental qui a été réalisé au cours de cette thèse. Le premier s'intéresse au développement d'une nouvelle

génération de nanocapsules lipidiques furtives portant à leur surface de longues chaînes de PEG. Le deuxième concerne la conception et la caractérisation des immunonanocapsules. Leurs évaluations *in vitro* et *in vivo* font l'objet du troisième et dernier chapitre

Références

(1) Brightman, M. W.; Reese, T. S., Junctions between intimately apposed cell membranes in the vertebrate brain. *J Cell Biol* **1969,** *40*, (3), 648-77.

(2) Ratcheson, R. A.; Ommaya, A. K., Experience with the subcutaneous cerebrospinal-fluid reservoir. Preliminary report of 60 cases. *N Engl J Med* **1968,** *279*, (19), 1025-31.

(3) Westphal, M.; Ram, Z.; Riddle, V.; Hilt, D.; Bortey, E., Gliadel wafer in initial surgery for malignant glioma: long-term follow-up of a multicenter controlled trial. *Acta Neurochir (Wien)* **2006,** *148*, (3), 269-75; discussion 275.

(4) Menei, P.; Benoit, J. P., Implantable drug-releasing biodegradable microspheres for local treatment of brain glioma. *Acta Neurochir Suppl* **2003,** *88*, 51-5.

(5) Westphal, M.; Hilt, D. C.; Bortey, E.; Delavault, P.; Olivares, R.; Warnke, P. C.; Whittle, I. R.; Jaaskelainen, J.; Ram, Z., A phase 3 trial of local chemotherapy with biodegradable carmustine (BCNU) wafers (Gliadel wafers) in patients with primary malignant glioma. *Neuro-oncol* **2003,** *5*, (2), 79-88.

(6) Cosolo, W. C.; Martinello, P.; Louis, W. J.; Christophidis, N., Blood-brain barrier disruption using mannitol: Time course and electron microscopy studies. *American Journal of Physiology - Regulatory Integrative and Comparative Physiology* **1989,** *256*, (2).

(7) Elliott, P. J.; Hayward, N. J.; Huff, M. R.; Nagle, T. L.; Black, K. L.; Bartus, R. T., Unlocking the blood-brain barrier: A role for RMP-7 in brain tumor therapy. *Experimental Neurology* **1996,** *141*, (2), 214-224.

(8) Sinkula, A. A.; Yalkowsky, S. H., Rationale for design of biologically reversible drug derivatives: prodrugs. *J Pharm Sci* **1975,** *64*, (2), 181-210.

(9) Sampath, P.; Amundson, E.; Wall, M. E.; Tyler, B. M.; Wani, M. C.; Alderson, L. M.; Colvin, M.; Brem, H.; Weingart, J. D., Camptothecin analogs in malignant gliomas: comparative analysis and characterization. *J Neurosurg* **2003,** *98*, (3), 570-7.

(10) Rautio, J.; Chikhale, P. J., Drug delivery systems for brain tumor therapy. *Current Pharmaceutical Design* **2004,** *10*, (12), 1341-1353.

(11) Cornford, E. M.; Young, D.; Paxton, J. W.; Finlay, G. J.; Wilson, W. R.; Pardridge, W. M., Melphalan penetration of the blood-brain barrier via the neutral amino acid transporter in tumor-bearing brain. *Cancer Research* **1992,** *52*, (1), 138-143.

(12) Schnyder, A.; Huwyler, J., Drug transport to brain with targeted liposomes. *NeuroRx* **2005,** *2*, (1), 99-107.

(13) Tamai, I.; Tsuji, A., Drug delivery through the blood-brain barrier. *Advanced Drug Delivery Reviews* **1996,** *19*, (3), 401-424.

(14) Chung, N. S.; Wasan, K. M., Potential role of the low-density lipoprotein receptor family as mediators of cellular drug uptake. *Advanced Drug Delivery Reviews* **2004,** *56*, (9), 1315-1334.

(15) Antohe, F.; Radulescu, L.; Puchianu, E.; Simionescu, M.; Kennedy, M. D.; Low, P. S., Increased uptake of folate conjugates by activated macrophages in experimental hyperlipemia. *Cell and Tissue Research* **2005,** *320*, (2), 277-285.

(16) Li, H.; Qian, Z. M., Transferrin/transferrin receptor-mediated drug delivery. *Medicinal Research Reviews* **2002,** *22*, (3), 225-250.

(17) Bickel, U.; Yoshikawa, T.; Landaw, E. M.; Faull, K. F.; Pardridge, W. M., Pharmacologic effects in vivo in brain by vector-mediated peptide drug delivery. *Proceedings of the National Academy of Sciences of the United States of America* **1993,** *90*, (7), 2618-2622.

(18) Wu, D.; Pardridge, W. M., Pharmacokinetics and blood-brain barrier transport of an anti-transferrin receptor monoclonal antibody (OX26) in rats after chronic treatment with the antibody. *Drug Metab Dispos* **1998,** *26*, (9), 937-9.
(19) Recht, L.; Torres, C. O.; Smith, T. W.; Raso, V.; Griffin, T. W., Transferrin receptor in normal and neoplastic brain tissue: implications for brain-tumor immunotherapy. *J Neurosurg* **1990,** *72*, (6), 941-5.
(20) Moghimi, S. M.; Hunter, A. C.; Murray, J. C., Long-circulating and target-specific nanoparticles: Theory to practice. *Pharmacological Reviews* **2001,** *53*, (2), 283-318.
(21) Kabanov, A. V.; Batrakova, E. V.; Melik-Nubarov, N. S.; Fedoseev, N. A.; Dorodnich, T. Y.; Alakhov, V. Y.; Chekhonin, V. P.; Nazarova, I. R.; Kabanov, V. A., A new class of drug carriers: Micelles of poly(oxyethylene)-poly(oxypropylene) block copolymers as microcontainers for drug targeting from blood in brain. *Journal of Controlled Release* **1992,** *22*, (2), 141-157.
(22) Huwyler, J.; Wu, D.; Pardridge, W. M., Brain drug delivery of small molecules using immunoliposomes. *Proceedings of the National Academy of Sciences of the United States of America* **1996,** *93*, (24), 14164-14169.
(23) Schnyder, A.; Krahenbuhl, S.; Drewe, J.; Huwyler, J., Targeting of daunomycin using biotinylated immunoliposomes: Pharmacokinetics, tissue distribution and in vitro pharmacological effects. *Journal of Drug Targeting* **2005,** *13*, (5), 325-335.
(24) Schnyder, A.; Krahenbuhl, S.; Torok, M.; Drewe, J.; Huwyler, J., Targeting of skeletal muscle in vitro using biotinylated immunoliposomes. *Biochem J* **2004,** *377*, (Pt 1), 61-7.
(25) Lockman, P. R.; Oyewumi, M. O.; Koziara, J. M.; Roder, K. E.; Mumper, R. J.; Allen, D. D., Brain uptake of thiamine-coated nanoparticles. *Journal of Controlled Release* **2003,** *93*, (3), 271-282.
(26) Olivier, J.-C.; Huertas, R.; Lee, H. J.; Calon, F.; Pardridge, W. M., Synthesis of Pegylated Immunonanoparticles. *Pharmaceutical Research* **2002,** *19*, (8), 1137-1143.
(27) Kreuter, J., *Application of nanoparticles for the delivery of drugs to the brain*. 1277 ed.; 2005; p 85-94.
(28) Aktas, Y.; Yemisci, M.; Andrieux, K.; Gursoy, R. N.; Alonso, M. J.; Fernandez-Megia, E.; Novoa-Carballal, R.; Quinoa, E.; Riguera, R.; Sargon, M. F.; Celik, H. H.; Demir, A. S.; Hincal, A. A.; Dalkara, T.; Capan, Y.; Couvreur, P., Development and brain delivery of chitosan-PEG nanoparticles fnnctionalized with the monoclonal antibody OX26. *Bioconjugate Chemistry* **2005,** *16*, (6), 1503-1511.
(29) Vonarbourg, A.; Passirani, C.; Saulnier, P.; Simard, P.; Leroux, J. C.; Benoit, J. P., Evaluation of pegylated lipid nanocapsules versus complement system activation and macrophage uptake. *Journal of Biomedical Materials Research - Part A* **2006,** *78*, (3), 620-628.
(30) Ballot, S.; Noiret, N.; Hindre, F.; Denizot, B.; Garin, E.; Rajerison, H.; Benoit, J. P., (99m)Tc/(188)Re-labelled lipid nanocapsules as promising radiotracers for imaging and therapy: formulation and biodistribution. *Eur J Nucl Med Mol Imaging* **2006**, 1-6.
(31) Coon, J. S.; Knudson, W.; Clodfelter, K.; Lu, B.; Weinstein, R. S., Solutol HS 15, nontoxic polyoxyethylene esters of 12-hydroxystearic acid, reverses multidrug resistance. *Cancer Research* **1991,** *51*, (3), 897-902.
(32) Buckingham, L. E.; Balasubramanian, M.; Emanuele, R. M.; Clodfelter, K. E.; Coon, J. S., Comparison of Solutol HS 15, Cremophor EL and novel ethoxylated fatty acid sulfactants as multidrug resistance modification agents. *International Journal of Cancer* **1995,** *62*, (4), 436-442.
(33) Garcion, E.; Lamprecht, A.; Heurtault, B.; Paillard, A.; Aubert-Pouessel, A.; Denizot, B.; Menei, P.; Benoit, J. P., A new generation of anticancer, drug-loaded, colloidal

vectors reverses multidrug resistance in glioma and reduces tumor progression in rats. *Mol Cancer Ther* **2006,** *5*, (7), 1710-22.

(34) Lamprecht, A.; Benoit, J.-P., Etoposide nanocarriers suppress glioma cell growth by intracellular drug delivery and simultaneous P-glycoprotein inhibition. *Journal of Controlled Release* **2006,** *112*, (2), 208-213.

REVUE BIBLIOGRAPHIQUE

Active targeting of brain tumors using nanocarriers

A. Beduneau [1], P. Saulnier [1,], J-P. Benoit [1, 2]

[1] Inserm, U646, Angers, F-49100 France ; Université d'Angers, Angers, F-49100 France.

[2] To whom correspondence should be addressed. (E-mail: jean-pierre.benoit@univ-angers.fr).

Abstract

The delivery of drugs to the brain tumors is limited by the presence of the blood-brain barrier (BBB) separating the blood from the cerebral parenchyma. The understanding of specific mechanisms occurring at the level of brain capillary endothelium, allowed to develop various strategies to enhance the penetration of drugs into the brain tissue. The active targeting is a non-invasive approach which consists in transporting drugs to target organs using site-specific ligands. Drug-loaded nanocarriers able to recognize brain capillary endothelial cells and cerebral tumoral cells have shown a promising potential in oncology. Endogenous and chimeric ligands binding to carriers or receptors of the BBB have been directly or indirectly conjugated to nanocarriers. This review indexes the main targeted colloidal systems used for drug delivery to the brain. Their pharmacological behavior and their therapeutic effect will be discussed.

Keywords

Nanocarriers, , brain targeting, endogenous ligands, monoclonal antibodies, carrier-mediated transport, receptor-mediated transcytosis, adsorptive-mediated transcytosis.

Contents

1 Introduction

The treatment of brain cancer represents one of the most difficult challenges in oncology. The three main brain tumors in adults are the astrocytomas, the oligodendrogliomas and the oliogoastrocytomas (1). The astrocytomas are tumors which arise from astrocytes, type of glial cells located into the brain. They include different subtypes of tumors classified according to their malignant grade. The anaplastic astrocytoma (grade III) and the glioblastoma (grade IV) occur more frequently than the other malignant gliomas and are the most aggressive due to their rapid proliferation and their property to infiltrate the healthy brain tissue. Despite the treatment combining surgical resection, radiotherapy and chemotherapy, the median survival of patients (1 year) has not been significantly changed for thirty years.

The failure of the chemotherapy is due to the inability of anticancer agents to reach the brain parenchyma after intravenous administration. Indeed, an endothelial cell monolayer in association with pericytes and astrocytes so-called the blood-brain barrier (BBB) separates the blood from the cerebral parenchyma and prevents from the penetration of drugs into the central nervous system (CNS). BBB first described by Erlich in 1885 protects the brain from substances (eg, potassium, glycine, and glutamate) which are neurotoxic in physiological concentrations (2). This physical barrier is characterized by tight intracellular junctions (*zona occludens*) (3) and by the absence of fenestrations limiting its crossing by therapeutic molecules such as antineoplastic agents. The deficiency in pinocytic vesicles and the high metabolic capacity of cerebral endothelial cells (4) contribute also to limit the exchange of anticancer agents between the plasma and the CNS. In addition, the cerebral endothelium has a high level of ATP-binding cassette (ABC) transporters such as the P-glycoprotein implied in the drug efflux mechanisms (5). Thus, the BBB prevents the brain uptake of all the large-

molecules drugs and more than 98% of pharmaceuticals small-molecule (6). Only the small (< 5000 Da), lipid–soluble and electrically-neutral molecules are able to diffuse passively across the BBB (7). However, the proliferation and the invasion of tumoral cells generate generally a local disruption of the BBB (2). Production of various mediators by the cancer cells such as arachidonic acid, leukotrienes, prostaglandin E and thromboxane B_2 increase the permeability of capillary endothelium (8). Moreover, the tumor secrets proangiogenic factors including basic fibroblast growth factor and vascular endothelial growth factor inducing the formation of new blood vessels into the tumor (9). These capillaries characterized by frequent fenestrations improve also the permeability of the blood-tumor interface and as a consequence, the penetration of drugs. Nevertheless, the disruption of the BBB does not occur in the healthy tissue surrounding the main tumor and so, the anticancer agents can not reach the adjacent tumors located in the normal tissue.

A second barrier separating the blood from the cerebrospinal fluid (CSF) resides in the choroid plexuses (10). The blood-CSF barrier is functionally and morphologically different of the BBB. The choroid epithelial cells form tight junction and are responsible for barrier function. Nevertheless, these cells have shown a low resistance in comparison with the endothelial cells of the BBB (11). The capillary endothelium in the choroid plexuses are fenestrated, allowing the diffusion of small molecules (12). Despite its permeability, blood-CSF barrier does not increase significantly the penetration of drugs into the brain. Indeed, the surface area of the blood-CSF barrier is 1000-fold less important than the surface area of the BBB (13).

Various invasive strategies (neurosurgical) were developed to improve the penetration of drugs into the brain. Among them, the interstitial drug delivery is an approach that was

sharply used for many years. Therapeutic agents were directly injected into the cerebral parenchyma. The implantation of polymeric matrix such as microspheres loaded with an anticancer agent was used for the treatment of malignant gliomas (14-17). The matrix after implantation releases the drug by hydrolytic degradation of the polymer. Besides, another intracavitary treatment using a controlled release system, the Gliadel® wafer, has been developed (18). This system was composed of a lipophilic anticancer agent, the carmustine, incorporated into a poly(carboxypropane)-sebacic acid (PCPP-SA) belonging to the series of polyanhydrides. The therapeutic effect of Gliadel® wafer has been tested in two phase III clinical trials (19, 20). In these randomized trials, the patients suffered from a recurrent malignant glioma including a majority of glioblastoma multiforme . Following resection of tumor, they received either Gliadel® or either placebo. The median survival time obtained with the treated patients, was significantly prolonged in comparison with untreated patients (2-month increase). Thus, Gliadel® was established as a safe and effective treatment for malignant gliomas. However, different side effects caused by this system have been reported. Infections, cerebral edemas due to the high concentration of carmustine and obstructive hydrocephalus resulting from the wafer dislodgment, were observed. Besides, intra-cerebroventricular infusion of drugs have been also perfected. The Ommaya reservoir, a catheter with pump system, (21) can deliver intermittent bolus injections of anticancer drugs directly into the cerebrospinal fluid. Disadvantages have been reported such as infection, catheter obstruction and discomfort for the patient. These invasive strategies rely on the diffusion of therapeutics molecules but this mechanism is very poor into the cerebral parenchyma. Indeed, the diffusion rate of drug decreases with the square of the diffusion distance (22).

Non-surgical strategies have been also investigated. One approach consisted to generate a transient disruption of the BBB in conjunction with the systemic administration of anticancer agents. The intracarotid administration of a hyperosmotic solution such as the mannitol led to a rapid diffusion of fluid across cerebral endothelium, moving out of endothelial cells into the vascular lumen and involving the opening of the tight junctions during a few hours (23). Mediators of inflammatory response, such as leukotrienes and vasoactive peptides were also used to increase the BBB permeability (24). However, with this method, neurotoxic chemotherapeutic agents reached also the healthy tissue, involving adverse effects.

Another approach concerns the modification of drugs in order to make them more lipophilic, improving their penetration into the brain by passive diffusion. In this way, lipophilic analogues and prodrugs (25) have been developed. However, despite the lipidization, no modified molecule demonstrated an anticancer activity superior to the parent drug. For example, the chlorambucil-tertiary characterized by a penetration into the brain 35-fold greater than the chlorambucil has not improved the treatment of brain-sequestered carcinosarcoma in rats (26). The weak solubility of these lipophilic molecules in the brain interstitial fluid could explain their inefficiency (27).

Active targeting of the BBB represents a promising non-invasive strategy for improving drug delivery to the brain tumors. It consists in using the various influx transport systems expressed within the cerebral endothelial, including the carrier-mediated transports (CMT), the receptor-mediated endocytosis (RME) and the adsorptive-mediated endocytosis (AME) systems. These transport systems have an essential physiological role in the delivery of vital substances to the brain. They play also a key role in the growth of cancerous cells and as a consequence, they are usually overexpressed on tumors. The CMT systems mediate the passage of small molecular weight nutrients though the BBB. Over 20 transporters highly

expressed on the cerebral capillaries of the BBB have been identified, such as the carriers for D-glucose (GLUT1), monocarboxylic acids (MCT1), large neutral amino acids (LAT1), small neutral amino acids (EAAT), cationic amino acids (CAT1), organic cations (OCT), etc. (28, 29). Besides, the concept of RME was initiated in the middle of 1970s in a study concerning the cellular cholesterol metabolism through the low density lipoproteins (LDL) (30). The specific receptors of the brain capillary endothelium have been identified for LDL, insulin, insulin-like growth factors (IGF-I, IGF-II), interleukin-1 (IL-1), folic acid (FA) and transferrin (Tf) (31). However, the receptor-mediated transcytosis (RMT) has only been showed for insulin and Tf receptors (TfR) (32, 33). AME systems have been also investigated for active targeting of brain tumors. The mechanism is based on an electrostatic interaction between a positively charged ligand and the negatively charged membrane of the BBB. The transport into the cerebral parenchyma of cationized albumins and cationized immunoglobulins was hence significantly improved in comparison with native proteins (34, 35).

A first approach of the active targeting consisted of the design of drugs with specific affinities with the CMT, RME or AME systems. This strategy aims at improving both the selective brain targeting and the brain uptake of therapeutics molecules. Active substances characterized by molecular structures which mimic endogenous nutrients, have been synthesized. The melphalan, a nitrogen mustard alkylating agent with a chemical structure close to phenylalanine, was able to cross the BBB via the LAT1 transporter (36). The attachment of glucose molecules to anticancer agent chlorambucil enabled the recognition by the GLUT1 transporters (37). However, in the case of peptide components, the glycosylation did not induce an enhanced BBB permeability but improved only their stability (38). The conjugation to drugs of endogenous ligands implied in RME and AME systems, promoted also their delivery to the brain. Tf has been used as an endogenous cellular transport system

for the delivery of diphteria toxin (CRM 107) to malignant brain tumors (39). Indeed, diphtheria toxin conjugated to Tf produced tumor responses without any systemic toxicity in patients with cerebral tumors refractory to conventional therapy. Moreover, beta-endorphin peptides were delivered with success to the brain after conjugation with cationized albumin (40). Besides, peptidomimetic monoclonal antibodies (MAbs) able to bind on the exofacial epitope of the RME systems have been developed (22). The MAb so-called OX26 recognizes an extracellular domain on the TfR, distinct from the Tf binding site and as a consequence does not interfere with endogenous Tf binding. Experiments have showed a specific targeting of OX26 on the brain capillary endothelial cells (BCECs) in rats and its ability to reach the cerebral parenchyma (41). Various applications have been developed using this OX26 MAb. Kurihara *et al.* (42) used with success this antibody as a neurodiagnostic agent for the early detection of primary brain cancers.

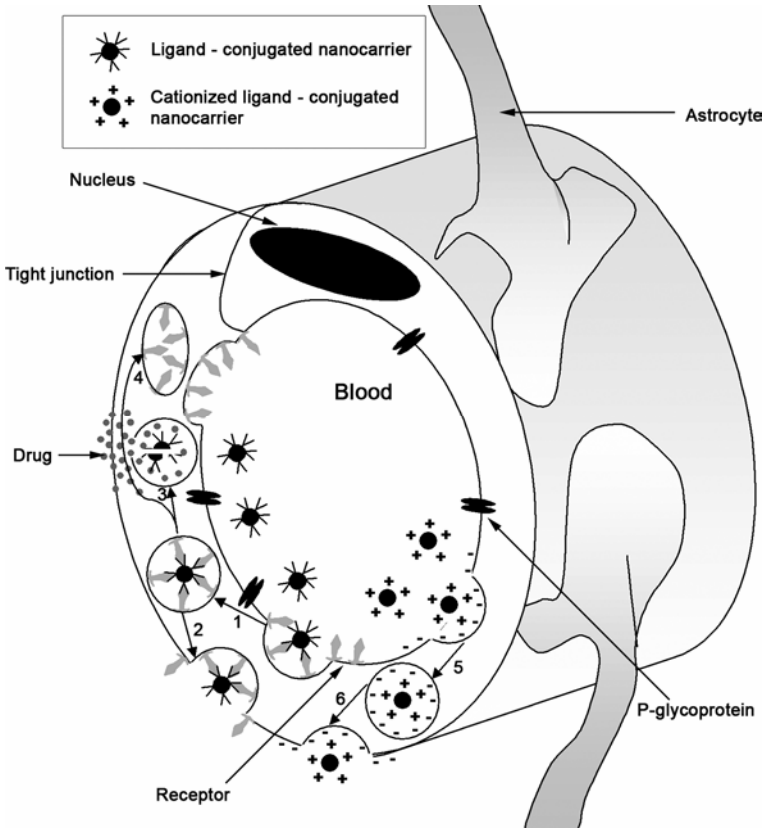

Figure 1. Mechanisms of drug transport through the BBB using nanocarriers conjugated to receptor-specific ligands (RME systems) and cationized ligands (AME systems). (1) Receptor-mediated endocytosis of the nanocarrier. (2) Exocytosis of the nanocarrier. (3) Dissociation of the receptor from the ligand-conjugated nanocarrier and acidification of the vesicle leading to the degradation of nanocarrier and the release of drug into the brain. (4) Recycling of receptors at the luminal cytoplasmic membrane. (5) Adsorptive-mediated endocytosis of nanocarrier conjugated to cationized ligands. (6) Exocytosis of positively charged nanocarriers.

Another approach of active targeting of brain is the conjugation of the ligands previously described on the surface of colloidal drug carriers. This coupling can be applied directly to the nanocarriers using covalent and non-covalent linkages or indirectly using a hydrophilic surfactant coating able to adsorb endogenous ligands after their intravenous administration. Thereby, these targeted nanovectors bind specifically to the brain capillary endothelium cells inducing an internalization mechanism (figure 1). The nanocarriers are either exocytosed and reach then the cerebral parenchyma or damaged within lysosomes leading to the drug release into the brain tissue. The main advantages of this strategy in comparison with drugs coupled directly to site-specific ligands is the reduction of the toxicity of the packaged molecule and the preservation of its biological activity. Besides, the structure of nanocarriers first developed in 1970 has been recently optimized in order to improve their biodistribution. Polyethylene glycol (PEG) has been grafted to nanoparticles and liposomes, increasing their stealthiness and, consequently, their systemic residence time into the bloodstream (43). Indeed, the steric barrier generated by this hydrophilic polymer surrounding the nanocarrier, prevents from the serum protein adsorption (opsonization process) (44) and hence, the recognition by the reticuloendothelial system (RES). This point represents an

essential parameter to take into account before designing one approach to target the cerebral tissue.

This review focuses on the various targeted nanocarriers which have been developed since the mid 1990's for the treatment of brain cancers. The colloidal systems conjugated to ligands implied in CMT, RME and AME systems and their pharmacokinetic properties will be described. Their interest in drug delivery to the brain and their therapeutic potential in oncology will be discussed. A technological approach concerning the conception of these nanocarriers including liposomes, polymeric micelles, polymeric and lipidic nanoparticles will be brought.

2 Nanocarriers for active targeting of brain: liposomes, polymeric micelles, polymeric and lipid nanoparticles

The nanocarriers injected by the systemic route and used for the drug delivery have to respect some essential conditions (45):

- Biodegradable,
- Biocompatible,
- non-immunogenic,
- physically stable in the blood.

2.1 Liposomes

Liposomes are structured in concentric bilayers of amphipathic phospholipids. Since 1997, the New York Academy of Science has distinguished three types of liposomal systems: multilamellar (MLV, 100 nm-20 mm), small unilamellar (SUV, 10-50 nm)) and large unilamellar (LUV, 50-1000 nm) vesicles (46). Various therapeutic molecules can be encapsulated inside the vesicles. Hydrophilic and hydrophobic substances are incorporated in the internal aqueous phase and into the lipid bilayer, respectively. The techniques of preparation were sharply described in literature (47, 48). Briefly, in each method, lipids are dissolved in an organic solvent. A dry lipid film is obtained after evaporation of the solvent and is then dispersed in an aqueous phase. The different preparation procedures differ according to the method used to disperse the lipids (thin lipid film hydration, mechanical method such as sonication, extrusion, etc..). Moreover, some components of liposomes inhibit the P-gp, improving hence the drug permeability across the BBB (49). For ten years, PEG coupled to phospholipids such as distearoylphosphatidylethanolamine (DSPE) were

introduced into the liposomal structure. In human, a 200-fold decrease of the systemic plasma clearance was then observed for pegylated liposomes in comparison with conventional liposomes (50). The polymers are incorporated during the formulation or by a post-insertion method developed by Uster *et al.* (51). This procedure consists in incubating pre-formed liposomes in a micellar solution of PEG coupled to phospholipids at 60°C between 1 and 2 hrs.

2.2 Polymeric micelles

The polymeric micelles are formed from a spontaneous association of amphiphilic copolymers in an aqueous phase. They are characterized by a diameter of a few tens of nanometers. The attractive force leading to the micellization, is based on an interaction between the hydrophobic or electrostatically neutral parts of copolymers. The self-assembly starts when the copolymer concentration reaches a threshold value so-called the critical micelle concentration (CMC). Usually, the CMC of amphiphilic copolymers was 1000-fold weaker than that of low molecular weight surfactants (10^{-6}-10^{-7} M) (52). Thus, this feature suggests the preservation of the micellar structure after the extreme dilution following the intravenous administration to patients. The micelle shape depends on the length of lipophilic chains (53). The nature of hydrophobic segments are classified in three groups (54, 55):

- polyester: poly(lactic acid) (PLA), poly(ε-caprolactone) (PCL),
- poly(L-amino acid): poly(aspartic acid) (PAsp), poly(glutamic acid) (PGlu),
- phospholipids: phosphatidylethanolamine (PE).

Most of them are biodegradable and biocompatible. The hydrophilic blocks commonly used in drug delivery are polyethers like the poly(propylene oxide) (PPO) and the PEG (56) with a

molecular mass comprised between 1 and 15 kDa (57). Other hydrophilic polymers may be used such as the poly(acryloylmorpholine) and poly(vinylpyrrolidone) (58). The polymeric nanocarriers must have a size larger than 42-50 kDa in order to prevent their elimination by the glomerular excretion of kidneys (59). Due to the PEG presence and their small size, micelles composed of PEG-*block*-poly(D,L-lactide) (PEG-*b*-PDLLA) were characterized by long-circulating properties with a half-life of 18 hrs after intravenous administration (60). Various hydrophobic anticancer agents including paclitaxel (61) and docetaxel (62) have been incorporated into the hydrophobic core of polymeric micelles. The drugs can be chemically conjugated to macromolecules. 40 nm-micelles composed of PEG-*block*-poly(aspartic acid) [PEG-*b*-P(asp)] coupled to doxorubicin have been developed by Nakanishi *et al*. (63).

2.3 Polymeric nanoparticles

Polymeric nanoparticles including nanospheres and nanocapsules are made from natural or artificial polymers and are characterized by sizes ranging between 10 and 1000 nm. Various biodegradable polymers such as PLA, poly(lactic-co-glycolic acid) PLGA, PCL, chitosan, poly(alkylcyanoacrylate) (PACA), poly(lysine) and PAsp are used to compose the core matrix (64-66). Polymeric nanoparticles are prepared from pre-formed polymers (67) or by polymerization of monomers (68).

A great number of nanoparticles are prepared with PLA, PLGA polymers due to their biodegradability and biocompatibility properties (69). They are mainly produced by solvent evaporation and by solvent diffusion (70). In the first method, an O/W emulsion is obtained by sonication, polymers have been previously dissolved in an organic solvent immiscible to water such as dichloromethane. The solvent is then evaporated to allow the formation of the polymeric matrix. Oils such as Miglyol® 810N can be added to the volatile organic solvent in

order to obtain nanocapsules (71). Hence, a polymer layer is deposited at the O/W interface, stabilizing the submicron oil drops as a steric barrier. Hydrophobic drugs can be incorporated into the colloidal particle after dissolution in the organic phase An alternative technique also based on the solvent evaporation has been developed for the hydrophilic component encapsulation. Instead of a simple emulsion, a multiple w/O/W emulsion is prepared and the hydrophilic drug is dissolved in the inner water phase. In the solvent diffusion method, polymers are dissolved in a water soluble solvent such as acetone or ethanol. The organic phase is then dispersed in water and the precipitation of the hydrophobic polymer occurred due the spontaneous diffusion of solvent in water. In order to improve the long-circulating properties of nanoparticles, PEG-PLA or PEG-PLGA copolymers were used for the preparation of nanoparticles (72). The PEG blocks are thus covalently linked to the nanoparticle surface. Pharmacokinetic behaviors of pegylated nanoparticles were significantly improved with a mean residence time (MRT) reaching 140.7 min (73). Nanoparticles were also prepared with hydrophilic polymers such as chitosan (74), maltodextrin (75), alginate (76) or gelatin. Biodegradable and non-toxic properties of chitosan confer it a great interest as a pharmaceutical excipient (77). The chitosan nanoparticles are produced by electrostatic interactions between positively charged chitosan and a polyanion sodium tripolyphosphate. PEG-grafted chitosan nanoparticles have been also produced in order to improve their long-circulating properties. Nevertheless, their important size, between 200 nm and 1 µm, represents a potential disadvantage for the delivery of drugs to the brain. Coacervation methods are also used to prepare chitosan (78) or gelatin nanoparticles (79).

Usually, production of nanocarriers by polymerization is realized from alkylcyanoacrylate monomers. Polyalkylcyanoacrylate nanoparticles were first developed by Couvreur *et al.* 25 years ago (68). The polymerization occurred in acidic aqueous solution and was initiated by the hydroxyl ions of water. A surfactant or a stabilizing agent (Pluronic® F68

or dextran 70) had been previously introduced in the aqueous solution in order to allow the dispersion of the monomer. The anionic polymerization anionic lasts a few hours at room temperature allowing the nanosphere formation with a size ranging from 50 to 300 nm (80). Nanocapsules can also be obtained by interfacial polymerization from microemulsion or O/W nanoemulsions (81-83). The organic phase is composed of oil, monomers and volatile solvent miscible with water such as acetone or ethanol. The monomers thanks to the solvent diffusion, move at the O/W interface and in contact with water, the polymerization is initiated. Nanocapsules with a high oil concentration are then obtained. The low degradation rate (84) and the toxicity depending on the length of the alkyl group (85) can limit the application of these polymeric nanoparticles when systemically administered. Isobutylcyanoacrylate and isohexylcyanoacrylate are usually used for the production of nanoparticles because of their weaker toxicity and their biodegradability. Besides, studies have shown the ability of these polymeric nanoparticles to circumvent the multidrug-resistant mechanisms (86, 87). PEG has been chemically conjugated to PACA polymers such as PEG-poly(isobuty2-cyanoacrylate) (PIBCA) (88) or PEG-poly(hexadecylcyanoacrylate) (PHDCA) (89) in order to obtain long-circulating nanoparticles. Moreover, an in-vitro cytotoxicity study revealed that the pegylation of the cyanoacrylate polymers reduces their toxicity (90).

2.4 Lipid nanoparticles

The lipids nanoparticles are classified in two main groups: the solid lipid nanoparticles (SLN) (91) and the lipidic nanocapsules (LNC) (92).

The SLN are composed of a solid lipid matrix stabilized by surfactants. The lipids used (triglycerides, complex glyceride mixtures and waxes) have the particularity to be in a solid form at room and physiological temperatures. These lipid nanoparticles are mainly

produced by high pressure homogenization (HPH) (93), via microemulsions (94) and by solvent emulsification-evaporation or diffusion (95). The physical stability of SLN (several years), the use of bioacceptable and biodegradable lipids, the size in the nanometer range and the protection of the encapsulated drug represent promising features for parenteral administration. However, the drug loading capacity of conventional SLN is limited by the weak solubility of drugs in the lipid melt and the drug expulsion after polymorphic transition (96). In order to overcome these problems, the lipid matrix and the drug structure have been modified. Nanostructured lipid carriers (NLC) (97) and lipid-drug conjugates (LDC) (98) have then been developed leading to a significant increase of the drug loading. Sterically stabilized SLN have been prepared with PEG_{2000} conjugated to phospholipids and glycerides (99).

On the contrary, LNC are composed of a liquid oily core (medium chain triglycerides) surrounded by hydrophilic (PEG_{660}-hydroxystearate) and lipophilic (phosphatidylethanolamine and phosphatidylcholine) surfactants. These nanocapsules are prepared by the phase inversion temperature method (PIT method) (100). Briefly, during three cycles of progressive heating and cooling, the oil-in-water (O/W) emulsion is inverted into W/O emulsion by passing through a phase inversion zone (92). At the last cycle, a fast cooling with cold water is performed at the PIT leading to formation of submicron-scale particles. LNC are obtained without organic solvent and with pharmaceutically acceptable excipients. Various anticancer drugs were encapsulated into these lipidic nanovectors such as etoposide, docetaxel and paclitaxel (101-103). The PEG_{660} hydroxystearate located on the external surface represents a steric barrier against opsonization and it inhibits the P-gp (104, 105). Hoarau *et al.* (106) have incorporated on the LNC surface PEG derivatives using post-insertion method previously described for liposomes. This surface modification improved their pharmacokinetic behavior with a MRT in blood reaching 216 min. Substituting the

PEG_{660} hydroxystearate for PEG_{1500} stearate and using the PIT method, stealth lipid nanocapsules were obtained with a half-life of about 330 min (107).

A great number of these pegylated nanocarriers have been used directly for the delivery of drugs to the brain tumors by passive transport. Among them, paclitaxel-loaded SLN have shown a significant accumulation of anticancer molecules into the brain tissue (108) and the therapeutic efficiency of doxorubicin-loaded liposomes has been evaluated in patients bearing recurrent high-grade glioma (109). These colloidal systems have been sharply described in literature (110). In order to optimize their biodistribution, these vectors have been decorated by site-specific biomolecules recognizing target tissues. The following focus on nanocarriers able to deliver specifically drugs to cerebral tissues.

Besides, other nanoparticle types exist such as mineral nanoparticles used in the diagnosis field. Iron oxide-based contrast agents showed excellent potential for imaging the CNS (111).

3 Strategies used for active targeting

3.1 Nanocarriers conjugated to ligands implied in CMT systems

The CMT systems are highly expressed on the cerebral endothelium. They allow the delivery of vital nutrients required for the normal brain homeostasis. Thus, these transporters can be an efficient strategy to target and enhance the drug delivery to the CNS. In this way, nanocarriers interacting with various nutrient carrier systems have been developed.

Among the facilitative (sodium-independent) glucose transporter (GLUT), the GLUT1 isoform is mainly expressed in the luminal surface of brain capillaries as well as choroid plexus (29). The GLUT1 transporter promotes the transport of D-glucose from blood into the brain. Like most of the nutrient transporters, it mediates the BBB passage of substances exhibiting similar structures, including 2-deoxyglucose, galactose, mannose, and glucose analogues (112). Its capacity to transport glucose through the BBB is sharply higher (1420 nmol/min · g tissue) than other nutrient transporters (91 nmol/min · g tissue for MCT1 and 28 nmol/min · g tissue for LAT1) (29). Besides, GLUT1 transporter is differentially regulated in human brain tumors. For example, it is overexpressed in cerebral hemangioblastoma but underexpressed in glioblastoma multiforme (113). Usually, the predominant glucose transporter in high-grade gliomas is the GLUT3 isoform, that is also expressed on neurons in healthy brain (114). Thus, considering their affinity for GLUT1 transporter, mannose derivatives have been incorporated onto the surface of liposomes. Mannose-liposomes prepared from *p*-aminophenyl-α mannoside were able to cross the BBB via the glucose transporter, to finally reach the mouse brain. (115). However, the rat brain accumulation was

not enhanced for liposomal systems composed of either *p*-aminophenyl-β-D-mannopyranoside or *p*-aminophenyl- β-D-glucopyranoside, compared with conventional formulations (116). Only an increase of their residence vascular time was noticed, especially for the mannose-liposomes.

The choline transporter consists of an anionic binding area which interacts with positively charged quaternary ammonium groups or simple cations (117). It plays a major role in the brain uptake of choline, acting as a precursor for the neurotransmitter acetylcholine and as an essential component of membrane phospholipids (phosphatidylcholine) (118). Moreover, the choline transporter interacts also with other quaternary ammoniums such as carnitine (119) and thiamine (120). No saturation of this carrier has been observed under physiological concentration, allowing the transport of other components without affecting the choline delivery to the brain (118). Besides, the concentration of choline containing components is increased in brain tumors (121), suggesting a high choline transport activity in cerebral cancerous cells. Ionically charged nanoparticles prepared from maltodextrin were surrounded with 1,2-dipalmitoyl-*sn*-glycero-3-phosphatidylcholine (DMPC). The coated nanoparticles were able to cross an *in-vitro* model of BBB (bovine brain capillary endothelial cells). Their passage through the endothelial cell monolayer was 3- or 4- fold higher than uncoated nanoparticles, without modification of the paracellular permeability, suggesting the effect of the BBB choline transporter (122). However, the lipophilic feature of DMPC may also explain the BBB crossing. In the same way, solid nanoparticles produced from microemulsion by emulsifying wax and Brij 78, were coated with thiamine (thiamine-PEG-DSPE) using a" post-insertion" procedure. The brain uptake transfer coefficient (K_{in}) of thiamine-nanoparticles was significantly greater than untargeted nanoparticles during the 45 to 120 s rat brain perfusion timeframe. In addition, the presence of free thiamine (50µM) into

the perfusion fluid did not induce a decrease of the brain distribution. These studies showed that thiamine did not induce a BBB penetration via the thiamine transporter but an interaction between the thiamine ligand and the thiamine BBB transporter. This association may improve the passive brain permeation, by increasing the concentration gradient. However, biodistribution of thiamine-nanoparticles has revealed no significant improvement of the brain radioactivity level at 2 hrs and 6 hrs postinjection, in comparison with conventional formulations (123).

These studies using the CMT systems as brain vector, showed contrasted results. Due to the endogenous feature of ligands, we could suppose interactions with the host biological environment such as erythrocytes and competition with the plasmatic nutrients, limiting thus their potential for the drug delivery to the brain tumors.

3.2 Nanocarriers conjugated to ligands implied in RME systems

RME systems require the binding of a ligand to a specific receptor located on the luminal membrane of the BBB. The receptor-ligand binding induces the internalization of receptor-ligand complexes within an endocytic vesicle. Four main intracellular mechanisms can occur: (124):

- Receptors leave ligands that are then degraded by the lysosomes and come back on the cell membrane.
- Simultaneous degradation of ligands and receptors after fusion with lysosomes.
- Receptors and ligands can be recycled after internalization (retroendocytosis).
- Receptors bound to ligands migrate within the cells to reach an other domain of the plasma membrane (transcytosis).

RME systems used in drug delivery to the brain are based both on endogenous and chimeric ligands.

3.2.1 Endogenous ligands

For many years, endogenous serum/blood ligands such as insulin and Tf, have been a major focus of research in dug delivery to the brain (125). FA represents also a promising site-specific ligand for brain targeting. The main advantage of these endogenous ligands is their high affinity for both brain and tumoral cells. Moreover, they are biocompatible and non-immunogenic (124).

In vitro and *in vivo* studies have shown the presence of a high concentration of insulin receptors on the animal (126, 127) and human cerebral capillaries (32). Duffy *et al.* (128) have demonstrated by autoradiography the transcytosis of the insulin through the BBB after injection into the carotid artery of one-month old rabbits. Furthermore, a high binding of insulin on brain tumors has been noticed (129). Hence, insulin seemed to be an interesting candidate to target drug-loaded nanoparticles to brain tumors. However, this peptidic hormone has a short systemic half-life and cause hypoglycemia at high concentrations. This side effect would be limited by substituting insulin by IGF which can be administered in a much higher concentration before hypoglycemia occurs. As in the case of insulin, IGF-I and IGF-II were shown to be endocytosed in isolated brain endothelium and crossed the BBB (130). Moreover, they are highly expressed by human cerebral tumors and their expression level increases with the tumor grade (glioblastoma multiforme, anaplastic astrocytoma, etc..) (131). However, their important interaction with serum IGF-binding proteins (IGFBPs) (132, 133) can limit their targeting properties. Studies concerning the grafting of insulin to the external surface of phosphatidylcholine liposomes have been performed twenty five years ago

(134). The coupling yield of hormone was evaluated as a function of the temperature and the lipid composition. A weak anchoring of insulin was observed in a distinct temperature range depending on the phospholipid type. Moreover, it has been reported that the cholesterol presence decreases the amount of peptides bound to small unilamellar vesicles. The incorporation of a glycosphingolipid, the sulfatide, within the lipid membrane improved the preferential interaction with insulin. After coupling, fusion and aggregation of liposomes was noticed via hydrophobic/hydrophilic interactions (135). Thus, the use of insulin as a transporter molecule set various problems due both to its biological activity and its intrinsic physico-chemical properties. Nevertheless, many scientific studies have exploited the interesting properties of insulin receptor for brain targeting because of the high density of receptors on the cerebral microvessels and the transcytosis triggered through these receptors . This matter will be discussed later.

Tf is a monomeric glycoprotein that can transport one (monoferric Tf) or two (diferric Tf) iron atoms (136). The TfR is overexpressed on the brain capillary endothelium (137) and at the surface of proliferating cells such as the brain tumor cells, especially the GBMs (138). In contrast, a low level of TfR is observed on the other healthy tissue. However, the TfR can be saturated under physiologic conditions due to a high endogenous plasma concentration of Tf (139). The receptor-mediated transcytosis of this peptide through the rat and human BBB have been also demonstrated (33, 140, 141). However, some scientists did not agree with these findings. Indeed, the study of the cerebral uptake of complex ^{59}Fe-[^{125}I]Tf showed the retroendocytosis of [^{125}I]-Tf after dissociation of the iron from the peptide in endosomal compartments (142-144). Only the ^{59}Fe was transcytosed to reach the cerebral parenchyma. These two mechanisms are still discussed. The interesting properties of Tf have been exploited for the delivery of various drugs to the brain. Tf coupled to pegylated

liposomes have been extensively developed for many years. Pharmacokinetic analysis have revealed a significant increase of the brain uptake for small Tf-PEG-liposomes (80 nm) in comparison with PEG-liposomes (145). Nevertheless, the brain targeting efficiency was not improved for large pegylated liposomes (140-180 nm) coupled to Tf. The internalization mechanism of Tf-PEG-liposomes/TfR complex in clathrin-coated pits through receptor-mediated endocytosis can explain this size-dependent efficiency (146). Furthermore, no immunogenicity increase was observed after coupling of Tf molecules on the pegylated liposome surface due to its endogenous feature (147). Anticancer agents were packaged within liposomal systems. Doxorubicin, an antineoplastic agent used against a wide range of human cancers, has been encapsulated within liposomes coupled to Tf (148). *In vitro* studies have revealed a 4-fold increase of pegylated Tf-liposome uptake by glioma cells in comparison with non-targeted liposomes. It has been also reported that the PEG chains incorporation on the liposome surface decrease significantly the doxorubicin uptake by the C6 glioma. Indeed, the steric barrier generated by the PEG can limit the binding of liposomes on the cell membrane and as a consequence decrease its internalization. Tf-liposomes used for the brain delivery of the antimetabolic drug 5-fluorouracile (5-FU) has also been investigated (149). The *in vivo* experiments have revealed that their accumulation within BCECs were 13-fold higher than that of the non-modified liposomes suggesting a likely enhanced brain uptake of 5-FU. Plasmid DNA (pDNA) has been packaged in pegylated Tf-polycyanoacrylate nanoparticles and the specific binding of this system to cells overexpressing TfR has been checked (150). Tf-polymeric micelles composed of a hydrophilic PEG shell have been also developed (151). The cytotoxicity against cancer cells of doxorubicin packaged within this targeted micellar system was significantly improved. Hence, Tf-nanocarriers seem to be an interesting carrier to deliver both drugs and genes to the brain.

Folates such as the folic acid (FA) and the 5'methyltetrahydrofolic acid (MTFA) are transported across the cell membranes by at least three mechanisms: the reduced folate carrier (RFC), the folate receptor (FR) and the folic acid export pump (152). The FR is expressed in a limited number of normal tissues like the thyroid, kidney, at the choroid plexus (153) and at the BBB (154). It has been identified as a tumor marker due its overexpression in a large number of tumors such as the ovarian carcinomas and the brain tumors (155). In addition, immediately after binding with its ligand, the FR is internalized in an early endosome and after a conformational change at acidic pH, the folate molecule is released (156). Studies performed by Wu *et. al* (154) suggested that the FR expressed at the BBB mediates the transport of MTFA and folic acid through the BBB. Folate-conjugated nanocarriers have been exploited to target selectively the cells expressing the FR. *In vitro* experiments have shown an enhanced uptake of doxorubicin-loaded FA-liposomes into C6 glioma. The amount of doxorubicin internalized into these tumoral cells was sufficient to limit the growth of cells (157). Furthermore, this preferential binding of FA-PEG-liposomes was observed through *in vitro* and *in vivo* experiments for cancer cells expressing a high level of FR such as murin lung carcinoma, human epidermal carcinoma and lymphoma (158-160). Folate-coupled copolymeric micelles were sharply used for the tumor-specific drug delivery (161). Doxorubicin-loaded FA-PEG-PLGA micelles have shown a significant accumulation of drug into the tumor tissue in mice (162). Paclitaxel-loaded PCL/MPEG micelles decorated with FA exhibited a higher cytotoxic effect against cancer cells such as MCF-7 and HeLa cell than non-targeted PCL/MPEG micelles (163). Folate targeting was also developed from PEG poly(cyanoacrylate) nanoparticles (164). A specific binding of the FA-PEG-nanoparticles to the soluble form of the FR so-called the folate-binding protein (FBP) has then been observed suggesting a potential interest of this system to target cell membranes expressing FR. Paclitaxel-loaded SLN composed of distearoylphosphatidylcholine

(DSPC)/triolein/cholesterol oleate/ PEG-cholesterol (40/40/18/2) have been also conjugated to FA (165). The toxicity effect of targeted lipid nanoparticles was enhanced only against tumoral cells overexpressing FR. Due to its ability to bind both to BCECs and tumoral cells, the colloidal carrier directed against FR should show interesting properties for drug transport to the brain tumors.

Hence, the conjugation of endogenous biomolecules on the nanocarrier surface represents an interesting tool to deliver drugs to cerebral tumors. Nevertheless, these components have a biological activity and as a consequence can interact with the host biological environment. A second approach for the active targeting of brain is the use of chimeric ligands such as the peptidomimetic MAbs involved in the RME systems.

3.2.2 Peptidomimetic MAbs

The peptidomimetic MAbs bind to an extracellular domain on the receptors, distinct from the endogenous ligand binding sites and consequently do not interfere with them. The first MAbs able to bind to specific tumors antigens have been developed in 1975 (166) but their interest in the cancer therapy field has only been exploited 20 years after. The OX26 murine MAb directed against the rat transferrin is one of chimeric peptides the most used for the drug targeting strategy. *In vivo* studies have demonstrated that this MAb passes through the BBB via a receptor-mediated transcytosis mechanism (41, 167). However, one scientific work was not consistent with this hypothesis. Indeed, Moos *et al.* (168) have shown that the OX26 accumulation in the pos-capillary compartment of BCECs was not sufficient to justify the transcytosis phenomenon. Despite these contradictions, the development of drug delivery systems using OX26 MAb has been sharply investigated. MAb-conjugated liposomes so-called immunoliposomes have shown a promising interest in the delivery of anticancer agents

to brain. Huwyler *et al.* (169) have worked on the *in vivo* evaluation of daunomycine-loaded immunoliposomes in rats. Pegylated 100-nm liposomes carrying more than 10 000 drug molecules were conjugated to OX26 MAbs. The brain delivery efficiency depended on the antibody density and was considered as optimal for a number of 29 OX26 per liposome (170). This density value was consistent with the studies of Maruyama *et al.* (171) who considered that the coupling of more than 34 MAbs per 110 nm-liposome does not increase the coupling efficiency on pulmonary endothelial cells. The $OX26_{29}$-immunoliposomes improved significantly the brain tissue distribution of daunomycine over 24 hrs in comparison with non-targeted pegylated liposomes. This pharmacokinetic behavior was changed after injection of 1 mg of pure OX26 MAb suggesting the specific targeting of the liposomal system. Moreover, the steric barrier conferred by the PEG on the particle surface decreased significantly the affinity of immunoliposomes for other organs such as the heart, the lung, the kidney, the liver and the spleen (169). Besides, an enhanced brain accumulation of daunomycine packaged within biotinylated immunoliposomes was also noticed suggesting the passing through the BBB by a receptor-mediated transcytosis (172). The transcytosis mechanism has been demonstrated by Cerletti *et al.* (173) using a BBB *in vitro* model composed of immortalized RBE4 rat BCECs and by *in vivo* experiments in rats. The crossing of the RBE4 cell monolayer by the OX26-conjugated liposomes was observed and characterized by a permeability coefficient (P_{app}) of about 1.6×10^{-5} ml/s. Moreover, after *in situ* perfusion in rats, OX26-immunoliposomes detected by scintillation counting were located in the postvascular compartment of the brain confirming the *in vitro* results. Nevertheless, these studies were not in agreement with the findings of Gosk *et al. (174)* who showed through immunohistochemical proofs, the inability of this liposomal system to reach the cerebral parenchyma.

OX26-immunoliposomes have been also employed for the controlled gene delivery to the brain. 6- to 7-kb expression plasmid encoding luciferase and beta-galactosidase have been packaged within these colloidal systems (175). The expression of luciferase genes in brain determined by a luminometer reached a maximal value 48 h after the intravenous injection in rats. The beta-galactosidase histochemistry revealed a high level of gene expression within the cerebral tissue such as the hippocampus and the thalamus. Besides, the weekly intravenous administration of OX26-immunoliposomes used for gene therapy did not involve inflammation within the target organs (176).

Moreover, immunoliposomes decorated with two different antibodies have been also developed by Zhang *et al.* (177) for gene therapy of brain cancers. The rat 8D3 MAb to the mouse TfR and the mouse 83-14 MAb to the human insulin receptor have been conjugated to 85 nm-pegylated immunoliposomes. The 8D3 MAb allowed the crossing of the BBB or of the tumor microvascular barrier by a transcytosis mechanism. The 83-14 MAb induced the receptor-mediated endocytosis of liposomal system into tumoral cells and the intracellular transport through the nuclear membrane (178). 8D3/83-14 MAb immunoliposomes carrying a plasmid DNA encoding the epidermal growth factor receptor (EGFR) antisense mRNA was intravenously injected in mice bearing the U87 brain tumors. The mRNA encapsulated induced a 79% reduction of immunoreactive EGFR protein (179). A 100% increase in survival was observed for the group treated by the plasmid mRNA-loaded immunoliposomes in comparison with the saline control and the luciferase gene therapy group. Hence, this survival study demonstrated the ability of immunoliposomes to deliver genes within brain tumoral cells. Besides, the coupling of two different antibodies on the liposome surface have been also used to target cell surface receptors on endothelium (180). The anti-transferrin OKT9 MAb allowing the internalization of the complex and the anti-E-selectin 1.2B6 MAb targeting the E-selectin, early marker of activated endothelium, have been also conjugated to

liposomes for the gene transfer. However, the presence of antibodies on the nanocarrier surface confers it immunogenic properties characterized by an increase of the plasma clearance. The recognition of the antibody Fc portion by the macrophages could mainly explain this rapid uptake by the RES (181). In this context, antibody fragments (Fab' and $F(ab')_2$) instead of the whole antibody, have been coupled to pegylated liposomes. This strategy has been developed in order to reduce the RES uptake via the Fc receptor-mediated mechanism. In this way, the fragment conjugation did not affect the long-circulating properties of pegylated liposomes. Unlike IgG-PEG-immunoliposomes, the same blood residence and the same level of liver uptake were obtained for both PEG-liposomes and Fab'-PEG immunoliposomes injected intravenously in mice (182). Moreover, the antibody fragments did not change the ability of immunoliposomes to bind to target cells.

Some immunoliposomes used for the cancer therapy have been transferred in Phase I clinical trials. The targeted liposomal system so-called the MCC-465 carrying doxorubicin was conjugated to $F(ab')_2$ fragments of GAH MAb (183). This biomolecule recognized various cancer cells such as gastric, colorectal, and mammary cancer tissues but negatively reacted with normal tissues (184). They have been administered in patients with metastatic or recurrent stomach cancers. This study illustrates the potential clinical application of immunoliposomes.

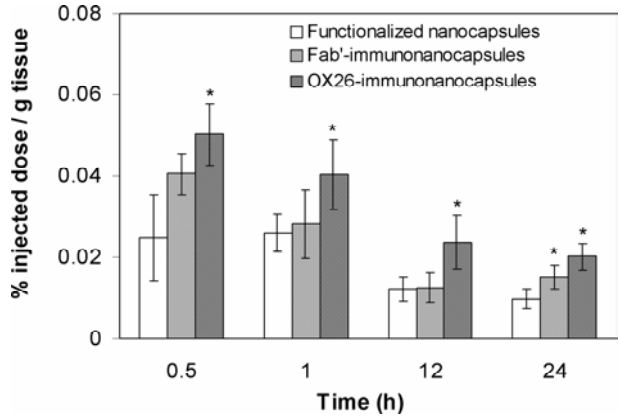

Figure 2. Brain targeting of ^{188}Re-functionalized nanocapsules and ^{188}Re-immunonanocapsules. Between 1.1 and 1.4 mg of ^{188}Re-LNC (≤ 5 µCi) was intravenously injected in the rat and the concentration of radioactivity in brain (% injected dose / g tissue) was determined at different times. Values represent means ± SEM (n = 5). * Statistical significance differences to pegylated nanocapsules (Mann-Whitney), $p<0.05$.

The strategy of active targeting using micelles, nanoparticles and nanocapsules conjugated to MAb have been developed later in comparison with immunoliposomes. Only a few studies concerning the design, the *in vitro* and *in vivo* evaluations of these targeted nanocarriers have been reported in literature. Micelles modified with fatty acid-conjugated Fab fragments of antibodies to antigens of brain glial cells (acid gliofibrillar antigen and α2-glycoprotein) were prepared to target the cerebral tissue (185). An increased activity of the trifluoperazine encapsulated into the nanocarrier was observed, suggesting the capacity of immunomicelles to reach the brain. Antibodies to α2 glycoprotein conjugated to Pluronic® micelles have also shown an improvement of the brain distribution of haloperidol (186). These micellar vectors may be used to deliver other drug types than neuroleptic agents such as anticancer agents. Moreover, cytotoxic effect of paclitaxel-loaded micelles coupled to tumor-specific monoclonal antibodies (MAb 2C5) was significantly improved in comparison with non-targeted micelles (187). LNC decorated with OX26 MAb or OX26 MAb Fab' fragments have

been very recently developed (manuscript in preparation). Densities comprised between 16 and 183 whole antibodies and between 42 and 173 Fab' fragments per LNC were obtained by monitoring their initial amount in the coupling reaction mixture. Their specific association to brain capillary endothelial cells has been demonstrated. 24hrs after their intravenous administration in rat, the brain accumulation of OX26-immunonanocapsules and Fab'-immunonanocapsules were 2 and 1.5 - fold higher than non-targeted LNC (Figure 2). Despite a prolonged vascular residence time of Fab'-immunonanocapsules, their brain association was lower than for OX26-immunonanocapsules. This result was explained by the Fc part, playing the role of a spacer between the LNC surface and the antigen binding sites**,** and thus promoting the recognition of target cells. Besides, chitosan-PEG nanoparticles conjugated to OX26 MAb were also synthesized (188) using the following copolymers: chitosan-PEG and chitosan-PEG-biotin. The colloidal system was administered intravenously in mice and the brain uptake was observed by fluorescent and electronic microscopies. A great number of OX26-immunonanoparticles were located in the brain tissue suggesting the crossing of the BBB by receptor-mediated transcytosis. OX26 has been also attached both on pegylated PLA nanoparticles and pegylated lipidic nanocapsules. Concerning the polymeric immunonanoparticles composed of $MPEG_{3500}$-PLA_{40000} and maleimide-PEG_{3500}-PLA_{40000}, between 60 and 76 antibodies were grafted (189). Besides, the lipidic pegylated immunonanocapsules were characterized by an antibody density comprised between 13 and 158. The immunospecific targeting of this lipidic nanovector has been shown on cells overexpressing TfR such as the BCECs and Y3.AG.1.2.3. cells. Furthermore, cationic SLN have been also developed for the targeted gene delivery (190). Indeed, DNA-coated SLN was bound to streptavidin by electrostatic interaction allowing the attachment of site-specific biotinylated ligands

3.3 Nanocarriers conjugated to ligands implied in AME systems

AME systems are triggered by an electrostatic interaction between a positively charged moiety of a peptide and the negatively charged plasma membrane. Anionic sites have been located on the luminal surface of brain capillaries due to the sialic acid residues of glycoproteins (191). The active targeting of drug using AME systems have been originally proposed for cationized albumin (192, 193). Cationization using hexamethylenediamine was a chemical modification of the protein leading to the conversion of carboxylic acids into extended primary amino groups . The adsorptive-mediated endocytosis of cationized albumin has been evaluated in isolated brain capillaries and in rat brain after carotid injection technique (193). An enhanced uptake of the positively charged albumin by brain capillaries has been noticed in comparison with native protein. *In vivo* studies in rats about the cationized albumin transport through the BBB have also been investigated using a carotid arterial infusion technique and a capillary depletion method (194). About 15 % of the cationized protein detected in the whole brain was located into the post-capillary extracellular space suggesting an adsorptive-mediated endocytosis. The pharmacokinetic behavior of cationized rat serum albumin intravenously injected in animals has also been characterized (35). Cationization improved the accumulation of the protein in brain tissues but its half-life decreased significantly from 4.8 h to 2.5 h in comparison with native rat serum albumin. The plasma-clearance was dependent on the degree of cationization. Isoelectric point (p*I*) values above 10 involved a very rapid clearance from the bloodstream of the cationized bovin serum albumin (CBSA) with a half-life time of about 1 minute (31). Besides, the cationized *heterologous* proteins have more immunogenic properties than the *homologou*s proteins (195). Moreover, adsorptive-mediated transcytosis or endocytosis of cationized albumin did

not occur exclusively in brain but also in kidneys, liver and less actively in lungs and myocardium (196).

At the beginning, the cationized proteins were investigated for the delivery of peptides into the brain. Pardridge *et. al* demonstrated that the beta-endorphin, a non-transportable chimeric peptide, covalently coupled to cationized albumin was able to reach the cerebral parenchyma (40). More recently, CBSA was conjugated to pegylated liposomes. These liposomal systems were taken up when in contact with isolated BCECs and a monolayer of porcine BCECs whereas no interaction was noticed between BSA-liposomes and endothelial cells (197). The cellular uptake of CBSA-liposomes has been demonstrated as an adsorptive-mediated endocytosis mechanism. CBSA coupled to polymeric nanoparticles have been also prepared for the drug delivery to the brain (198). 100 nm-nanocarriers were synthesized using the emulsion/solvent evaporation technique from MPEG-PLA and maleimide-PEG-PLA copolymers. The BSA was mildly cationized (P*I* = 8-9) in order to have optimal pharmacokinetic properties: a long serum half-life and a great degree of selectivity to brain as previously discussed. The uptake of CBSA-nanocarriers into isolated BCECs was significantly improved but a cytotoxic effect on these cells was noticed for concentrations above 1 mg/ml. 30 minutes after intravenous injection in mice, fluorescent CBSA-nanoparticles were localized by microscopy in the periventricular region of the third ventricle. In contrast, the amount of nanoparticles bearing BSA in the cerebral parenchyma was not significant. These results showed the ability of CBSA-nanoparticles to pass through the BBB to reach the cerebral parenchyma by an adsorptive-mediated transcytosis. The transport mechanism of CBSA-nanoparticles was studied using an *in vitro* BBB model composed both of BCECs and astrocytes isolated from newborn rats (199). The transport of CBSA-nanoparticles across the coculture was observed and was characterized by an apparent permeability value about 7.8 fold higher than that of BSA-nanocarriers. This transport was

inhibited by competition with an excess of free CBSA. Hence, considering that the nanocarrier amount added to the luminal compartment (0.2 mg/ml) did not impact the BBB integrity, the authors concluded that the adsorptive-mediated transcytosis was implied in the CBSA-nanoparticles transport through the BBB.

A few examples of nanovectors used for the active targeting of brain tumors was indexed in Table I.

Table I. Nanocarriers targeting both the BBB and the brain tumors

Nanocarrier	Targeting system	Ligand	Drug	Study type	Relevant results	Ref
Pegylated liposome	TfR	Tf	5-FU	*In vivo*	Accumulation into BCECs	(149)
Pegylated liposome	FR	FA	Doxorubicin	*In vitro*	Enhanced uptake into C6 glioma cells	(157)
Pegylated liposome	TfR	OX26 MAb	Daunomycine	*In vivo*	Enhanced delivery of daunomycine into brain tissue	(169, 247)
PEG-PLA nanoparticle	Anionic sites	CBSA	/	*In vivo*	Localization of nanoparticles in the lateral ventricle, third ventricle and periventricular region	(198, 199)
PEG-chitosan nanoparticle	TfR	OX26 MAb	/	*In vivo*	Enhanced brain uptake	(188)
SLN	Thiamine transporter	Thiamine	/	*In vivo*	Association with BBB and improvement of the passive brain permeation	(123)
LNC	TfR	OX26 MAb and Fab' fragment of OX26 MAb	/	*In vivo*	Enhanced brain uptake	

3.4 Coating of nanocarriers

Coating of nanoparticles using hydrophilic surfactants have shown a promising effect for the delivery of drugs to the brain (200). Their targeted effect depended on the surfactant nature (e.g., chemical structure, physical-chemical and biochemical parameters). Only a few polysorbates (20, 40, 60 or 80) and not polysorbates 81 and 85 which are more hydrophobic, neither poloxamers (184, 188, 388, 407 or 908), nor Cremophor® (EL or RM40) interact with brain endothelium (200). Numerous explanations have been reported to understand the coating influence on the drug transport to the brain. One of them concerned the adsorption of plasma proteins such as the apolipoproteins (APO) on the surface of coated nanoparticles after intravenous administration. Indeed, Lück *et al.* (201) observed the APO E adsorption on the surface of nanoparticles coated with polysorbate 20, 40, 60 and 80 after a 5 min-incubation in human citrate-stabilized plasma at 37°C. In contrast, nanoparticles recovered by the poloxamers and Cremophor® previously mentioned, did not interact with APO E. This apolipoprotein is implied in the transport of low density lipoprotein (LDL) into the brain. LDL characterized by a size varying between 18 and 25 nm carry fatty acid molecules which are essential for the CNS. A high level of LDL receptors implied in RME systems was expressed on the BCECs (202, 203). Moreover, *in vitro* transcytosis of LDL through the BBB was observed by Dehouck *et. al* (204). This mechanism was fully inhibited by the C7 monoclonal antibody interacting with the LDL receptor. Hence, the nanocarriers coated with polysorbate may mimic the LDL after APO E adsorption. Moreover, this protein is expressed at a high level in brain tumors such as astrocytomas and glioblastomas (205).

The coating using polysorbates has been applied to numerous nanocarriers for the drug delivery to the brain. The effect of nanoparticles made of PBCA coated with polysorbates such as polysorbate 80 have been sharply investigated since 1995 (206). Polysorbate 80-

coated PBCA nanoparticles were taken up into human and bovine endothelial cells more rapidly and in an amount 20-fold higher than with conventional nanocarriers (207). Various drugs have been transported successfully into the brain including dalargin (207), kytorphin (208), loperamide (209), tubocurarine (210) and doxorubicin (211). The pharmacokinetic behavior of doxorubicin packaged within coated PBCA nanoparticles was significantly enhanced after intravenous injection in healthy rats. This formulation allowed a considerable accumulation of drug into the brain with a concentration reaching 6 µg/g, 2 hrs after systemic administration (211). In contrast, a weak drug level (< 0.1 µg/g) was present into the cerebral tissues with three other preparations including free doxorubicin, doxorubicin in a 1% polysorbate 80/saline solution and doxorubicin-loaded uncoated PBCA nanoparticles. Therapeutic potential of doxorubicin-loaded PBCA-nanoparticles coated with polysorbate 80 was evaluated for the treatment of glioblastoma intracranially implanted in rats (212, 213). Animals bearing 101/8 glioblastoma tumor were treated by three intravenous injections on Day 2, 5 and 8 of 1.5 or 2.5 mg/kg doxorubicin bound to polysorbate 80-coated PBCA nanoparticles. Antitumor efficiency based on the increase of the median survival time as compared to doxorubicin (IST_D) was improved with coated nanoparticles in comparison with uncoated nanocarriers with IST_D values of about 24 and 43 % for dosages of 3 × 1.5 and 3 × 2.5 mg/kg, respectively. For one group, the rats showed a long-term remission. These animals were sacrificed after six months and the histology revealed a slower tumor growth with lower tumors sizes. Besides, doxorubicin in a polysorbate 80 solution showed also a slight effect with IST_D comprised between 7.5 and 10 %.

Thus, all these studies demonstrated the therapeutic potential of PBCA nanoparticles coated with polysorbate 80 and their ability to deliver drug into the brain. However, a recent biodistribution study performed in glioma-bearing rats questioned the interest of polysorbate 80 on the drug delivery to the brain (214). Indeed, no difference of pharmacokinetic behaviors

between uncoated PBCA nanoparticles and doxorubicin-loaded polysorbate 80-coated PBCA nanoparticles were observed. Moreover, the unloaded nanocarriers coated with polysorbate 80 showed a significant improvement of PBCA nanocarriers accumulation into glioma and a reduction of their concentration in RES organs including liver and spleen. These surprising results may be due to the positive charges of the doxorubicin which prevent the plasma component adsorption from playing a major role in the brain targeting. Besides, another scientific work has shown that the PEG-polyhexadecylcyanoacrylate (PHDCA) nanoparticles injected intravenously was detected in a significant amount into the mouse and the rat brains whereas this accumulation was not observed for polysorbate 80 coated PHDCA nanoparticles (215). In this context, other reasons that the interaction between APO E and polysorbate 80 could explain the transport of drug to the CNS. A work of Olivier *et al.* (216) suggested that the mechanism involved in the crossing of the BBB was not due to the interaction between polysorbate 80 and APO E as previously mentioned but to toxic effects of coated nanocarriers. Various scientific results supported this hypothesis. Firstly, BBB permeability studies were evaluated using an *in vitro* BBB model composed of a coculture of bovine BCECs and rat astrocytes. For concentrations of 10 µg/ml and above, coated and uncoated nanoparticles generated a progressive disruption of the tight junctions. Secondly, for a long time, BBB impairment was noticed after intravenous injection of polysorbate 80 at a dose about 3 mg/kg (217). These amounts were used in some *in vivo* experiments previously described (211). Lastly, it has been reported that the polysorbate 80 coating led to a desorption of the drug located on the nanoparticle surface. Thus, in the case of dalargin, the polysorbate 80-coated dalargin-loaded nanoparticle formulation corresponded in fact to a mixture of dalargin, nanoparticles and polysorbate 80. Thus, Olivier *et al.* (216) supposed that a synergistic effect on the BBB permeabilization was induced by the combined toxicity of PBCA nanoparticles and polysorbate 80. According to the authors, only a disruption of the

BBB due to coated nanocarriers allowed the penetration of drug into the cerebral parenchyma and no specific targeting and transcytosis mechanism were involved. Nevertheless, this hypothesis was disproved by Kreuter *et al.* through *in vitro* and *in vivo* studies (218). Indeed, no modification of the BBB integrity was observed after addition of PBCA nanoparticles and polysorbate 80 (10 and 20 µg/ml) in a coculture of bovine BCECs and rat astrocytes. Moreover, free dalargin injected in mice immediately with empty polysorbate 80-coated PBCA nanoparticles or after 5 and 30 minutes did not penetrate into the brain. These results suggested that the delivery of drug to the CNS can not be only explained by the opening of tight junctions of the BBB due to the combined effect of the surfactants and the nanoparticles. Nevertheless, the biocompatible properties of polymers used being not well demonstrated, we could suppose that they can interact with the host biological environment.

The coating by a hydrophilic surfactant was applied to more biocompatible nanocarriers such as lipidic colloidal systems for the drug delivery to the brain. SLN surface was recovered by various hydrophilic surfactants (219, 220). Polysorbate-coated on SLN showed a specific adsorption of plasma proteins interacting with brain such as APO E and hence, by referring to previous works on PBCA nanoparticles, suggested a potential interest for the brain targeting. Polysorbate 80-coated atovaquone-loaded SLN were used for the treatment of the toxoplasmic encephalitis (TE) (221). A promising therapeutic effect was obtained in infected mice after intravenous administration. The role of polysorbate 80 on the brain targeting of PLA nanoparticles was also investigated (222). The coated nanocarriers so-called model nanoparticles (MNPs) were labeled with FITC-dextran and injected in healthy mice. Fluorescence microscopy showed the presence of MNPs into brain tissue. In contrast, a simple mixture of PLA nanoparticles, polysorbate 80 and dextran-FITC in saline revealed no fluorescence intensity into the brain. Recently, nanoparticles were prepared using a novel PLA-polysorbate 80 copolymer with 8.5 % and 15.3 % polysorbate 80 ratio (223).

Thus, coating of nanocarriers with polysorbate 80 have shown a promising interest for the delivery of drugs to the brain. In fact, this approach corresponded to an indirect conjugation of site-specific ligand implied in RME systems. Indeed, after intravenous injection, the APO E located in the plasma was adsorbed on the surfactant coating and was involved in the receptor-mediation of drug transport. In this context, novel targeted nanocarriers were developed by covalent linkage of APO E and APO E-derived peptides on albumin nanoparticles (224) and liposomes (225), respectively. Furthermore, dipalmitoylated APO E-derived peptides characterized by a high lipid affinity were anchored on liposomes (226). These novel systems were taken up within BCECs and the transport of loperamide into the brain was significantly improved with APO E conjugated to albumin nanoparticles.

3.5 Coupling of ligands

3.5.1 Covalent coupling

The coupling strategies first described 25 years ago, are most frequently used to attach covalently proteins including MAbs and peptides, to nanocarriers. To allow the conjugation, pegylated liposomes were functionalized using a bifunctionnal PEG containing a hydrophobic lipid anchor at one end and a crosslinker at the other one. The crosslinker could be amine reactive such as the *N*-hydroxysuccinimide group (NHS) derivatives or thiol reactive such as the maleimide and pyridyldithiopropionylamine (PDP) derivatives (227). The lipid part was often phospholipids such as the DSPE (170) and dipalmitoyphosphatidylethanolamine (DPPE) (182). The bifunctionnal PEG were introduced either by pre-insertion procedure or by post-insertion into preformed liposomes (51) or LNC (REF). In order to functionalize the surface of PLA nanoparticles, amine and sulfhydryl reactive end-groups have been conjugated

to PEG-PLA copolymers leading to the synthesis of PEG-PLA-NHS (228), PEG-PLA-aldehyde (229) and PEG-PLA-maleimide (189).

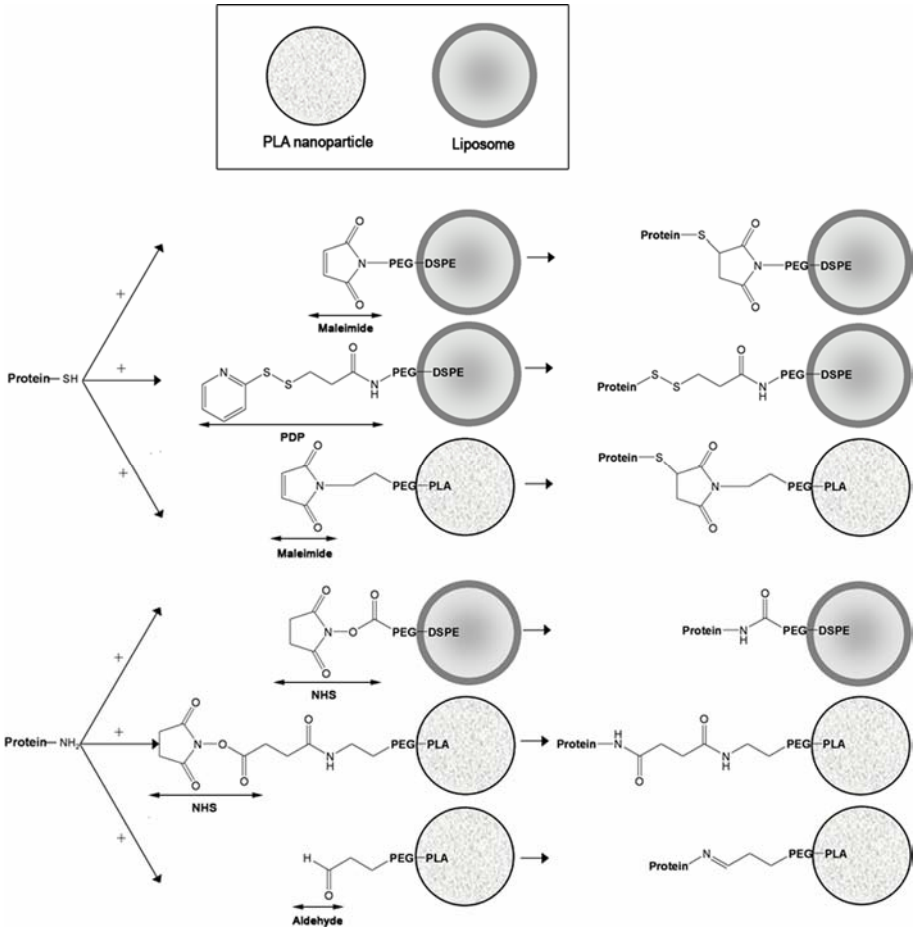

Figure 3. Various coupling strategies of proteins to liposomes and PLA nanoparticles. The covalent linkage was performed via the primary amine groups or via the sulfhydryl function located on the native ligand or previously inserted in its structure.

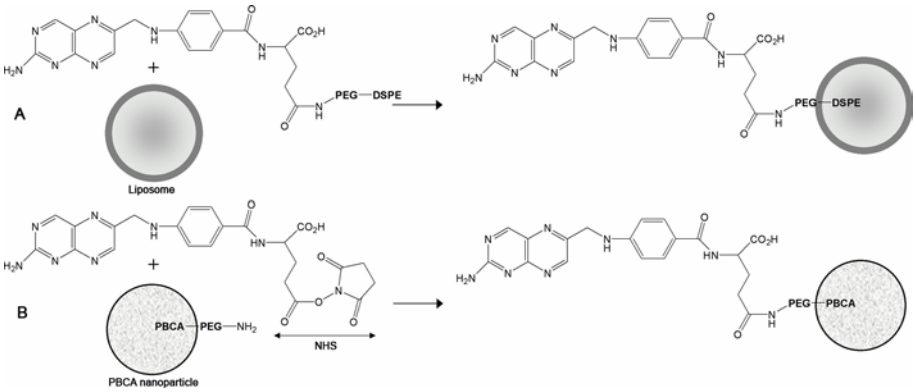

Figure 4. Covalent coupling of folic acid to liposomes and PBCA nanoparticles. (A) Incorporation of folate-PEG-DSPE in liposomes by the post-insertion procedure. (B) Conjugation of folate - NHS by reaction with the primary amine group located on the surface of the PBCA nanoparticles.

Functionalized nanocarriers were then covalently coupled to proteins via their primary amine or their sulfhydryl groups (figure 3). The amine groups are located on the side chain of some amino acids such as lysine, arginine, glutamine residues and at the amine terminus. Sulfhydryls are available in cysteine residues, in the hinge region of Fab' fragments or could be inserted in the protein structure through different ways, via the primary amine groups or the carbohydrates. The following amine reactive crosslinkers, the *N*-succinimidyl-3(2-pyridyldithio)propionate (SPDP) (230) and the *N*-succinimidyl-2-mercapto-[S-acetyl]acetic acid (SATA) (231) have been sharply used for the protein thiolation. The reaction required two steps corresponding for the first one to the crosslinker conjugation and for the second one to the deprotection of the sulfhydryl groups. Besides, a reaction between 2-iminothiolane hydrochloride so-called Traut's Reagent and amine groups represented an alternative to SATA and SPDP and required only one step (232). However, these procedures using primary amines involved sometimes partial or complete loss of recognition activity due to the

modification of the antigen binding sites (233). Moreover, during conjugation, the NHS-based reagents converted positively charged lysines to neutral groups leading to a probable loss of recognizing activity (234). In contrast, thiolation with the carbohydrates located within the Fc portion was supposed to preserve the antibody activity. Briefly, the sugar parts were oxidized using sodium meta periodate to convert vicinal hydroxyls to aldehydes or ketones. 3-(2-pyridyldithio) propionic acid hydrazide (PDPH) reacted then with aldehydes or ketones. Reduction of disulfide bonds was then performed with dithiotreitol (DTT) resulting in the formation of sulfhydryl groups (235).

Other strategies have been developed to conjugate site-directing biomolecules to the nanocarrier surface. PEG poly(cyanoacrylate) nanoparticles have been covalently coupled with folic acid by reaction between terminal amino groups located on the nanoparticle surface and the *N*-hydroxysuccinimide added by esterification on the folic acid (164) (figure 4A). Lipid-PEG-folate conjugates including cholesterol-PEG-folate (236), DPPE-PEG-folate (157) and DSPE-PEG-folate (237) were incorporated into SLN and liposomes (figure 4B). "Post-insertion" procedure was also used to conjugate thiamine (thiamine-PEG-DSPE) to SLN nanoparticles (123).

3.5.2 Non-covalent coupling

Methods using non-covalent linkage have been used to conjugate ligands to nanocarriers. Immunoliposomes have been prepared by interaction between protein A and the Fc portion of some IgG classes (238). However, this method was applied only to antibodies.

Linkage strategy using avidin-biotin technology was also used. The nature of the non-covalent binding between avidin and biotin was characterized by an extremely high affinity

with a K_D of about 10^{-15} M and a dissociation half-time of 89 days (239). The avidin which has four biotin binding sites could be substituted by its neutral form such as the streptavidin (SA) characterized by a lower clearance from plasma (240). Two approaches were developed to non-covalently conjugate ligands to nanocarriers using avidin/biotin strategy. The first one corresponded to the insertion of SA or avidin in the ligand structure (241). The avidin or SA were activated with N-maleimidobenzoyl-*N*-hydroxysuccinimide (MBS) and reacted then with sulfhydryl groups previously introduced on the protein leading to the formation of a thioether bond. In parallel, biotinylated nanocarriers were prepared. Lipid-PEG-biotin constructs such as DSPE-PEG-biotin were introduced into liposomes (172). Functionalized chitosan and PLA nanoparticles were produced using chitosan-PEG-biotin (188) and PLA-PEG-biotin (242), respectively. SA was also associated to cationic SLN via electrostatic interactions (190). Thereby, SA/avidin-conjugated ligands were directly coupled to biotinylated nanocarriers. The second approach concerned the ligand biotinylation. NHS-PEG-biotin was commonly used to insert biotin molecules on proteins bearing primary amine groups (243). The biotinylated nanocarriers previously described were incubated with avidin or SA and finally added with biotinylated ligands for the coupling.

4 Conclusion

Targeted nanocarriers represent a promising tool to deliver drugs and genes to cerebral tumors. Surface-modified nanocarriers were developed by direct conjugation of site-directing ligands or indirectly by coating of surfactants. This active targeting strategy initiated thirty years ago (244) has been significantly developed for 1990s after the developpement of stealth nanocarriers using gangliosides and PEG derivatives. Indeed, a low level of RES uptake allowed to increase the systemic residence time of nanocarriers and consequently, optimize the access to target cells. The various brain active targeting strategies which have been established, consisted in grafting on nanocarriers, a ligand recognizing an antigen overexpressed on BCECs. Endogenous and chimeric ligands including small molecular weight nutrients, proteins, peptides were conjugated directly to nanocarriers using a covalent or a non-covalent linkage. This approach has been sharply developed for liposomal systems. In contrast, a few works concerned polymeric micelles, polymeric and lipidic nanoparticle (123, 186, 188, 245). An indirect conjugation was also performed in coating the particle surface with a hydrophilic surfactant such as polysorbate 80, interacting with plasmatic proteins such as the APO E. Considering the various studies reported in this review, the conjugation of site-specific ligands to nanocarriers allowed usually to improve significantly the brain accumulation.

For the moment, only a few studies have demonstrated clearly the therapeutic effect of targeted nanocarriers in the treatment of cerebral tumors. Doxorubicin-loaded polysorbate 80-coated PBCA nanoparticles have shown promising results for the chemotherapy of rat glioblastoma (246). Non-viral gene therapy against human glial brain tumors implanted in mice, were also investigated with success using immunoliposomes conjugated to two different antibodies and carrying a plasmid DNA (177). Moreover, the mechanism of the nanocarrier-

mediated transport of drugs or genes across the BBB were not well-known or still discussed. For example, the opinions are not unanimous concerning the case of the TfR and its ability to mediate transcytosis. In the case where drug-loaded nanocarriers would reach the brain by a receptor-mediated transcytosis mechanism, it may access to cerebral tumors via the ligands which have also a high affinity for brain tumors.

These targeted colloidal systems must still be optimized in order to allow their transfer in clinical applications. The influence of some parameters such as the size, the polymer type, the hydrophilic / lipophilic nature of the particle surface and the surface charge, on the targeting efficiency and the cerebral uptake is not been well defined . Moreover, a detailed understanding of the internalization of particles into the BCECs and of the drug transport from the BBB to the brain tissue would be very helpful.

Acknowledgments

This work was supported by the "ARC" (Association pour la Recherche sur le Cancer) and by the departmental committee of Maine-et-Loire of "la Ligue contre le Cancer".

Bibliography

1. A. Behin, K. Hoang-Xuan, A. F. Carpentier, and J. Y. Delattre. Primary brain tumours in adults. *Lancet* **361**: 323-31 (2003).
2. S. Gururangan and H. S. Friedman. Innovations in design and delivery of chemotherapy for brain tumors. *Neuroimaging Clinics of North America* **12**: 583-597 (2002).
3. M. W. Brightman and T. S. Reese. Junctions between intimately apposed cell membranes in the vertebrate brain. *J Cell Biol* **40**: 648-77 (1969).
4. T. S. Reese and M. J. Karnovsky. Fine structural localization of a blood-brain barrier to exogenous peroxidase. *J Cell Biol* **34**: 207-17 (1967).
5. P. L. Golden and G. M. Pollack. Blood-brain barrier efflux transport. *J Pharm Sci* **92**: 1739-53 (2003).
6. W. M. Pardridge. BBB-Genomics: creating new openings for brain-drug targeting. *Drug Discovery Today* **6**: 381-383 (2001).
7. M. H. Abraham, H. S. Chadha, and R. C. Mitchell. Hydrogen bonding. 33. Factors that influence the distribution of solutes between blood and brain. *J Pharm Sci* **83**: 1257-68 (1994).
8. M. Wahl, L. Schilling, A. Unterberg, and A. Baethmann. Mediators of vascular and parenchymal mechanisms in secondary brain damage. *Acta Neurochirurgica, Supplement* **57**: 64-72 (1993).
9. J. Folkman. Angiogenesis in cancer, vascular, rheumatoid and other disease. *Nat Med* **1**: 27-31 (1995).
10. H. Wolburg, K. Wolburg-Buchholz, S. Liebner, and B. Engelhardt. Claudin-1, claudin-2 and claudin-11 are present in tight junctions of choroid plexus epithelium of the mouse. *Neurosci Lett* **307**: 77-80 (2001).
11. Y. Saito and E. M. Wright. Bicarbonate transport across the frog choroid plexus and its control by cyclic nucleotides. *J Physiol* **336**: 635-48 (1983).
12. G. D. Pappas and V. M. Tennyson. An electron microscopic study of the passage of colloidal particles from the blood vessels of the ciliary processes and choroid plexus of the rabbit. *J Cell Biol* **15**: 227-39 (1962).
13. W. M. Pardridge. Drug delivery to the brain. *J Cereb Blood Flow Metab* **17**: 713-31 (1997).
14. P. Menei, M. C. Venier, E. Gamelin, J. P. Saint-Andre, G. Hayek, E. Jadaud, D. Fournier, P. Mercier, G. Guy, and J. P. Benoit. Local and sustained delivery of 5-fluorouracil from biodegradable microspheres for the radiosensitization of glioblastoma: a pilot study. *Cancer* **86**: 325-30 (1999).
15. F. DiMeco, K. W. Li, B. M. Tyler, A. S. Wolf, H. Brem, and A. Olivi. Local delivery of mitoxantrone for the treatment of malignant brain tumors in rats. *J Neurosurg* **97**: 1173-8 (2002).
16. P. B. Storm, J. L. Moriarity, B. Tyler, P. C. Burger, H. Brem, and J. Weingart. Polymer delivery of camptothecin against 9L gliosarcoma: release, distribution, and efficacy. *J Neurooncol* **56**: 209-17 (2002).
17. M. S. Lesniak, U. Upadhyay, R. Goodwin, B. Tyler, and H. Brem. Local delivery of doxorubicin for the treatment of malignant brain tumors in rats. *Anticancer Res* **25**: 3825-31 (2005).
18. M. Westphal, Z. Ram, V. Riddle, D. Hilt, and E. Bortey. Gliadel wafer in initial surgery for malignant glioma: long-term follow-up of a multicenter controlled trial. *Acta Neurochir (Wien)* **148**: 269-75; discussion 275 (2006).

19. M. Westphal, D. C. Hilt, E. Bortey, P. Delavault, R. Olivares, P. C. Warnke, I. R. Whittle, J. Jaaskelainen, and Z. Ram. A phase 3 trial of local chemotherapy with biodegradable carmustine (BCNU) wafers (Gliadel wafers) in patients with primary malignant glioma. *Neuro-oncol* **5**: 79-88 (2003).
20. H. Brem, S. Piantadosi, P. C. Burger, M. Walker, R. Selker, N. A. Vick, K. Black, M. Sisti, S. Brem, G. Mohr, and et al. Placebo-controlled trial of safety and efficacy of intraoperative controlled delivery by biodegradable polymers of chemotherapy for recurrent gliomas. The Polymer-brain Tumor Treatment Group. *Lancet* **345**: 1008-12 (1995).
21. R. A. Ratcheson and A. K. Ommaya. Experience with the subcutaneous cerebrospinal-fluid reservoir. Preliminary report of 60 cases. *N Engl J Med* **279**: 1025-31 (1968).
22. W. M. Pardridge. Non-invasive drug delivery to the human brain using endogenous blood-brain barrier transport systems. *Pharm. Sci. Technol. Today* **2**: 49-59 (1999).
23. W. C. Cosolo, P. Martinello, W. J. Louis, and N. Christophidis. Blood-brain barrier disruption using mannitol: Time course and electron microscopy studies. *American Journal of Physiology - Regulatory Integrative and Comparative Physiology* **256**: (1989).
24. T. F. Cloughesy and K. L. Black. Pharmacological blood-brain barrier modification for selective drug delivery. *Journal of Neuro-Oncology* **26**: 125-132 (1995).
25. A. A. Sinkula and S. H. Yalkowsky. Rationale for design of biologically reversible drug derivatives: prodrugs. *J Pharm Sci* **64**: 181-210 (1975).
26. N. H. Greig, S. Genka, E. M. Daly, D. J. Sweeney, and S. I. Rapoport. Physicochemical and pharmacokinetic parameters of seven lipophilic chlorambucil esters designed for brain penetration. *Cancer Chemother Pharmacol* **25**: 311-9 (1990).
27. J. Rautio and P. J. Chikhale. Drug delivery systems for brain tumor therapy. *Current Pharmaceutical Design* **10**: 1341-1353 (2004).
28. D. D. Allen and W. J. Geldenhuys. Molecular modeling of blood-brain barrier nutrient transporters: In silico basis for evaluation of potential drug delivery to the central nervous system. *Life Sciences* **78**: 1029-1033 (2006).
29. A. Tsuji. Small molecular drug transfer across the blood-brain barrier via carrier-mediated transport systems. *NeuroRx* **2**: 54-62 (2005).
30. R. G. W. Anderson, M. S. Brown, and J. L. Golstein. Role of the coated endocytic vesicle in the uptake of receptor bound low density lipoprotein in human fibroblasts. *Cell* **10**: 351-364 (1977).
31. U. Bickel, T. Yoshikawa, and W. M. Pardridge. Delivery of peptides and proteins through the blood-brain barrier. *Advanced Drug Delivery Reviews* **46**: 247-279 (2001).
32. W. M. Pardridge, J. Eisenberg, and J. Yang. Human blood-brain barrier insulin receptor. *J Neurochem* **44**: 1771-8 (1985).
33. W. M. Pardridge, J. Eisenberg, and J. Yang. Human blood-brain barrier transferrin receptor. *Metabolism* **36**: 892-5 (1987).
34. D. Triguero, J. B. Buciak, J. Yang, and W. M. Pardridge. Blood-brain barrier transport of cationized immunoglobulin G: enhanced delivery compared to native protein. *Proc Natl Acad Sci U S A* **86**: 4761-5 (1989).
35. W. M. Pardridge, D. Triguero, J. Buciak, and J. Yang. Evaluation of cationized rat albumin as a potential blood-brain barrier drug transport vector. *J Pharmacol Exp Ther* **255**: 893-9 (1990).
36. E. M. Cornford, D. Young, J. W. Paxton, G. J. Finlay, W. R. Wilson, and W. M. Pardridge. Melphalan penetration of the blood-brain barrier via the neutral amino acid transporter in tumor-bearing brain. *Cancer Research* **52**: 138-143 (1992).

37. T. Halmos, M. Santarromana, K. Antonakis, and D. Scherman. Synthesis of glucose-chlorambucil derivatives and their recognition by the human GLUT1 glucose transporter. *European Journal of Pharmacology* **318**: 477-484 (1996).
38. K. A. Witt, T. J. Gillespie, J. D. Huber, R. D. Egleton, and T. P. Davis. Peptide drug modifications to enhance bioavailability and blood-brain barrier permeability. *Peptides* **22**: 2329-2343 (2001).
39. D. W. Laske, R. J. Youle, and E. H. Oldfield. Tumor regression with regional distribution of the targeted toxin TF- CRM107 in patients with malignant brain tumors. *Nature Medicine* **3**: 1362-1368 (1997).
40. W. M. Pardridge, D. Triguero, and J. L. Buciak. Beta-endorphin chimeric peptides: transport through the blood-brain barrier in vivo and cleavage of disulfide linkage by brain. *Endocrinology* **126**: 977-84 (1990).
41. W. M. Pardridge, J. L. Buciak, and P. M. Friden. Selective transport of an anti-transferrin receptor antibody through the blood-brain barrier in vivo. *Journal of Pharmacology and Experimental Therapeutics* **259**: 66-70 (1991).
42. A. Kurihara and W. M. Pardridge. Imaging brain tumors by targeting peptide radiopharmaceuticals through the blood-brain barrier. *Cancer Res* **59**: 6159-63 (1999).
43. S. M. Moghimi and J. Szebeni. Stealth liposomes and long circulating nanoparticles: critical issues in pharmacokinetics, opsonization and protein-binding properties. *Progress in Lipid Research* **42**: 463-478 (2003).
44. S. I. Jeon, J. H. Lee, J. D. Andrade, and P. G. De Gennes. Protein-surface interactions in the presence of polyethylene oxide. I. Simplified theory. *Journal of Colloid and Interface Science* **142**: 149-158 (1991).
45. P. R. Lockman, R. J. Mumper, M. A. Khan, and D. D. Allen. Nanoparticle technology for drug delivery across the blood-brain barrier. *Drug Development and Industrial Pharmacy* **28**: 1-13 (2002).
46. S. S. Chrai, R. Murari, and I. Ahmad. Liposomes (a review), part one: Manufacturing issues. *BioPharm* **14**: 10-14 (2001).
47. W. H. Hargreaves. If I had...a sigmoidoscopy. *Br Med J* **2**: 699 (1978).
48. F. Szoka, F. Olson, T. Heath, W. Vail, E. Mayhew, and D. Papahadjopoulos. Preparation of unilamellar liposomes of intermediate size (0.1-0.2 mumol) by a combination of reverse phase evaporation and extrusion through polycarbonate membranes. *Biochim Biophys Acta* **601**: 559-71 (1980).
49. A. Rahman, S. R. Husain, J. Siddiqui, M. Verma, M. Agresti, M. Center, A. R. Safa, and R. I. Glazer. Liposome-mediated modulation of multidrug resistance in human HL-60 leukemia cells. *J Natl Cancer Inst* **84**: 1909-15 (1992).
50. T. M. Allen. Long-circulating (sterically stabilized) liposomes for targeted drug delivery. *Trends Pharmacol Sci* **15**: 215-20 (1994).
51. P. S. Uster, T. M. Allen, B. E. Daniel, C. J. Mendez, M. S. Newman, and G. Z. Zhu. Insertion of poly(ethylene glycol) derivatized phospholipid into pre-formed liposomes results in prolonged in vivo circulation time. *FEBS Letters* **386**: 243-246 (1996).
52. S. B. La, T. Okano, and K. Kataoka. Preparation and characterization of the micelle-forming polymeric drug indomethacin-incorporated poly(ethylene oxide)-poly(beta-benzyl L-aspartate) block copolymer micelles. *J Pharm Sci* **85**: 85-90 (1996).
53. L. Zhang, K. Yu, and A. Eisenberg. Ion-induced morphological changes in 'crew-cut' aggregates of amphiphilic block copolymers. *Science* **272**: 1777-1779 (1996).
54. G. Gaucher, M. H. Dufresne, V. P. Sant, N. Kang, D. Maysinger, and J. C. Leroux. Block copolymer micelles: preparation, characterization and application in drug delivery. *J Control Release* **109**: 169-88 (2005).

55. V. S. Trubetskoy and V. P. Torchilin. Use of polyoxyethylene-lipid conjugates as long-circulating carriers for delivery of therapeutic and diagnostic agents. *Advanced Drug Delivery Reviews* **16**: 311-320 (1995).
56. R. Vakil and G. S. Kwon. PEG-phospholipid micelles for the delivery of amphotericin B. *Journal of controlled release : official journal of the Controlled Release Society* **101**: 386-389 (2005).
57. V. P. Torchilin. Targeted polymeric micelles for delivery of poorly soluble drugs. *Cellular and Molecular Life Sciences* **61**: 2549-2559 (2004).
58. V. P. Torchilin, V. S. Trubetskoy, K. R. Whiteman, P. Caliceti, P. Ferruti, and F. M. Veronese. New synthetic amphiphilic polymers for steric protection of liposomes in vivo. *Journal of Pharmaceutical Sciences* **84**: 1049-1053 (1995).
59. L. W. Seymour, R. Duncan, J. Strohalm, and J. Kopecek. Effect of molecular weight (Mw) of N-(2-hydroxypropyl)methacrylamide copolymers on body distribution and rate of excretion after subcutaneous, intraperitoneal, and intravenous administration to rats. *J Biomed Mater Res* **21**: 1341-58 (1987).
60. Y. Yamamoto, Y. Nagasaki, Y. Kato, Y. Sugiyama, and K. Kataoka. Long-circulating poly(ethylene glycol)-poly(-lactide) block copolymer micelles with modulated surface charge. *Journal of Controlled Release* **77**: 27-38 (2001).
61. M. Nakayama and T. Okano. Preparation and characterization of paclitaxel-loaded thermoresponsive polymeric micelles, *Polymer Preprints, Japan*, Vol. 55, 2006, pp. 2020.
62. D. Le Garrec, S. Gori, D. Karkan, L. Luo, D. G. Lessard, D. Smith, M. Ranger, M.-A. Yessine, and J.-C. Leroux. Preparation, characterization, cytotoxicity and biodistribution of docetaxel-loaded polymeric micelle formulations. *Journal of Drug Delivery Science and Technology* **15**: 115-120 (2005).
63. T. Nakanishi, S. Fukushima, K. Okamoto, M. Suzuki, Y. Matsumura, M. Yokoyama, T. Okano, Sakurai, Y., and K. Kataoka. Development of the polymer micelle carrier system for doxorubicin. *Journal of Controlled Release* **74**: 295-302 (2001).
64. R. Gref, P. Couvreur, G. Barratt, and E. Mysiakine. Surface-engineered nanoparticles for multiple ligand coupling. *Biomaterials* **24**: 4529-4537 (2003).
65. P. Calvo, C. Remunan-Lopez, J. L. Vila-Jato, and M. J. Alonso. Development of positively charged colloidal drug carriers: Chitosan-coated polyester nanocapsules and submicron-emulsions. *Colloid and Polymer Science* **275**: 46-53 (1997).
66. R. Gaspar. Polyalkylcyanoacrylate nanoparticles in drug targeting. *Revista Portuguesa de Farmacia* **41**: 36-45 (1991).
67. I. Montasser, S. Briancon, J. Lieto, and H. Fessi. Obtaining methods and formation mechanisms of polymeric nanoparticles
[Methodes d'obtention et mecanismes de formation de nanoparticules polymeriques]. *Journal de Pharmacie de Belgique* **55**: 155-167 (2000).
68. P. Couvreur, B. Kante, M. Roland, P. Guiot, P. Bauduin, and P. Speiser. Polycyanoacrylate nanocapsules as potential lysosomotropic carriers: preparation, morphological and sorptive properties. *J Pharm Pharmacol* **31**: 331-2 (1979).
69. M. D. Hayes, M. J. Hallihan, B. J. Love, A. O. Aning, A. Habenschuss, and T. Theiss. PGA and PLA as biodegradable polymers, *Transactions of the Annual Meeting of the Society for Biomaterials in conjunction with the International Biomaterials Symposium*, Vol. 2, 1996, pp. 400.
70. H. Fessi, F. Piusieux, J. P. Devissaguet, N. Ammoury, and S. Benita. Nanocapsule formation by interfacial polymer deposition following solvent displacement. *International Journal of Pharmaceutics* **55**: (1989).

71. S. Guinebretiere, S. Briancon, J. Lieto, C. Mayer, and H. Fessi. Study of the emulsion-diffusion of solvent: Preparation and characterization of nanocapsules. *Drug Development Research* **57**: 18-33 (2002).
72. R. Gref, Y. Minamitake, M. T. Peracchia, V. Trubetskoy, V. Torchilin, and R. Langer. Biodegradable long-circulating polymeric nanospheres. *Science* **263**: 1600-3 (1994).
73. V. C. F. Mosqueira, P. Legrand, J.-L. Morgat, M. Vert, E. Mysiakine, R. Gref, J.-P. Devissaguet, and G. Barratt. Biodistribution of long-circulating PEG-grafted nanocapsules in mice: Effects of PEG chain length and density. *Pharmaceutical Research* **18**: 1411-1419 (2001).
74. P. Calvo, C. Remunan-Lopez, J. L. Vila-Jato, and M. J. Alonso. Chitosan and chitosan/ethylene oxide-propylene oxide block copolymer nanoparticles as novel carriers for proteins and vaccines. *Pharm Res* **14**: 1431-6 (1997).
75. M. Major, E. Prieur, J. F. Tocanne, D. Betbeder, and A. M. Sautereau. Characterisation and phase behaviour of phospholipid bilayers adsorbed on spherical polysaccharidic nanoparticles. *Biochimica et Biophysica Acta - Biomembranes* **1327**: 32-40 (1997).
76. J. E. Diederichs, C. Vauthier, H. Alphandary, P. Couvreur, and R. H. Muller. Formation process and determination of microviscosity of alginate nanoparticles. *Proceedings of the Controlled Release Society* 511-512 (1994).
77. L. Illum. Chitosan and its use as a pharmaceutical excipient. *Pharmaceutical Research* **15**: 1326-1331 (1998).
78. B. Sarmento, S. Martins, A. Ribeiro, F. Veiga, R. Neufeld, and D. Ferreira. Development and comparison of different nanoparticulate polyelectrolyte complexes as insulin carriers. *International Journal of Peptide Research and Therapeutics* **12**: 131-138 (2006).
79. B. Mohanty, V. K. Aswal, J. Kohlbrecher, and H. B. Bohidar. Synthesis of gelatin nanoparticles via simple coacervation. *Journal of Surface Science and Technology* **21**: 149-160 (2005).
80. S. J. Douglas, L. Illum, and S. S. Davis. Particle size size distribution of poly(butyl 2-cyanoacrylate) nanoparticles. II. Influence of stabilizers. *Journal of Colloid and Interface Science* **103**: 154-163 (1985).
81. M. R. Gasco and M. Trotta. Nanoparticles from microemulsions. *International Journal of Pharmaceutics* **29**: 267-268 (1986).
82. N. Al Khouri Fallouh, L. Roblot-Treupel, and H. Fessi. Development of a new process for the manufacture of polyisobutylcyanoacrylate nanocapsules. *International Journal of Pharmaceutics* **28**: 125-132 (1986).
83. K. Krauel, N. M. Davies, S. Hook, and T. Rades. Using different structure types of microemulsions for the preparation of poly(alkylcyanoacrylate) nanoparticles by interfacial polymerization. *Journal of Controlled Release* **106**: 76-87 (2005).
84. C. Lherm, R. H. Muller, F. Puisieux, and P. Couvreur. Alkylcyanoacrylate drug carriers: II. Cytotoxicity of cyanoacrylate nanoparticles with different alkyl chain length. *International Journal of Pharmaceutics* **84**: 13-22 (1992).
85. R. H. Muller, C. Lherm, J. Herbort, T. Blunk, and P. Couvreur. Alkylcyanoacrylate drug carriers: I. Physicochemical characterization of nanoparticles with different alkyl chain length. *International Journal of Pharmaceutics* **84**: 1-11 (1992).
86. S. Bennis, C. Chapey, P. Couvreur, and J. Robert. Enhanced cytotoxicity of doxorubicin encapsulated in polyisohexylcyanoacrylate nanospheres against multidrug-resistant tumour cells in culture. *Eur J Cancer* **30A**: 89-93 (1994).
87. A. C. De Verdiere, C. Dubernet, F. Ne?mati, E. Soma, M. Appel, J. Ferte?, S. Bernard, F. Puisieux, and P. Couvreur. Reversion of multidrug resistance with

polyalkylcyanoacrylate nanoparticles: Towards a mechanism of action. *British Journal of Cancer* **76**: 198-205 (1997).
88. M. T. Peracchia, C. Vauthier, F. Puisieux, and P. Couvreur. Development of sterically stabilized poly(isobutyl 2-cyanoacrylate) nanoparticles by chemical coupling of poly(ethylene glycol). *Journal of Biomedical Materials Research* **34**: 317-326 (1997).
89. M. T. Peracchia, C. Vauthier, D. Desmae?le, A. Gulik, J.-C. Dedieu, M. Demoy, J. D'Angelo, and P. Couvreur. Pegylated nanoparticles from a novel methoxypolyethylene glycol cyanoacrylate-hexadecyl cyanoacrylate amphiphilic copolymer. *Pharmaceutical Research* **15**: 550-556 (1998).
90. M. T. Peracchia, E. Fattal, D. Desmaële, M. Besnard, J. P. Noe?l, J. M. Gomis, M. Appel, J. D'Angelo, and P. Couvreur. Stealth(®) PEGylated polycyanoacrylate nanoparticles for intravenous administration and splenic targeting. *Journal of Controlled Release* **60**: 121-128 (1999).
91. S. A. Wissing, O. Kayser, and R. H. Mu?ller. Solid lipid nanoparticles for parenteral drug delivery. *Advanced Drug Delivery Reviews* **56**: 1257-1272 (2004).
92. B. Heurtault, P. Saulnier, B. Pech, J.-E. Proust, and J.-P. Benoit. A Novel Phase Inversion-Based Process for the Preparation of Lipid Nanocarriers. *Pharmaceutical Research* **19**: 875-880 (2002).
93. R. Cortesi, E. Esposjto, G. Luca, and C. Nastruzzi. Production of lipospheres as carriers for bioactive compounds. *Biomaterials* **23**: 2283-94 (2002).
94. R. Cavalli, O. Caputo, and M. R. Gasco. Preparation and characterization of solid lipid nanospheres containing paclitaxel. *Eur J Pharm Sci* **10**: 305-9 (2000).
95. B. Sjostrom, A. Kaplun, Y. Talmon, and B. Cabane. Structures of nanoparticles prepared from oil-in-water emulsions. *Pharm Res* **12**: 39-48 (1995).
96. C. Freitas and R. H. Muller. Correlation between long-term stability of solid lipid nanoparticles (SLN(TM)) and crystallinity of the lipid phase. *European Journal of Pharmaceutics and Biopharmaceutics* **47**: 125-132 (1999).
97. R. H. Muller, M. Radtke, and S. A. Wissing. Nanostructured lipid matrices for improved microencapsulation of drugs. *Int J Pharm* **242**: 121-8 (2002).
98. C. Olbrich, A. Gessner, O. Kayser, and R. H. Mu?ller. Lipid-drug-conjugate (LDC) nanoparticles as novel carrier system for the hydrophilic antitrypanosomal drug diminazenediaceturate. *Journal of Drug Targeting* **10**: 387-396 (2002).
99. R. Cavalli, C. Bocca, A. Miglietta, O. Caputo, and M. R. Gasco. Albumin adsorption on stealth and non-stealth solid lipid nanoparticles. *S.T.P. Pharma Sciences* **9**: 183-189 (1999).
100. K. Shinoda. The stability of O/W Type Emulsions as Functions of Temperature and the HLB of Emulsifiers: The Emulsification by PIT-Method. *Journal of Colloid and Interface Science* **30**: 258-263 (1969).
101. M. N. Khalid, P. Simard, D. Hoarau, A. Dragomir, and J.-C. Leroux. Long circulating poly(ethylene glycol)-decorated lipid nanocapsules deliver docetaxel to solid tumors. *Pharmaceutical Research* **23**: 752-758 (2006).
102. A. Lamprecht and J.-P. Benoit. Etoposide nanocarriers suppress glioma cell growth by intracellular drug delivery and simultaneous P-glycoprotein inhibition. *Journal of Controlled Release* **112**: 208-213 (2006).
103. S. Peltier, J. M. Oger, F. Lagarce, W. Couet, and J. P. Benoit. Enhanced oral paclitaxel bioavailability after administration of paclitaxel-loaded lipid nanocapsules. *Pharm Res* **in press**: (2006).
104. L. E. Buckingham, M. Balasubramanian, R. M. Emanuele, K. E. Clodfelter, and J. S. Coon. Comparison of Solutol HS 15, Cremophor EL and novel ethoxylated fatty acid

sulfactants as multidrug resistance modification agents. *International Journal of Cancer* **62**: 436-442 (1995).
105. J. S. Coon, W. Knudson, K. Clodfelter, B. Lu, and R. S. Weinstein. Solutol HS 15, nontoxic polyoxyethylene esters of 12-hydroxystearic acid, reverses multidrug resistance. *Cancer Research* **51**: 897-902 (1991).
106. D. Hoarau, P. Delmas, S. David, E. Roux, and J.-C. Leroux. Novel long-circulating lipid nanocapsules. *Pharmaceutical Research* **21**: 1783-1789 (2004).
107. A. Beduneau, P. Saulnier, N. Anton, F. Hindre, C. Passirani, H. Rajerison, N. Noiret, and J. P. Benoit. Pegylated Nanocapsules Produced by an Organic Solvent-Free Method: Evaluation of their Stealth Properties. *Pharm Res* **23**: 2190-9 (2006).
108. J. M. Koziara, P. R. Lockman, D. D. Allen, and R. J. Mumper. Paclitaxel nanoparticles for the potential treatment of brain tumors. *Journal of Controlled Release* **99**: 259-269 (2004).
109. P. Hau, K. Fabel, U. Baumgart, P. Ru?mmele, O. Grauer, A. Bock, C. Dietmaier, W. Dietmaier, J. Dietrich, C. Dudel, F. Hu?bner, T. Jauch, E. Drechsel, I. Kleiter, C. Wismeth, A. Zellner, A. Brawanski, A. Steinbrecher, J. Marienhagen, and U. Bogdahn. Pegylated Liposomal Doxorubicin-Efficacy in Patients with Recurrent High-Grade Glioma. *Cancer* **100**: 1199-1207 (2004).
110. J. M. Koziara, P. R. Lockman, D. D. Allen, and R. J. Mumper. The blood-brain barrier and brain drug delivery. *J Nanosci Nanotechnol* **6**: 2712-35 (2006).
111. Y.-E. L. Koo, G. R. Reddy, M. Bhojani, R. Schneider, M. A. Philbert, A. Rehemtulla, B. D. Ross, and R. Kopelman. Brain cancer diagnosis and therapy with nanoplatforms. *Advanced Drug Delivery Reviews* **58**: 1556-1577 (2006).
112. W. M. Pardridge. Transport of small molecules through the blood-brain barrier: biology and methodology. *Advanced Drug Delivery Reviews* **15**: 5-36 (1995).
113. H. Tsukamoto, R. J. Boado, and W. M. Pardridge. Differential expression in glioblastoma multiforme and cerebral hemangioblastoma of cytoplasmic proteins that bind two different domains within the 3?-untranslated region of the human glucose transporter 1 (GLUT1) messenger RNA. *Journal of Clinical Investigation* **97**: 2823-2832 (1996).
114. R. J. Boado, K. L. Black, and W. M. Pardridge. Gene expression of GLUT3 and GLUT1 glucose transporters in human brain tumors. *Molecular Brain Research* **27**: 51-57 (1994).
115. F. Umezawa and Y. Eto. Liposome targeting to mouse brain: Mannose as a recognition marker. *Biochemical and Biophysical Research Communications* **153**: 1038-1044 (1988).
116. M. Mora, M.-L. Sagrista?, D. Trombetta, F. P. Bonina, A. De Pasquale, and A. Saija. Design and characterization of liposomes containing long-chain N-acylPEs for brain delivery: Penetration of liposomes incorporating GM1 into the rat brain. *Pharmaceutical Research* **19**: 1430-1438 (2002).
117. P. R. Lockman and D. D. Allen. The transport of choline. *Drug Development and Industrial Pharmacy* **28**: 749-771 (2002).
118. D. D. Allen and Q. R. Smith. Characterization of the blood-brain barrier choline transporter using the in situ rat brain perfusion technique. *Journal of Neurochemistry* **76**: 1032-1041 (2001).
119. E. M. Cornford, L. D. Braun, and W. H. Oldendorf. Carrier mediated blood-brain barrier transport of choline and certain choline analogs. *Journal of Neurochemistry* **30**: 299-308 (1978).

120. Y. S. Kang, T. Terasaki, T. Ohnishi, and A. Tsuji. In vivo and in vitro evidence for a common carrier mediated transport of choline and basic drugs through the blood-brain barrier. *J Pharmacobiodyn* **13**: 353-60 (1990).
121. G. Tedeschi, N. Lundbom, R. Raman, S. Bonavita, J. H. Duyn, J. R. Alger, and G. Di Chiro. Increased choline signal coinciding with malignant degeneration of cerebral gliomas: A serial proton magnetic resonance spectroscopy imaging study. *Journal of Neurosurgery* **87**: 516-524 (1997).
122. L. Fenart, A. Casanova, B. Dehouck, C. Duhem, S. Slupek, R. Cecchelli, and D. Betbeder. Evaluation of effect of charge and lipid coating on ability of 60-nm nanoparticles to cross an in vitro model of the blood-brain barrier. *Journal of Pharmacology and Experimental Therapeutics* **291**: 1017-1022 (1999).
123. P. R. Lockman, M. O. Oyewumi, J. M. Koziara, K. E. Roder, R. J. Mumper, and D. D. Allen. Brain uptake of thiamine-coated nanoparticles. *Journal of Controlled Release* **93**: 271-282 (2003).
124. S. P. Vyas and V. Sihorkar. Endogenous carriers and ligands in non-immunogenic site-specific drug delivery. *Adv Drug Deliv Rev* **43**: 101-64 (2000).
125. W. M. Pardridge. Drug and gene targeting to the brain with molecular Trojan horses. *Nature Reviews Drug Discovery* **1**: 131-139 (2002).
126. H. J. Frank and W. M. Pardridge. A direct in vitro demonstration of insulin binding to isolated brain microvessels. *Diabetes* **30**: 757-61 (1981).
127. M. van Houten and B. I. Posner. Insulin binds to brain blood vessels in vivo. *Nature* **282**: 623-5 (1979).
128. K. R. Duffy and W. M. Pardridge. Blood-brain barrier transcytosis of insulin in developing rabbits. *Brain Res* **420**: 32-8 (1987).
129. R. P. Glick, R. Gettleman, K. Patel, R. Lakshman, and J. C. M. Tsibris. Insulin and insulin-like growth factor I in brain tumors: Binding and in vitro effects, *Neurosurgery*, Vol. 24, 1989, pp. 791-797.
130. R. R. Reinhardt and C. A. Bondy. Insulin-like growth factors cross the blood-brain barrier. *Endocrinology* **135**: 1753-61 (1994).
131. M. W. Elmlinger, M. H. Deininger, B. S. Schuett, R. Meyermann, F. Duffner, E. H. Grote, and M. B. Ranke. In vivo expression of insulin-like growth factor-binding protein-2 in human gliomas increases with the tumor grade. *Endocrinology* **142**: 1652-1658 (2001).
132. R. G. Rosenfeld, G. Lamson, H. Pham, Y. Oh, C. Conover, D. D. De Leon, S. M. Donovan, I. Ocrant, and L. Giudice. Insulinlike growth factor-binding proteins. *Recent Prog Horm Res* **46**: 99-159; discussion 159-63 (1990).
133. I. Ocrant. Insulin-like growth factor binding proteins in the nervous system. *Adv Exp Med Biol* **293**: 471-82 (1991).
134. J. H. Wiessner and K. J. Hwang. Binding of insulin to the external surface of liposomes. Effect of surface curvature, temperature, and lipid composition. *Biochimica et Biophysica Acta* **689**: 490-498 (1982).
135. J. H. Wiessner, H. Mar, D. G. Baskin, and K. J. Hwang. Peptide-carrier interaction: induction of liposome fusion and aggregation by insulin. *J Pharm Sci* **75**: 259-63 (1986).
136. T. R. Daniels, T. Delgado, G. Helguera, and M. L. Penichet. The transferrin receptor part II: Targeted delivery of therapeutic agents into cancer cells. *Clinical Immunology* **In Press, Corrected Proof**.
137. W. A. Jefferies, M. R. Brandon, S. V. Hunt, A. F. Williams, K. C. Gatter, and D. Y. Mason. Transferrin receptor on endothelium of brain capillaries. *Nature* **312**: 162-3 (1984).

138. L. Recht, C. O. Torres, T. W. Smith, V. Raso, and T. W. Griffin. Transferrin receptor in normal and neoplastic brain tissue: Implications for brain-tumor immunotherapy. *Journal of Neurosurgery* **72**: 941-945 (1990).
139. P. A. Seligman. Structure and function of the transferrin receptor. *Prog Hematol* **13**: 131-47 (1983).
140. J. B. Fishman, J. B. Rubin, J. V. Handrahan, J. R. Connor, and R. E. Fine. Receptor-mediated transcytosis of transferrin across the blood-brain barrier. *Journal of Neuroscience Research* **18**: 299-304 (1987).
141. L. Descamps, M.-P. Dehouck, G. Torpier, and R. Cecchelli. Receptor-mediated transcytosis of transferrin through blood-brain barrier endothelial cells. *American Journal of Physiology - Heart and Circulatory Physiology* **270**: (1996).
142. C. M. Morris, A. B. Keith, J. A. Edwardson, and R. G. Pullen. Uptake and distribution of iron and transferrin in the adult rat brain. *J Neurochem* **59**: 300-6 (1992).
143. E. M. Taylor and E. H. Morgan. Developmental changes in transferrin and iron uptake by the brain in the rat. *Developmental Brain Research* **55**: 35-42 (1990).
144. R. L. Roberts, R. E. Fine, and A. Sandra. Receptor-mediated endocytosis of transferrin at the blood-brain barrier. *J Cell Sci* **104 (Pt 2)**: 521-32 (1993).
145. H. Hatakeyama, H. Akita, K. Maruyama, T. Suhara, and H. Harashima. Factors governing the in vivo tissue uptake of transferrin-coupled polyethylene glycol liposomes in vivo. *International Journal of Pharmaceutics* **281**: 25-33 (2004).
146. A. C. Steven, J. F. Hainfeld, J. S. Wall, and C. J. Steer. Mass distributions of coated vesicles isolated from liver and brain: Analysis by scanning transmission electron microscopy. *Journal of Cell Biology* **97**: 1714-1723 (1983).
147. O. Ishida, K. Maruyama, H. Tanahashi, M. Iwatsuru, K. Sasaki, M. Eriguchi, and H. Yanagie. Liposomes bearing polyethyleneglycol-coupled transferrin with intracellular targeting property to the solid tumors in vivo. *Pharmaceutical Research* **18**: 1042-1048 (2001).
148. D. A. Eavarone, X. Yu, and R. V. Bellamkonda. Targeted drug delivery to C6 glioma by transferrin-coupled liposomes. *Journal of Biomedical Materials Research* **51**: 10-14 (2000).
149. V. Soni, D. V. Kohli, and S. K. Jain. Transferrin coupled liposomes as drug delivery carriers for brain targeting of 5-florouracil. *Journal of Drug Targeting* **13**: 245-250 (2005).
150. Y. Li, M. Ogris, E. Wagner, J. Pelisek, and M. Ruffer. Nanoparticles bearing polyethyleneglycol-coupled transferrin as gene carriers: preparation and in vitro evaluation. *International Journal of Pharmaceutics* **259**: 93-101 (2003).
151. S. K. Lai, J. Fu, S. T. Man, and J. Hanes. Doxorubicin-loaded transferrin-targeted polymeric micelles rapidly enter cancer cells and accumulate near the cell nucleus, *AIChE Annual Meeting, Conference Proceedings*, 2005, pp. 14370.
152. R. Zhao, R. Seither, K. E. Brigle, I. G. Sharina, P. J. Wang, and I. D. Goldman. Impact of overexpression of the reduced folate carrier (RFC1), an anion exchanger, on concentrative transport in murine L1210 leukemia cells. *J Biol Chem* **272**: 21207-12 (1997).
153. J. F. Ross, P. K. Chaudhuri, and M. Ratnam. Differential regulation of folate receptor isoforms in normal and malignant tissues in vivo and in established cell lines. Physiologic and clinical implications. *Cancer* **73**: 2432-43 (1994).
154. D. Wu and W. M. Pardridge. Blood-brain barrier transport of reduced folic acid. *Pharmaceutical Research* **16**: 415-419 (1999).

155. S. D. Weitman, R. H. Lark, L. R. Coney, D. W. Fort, V. Frasca, V. R. Zurawski, Jr., and B. A. Kamen. Distribution of the folate receptor GP38 in normal and malignant cell lines and tissues. *Cancer Res* **52**: 3396-401 (1992).
156. R. J. Lee, S. Wang, and P. S. Low. Measurement of endosome pH following folate receptor-mediated endocytosis. *Biochim Biophys Acta* **1312**: 237-42 (1996).
157. J. M. Saul, A. Annapragada, J. V. Natarajan, and R. V. Bellamkonda. Controlled targeting of liposomal doxorubicin via the folate receptor in vitro. *J Control Release* **92**: 49-67 (2003).
158. H. Shmeeda, L. Mak, D. Tzemach, P. Astrahan, M. Tarshish, and A. Gabizon. Intracellular uptake and intracavitary targeting of folate-conjugated liposomes in a mouse lymphoma model with up-regulated folate receptors. *Molecular Cancer Therapeutics* **5**: 818-824 (2006).
159. A. Gabizon, H. Shmeeda, A. T. Horowitz, and S. Zalipsky. Tumor cell targeting of liposome-entrapped drugs with phospholipid-anchored folic acid-PEG conjugates. *Advanced Drug Delivery Reviews* **56**: 1177-1192 (2004).
160. A. Gabizon, A. T. Horowitz, D. Goren, D. Tzemach, F. Mandelbaum-Shavit, M. M. Qazen, and S. Zalipsky. Targeting folate receptor with folate linked to extremities of poly(ethylene glycol)-grafted liposomes: In vitro studies. *Bioconjugate Chemistry* **10**: 289-298 (1999).
161. N. Nishiyama and K. Kataoka. Current state, achievements, and future prospects of polymeric micelles as nanocarriers for drug and gene delivery. *Pharmacology & Therapeutics* **112**: 630-648 (2006).
162. H. S. Yoo and T. G. Park. Folate receptor targeted biodegradable polymeric doxorubicin micelles. *Journal of Controlled Release* **96**: 273-283 (2004).
163. E. K. Park, S. Y. Kim, S. B. Lee, and Y. M. Lee. Folate-conjugated methoxy poly(ethylene glycol)/poly(E-caprolactone) amphiphilic block copolymeric micelles for tumor-targeted drug delivery. *Journal of Controlled Release* **109**: 158-168 (2005).
164. B. Stella, S. Arpicco, M. T. Peracchia, D. Desmaele, J. Hoebeke, M. Renoir, J. D'Angelo, L. Cattel, and P. Couvreur. Design of folic acid-conjugated nanoparticles for drug targeting. *J Pharm Sci* **89**: 1452-64 (2000).
165. P. J. Stevens, M. Sekido, and R. J. Lee. A folate receptor-targeted lipid nanoparticle formulation for a lipophilic paclitaxel prodrug, *Pharmaceutical Research*, Vol. 21, 2004, pp. 2153-2157.
166. G. Kohler and C. Milstein. Continuous cultures of fused cells secreting antibody of predefined specificity. *Nature* **256**: 495-7 (1975).
167. S. Skarlatos, T. Yoshikawa, and W. M. Pardridge. Transport of [125I]transferrin through the rat blood-brain barrier. *Brain Res* **683**: 164-71 (1995).
168. T. Moos and E. H. Morgan. Restricted transport of anti-transferrin receptor antibody (OX26) through the blood-brain barrier in the rat. *J Neurochem* **79**: 119-129 (2001).
169. J. Huwyler, J. Yang, and W. M. Pardridge. Receptor mediated delivery of daunomycin using immunoliposomes: Pharmacokinetics and tissue distribution in the rat. *Journal of Pharmacology and Experimental Therapeutics* **282**: 1541-1546 (1997).
170. J. Huwyler, D. Wu, and W. M. Pardridge. Brain drug delivery of small molecules using immunoliposomes. *Proceedings of the National Academy of Sciences of the United States of America* **93**: 14164-14169 (1996).
171. K. Maruyama, T. Takizawa, T. Yuda, S. J. Kennel, L. Huang, and M. Iwatsuru. Targetability of novel immunoliposomes modified with amphipathic poly(ethylene glycol) s conjugated at their distal terminals to monoclonal antibodies. *Biochimica et Biophysica Acta (BBA) - Biomembranes* **1234**: 74-80 (1995).

172. A. Schnyder, S. Krahenbuhl, J. Drewe, and J. Huwyler. Targeting of daunomycin using biotinylated immunoliposomes: Pharmacokinetics, tissue distribution and in vitro pharmacological effects. *Journal of Drug Targeting* **13**: 325-335 (2005).
173. A. Cerletti, J. Drewe, G. Fricker, A. N. Eberle, and J. Huwyler. Endocytosis and transcytosis of an immunoliposome-based brain drug delivery system. *J Drug Target* **8**: 435-46 (2000).
174. S. Gosk, T. Moos, C. Vermehren, and G. Storm. Targeting anti-transferrin receptor antibody (OX26) and OX26-conjugated liposomes to brain capillary endothelial cells using in situ perfusion. *Journal of Cerebral Blood Flow and Metabolism* **24**: 1193-1204 (2004).
175. N. Shi and W. M. Pardridge. Noninvasive gene targeting to the brain. *Proceedings of the National Academy of Sciences of the United States of America* **97**: 7567-7572 (2000).
176. Y.-f. Zhang, R. J. Boado, and W. M. Pardridge. Absence of Toxicity of Chronic Weekly Intravenous Gene Therapy with Pegylated Immunoliposomes. *Pharmaceutical Research* **20**: 1779-1785 (2003).
177. Y. Zhang, C. Zhu, and W. M. Pardridge. Antisense gene therapy of brain cancer with an artificial virus gene delivery system. *Molecular Therapy* **6**: 67-72 (2002).
178. D. A. Podlecki, R. M. Smith, M. Kao, P. Tsai, T. Huecksteadt, D. Brandenburg, R. S. Lasher, L. Jarett, and J. M. Olefsky. Nuclear translocation of the insulin receptor. A possible mediator of insulin's long term effects. *J Biol Chem* **262**: 3362-8 (1987).
179. Y. Zhang, H. Jeong Lee, R. J. Boado, and W. M. Pardridge. Receptor-mediated delivery of an antisense gene to human brain cancer cells. *J Gene Med* **4**: 183-94 (2002).
180. P. H. Tan, M. Manunta, N. Ardjomand, S. A. Xue, D. F. P. Larkin, D. O. Haskard, K. M. Taylor, and A. J. T. George. Antibody targeted gene transfer to endothelium. *Journal of Gene Medicine* **5**: 311-323 (2003).
181. J. A. Harding, C. M. Engbers, M. S. Newman, N. I. Goldstein, and S. Zalipsky. Immunogenicity and pharmacokinetic attributes of poly(ethylene glycol)-grafted immunoliposomes. *Biochimica et Biophysica Acta (BBA) - Biomembranes* **1327**: 181-192 (1997).
182. K. Maruyama, N. Takahashi, T. Tagawa, K. Nagaike, and M. Iwatsuru. Immunoliposomes bearing polyethyleneglycol-coupled Fab' fragment show prolonged circulation time and high extravasation into targeted solid tumors in vivo. *FEBS Letters* **413**: 177-180 (1997).
183. Y. Matsumura, M. Gotoh, K. Muro, Y. Yamada, K. Shirao, Y. Shimada, M. Okuwa, S. Matsumoto, Y. Miyata, H. Ohkura, K. Chin, S. Baba, T. Yamao, A. Kannami, Y. Takamatsu, K. Ito, and K. Takahashi. Phase I and pharmacokinetic study of MCC-465, a doxorubicin (DXR) encapsulated in PEG immunoliposome, in patients with metastatic stomach cancer. *Annals of Oncology* **15**: 517-525 (2004).
184. T. Hamaguchi, Y. Matsumura, Y. Nakanishi, K. Muro, Y. Yamada, Y. Shimada, K. Shirao, H. Niki, S. Hosokawa, T. Tagawa, and T. Kakizoe. Antitumor effect of MCC-465, pegylated liposomal doxorubicin tagged with newly developed monoclonal antibody GAH, in colorectal cancer xenografts. *Cancer Science* **95**: 608-613 (2004).
185. V. P. Chekhonin, A. V. Kabanov, Y. A. Zhirkov, and G. V. Morozov. Fatty acid acylated Fab-fragments of antibodies to neurospecific proteins as carriers for neuroleptic targeted delivery in brain. *FEBS Letters* **287**: 149-152 (1991).
186. A. V. Kabanov, E. V. Batrakova, N. S. Melik-Nubarov, N. A. Fedoseev, T. Y. Dorodnich, V. Y. Alakhov, V. P. Chekhonin, I. R. Nazarova, and V. A. Kabanov. A new class of drug carriers: Micelles of poly(oxyethylene)-poly(oxypropylene) block

copolymers as microcontainers for drug targeting from blood in brain. *Journal of Controlled Release* **22**: 141-157 (1992).
187. Z. Gao, A. N. Lukyanov, A. R. Chakilam, and V. P. Torchilin. PEG-PE/phosphatidylcholine mixed immunomicelles specifically deliver encapsulated taxol to tumor cells of different origin and promote their efficient killing. *Journal of Drug Targeting* **11**: 87-92 (2003).
188. Y. Aktas, M. Yemisci, K. Andrieux, R. N. Gursoy, M. J. Alonso, E. Fernandez-Megia, R. Novoa-Carballal, E. Quinoa, R. Riguera, M. F. Sargon, H. H. Celik, A. S. Demir, A. A. Hincal, T. Dalkara, Y. Capan, and P. Couvreur. Development and brain delivery of chitosan-PEG nanoparticles fnnctionalized with the monoclonal antibody OX26. *Bioconjugate Chemistry* **16**: 1503-1511 (2005).
189. J.-C. Olivier, R. Huertas, H. J. Lee, F. Calon, and W. M. Pardridge. Synthesis of Pegylated Immunonanoparticles. *Pharmaceutical Research* **19**: 1137-1143 (2002).
190. N. Pedersen, S. Hansen, A. V. Heydenreich, H. G. Kristensen, and H. S. Poulsen. Solid lipid nanoparticles can effectively bind DNA, streptavidin and biotinylated ligands. *European Journal of Pharmaceutics and Biopharmaceutics* **62**: 155-162 (2006).
191. A. W. Vorbrodt. Ultracytochemical characterization of anionic sites in the wall of brain capillaries. *J Neurocytol* **18**: 359-68 (1989).
192. W. M. Pardridge, A. K. Kumagai, and J. B. Eisenberg. Chimeric peptides as a vehicle for peptide pharmaceutical delivery through the blood-brain barrier. *Biochem Biophys Res Commun* **146**: 307-13 (1987).
193. A. K. Kumagai, J. B. Eisenberg, and W. M. Pardridge. Absorptive-mediated endocytosis of cationized albumin and a ?-endorphin-cationized albumin chimeric peptide by isolated brain capillaries. Model system of blood-brain barrier transport. *Journal of Biological Chemistry* **262**: 15214-15219 (1987).
194. D. Triguero, J. Buciak, and W. M. Pardridge. Capillary depletion method for quantification of blood-brain barrier transport of circulating peptides and plasma proteins. *J Neurochem* **54**: 1882-8 (1990).
195. A. Muckerheide, R. J. Apple, A. J. Pesce, and J. G. Michael. Cationization of protein antigens. I. Alteration of immunogenic properties. *J Immunol* **138**: 833-7 (1987).
196. P. Bergmann, R. Kacenelenbogen, and A. Vizet. Plasma clearance, tissue distribution and catabolism of cationized albumins with increasing isoelectric points in the rat. *Clinical Science* **67**: 35-43 (1984).
197. M. Thole, S. Nobmanna, J. Huwyler, A. Bartmann, and G. Fricker. Uptake of cationzied albumin coupled liposomes by cultured porcine brain microvessel endothelial cells and intact brain capillaries. *J Drug Target* **10**: 337-44 (2002).
198. W. Lu, Y. Zhang, Y. Z. Tan, K. L. Hu, X. G. Jiang, and S. K. Fu. Cationic albumin-conjugated pegylated nanoparticles as novel drug carrier for brain delivery. *J Control Release* **107**: 428-48 (2005).
199. W. Lu, Y.-Z. Tan, K.-L. Hu, and X.-G. Jiang. Cationic albumin conjugated pegylated nanoparticle with its transcytosis ability and little toxicity against blood-brain barrier. *International Journal of Pharmaceutics* **295**: 247-260 (2005).
200. J. Kreuter, V. E. Petrov, D. A. Kharkevich, and R. N. Alyautdin. Influence of the type of surfactant on the analgesic effects induced by the peptide dalargin after its delivery across the blood-brain barrier using surfactant-coated nanoparticles. *Journal of Controlled Release* **49**: 81-87 (1997).
201. M. Luck. Plasmaproteinadsorption als möglicher Schlüsselfaktor für eine kontrollierte Arzneistoffapplikation mit partikulären Trägern, Freie Universität, Berlin, 1997, pp. 14 - 24 and 137-154.

202. B. Dehouck, M. P. Dehouck, J. C. Fruchart, and R. Cecchelli. Upregulation of the low density lipoprotein receptor at the blood-brain barrier: intercommunications between brain capillary endothelial cells and astrocytes. *J Cell Biol* **126**: 465-73 (1994).
203. S. Meresse, C. Delbart, J. C. Fruchart, and R. Cecchelli. Low-density lipoprotein receptor on endothelium of brain capillaries. *J Neurochem* **53**: 340-5 (1989).
204. B. Dehouck, L. Fenart, M. P. Dehouck, A. Pierce, G. Torpier, and R. Cecchelli. A new function for the LDL receptor: transcytosis of LDL across the blood-brain barrier. *J Cell Biol* **138**: 877-89 (1997).
205. M. Murakami, Y. Ushio, Y. Morino, T. Ohta, and Y. Matsukado. Immunohistochemical localization of apolipoprotein E in human glial neoplasms. *Journal of Clinical Investigation* **82**: 177-188 (1988).
206. J. Kreuter, R. N. Alyautdin, D. A. Kharkevich, and A. A. Ivanov. Passage of peptides through the blood-brain barrier with colloidal polymer particles (nanoparticles). *Brain Res* **674**: 171-4 (1995).
207. P. Ramge, R. E. Unger, J. B. Oltrogge, D. Zenker, D. Begley, J. Kreuter, and H. Von Briesen. Polysorbate-80 coating enhances uptake of polybutylcyanoacrylate (PBCA)-nanoparticles by human and bovine primary brain capillary endothelial cells. *Eur J Neurosci* **12**: 1931-40 (2000).
208. J. Kreuter. Nanoparticulate systems for brain delivery of drugs. *Advanced Drug Delivery Reviews* **47**: 65-81 (2001).
209. R. N. Alyautdin, V. E. Petrov, K. Langer, A. Berthold, D. A. Kharkevich, and J. Kreuter. Delivery of loperamide across the blood-brain barrier with polysorbate 80-coated polybutylcyanoacrylate nanoparticles. *Pharm Res* **14**: 325-8 (1997).
210. R. N. Alyautdin, E. B. Tezikov, P. Ramge, Y. Kroiter, D. Begly, and D. A. Kharkevich. Polybutylcyanoacrylate nanoparticles covered with polysorbate-80 are responsible for the transport of tubocurarine sorbed on them to the brain perfused in situ. *Eksperimental'naya i Klinicheskaya Farmakologiya* **61**: 26 (1998).
211. A. E. Gulyaev, S. E. Gelperina, I. N. Skidan, A. S. Antropov, G. Y. Kivman, and J. Kreuter. Significant transport of doxorubicin into the brain with polysorbate 80-coated nanoparticles. *Pharm Res* **16**: 1564-9 (1999).
212. S. C. J. Steiniger, J. Kreuter, A. S. Khalansky, I. N. Skidan, A. I. Bobruskin, Z. S. Smirnova, S. E. Severin, R. Uhl, M. Kock, K. D. Geiger, and S. E. Gelperina. Chemotherapy of glioblastoma in rats using doxorubicin-loaded nanoparticles. *International Journal of Cancer* **109**: 759-767 (2004).
213. S. E. Gelperina, A. S. Khalansky, I. N. Skidan, Z. S. Smirnova, A. I. Bobruskin, S. E. Severin, B. Turowski, F. E. Zanella, and J. Kreuter. Toxicological studies of doxorubicin bound to polysorbate 80-coated poly(butyl cyanoacrylate) nanoparticles in healthy rats and rats with intracranial glioblastoma. *Toxicology Letters* **126**: 131-141 (2002).
214. A. Ambruosi, A. S. Khalansky, H. Yamamoto, S. E. Gelperina, D. J. Begley, and J. Kreuter. Biodistribution of polysorbate 80-coated doxorubicin-loaded [14C]-poly(butyl cyanoacrylate) nanoparticles after intravenous administration to glioblastoma-bearing rats. *Journal of Drug Targeting* **14**: 97-105 (2006).
215. P. Calvo, B. Gouritin, H. Chacun, D. Desmaele, J. D'Angelo, J. P. Noel, D. Georgin, E. Fattal, J. P. Andreux, and P. Couvreur. Long-circulating PEGylated polycyanoacrylate nanoparticles as new drug carrier for brain delivery. *Pharm Res* **18**: 1157-66 (2001).
216. J. C. Olivier, L. Fenart, R. Chauvet, C. Pariat, R. Cecchelli, and W. Couet. Indirect evidence that drug brain targeting using polysorbate 80-coated polybutylcyanoacrylate nanoparticles is related to toxicity. *Pharm Res* **16**: 1836-42 (1999).

217. M. N. Azmin, J. F. Stuart, and A. T. Florence. The distribution and elimination of methotrexate in mouse blood and brain after concurrent administration of polysorbate 80. *Cancer Chemother Pharmacol* **14**: 238-42 (1985).
218. J. Kreuter, P. Ramge, V. Petrov, S. Hamm, S. E. Gelperina, B. Engelhardt, R. Alyautdin, H. Von Briesen, and D. J. Begley. Direct evidence that polysorbate-80-coated poly(butylcyanoacrylate) nanoparticles deliver drugs to the CNS via specific mechanisms requiring prior binding of drug to the nanoparticles. *Pharmaceutical Research* **20**: 409-416 (2003).
219. T. M. Goppert and R. H. Muller. Polysorbate-stabilized solid lipid nanoparticles as colloidal carriers for intravenous targeting of drugs to the brain: comparison of plasma protein adsorption patterns. *J Drug Target* **13**: 179-87 (2005).
220. T. M. Goppert and R. H. Muller. Plasma protein adsorption of Tween 80- and poloxamer 188-stabilized solid lipid nanoparticles. *J Drug Target* **11**: 225-31 (2003).
221. N. Scholer, K. Krause, O. Kayser, R. H. Muller, K. Borner, H. Hahn, and O. Liesenfeld. Atovaquone nanosuspensions show excellent therapeutic effect in a new murine model of reactivated toxoplasmosis. *Antimicrob Agents Chemother* **45**: 1771-9 (2001).
222. W. Sun, C. Xie, H. Wang, and Y. Hu. Specific role of polysorbate 80 coating on the targeting of nanoparticles to the brain. *Biomaterials* **25**: 3065-3071 (2004).
223. Z. Zhang and S.-S. Feng. In vitro investigation on poly(lactide)-tween 80 copolymer nanoparticles fabricated by dialysis method for chemotherapy. *Biomacromolecules* **7**: 1139-1146 (2006).
224. K. Michaelis, M. M. Hoffmann, S. Dreis, E. Herbert, R. N. Alyautdin, M. Michaelis, J. Kreuter, and K. Langer. Covalent linkage of apolipoprotein e to albumin nanoparticles strongly enhances drug transport into the brain. *J Pharmacol Exp Ther* **317**: 1246-53 (2006).
225. I. Sauer, I. R. Dunay, K. Weisgraber, M. Bienert, and M. Dathe. An apolipoprotein E-derived peptide mediates uptake of sterically stabilized liposomes into brain capillary endothelial cells. *Biochemistry* **44**: 2021-9 (2005).
226. I. Sauer, H. Nikolenko, S. Keller, K. Abu Ajaj, M. Bienert, and M. Dathe. Dipalmitoylation of a cellular uptake-mediating apolipoprotein E-derived peptide as a promising modification for stable anchorage in liposomal drug carriers. *Biochim Biophys Acta* **1758**: 552-61 (2006).
227. M. Mercadal, J. C. Domingo, J. Petriz, J. Garcia, and M. A. de Madariaga. Preparation of immunoliposomes bearing poly(ethylene glycol)-coupled monoclonal antibody linked via a cleavable disulfide bond for ex vivo applications. *Biochimica et Biophysica Acta (BBA) - Biomembranes* **1509**: 299-310 (2000).
228. J. K. Tessmar, A. G. Mikos, and A. Gopferich. Amine-reactive biodegradable diblock copolymers. *Biomacromolecules* **3**: 194-200 (2002).
229. Y. Nagasaki, T. Okada, C. Scholz, M. Iijima, M. Kato, and K. Kataoka. The reactive polymeric micelle based on an aldehyde-ended poly(ethylene giycol)/poly(lactide) block copolymer. *Macromolecules* **31**: 1473-1479 (1998).
230. J. Barbet, P. Machy, and L. D. Leserman. Monoclonal antibody covalently coupled to liposomes: Specific targeting to cells. *Journal of Supramolecular and Cellular Biochemistry* **16**: 243-258 (1981).
231. R. J. S. Duncan, P. D. Weston, and R. Wrigglesworth. A new reagent which may be used to introduce sulfhydryl groups into proteins, and its use in the preparation of conjugates for immunoassay. *Analytical Biochemistry* **132**: 68-73 (1983).

232. T. O. Harasym, M. B. Bally, and P. Tardi. Clearance properties of liposomes involving conjugated proteins for targeting. *Advanced Drug Delivery Reviews* **32**: 99-118 (1998).
233. P. L. Domen, J. R. Nevens, A. K. Mallia, G. T. Hermanson, and D. C. Klenk. Site-directed immobilization of proteins. *Journal of Chromatography* **510**: 293-302 (1990).
234. R. G. Melton. Preparation and purification of antibody-enzyme conjugates for therapeutic applications. *Advanced Drug Delivery Reviews* **22**: 289-301 (1996).
235. S. M. Ansell, P. G. Tardi, and S. S. Buchkowsky. 3-(2-pyridyldithio)propionic acid hydrazide as a cross-linker in the formation of liposome-antibody conjugates. *Bioconjug Chem* **7**: 490-6 (1996).
236. W. Guo, T. Lee, J. Sudimack, and R. J. Lee. Receptor-specific delivery of liposomes via folate-PEG-Chol. *Journal of Liposome Research* **10**: 179-195 (2000).
237. R. J. Lee and P. S. Low. Folate-mediated tumor cell targeting of liposome-entrapped doxorubicin in vitro. *Biochimica et Biophysica Acta - Biomembranes* **1233**: 134-144 (1995).
238. P. Machy and L. D. Leserman. Elimination or rescue of cells in culture by specifically targeted liposomes containing methotrexate or formyl-tetrahydrofolate. *Embo J* **3**: 1971-7 (1984).
239. N. M. Green. Avidin and streptavidin. *Methods Enzymol* **184**: 51-67 (1990).
240. Y.-S. Kang, Y. Saito, and W. M. Pardridge. Pharmacokinetics of [3H]biotin bound to different avidin analogues. *Journal of Drug Targeting* **3**: 159-165 (1995).
241. W. M. Pardridge. Vector-mediated peptide drug delivery to the brain. *Advanced Drug Delivery Reviews* **15**: 109-146 (1995).
242. A. K. Salem, S. M. Cannizzaro, M. C. Davies, S. J. Tendler, C. J. Roberts, P. M. Williams, and K. M. Shakesheff. Synthesis and characterisation of a degradable poly(lactic acid)-poly(ethylene glycol) copolymer with biotinylated end groups. *Biomacromolecules* **2**: 575-80 (2001).
243. N. C. Phillips, L. Gagne, C. Tsoukas, and J. Dahman. Immunoliposome targeting to murine CD4+ leucocytes is dependent on immune status. *J Immunol* **152**: 3168-74 (1994).
244. J. N. Weinstein, R. Blumenthal, S. O. Sharrow, and P. A. Henkart. Antibody-mediated targeting of liposomes. Binding to lymphocytes does not ensure incorporation of vesicle contents into the cells. *Biochimica et Biophysica Acta* **509**: 272-288 (1978).
245. J.-C. Olivier. Drug transport to brain with targeted nanoparticles. *NeuroRx* **2**: 108-119 (2005).
246. S. S. C.J. and K. J. , S. Khalansky Alexander ,Skidan Igor N. , Bobruskin Alexey I. , Smirnova Zoya S. , Severin Sergey E. , Uhl Reiner , Kock Martin , D. Geiger Kathrin , Gelperina Svetlana E. Chemotherapy of glioblastoma in rats using doxorubicin-loaded nanoparticles. *International Journal of Cancer* **109**: 759-767 (2004).
247. A. Schnyder and J. Huwyler. Drug transport to brain with targeted liposomes. *NeuroRx* **2**: 99-107 (2005).

TRAVAIL EXPERIMENTAL

CHAPITRE I

CONCEPTION D'UNE NOUVELLE GENERATION DE NANOCAPSULES LIPIDIQUES FURTIVES

CONCEPTION D'UNE NOUVELLE GENERATION DE NANOCAPSULES LIPIDIQUES FURTIVES

Dans cette première partie, l'objectif est de concevoir un nouveau vecteur lipidique caractérisé par un temps de résidence vasculaire prolongé. En effet, ce paramètre est essentiel pour favoriser la reconnaissance des tissus cibles. L'utilisation de polymères hydrophiles comme le poly(éthylène glycol) (PEG) à la surface de systèmes colloïdaux constitue une des approches les plus efficaces pour augmenter le temps de circulation dans le sang. Le PEG génère une barrière stérique autour de la particule qui empêche l'adsorption d'opsonines impliquées dans les mécanismes de phagocytose. Cet effet est notamment influencé par la masse moléculaire du polymère hydrophile. Dans ce contexte, de nouvelles nanocapsules lipidiques ont été mises au point en utilisant un PEG plus long que celui de la formulation conventionnelle. L'hydroxystearate de PEG_{660} a ainsi été remplacé par le stéarate de PEG_{1500}. L'influence de ce polymère sur la formulation des nanocapsules et sur leur furtivité a été évaluée. Ce travail a été publié dans Pharmaceutical Research (Arnaud Béduneau, Patrick Saulnier, Nicolas Anton, François Hindré, Catherine Passirani, Holisoa Rajerison, Nicolas Noiret, Jean-Pierre Benoit. *Pegylated nanocapsules produced by an organic solvent-free method: Evaluation of their stealth properties.* Volume 23, issue 9, p : 2190-2199,).

Pegylated nanocapsules produced by an organic solvent-free method: evaluation of their stealth properties

Arnaud Béduneau [1], Patrick Saulnier [1, 3], Nicolas Anton [1], François Hindré [1], Catherine Passirani [1], Holisoa Rajerison [2], Nicolas Noiret [2], Jean-Pierre Benoit [1]

[1] Inserm, U646, Angers, F-49100 France ; Université d'Angers, Angers, F-49100 France.
[2] UMR-CNRS 6052, Rennes, F-35700 France ; ENSC, Rennes, F-35700 France.
[3] To whom correspondence should be addressed. (E-mail: patrick.saulnier@univ-angers.fr).

ABSTRACT

Purpose. To develop from an original process, a novel generation of stealth lipidic nanocapsules in order to improve the lipophilic drug delivery in accessible sites.

Methods. Nanocapsules covered by PEG_{1500} stearate were obtained by a low energy emulsification method. Conductivity measurements and ternary diagram were performed to describe the formulation mechanism. Hemolytic dosage CH50 and pharmacokinetic study in rats have been achieved in order to study the stealth properties of nanocapsules.

Results. Transition from an O/W emulsion to a w/O/W emulsion was necessary to produce PEG_{1500} stearate nanocapsules. Interestingly nanocapsules with a size around 26 nm and a polydispersity index inferior to 0.1 were obtained. The CH50 test has revealed a very weak complement consumption in the presence of such nanocapsules. Moreover, after intravenous injection into rats, PEG_{1500} stearate nanocapsules exhibited long circulating properties. The

experimental data support the concept of steric repulsion of the surface towards proteins, displayed by nanocapsules covered with PEG_{1500} stearate. These *in vivo* results were in agreement with the PEG_{1500} density calculated at the nanocarrier surface.

Conclusions. Injectable drug carriers have been developed. Their long-circulating properties could confer them a strong potential for lipophilic drug targeting.

KEY WORDS

Lipidic nanocapsules; PEG chain density; "stealth" colloids; polyethylene glycol; transitional inversion.

INTRODUCTION

For 40 years, drug carriers in the nanometer range have been in development. Most of them are used in the field of cancer therapy and diagnosis. Indeed, these submicronic systems, after intravenous administration, are expected to improve the targeting and release of the encapsulated drug. Liposomes and more recently, nanocapsules represent an important part of these carriers. They are composed of nonionic surfactants, macromolecules and / or phospholipids.

Unfortunately, following intravenous injection, these nanocarriers are rapidly cleared from the blood. Macrophages of the mononuclear phagocytic system, particularly Kuppfer cells in the liver, recognized and removed them from the bloodstream. The adsorption of plasma proteins at the surface of these particles (opsonization process) seems to be

responsible of the short lifetime in the bloodstream because of their interaction with specific plasma membrane receptors on monocytes and various subsets of tissue macrophages (1). Therefore, to increase the circulating half-time of nanocarriers, some studies have shown the impact of grafting polyethylene-glycol (PEG) derivatives at their surface (2). Indeed, the presence of such polymers reduces the protein adsorption by ensuring an efficient steric stabilization. The PEG density, corona thickness and PEG chain length are important parameters to consider to avoid opsonization (3).

In this context, lipid nanocarriers covered with PEG_{660} hydroxystearate have been developed by Heurtault *et al.* (4) over the last five years. These standard nanocapsules were prepared according to an organic solvent-free process using the Phase Inversion Temperature (PIT) method (5). When an oil-in-water (O/W) emulsion prepared with a nonionic surfactant of the ethylene oxide type is heated to a critical temperature (PIT), the emulsion inverts to a water-in-oil emulsion (W/O) (6). During a rapid cooling at PIT, the system crosses a point of zero spontaneous curvature promoting the formation of submicron-scale particles. Despite of the presence of PEG, these lipid nanocapsules exhibit an early disappearance half-time of 21 minutes after injection in the bloodstream (7). In order to extend the disappearance half-time, a novel long-circulating particle with longer PEG chain (PEG_{1500} stearate) based on low-energy emulsification method, without phase inversion, was developed.

In this study, the formulation process of these nanocarriers was investigated. The nanocapsule structure was then explored by cryo-transmission electron microscopy (Cryo-TEM). The influence of the PEG length on the electrokinetic properties of the particles was compared to the standard nanocapsules developed by Heurtault *et al.* (8). The ability of the PEG_{1500} stearate (density and length) to inhibit the in-vitro activation of the complement system and to prolong the lifetime of the nanocapsules after intravenous injection in rats was also evaluated in comparison with PEG_{660} hydroxystearate nanocapsules.

MATERIALS AND METHODS

Lipoïd® S75-3 (soybean lecithin at 69% of phosphatidylcholine and 10% phosphatidylethanolamine) and DUB SPEG 30S® (PEG_{1500} stearate) were kind gifts from Lipoïd GmbH (Ludwigshafen, Germany) and Stearinerie Dubois (Citron, France), respectively. Due to its complex composition, the brand name of soybean lecithin will be used in the following. The lipophilic Labrafac® WL 1349 (caprylic-capric acid triglycerides) was generously provided by Gattefossé S.A. (Saint-Priest, France). NaCl was purchased from Prolabo (Fontenay-sous-bois, France). Deionised water was obtained from a Milli-Q plus® system (Millipore, Paris, France).

Formulation of stearate PEG_{1500} nanocapsules

An aqueous phase containing deionised water, NaCl, and hydrophilic non-ionic surfactant (DUB SPEG 30S®) was added to the oil phase (Labrafac®) and lecithin (Lipoïd®) (Table I) under magnetic stirring at an agitation speed of 200 rpm. As for the preparation of standard nanocapsules, at least three temperature cycles alternating from 60°C to 95°C at a rate of 4°C/min were realized to obtain stable nanocapsules (9). During the last cooling, the formulation reaching 80°C, was rapidly diluted (1:3.5) with 12.5 ml cold water to form particles, and then continuously stirred for thirty minutes.

Table I. Composition of PEG_{1500} stearate nanocapsules A.

PEG_{1500} stearate nanocapsules (26nm)	
Constituents	Quantity
PEG_{1500} stearate	1.403 g
Lipoïd®	0.075 g
NaCl	0.250 g
Labrafac®	0.468 g
Deionized water	2.805 g
Deionized water at 0°C	12.50 g

Conductivity measurement

The conductivity of the bulk phase was measured using a conductimeter LF 325B (WTW, Weilheim, Germany) with two platinum plate attachments. Conductivity was determined during heating, between 60°C and 100°C, under magnetic stirring at an agitation speed of 200 rpm. The conductivimeter mode used was the nonlinear temperature compensation (nLF). Four different compositions corresponding to high, low and intermediate water fraction Fw (0.85, 0.66, 0.5 and 0.33) have been studied with Fw described as:

$$Fw = \frac{V_{water}}{(V_{water} + V_{oil})} \quad (1)$$

Where V_{water} and V_{oil} were the volumes of water and oil, respectively, in the nanocapsule suspension before dilution. Moreover, concentration of PEG_{1500} stearate was fixed at 30% w/w. The conductivity measurements were performed in triplicate indicating an accuracy around 1.5%.

Feasibility domain

In order to optimize constituent proportions, a ternary diagram was built. For each plot, the preparation process was unchanged but the proportions of water, oil and PEG_{1500} stearate were modified. The sum of the amounts of these three components was considered to be 100% (w/w). Concentrations of Lipoïd® S75-3 and NaCl in water were fixed at 1.5% (w/w) and 5% (w/w), respectively. The feasibility domain was defined as an area that allowed the formation of nanocapsules. After dilution, the hydrodynamic diameter range and the polydispersity index of each formulation were characterized by dynamic light scattering spectroscopy.

Particle characterization

Size measurements

The average hydrodynamic diameter and the polydispersity index (PI) of nanocapsules were determined by dynamic light scattering using a Malvern Autosizer 4700 (Malvern Instruments S.A., Worcestershire, United Kingdom) fitted with a 488 nm laser beam at a fixed angle of 90°. The polydispersity index was used as a measurement of the size distribution. A small value of PI (< 0.1) indicates an unimodale size distribution, while a PI > 0.3 indicates a higher heterogeneity. The temperature of the cell was maintained at 25°C. Nanocapsules were diluted 1:100 (v/v) in deionised water in order to assure a convenient scattered intensity on the detector.

Cryo transmission electron microscopy (Cryo-TEM)

Cryo-TEM observations were performed at –170°C on a Philips CM120 electron microscope operating at –120 kV following the method previously developed by Lambert *et al.* (10).

Determination of the proportion of free PEG_{1500} stearate in the nanocapsule suspension

We assumed that the whole quantity of Labrafac® and Lipoïd® used in the preparation was confined into spherical particles. On the contrary, a release of the PEG_{1500} stearate from the nanocapsule shell has been noticed. So, an assessment of PEG_{1500} stearate amount in the external phase of the suspension was performed. The free hydrophilic polymer was separated from the nanocapsules by steric exclusion chromatography. Nanocapsule suspension was deposited on 1.5 × 40 cm Sepharose CL-4B column and was eluted with distilled water. About 200 fractions of 400 µl were successively collected and the PEG concentration was determined from a colorimetric method taking advantage of the formation of a complex between PEG and iodine (11). 50µl of KI/I_2 solution was added to 100 µl of sample diluted at 1:4 (v/v) and the turbidity of the medium was then detected spectrophotometrically at 492 nm. Three measurements by fraction were performed to evaluate the PEG concentration indicating a 1% accuracy. After chromatography, the amount of PEG_{1500} stearate adsorbed on the Sepharose gel was determined according to the same method.

Measurement of the electrophoretic mobility

Electrophoretic mobility measurements of nanocapsules were carried out using a Zetasizer 2000, (Malvern Instruments S.A.) based on the laser Doppler effect. Measurements were made in water at pH 7.4 with cell voltage 150 V. The nanocarriers were diluted in water at 1:10 (w/w) and seven NaCl concentrations were chosen: 1, 2, 10,15, 25, 50 and 100 mM.

The electrophoretic mobility measurements were carried out in triplicate. All the values were measured with a relative accuracy of 1%.

From these experimental electrophoretic mobilities, a soft particle analysis theory (12) was applied. It aimed at characterizing the surface electric properties of PEG_{1500} stearate nanocapsules (13). Two physical constants ZN and $1/\lambda$ were then determined: ZN ($C.m^3$) represented spatial charge density in the polyelectrolyte region and λ^{-1} (m) was the depth of the layer accessible by counterions like Na^+.

Complement consumption studies

Complement consumption was assessed in human serum (HS) by measuring the residual hemolytic capacity of the complement system after contact with nanocapsules. Various amounts of the nanocapsule suspension (50,100, 125, 150, 200, 250 µl) were diluted with VBS^{2+} (Veronal Buffer Saline) in order to obtain a total volume of 300 µl for each sample. After addition of 100 µl of HS, the suspensions were incubated at 37°C for 60 minutes, under gentle agitation. Simultaneously, sheep erythrocytes were sensitized with hemolysine diluted at 1:1600 (v/v) in VBS^{2+} and suspended to a final concentration of 1.10^8 cells/ml. After incubation, nanocapsules in HS were diluted to 1:24 (v/v) and different amounts of the mixture nanocapsules / serum (0.2, 0.25, 0.3, 0.35, 0.4, 0.6 ml) were diluted with VBS^{2+} to reach a total volume of 0.8 ml. The sensitized sheep erythrocytes (0.2 ml) were also added and the sample were incubated at 37°C for 45 minutes. After addition of 2 ml of NaCl, unlysed erythrocytes were separated by centrifugation. The lysis of cells measured at 405 nm allowed to determine the level of residual active complement in HS previously exposed to nanocapsules. Zymosan particles, a strong complement activator (14), were used as a positive control. Results were expressed as CH50 units consumption (15). The CH50

units represent the concentration of serum of hemolytic complement units per ml of serum able to cause 50% hemolysis of a fixed volume of these sheep red cells.

In vivo **studies**

Preparation of radiolabeled nanocapsules

Nanocapsules were labeled by incorporating in their oily core a lipophilic complex: ^{99m}Tc $(S_3CPh)_2(S_2CPh)$ or ^{99m}Tc–SSS complex, prepared according to Mevellec *et al.* (16). ^{99m}Tc was obtained from a $^{99}Mo/^{99m}Tc$ generator purchased from CIS bio International/Schering (Gif sur Yvette, France). 1 ml of deionised water was added to a vial containing 7.5 mg sodium gluconate and 0.075 mg $SnCl_2.2H_2O$ in a freeze-dried form. Pertechnetate (370 Mbq, 0.5 ml) was mixed with this solution at room temperature for 10 minutes. 4 mg of a sodium dithiobenzoate and trithiobenzoate mixture in 0.5 ml of deionised water were finally added and heated for 30 minutes at 100°C. The radiochemical purity of the lipophilic complex was determined by thin layer chromatography and the migration was evaluated using a phospho-imager apparatus (Packard, Cyclone™ storage phosphor system). The chromatography was carried out on silica/alumina 60 F_{254} gel plates (Merck), using a solution of petroleum (6/4) as eluant (Rf 0.7). PEG_{1500} stearate nanocapsules were prepared in adding ^{99m}Tc–SSS complex to the raw materials . Its volume was deduced of the total amount of deionised water before dilution. The rest of the preparation process previously described remained then unchanged. The nanocapsules were finally dialyzed against distilled water (2 l), at room temperature during 2 hours.

Animal experimentation

Animal studies were carried out in accordance with the French regulation (law 0189.4 of January 24, 1990) on male Wistar rats (400-450 g). The ^{99m}Tc nanocapsules (500 µl, 0.2 MBq) were injected intravenously in the penile vein under gaseous isoflurane anesthesia. Blood samples (0.5 ml) were withdrawn on four animals intracardially at 15, 45, 90 min, 2, 4, 6, 16, 24, 41 and 48 h after injection. They were then introduced into vials, weighted and counted in a gamma counter (Packard Auto-Gamma 5000 series) for activity. Nanocapsule concentrations in blood at the various time points were calculated based on the assumption that blood represents 7% of rat body weight and were expressed as percent of the injected dose.

Data analysis

The pharmacokinetic data were analyzed by a noncompartmental analysis. The time corresponding to the disappearance of 50% of the total injected dose was determined by linear interpolation. The $AUC_{[0-24]}$ and $AUC_{[0-48]}$ calculations were performed by the trapezoidal method during the experimental period.

RESULTS AND DISCUSSION

Conductivity measurements

The conductivity study was performed on four formulations containing a constant PEG_{1500} stearate concentration (30% w/w) and different Fw. The conductivity evolutions were determined under magnetic stirring while the temperature was increased. Two different

behaviors were observed for systems with high and low water proportions. In order to describe these profiles, two representative preparations (Table II) among the four were chosen: the formulation A (Fw = 0.85) and the formulation B (Fw = 0.5).

Table II. Composition of preparations used for conductivity studies. The water fractions (Fw) for formulations A and B were 0.85 and 0.5, respectively. For each preparation, the NaCl concentration in aqueous phase was constant (89 g/l).

Quantity (g)	Formulation A	Formulation B
PEG_{1500} stearate	28.05	28.05
Lipoïd®	1.5	1.5
NaCl	5	2.92
Labrafac®	9.35	32.73
Deionized water	56.1	32.73

The conductivity of the system A as a function of the temperature was exhibited in Figure 1A. A constant conductivity around 33 mS/cm corresponding to a O/W emulsion was observed until 76°C. Then, the conductivity exhibited a variation zone between 76 and 90°C to attain afterwards a threshold value of 29 mS/cm. This significant conductivity above 90°C denoted an aqueous external phase. So, this behavior was not suggestive of a phase inversion but of a transition from a O/W emulsion to a w/O/W emulsion (17) by passing through a transitional zone characterized by conductivity changes (in gray on the graph). The proportion of inner water (Fw_{in}) contained in the multiple emulsion was calculated from the difference between the experimental conductivity and the expected one predicted by Bruggeman's law described below:

$$\kappa = \kappa_w \times F_W^{3/2} \qquad (5)$$

Where κ was the emulsion conductivity and κ_w, the aqueous phase conductivity with the same NaCl concentration. For temperatures below 76°C corresponding to a O/W emulsion, this equation was applied. The experimental conductivity was around 33 mS/cm and the conductivity calculated from Bruggeman's law was 33.7 mS/cm with κ_w = 43 mS/cm. On the contrary, after the transitional zone, the conductivity measured (29 mS/cm) was lower than the one determined from Bruggeman's law suggesting the presence of water within the oil drops. The inner water amount was determined from these conductivity differences to be about 8% (w/w) and the total internal phase of the w/O/W emulsion was around 25% (w/w).

The conductivity of the composition B containing equal amount of oil and water (Fw = 0.5) is illustrated in Figure 1B. As in the case of the system A, the conductivity stayed constant (i.e., 8.5 mS/cm) for temperatures below 75°C. This conductivity value was in agreement with the one determined with the Bruggeman's equation (i.e., 8.1 mS/cm with κ_w = 23 mS/cm). Between 75 and 95°C, a rapid conductivity decrease was observed until 0 mS/cm corresponding to an external phase inversion. Indeed, during the temperature increase, the inner oil phase moved to the external phase in crossing a transitional zone and the O/W emulsion became a W/O emulsion. This behavior is representative of classical PIT method used by Heurtault *et al.* (9).

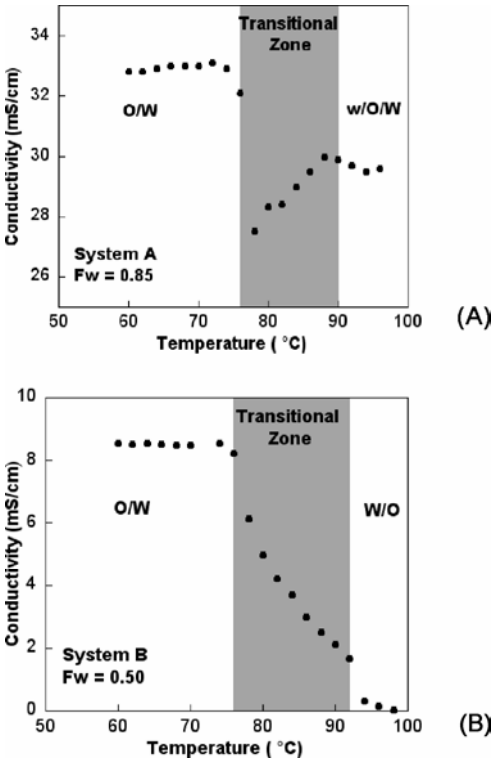

Figure 1. Evolution of the conductivity as the temperature increases. The PEG_{1500} stearate concentration was 30% (w/w). The conductivity variations occurred in the transitional zone represented in gray on the graphics. (A) For the system A composed of a water fraction (Fw) of 0.85, the crossing of the gray zone corresponded to a transition from a O/W emulsion to a multiple w/O/W emulsion. (B) For system with a lower water fraction (Fw = 0.5), the conductivity when temperature increased, sharply decreased up to 0 mS/cm denoting a phase inversion.

The conductivity changes observed for each formulation occurred at the same range of temperature, between 75 and 90°C into a transitional zone corresponding to the gray region in Figure 2. For emulsions composed of 30 to 65% of water, the interfacial curvature was inverted with temperature increase according to the Bancroft's rules (18) while crossing the transitional zone. Phase inversion was not possible for systems with higher water fraction because the oil amount is too small, and their interfacial curvature is opposite to the one

naturally induced by the non-ionic surfactant leading to multiple emulsion w/O/W (19). During the temperature cycles, these morphology changes were due to the variation of surfactant affinity for aqueous and oily phases defined by an empirical formulation variable so-called the hydrophilic-lipophilic balance (HLD). HLD > 0 and HLD < 0 correspond to surfactant affinity for oil and for water, respectively (20). A HLD value equal to 0 represents an optimum formulation where an uniform repartition of surfactant between the two phases occurs. A formulation-composition map introduced 20 years ago described the variations of the emulsion morphology according to the water fraction Fw and the HLD (21). Thus, making a correlation between this map and the figure 2, we hypothesized that the transitional zone corresponds to the optimum formulation of system with a HLD value close to 0. In this narrow domain, the spontaneous curvature of the PEG_{1500} stearate is near zero leading to the disappearance of droplets (22). Then, a bicontinuous microemulsion phase with excess water and /or oil takes place (23).

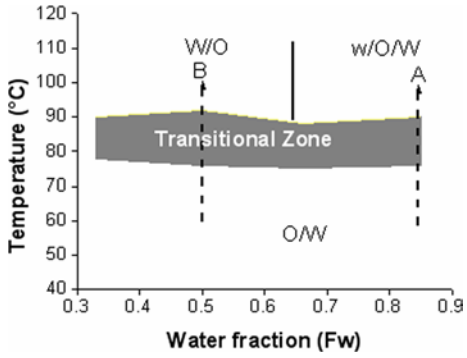

Figure 2. Morphology evolutions as a function of temperature for four systems containing 30% (w/w) of PEG_{1500} stearate and different water fractions: Fw = 0.33; 0.5; 0.66; 0.85. Transitional zone (in gray on the graphic) represented conductivity variations denoting a morphology change. For preparations composed of high water fractions (Fw > 0.6), temperature increase led to a transition from a O/W emulsion to a multiple w/O/W emulsion. For systems with lower water proportions, phase inversion took place in the transitional zone.

After three temperature cycles, the preparations A and B were diluted with cold water and were analyzed by photon correlation spectroscopy (PCS). Some nanocapsules exhibiting a small hydrodynamic diameter (26 nm) and a monomodal distribution (PI < 0.1) were produced from the composition A. On the contrary, despite the inversion phase observed during the temperature increase, no structure was obtained for the formulation B. These results could be correlated with the work of Wadledtyrf *et al.* (24) who had demonstrated that the occurrence of phase inversion was not a guaranty of the nanocapsule formation. Moreover, according to Morales *et al*. (25), the preparation of nano-emulsion implies a complete solubilization of the oil phase in a bicontinuous microemulsion, at PIT. Thus, we could suppose that for low Fw inducing phase inversion during temperature cycles, the oil is not entirely soluble. Concerning the standard nanocapsules developed by Heurtault *et al.,* their preparation required the crossing of a phase inversion zone between 70 and 85°C (9). These formulations composed of PEG_{660} hydroxystearate were characterized by lower water fractions leading to phase changes (8). Hence, for these systems, a significant oil solubilization occurs within the bicontinuous microemulsion .

Feasibility domain

A ternary diagram was established to define the constituents proportions of salted water, Labrafac® and PEG_{1500} stearate allowing the formation of submicron particles with a monodisperse size distribution. The formulation process, previously described, was applied for each point of the diagram (Figure 3). Particle size and distribution were then determined for each formulation. A feasibility domain, in gray on the graphic, corresponding to the formation of nanocapsules with a size comprised between 20 and 150 nm and an polydispersity index inferior to 0.3 was revealed. It is described as a parallelogram whose relative proportions are comprised between 20 and 40% (w/w) of non-ionic surfactant, 40 and

75% (w/w) of salted water and 5 and 20% of Labrafac®. Furthermore, as in the case of system A, we noticed that the particle formation occurred only at Fw above 0.65. Thus, we could suppose that for all the systems within the feasibility domain, the process of particle formation is similar to the one occurring during the preparation of A: no phase inversion but a transition from a W/O emulsion to a w/O/W emulsion by passing through a zone corresponding to a bicontinuous phase allowing the formation of nanocapsules.

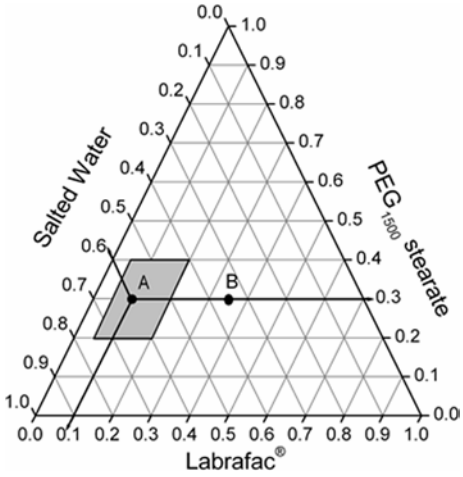

Figure 3. Ternary diagram allowing the determination of feasibility domain comprising nanocapsules with a size smaller than 150 nm and a polydispersity index inferior to 0.3. The composition A characterized by a water fraction Fw = 0.85, led to the formation of nanocapsules with a size around 26 nm and a monomodal distribution. On the contrary, the formulation B composed of a lower water amount (Fw = 0.5) was located outside of the feasibility domain.

In conclusion, the complete process leading to the nanocapsule formation is illustrated in Figure 4, where the morphology changes of systems occurring during the temperature cycle is exhibited. A transition from a O/W emulsion into a w/O/W is induced when the

temperature is increased to 95°C and vice-versa. Three temperature cycles were applied and a rapid cooling was performed inside the transitional zone.

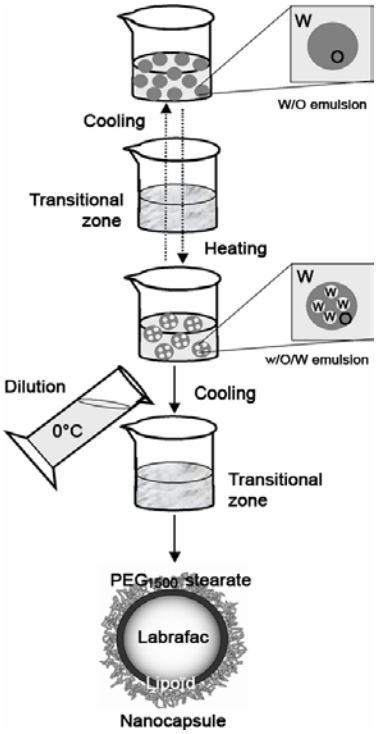

Figure 4. Formulation process of lipid nanocapsules composed of a high water fraction and description of morphology changes during the temperature cycles.

The previously mentioned system (A) was subjected to Cryo-TEM observation (Figure 5). The capsules analyzed by using electron beam at different angles (results not shown) were spherical. The size observed was around 25 nm, similarly to the hydrodynamic diameter determined by PCS (26 nm). The narrow size distribution characterized by both Cryo-TEM and PCS (PI < 0.1) contributed to improve the stability of the suspension by reducing the Ostwald ripening (6). This hypothesis was confirmed by macroscopic observations at 4°C and

37°C and at different pH (6, 7.4 and 8) showing a stability of the suspension over three months.

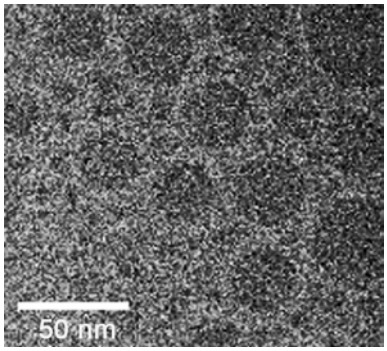

Figure 5. Cryo-TEM image of nanocapsules A.

The next studies have been carried out on the system A which exhibited a monomodal granulometric distribution and an interesting size (26 nm) for drug delivery. Each experiment was performed immediately after the preparation of nanocapsules.

Influence of the PEG_{1500} stearate on the stealthiness of nanocapsules

The capacity of PEG_{1500} stearate into the nanocapsule shell to reduce complement consumption has been exhibited in Figure 6. The results were then compared to a previous study of Vonarbourg *et al*. (26) concerning the evaluation of the complement activation by 50 nm PEG_{660} hydroxystearate nanocapsules. Complement activation expressed as CH50 units consumption was evaluated as the residual lytic capacity of the serum after contact with nanocapsules. A strong complement activation occurred in the presence of very small amount of Zymosan particles. On the contrary, nanocapsules did not induce any response of the complement system for a surface area lower than 1000 cm^2. For higher surface area, between 2000 and 5000 cm^2, the complement consumption took place reaching a maximum of 20%

and 15% for PEG_{1500} stearate and PEG_{660} hydroxystearate nanocapsules, respectively. This very weak complement activation observed for each type of nanocapsules was mainly due to the synergistic effect between the nanocapsule size and PEG layer. Indeed, the complement cascade involving a chain reaction of several complement components requires a certain local area on the nanocapsule surface. Ishida *et al.* (27) reported that the surface area of liposomes recognized by complement surface (SRC) was proportional to their diameter. Thus, the small size of nanocapsules limits the recognition of complement system (28). In addition to the size, the PEG layer surrounding the particle plays a major role in the weak complement activation observed in this study. The steric repulsion exerted by the PEG reduces adsorption of complement fragments (29). This protein-resistant effect was dependent on both polymer chain length and polymer surface density (1). However, Jeon *et al.* (30) demonstrated that the PEG surface density had a greater effect than length on steric repulsion.

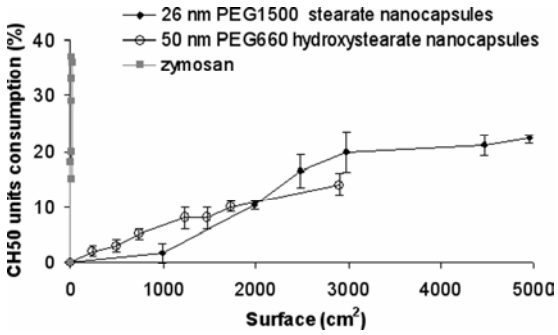

Figure 6. Consumption of CH 50 units in the presence of 26 nm PEG_{1500} stearate nanocapsules A , 50 nm PEG_{660} hydroxystearate nanocapsules and Zymosan particles as function of surface area.

In this context, the stearate PEG_{1500} density at the surface of nanocapsules has been assessed. The method used to evaluate the number of nanocapsules by volume unit (N_{caps}) has been developed by Minkov *et al.* (31) and was applied to PEG_{660} hydroxystearate nanocapsules. The authors hypothesized that the thickness of the particle shell was mainly influenced by the Lipoid® and corresponded to a 4.5 nm bilayer membrane. As a consequence, the shell thickness of 26 nm nanocapsules was estimated to about 4.5 nm and the diameter of the Labrafac® core (d) to about 17 nm. Moreover, the free PEG_{1500} stearate contained in suspension was separated by Sepharose CL-4B column chromatography. Its assessment was performed by a colorimetric method. Two peaks were observed from the chromatogram in Figure 7, the nanocapsules were first eluted, their diameter analyzed by dynamic light scattering was about 30 nm.

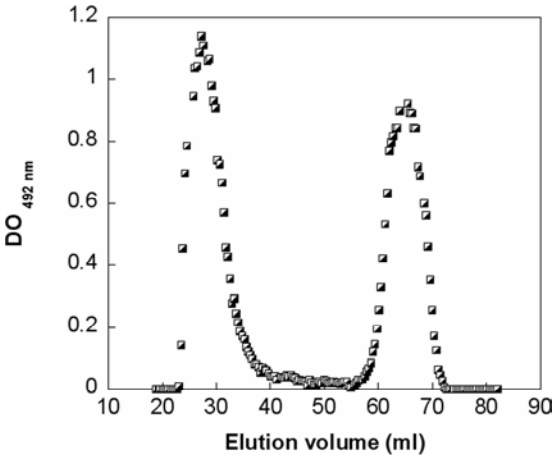

Figure 7. Elution profile of PEG_{1500} stearate nanocapsules A obtained by Sepharose CL-4B gel filtration chromatography. The first peak corresponded to nanocapsules and the second one to free PEG_{1500} stearate.

The free PEG_{1500} stearate corresponding to the second peak was composed of 43% (w/w) of the total amount of PEG contained in the nanoparticle suspension. Moreover, a negligible amount of PEG_{1500} adsorbed on the Sepharose gel was determined after chromatography. Thus, we could consider that the nanocapsule shell contained 57% (w/w) of the total PEG_{1500} stearate amount incorporated in the formulation. From this value ($P_{st\ PEG1500}$ = 0.57) and the other approximations, the surface of one PEG_{1500} stearate molecule confined into the nanocapsule corona ($S_{st\ PEG1500}$) was calculated by the following equation:

$$S_{st\ PEG1500} = \frac{(N_{caps} \times S_{caps})}{(N_{st\ PEG1500} \times P_{st\ PEG1500})} \quad (2)$$

Where $N_{st\ PEG1500}$ was the total number of PEG_{1500} stearate molecules per unit volume in the preparation, $P_{st\ PEG1500}$ was the proportion of surfactant molecules in the nanocapsule shell, S_{caps} was the surface area of one nanocapsule and N_{caps} was the number of nanocapsules per unit volume, N_{caps} was given by:

$$N_{caps} = \frac{N_{lab}}{n_{lab}} \quad (3)$$

Where N_{lab} was the total number of Labrafac® molecules per unit volume and n_{lab} was the number of Labrafac® molecules confined in the nanocapsule core, n_{lab} was given by:

$$n_{lab} = \frac{V_{core}}{V_{lab}} \quad (4)$$

Where V_{core} was the volume of the Labrafac® core and V_{lab} (32, 33) was the volume of one Labrafac® molecule. The numerical data used:

$P_{st\ PEG1500}$ = 0.57

$N_{st\ PEG1500} = 2.7 \times 10^{19}$

$S_{caps} = 2124\ nm^2$

$N_{lab} = 3.4 \times 10^{19}$

$V_{core} = 2572\ nm^3$

$V_{lab} = 1.54\ nm^3$

The surface covered by one molecule of PEG_{1500} stearate was then estimated to about 2.8 nm^2, corresponding to a distance *D* between two PEG chains of about 1.7 nm. From previous studies about interactions between protein adsorption and PEG density, the polymer surface density is believed to be sufficient to prevent the opsonization process. Indeed, Jeon *et al*. (30) demonstrated that *D* = 1 nm and *D* = 1.5 nm were the optimal distances to prevent the adsorption of small and large proteins, respectively. Furthermore, Gref *et al.* (3) have shown that nanospheres made from copolymer block PEG-PLA allowed a maximum protein repelling when *D* = 1.4 nm. A weak complement consumption has been obtained for nanocapsules possessing on their surface some PEG chains separated by a distance D of about 2 nm (34). Therefore, these results are in agreement with previous assessments of the complement consumption. Indeed, the complement system was weakly activated by the nanocapsules because of the optimal PEG_{1500} stearate density surface which prevented the adsorption of complement protein fragments. The presence of such a surfactant strongly reduced Van Der Vaals forces and increased steric repulsion between particles and proteins. Concerning the standard nanocapsules, the PEG density has not been assessed. However, Vonarbourg *et al. (35)* showed that PEG_{660} hydroxystearate was organized in brush conformation suggesting a high PEG density on the particle surface.

The electrokinetic properties of the PEG_{1500} stearate nanocapsules have also been assessed from a soft particle electrophoresis analysis (12). The electrophoretic mobilities of nanocapsules as a function of the salt concentration were observed in Figure 8. The best fit between experimental points and those corresponding to the theoretical model was obtained when ZN = -1.12×10^{6} $C.m^{-3}$ and $\lambda^{-1} = 1.0 \times 10^{-9}$ m with $R^2 = 0.97$. ZN corresponded to spatial charge density and λ^{-1} represented the depth of the layer accessible to the counterions. The correlation coefficient > 0.95 proved that nanocapsules verified the theory of soft particle. These results have been compared to the values obtained for standard lipid nanocapsules (LNC) with PEG_{660} hydroxystearate and the same Lipoïd® amount (Table III). We noticed that the charge density of PEG_{1500} stearate nanocapsules was three-fold higher than LNC. Vonarbourg *et al.* (35) demonstrated that PEG chains own negative dipolar charges playing a major role in the particle electrokinetic properties. So, this important ZN value could explain a higher PEG_{1500} stearate density into the nanocapsule shell. Furthermore, in spite of the longer PEG chain, the thickness of the accessible layer to Na^+ ions was thinner for PEG_{1500} nanocapsules than for LNC. We could hypothesize that λ^{-1} was weaker because of the short distance between two polymer chains, preventing the penetration of counterions into the accessible layer. In consequence, both ZN and λ^{-1} suggest, as the previous study, a high PEG_{1500} stearate density at the nanocapsule surface.

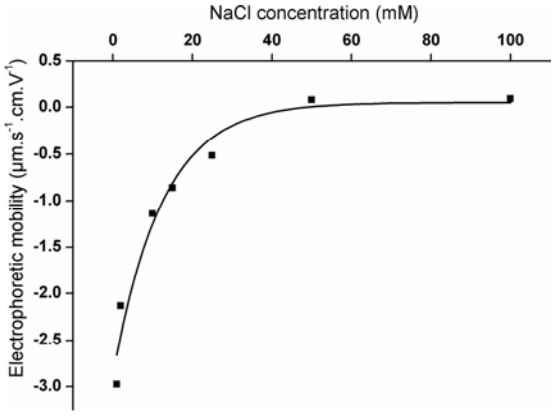

Figure 8. Evolution of the electrophoretic mobility as a function of NaCl concentration for PEG_{1500} stearate nanocapsules A.

Table III. ZN and 1/λ parameters for classic lipid nanocapsules prepared with PEG_{660} hydroxystearate and novel nanocapsules A composed of PEG_{1500} stearate. R^2 corresponded to the correlation coefficient obtained from the fitting.

Type of LNC	ZN (10^6 C.m^{-3})	1/λ (10^{-9} m)	R^2
PEG_{660} nanocapsules 20 nm	-0.32 ± 0.08	2.5 ± 0.5	0.99
PEG_{1500} nanocapsules 26 nm	-1.12 ± 0.08	1 ± 0.5	0.97

In a last part, the PEG_{1500} stearate nanocapsule pharmacokinetics were investigated in healthy rats in order to study the correlation between the low complement consumption by the particles and their circulation time in the bloodstream. The nanocapsule concentration in the bloodstream was determined versus time (Figure 9). The results were compared to a pharmacokinetic study realized on standard ^{99m}Tc-labelled nanocapsules (7). The free ^{99m}Tc–SSS complex in the suspension was previously removed by dialysis. The half disappearance time of PEG1500 stearate nanocapsules was observed around 5.5 h. Moreover, 20% of the

dose was still present in the blood 24 h after injection. These pharmacokinetic characteristics are more advantageous in comparison with standard LNC. Indeed, Ballot *et al.* demonstrated the rapid clearance from blood of nanocarriers composed of PEG_{660} hydroxystearate with a $t_{1/2}$ of 21 min. Although these capsules activate very weakly the complement system, they are rapidly recognized by the reticulo-endothelial system (RES) organs. These results could be explained by the change of physicochemical properties of standard nanocapsules after their intravenous administration. Indeed, we could hypothesize a possible leakage of PEG_{660} hydroxystearate from shell and / or a modification of the surfactant organization after injection in the blood. Moreover, by grafting DSPE-PEG_{2000} and DSPE-PEG_{5000} on the surface of these nanocapsules, Hoarau *et al.* (2) showed a significant improvement of their circulation time. This pharmacokinetic behavior was due to the length of PEG chains which reduced protein adsorption (36). Gref *et al.* (37) reported that the blood circulation time for nanospheres composed of PLA-PEG copolymers was significantly improved with increasing of molecular weight of PEG chains. Nevertheless, although the nanocapsules modified by Hoarau *et al.* were composed of PEG chains with a molecular weight superior to 1500 g/mol, their $AUC_{[0\text{-}24]\ blood}$ (796 %dose.h) corresponded to only 75% of that of PEG_{1500} stearate nanocapsules (1053 %dose.h). So, this difference suggested that the protein-resistant effect of the PEG density was greater than the length of the polymer chain.

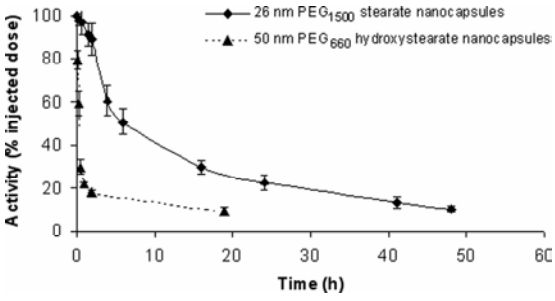

Figure 9. Blood concentration-time profile for PEG_{1500} stearate nanocapsule A. Formulation was intravenously injected at a dose of 500 µl nanocapsules/rat and evolution of blood activity was expressed in percentage of injected dose. The results were compared to 50 nm PEG_{660} hydroxystearate nanocapsules .

Moreover, this experiment allowed to correlate the low complement activation by the nanocapsules with their long-circulating properties. Indeed, by reducing the complement proteins consumption, the injected nanocapsules were not rapidly recognized by macrophages, increasing their residence time in the bloodstream (38, 39). Thus, decreasing the recognition by complement system, the PEG density and the size of colloids represent essential parameters to confer stealth properties to particles. Nevertheless, an other parameter, the lecithin presence, could be taken into account. Mosqueira *et al.* (40) has compared nanocapsules composed of PLA-$PEG_{20\ 000}$ copolymers and of lecithin with nanospheres without phospholipids and characterized by a higher PLA-$PEG_{20\ 000}$ density. The results showed that liver association of nanocapsules was 2- to 3-fold lower for nanocapsules in spite of their low PEG density. The authors have explained this phenomenon by the presence of lecithin that confers hydrophilic properties to the nanocapsule surface. Indeed, hydrophilic coating is known to decrease the opsonization process (41). However, their $AUC_{[0\text{-}24]\ blood}$ was sharply lower in comparison with PEG_{1500} nanocapsules (190 %dose.h) probably due to their larger size (197 nm). Consequently, the Lipoïd® inside the PEG_{1500} stearate shell could contribute to long-circulating properties. Furthermore, the lipidic nanocapsules show an other advantage for lipophilic drug delivery in comparison with submicron lipid emulsions. Lundberg *et al.*(42) reported that the rapid clearance of 44 nm nanoemulsion composed of triolein (TO), dipalmitoyl phosphatidylcholine (DPPC) and polyethylene glycol modified

phosphatidylethalonamine (PEG-PEG) was mainly due to the lypolis of the TO and not by uptake of whole emulsion droplets. In our case, the enzymatic degradation of nanocapsules was prevented by the polymeric shell protecting the oily core.

CONCLUSIONS

In this study, we have developed a new generation of nanocapsules composed of an oily core surrounded by a PEG_{1500} stearate layer with phospholipids and where no coating was necessary to make them stealthy. Their preparation did not allow the crossing of an inversion zone as in the case of the PIT method, but a transition from a O/W emulsion into a w/O/W multiple emulsion. *In vitro* and *in vivo* studies have revealed the long-circulating properties of these novel nanocapsules. Indeed, the complement system playing a major role in phagocytosis of colloidal drug carriers was only slightly activated in the presence of nanocapsules. This *in vitro* behavior also corroborated *in vivo* results. When nanocarriers were injected intravenously to rats, 20% of the total dose was still in the bloodstream 24h after administration. Hence, we could suppose that these capsules prevented the opsonization process, consequently reducing their uptake by the mononuclear phagocytic system. The optimal protein-resistant effect of PEG_{1500} stearate on nanocapsule surfaces was considered to be dependent on both chain length and surface density. The PEG_{1500} stearate density calculated on the nanocapsule surface was consistent with the literature findings. Indeed, the distance of 1.7 nm between each PEG chain corresponded to a threshold value for optimal protein resistance. Moreover, the small size (26 nm) and the presence of lecithin on the nanocapsule surface contribute also to their stealth properties.

So, these PEG_{1500} stearate nanocapsules characterized by long-circulating properties allowed a potential application for delivery of lipophilic drugs to solid tumors. Indeed, contrary to the standard colloidal carriers that were rapidly recognized by macrophages, the stealth properties of these nanocapsules could lead to an important accumulation of drugs in accessible sites.

ACKNOWLEDGEMENTS

The authors thank O. Lambert for Cryo-TEM studies (UMR-CNRS 5471, Bordeaux, F-33405 France ; Université de Bordeaux 1, Bordeaux, F-33405 France). We also want to thank Andréanne Bouchard (University of Technology, Delft, NL-2600 AA The Netherlands) for her valuable comments and suggestions. This work was supported by the departmental committee of Maine-et-Loire of "Ligue contre le cancer".

REFERENCES

1. C. Passirani and J. Benoit. Complement activation by injectable colloidal drug carriers. In R. I. Mahato (ed), *Biomaterials for Delivery and Targeting of Proteins and Nucleic Acids* (R. I. Mahato, ed), CRC Press, 2005, pp. 187-230.
2. D. Hoarau, P. Delmas, S. x. E. p. David, E. Roux, and J.-C. Leroux. Novel Long-Circulating Lipid Nanocapsules. *Pharmaceutical Research* **21**: 1783-1789 (2004).
3. R. Gref, M. Luck, P. Quellec, M. Marchand, E. Dellacherie, S. Harnisch, T. Blunk, and R. H. Muller. 'Stealth' corona-core nanoparticles surface modified by polyethylene glycol (PEG): influences of the corona (PEG chain length and surface density) and of the core composition on phagocytic uptake and plasma protein adsorption. *Colloids and Surfaces B: Biointerfaces* **18**: 301-313 (2000).
4. B. Heurtault, P. Saulnier, B. Pech, J. E. Proust, and J. P. Benoit. Properties of polyethylene glycol 660 12-hydroxy stearate at a triglyceride/water interface. *International Journal of Pharmaceutics* **242**: 167-170 (2002).
5. K. Shinoda. The stability of O/W Type Emulsions as Functions of Temperature and the HLB of Emulsifiers: The Emulsification by PIT-Method. *Journal of Colloid and Interface Science* **30**: 258-263 (1969).
6. T. Tadros, P. Izquierdo, J. Esquena, and C. Solans. Formation and stability of nano-emulsions. *Advances in Colloid and Interface Science* **108-109**: 303-318 (2004).
7. S. Ballot, N. Noiret, F. Hindre, B. Denizot, E. Garin, H. Rajerison, and J. P. Benoit. (99m)Tc/(188)Re-labelled lipid nanocapsules as promising radiotracers for imaging and therapy: formulation and biodistribution. *Eur J Nucl Med Mol Imaging* 1-6 (2006).
8. B. Heurtault, P. Saulnier, B. Pech, M.-C. Venier-Julienne, J.-E. Proust, R. Phan-Tan-Luu, and J.-P. Benoit. The influence of lipid nanocapsule composition on their size distribution. *European Journal of Pharmaceutical Sciences* **18**: 55-61 (2003).
9. B. a. Heurtault, P. Saulnier, B. Pech, J.-E. Proust, and J.-P. Benoit. A Novel Phase Inversion-Based Process for the Preparation of Lipid Nanocarriers. *Pharmaceutical Research* **19**: 875-880 (2002).
10. O. Lambert, N. Cavusoglu, J. Gallay, M. Vincent, J. L. Rigaud, J. P. Henry, and J. Ayala-Sanmartin. Novel organization and properties of annexin 2-membrane complexes. *J Biol Chem* **279**: 10872-82 (2004).
11. G. E. C. Sims and T. J. A. Snope. Method for the estimation of poly(ethylene glycol) in plasma protein fractions. *Anal. Biochem.* **107**: 60-63 (1980).
12. H. Ohshima. Dynamic Electrophoretic Mobility of a Soft Particle. *Journal of Colloid and Interface Science* **233**: 142-152 (2001).
13. V. Ducel, P. Saulnier, J. Richard, and F. Boury. Plant protein-polysaccharide interactions in solutions: application of soft particle analysis and light scattering measurements. *Colloids and Surfaces B: Biointerfaces* **41**: 95-102 (2005).
14. W. Wang, K. Okamoto, J. Rounds, E. Chambers, and D. O. Jacobs. In vitro complement activation favoring soluble C5b-9 complex formation alters myocellular sodium homeostasis. *Surgery* **129**: 209-219 (2001).
15. M. T. Peracchia, C. Vauthier, C. Passirani, P. Couvreur, and D. Labarre. Complement consumption by poly(ethylene glycol) in different conformations chemically coupled to poly(isobutyl 2-cyanoacrylate) nanoparticles. *Life Sci* **61**: 749-61 (1997).
16. F. Mevellec, F. Tisato, F. Refosco, A. Roucoux, N. Noiret, H. Patin, and G. Bandoli. Synthesis and characterization of the "sulfur-rich"

bis(perthiobenzoato)(dithiobenzoato)technetium(III) heterocomplex. *Inorg Chem* **41**: 598-601 (2002).

17. J. Allouche, E. Tyrode, V. Sadtler, L. Choplin, and J. L. Salager. Simultaneous conductivity and viscosity measurements as a technique to track emulsion inversion by the phase-inversion-temperature method. *Langmuir* **20**: 2134-40 (2004).
18. W. D. Bancroft. The theory of emulsification. *J. Phys. Chem.* **17**: (1913).
19. J. Allouche, E. Tyrode, V. Sadtler, L. Choplin, and J. L. Salager. Single and two steps emulsification to prepare a persistent multiple emulsion with a surfactant-polymer mixture. *Industrial and Ingineering Chemistry Research* **42**: 3982-3988 (2003).
20. S. Marfisi, M. P. Rodriguez, G. Alvarez, M.-T. Celis, A. Forgiarini, J. Lachaise, and J.-L. Salager. Complex emulsion inversion pattern associated with the partitioning of nonionic surfactant mixtures in the presence of alcohol cosurfactant. *Langmuir* **21**: 6712-6716 (2005).
21. J. L. Salager, M. Minana-Perez, M. Perez-Sanchez, M. Ramirez-Gouveia, and C. I. Rojas. SURFACTANT-OIL-WATER SYSTEMS NEAR THE AFFINITY INVERSION. PART III: THE TWO KINDS OF EMULSION INVERSION. *Journal of Dispersion Science and Technology* **4**: 313-329 (1983).
22. M. C. Elisabeth Van Hecke, Jérôme Poprawski, Jean-Marie Aubry, Jean-Louis Salager,. A novel criterion for studying the phase equilibria of non-ionic surfactant-triglyceride oil-water systems. *Polymer International* **52**: 559-562 (2003).
23. J. Poprawski, M. Catte, L. Marquez, M.-J. Marti, J.-L. Salager, and J.-M. Aubry. Application of hydrophilic-lipophilic deviation formulation concept to microemulsions containing pine oil and nonionic surfactant. *Polymer International* **52**: 629-632 (2003).
24. A. Wadle, T. Forster, and W. von Rybinski. Influence of the microemulsion phase structure on the phase inversion temperature emulsification of polar oils. *Colloids and Surfaces A: Physicochemical and Engineering Aspects* **76**: 51-57 (1993).
25. D. Morales, J. M. Gutiérrez, M. J. García-Celma, and Y. C. Solans. A study of the relation between bicontinuous microemulsions and oil/water nano-emulsion formation. *Langmuir* **19**: 7196-7200 (2003).
26. A. Vonarbourg, C. Passirani, P. Saulnier, and J. P. Benoit. Evaluation of pegylated lipid nanocapsules versus complement system activation and macrophage uptake. *J biomed Mater Res A* **In Press**: (2006).
27. T. Ishida, H. Harashima, and H. Kiwada. Liposome clearance. *Bioscience Reports* **22**: 197-224 (2002).
28. H. Harashima, K. Sakata, K. Funato, and H. Kiwada. Enhanced hepatic uptake of liposomes through complement activation depending on the size of liposomes. *Pharmaceutical Research* **11**: 402-406 (1994).
29. S. M. Moghimi and J. Szebeni. Stealth liposomes and long circulating nanoparticles: critical issues in pharmacokinetics, opsonization and protein-binding properties. *Progress in Lipid Research* **42**: 463-478 (2003).
30. S. I. Jeon, J. H. Lee, J. D. Andrade, and P. G. De Gennes. Protein--surface interactions in the presence of polyethylene oxide : I. Simplified theory. *Journal of Colloid and Interface Science* **142**: 149-158 (1991).
31. I. Minkov, T. Ivanova, I. Panaiotov, J. Proust, and P. Saulnier. Reorganization of lipid nanocapsules at air-water interface: I. Kinetics of surface film formation. *Colloids and Surfaces B: Biointerfaces* **45**: 14-23 (2005).
32. V. G. Ivkov and G. N. Berestovskii. [Conformation of hydrocarbon chains in a lipid bilayer]. *Biofizika* **24**: 633-6 (1979).

33. J. M. Smaby, W. J. Baumann, and H. L. Brockman. Lipid structure and the behavior of cholesteryl esters in monolayer and bulk phases. *J Lipid Res* **20**: 784-8 (1979).
34. M. Vittaz, D. Bazile, G. Spenlehauer, T. Verrecchia, M. Veillard, F. Puisieux, and D. Labarre. Effect of PEO surface density on long-circulating PLA-PEO nanoparticles which are very low complement activators. *Biomaterials* **17**: 1575-1581 (1996).
35. A. Vonarbourg, P. Saulnier, C. Passirani, and J. P. Benoit. Electrokinetic properties of noncharged lipid nanocapsules: influence of the dipolar distribution at the interface. *Electrophoresis* **26**: 2066-75 (2005).
36. A. Mori, A. L. Klibanov, V. P. Torchilin, and L. Huang. Influence of the steric barrier activity of amphipathic poly(ethyleneglycol) and ganglioside GM1 on the circulation time of liposomes and on the target binding of immunoliposomes in vivo. *FEBS Letters* **284**: 263-266 (1991).
37. R. Gref, Y. Minamitake, M. T. Peracchia, V. Trubetskoy, V. Torchilin, and R. Langer. Biodegradable long-circulating polymeric nanospheres. *Science* **263**: 1600-3 (1994).
38. J.-C. Leroux, E. Allemann, F. De Jaeghere, E. Doelker, and R. Gurny. Biodegradable nanoparticles -- From sustained release formulations to improved site specific drug delivery. *Journal of Controlled Release* **39**: 339-350 (1996).
39. J.-C. Leroux, F. De Jaeghere, B. Anner, E. Doelker, and R. Gurny. An investigation on the role of plasma and serum opsonins on the internalization of biodegradable poly(D,L-lactic acid) nanoparticles by human monocytes. *Life Sciences* **57**: 695-703 (1995).
40. V. C. F. Mosqueira, P. Legrand, J.-L. Morgat, M. Vert, E. Mysiakine, R. Gref, J.-P. Devissaguet, and G. Barratt. Biodistribution of long-circulating PEG-grafted nanocapsules in mice: Effects of PEG chain length and density. *Pharmaceutical Research* **18**: 1411-1419 (2001).
41. S. I. Jeon, J. H. Lee, J. D. Andrade, and P. G. De Gennes. Protein-surface interactions in the presence of polyethylene oxide. I. Simplified theory. *Journal of Colloid and Interface Science* **142**: 149-158 (1991).
42. B. B. Lundberg, B.-C. Mortimer, and T. G. Redgrave. Submicron lipid emulsions containing amphipathic polyethylene glycol for use as drug-carriers with prolonged circulation time. *International Journal of Pharmaceutics* **134**: 119-127 (1996).

CHAPITRE II

CONCEPTION ET CARACTERISATION DES IMMUNONANOCAPSULES

CONCEPTION ET CARACTERISATION DES IMMUNONANOCAPSULES

Ce chapitre décrit la conception des immunonanocapsules. Afin de conjuguer de façon covalente, les anticorps monoclonaux OX26 dirigés contre le récepteur à la transferrine ainsi que les fragments Fab', des fonctions maléimides liées au PEG_{2000}-DSPE, ont été incorporées sur la surface des NCL par une technique de « post-insertion ». Afin de mieux comprendre les paramètres influençant cette post-insertion, nous avons étudié l'adsorption du DSPE-PEG_{2000}-maleimide à l'interface huile/eau à partir d'un tensiomètre à goutte montante. L'influence de la température et des constituants localisés à la surface des nanocapsules lipidiques (Lipoïd® S75-3 et Solutol® HS15) a été recherchée à travers des mesures de pression superficielle. En considérant que les monocouches interfaciales étaient assimilables au solide de Maxwell généralisé, leur comportement rhéologique a été défini. Le but était de caractériser la cohésion des films de DSPE-PEG_{2000}-Maleimide adsorbés à l'interface huile/eau. Par extrapolation, des conclusions sur le mécanisme d'adsorption et la stabilité de l'ancrage du polymère bifonctionnel sur les nanocapsules lipidiques ont été tirées. Par ailleurs, pour permettre la réaction avec les fonctions maléimides, des groupements sulfhydryles ont été insérés dans la structure des OX26. Parallèlement, des fragments Fab' obtenus à partir de cette même immunoglobuline et portant au niveau de leurs chaînes lourdes, des fonctions thiols, ont été couplés aux nanocapsules. Après couplage, la taille des immunonanocapsules et la densité des ligands ont été caractérisées. La capacité de ces immunonanocapsules à s'associer spécifiquement aux cellules surexprimant le récepteur à la transferrine a ensuite été évaluée.

Design of novel targeted lipid nanocapsules by conjugation of whole antibodies and antibody Fab' fragments

A. Béduneau[1], P. Saulnier[1], F. Hindre[1], A. Clavreul[2] and J-P. Benoit[1, 3]

[1] Inserm, U646, Angers, F-49100 France ; Université d'Angers, Angers, F-49100 France

[2]Département de Neurochirurgie CHU d'Angers, Angers, F-49033 France

[3]To whom correspondence should be addressed. (E-mail: jean-pierre@univ-angers.fr)

Abstract

Immunonanocapsules were synthesized by conjugation to lipid nanocapsules (LNC) of whole OX26 monoclonal antibodies (OX26 MAb) directed against the transferrin receptor (TfR). The TfR is overexpressed on the cerebral endothelium and mediates the transcytosis mechanism. Fab' fragments known for their reduced interaction with the reticuloendothelial system, were also conjugated to LNC. To allow the coupling, lipid PEG_{2000} functionalized with reactive-sulfhydryl maleimide groups (DSPE-PEG_{2000}-maleimide) were incorporated into LNC shell by a post-insertion procedure, developed initially for the liposome pegylation. Interfacial model using the dynamic rising drop technique allowed to determine the parameters influencing the DSPE-PEG_{2000}-maleimide insertion and the quality of the anchorage. The heating was essential to promote both an important and stable adsorption of DSPE-PEG_{2000}-maleimide on LNC. In order to react with maleimide functions, OX26 MAb were thiolated whereas thiol residues on Fab' fragments were directly used. The number of ligands per nanocapsule was adjusted according to their initial amount in the coupling

reaction mixture, with densities comprised between 16 and 183 whole antibodies and between 42 and 173 Fab' fragments per LNC. The specific association of immunonanocapsules to cells overexpressing TfR has then been demonstrated, thus suggesting their ability to deliver drugs to the brain.

Keywords

Immunonanocapsules, OX26 monoclonal antibody, Fab' fragment, transferrin receptor, brain targeting, interfacial rheology.

1. Introduction

Colloidal drug carriers such as liposomes and nanoparticles, have been sharply used for systemic drug delivery. Packaged into the nanocontainer, the drug is protected from chemical and enzymatic degradations. The first generation of nanocarriers developed 40 years ago, is rapidly eliminated from the bloodstream by the reticuloendothelial system (RES). Consequently, the drug is only delivered into the liver and the spleen. In order to improve the vascular residence time of colloidal systems, hydrophilic and flexible polymers such as poly(ethylene) glycol (PEG) have been grafted on their surface, thus conferring a steric protection [1]. Their main therapeutic application concerned the drug delivery into the tumor sites thanks to the enhanced permeability and retention effect (EPR effect) [2].

Lipid nanocapsules (LNC) [3] are included in this generation of stealth nanovector. These colloidal carriers, in the nanometer size range, are produced using a solvent-free process with biocompatible excipients. They are formed by an oily core surrounded by a

hydrophilic surfactant, Solutol® HS15 (70% PEG_{660} hydroxystearate and 30% free PEG_{660}) conferring long-circulating properties [4] and inhibiting the P-glycoprotein efflux pump (P-gp) [5, 6]. LNC can be loaded with anti-cancer agents such as etoposide and paclitaxel and deliver efficiently drugs to glioma cells [7, 8].

As most of stealth nanocarriers, the therapeutic limitation of LNC is due to their non-specificity and their inability to cross the poorly permeable endothelia. Thus, these nanovectors can not be used for drug delivery to the central nervous system (CNS). Indeed, the blood brain barrier (BBB), which separates the blood and the cerebral parenchyma, is mainly composed of brain capillary endothelial cells (BCEC) sealed together by continuous tight junctions, decreasing drastically its permeability. In this context, included in a strategy of active targeting, the LNC have been modified using site-specific ligands to allow drug delivery to the cerebral nervous system (CNS). OX26 murine monoclonal antibodies (OX26 MAb) recognizing transferrin receptor (TfR), have been conjugated to LNC (OX26-immunonanocapsules). This antibody targets specifically the BCEC [9] thanks to a high concentration of TfR expressed on their luminal side and is able to cross the BBB via a receptor-mediated transcytosis mechanism [10]. The OX26 MAb binds to an extracellular domain of the TfR, distinct from the transferrin binding site, thus avoiding the competition with the endogenous transferrin in the circulation. Besides, the Fc part of the whole antibody is known to activate both the classic pathway of complement system and the macrophages, which bear Fc receptors on their surface. Consequently, the conjugation of entire antibodies may decrease significantly the vascular residence time of immunonanocapsules [11]. Thus, OX26 MAb Fab' fragments characterized by the absence of Fc part, have been also conjugated to LNC (Fab'-immunonanocapsules).

The feasibility and the potential of this active targeting strategy using nanocarriers have been already demonstrated. OX26-immunoliposomes have shown a promising interest

for the delivery of doxorubicin and daunomycine to the brain [12, 13]. The conception of OX26-PLA nanoparticles [14] and OX26-chitosan nanoparticles [15] have been achieved and the chitosan immunonanoparticles were able to reach cerebral parenchyma.

To allow the covalent attachment of site-directed biomolecules, bifunctional polymer, the distearoylphosphatidylethanolamine-PEG_{2000}-maleimide (DSPE-PEG_{2000}-maleimide) has been incorporated into the LNC shell. The maleimide functions react with sulfhydryl groups to form thioether bonds. In contrast to Fab' fragments which bear thiol residues on the intra-heavy, this reaction required the thiolation of OX26 MAb. Besides, the incorporation of DSPE-PEG_{2000}-maleimide was performed using a post-insertion procedure. This last method was initially developed for the pegylation of liposomes. It consisted in incubating particles in a micellar solution of PEG lipids. During the incubation, a transfer depending on the temperature occurred between phospholipids located into the liposomal system and lipid-conjugated polymers. Uster *et al.* [16] have shown that the incorporation rate of PEG_{1900}-DSPE into liposomes was close to the optimum value after an incubation at 60°C during 1 hr.

This work describes the synthesis of immunonanocapsules. Firstly, the DSPE-PEG_{2000}-maleimide incorporation into the LNC shell was characterized using an interfacial model. The temperature effect and the interactions between the bifunctional polymer and the components located at the LNC surface was studied. We could suppose that, as in the case of liposomes, the presence of phospholipids at the interface was necessary to allow the matter transfer. In contrast, the presence of Solutol® HS15 generating a steric barrier around the nanocapsule, could reduce the DSPE-PEG_{2000}-maleimide insertion. The polymer was adsorbed at pure O/W interface and on interfacial monolayers composed of Lipoïd® S75-3 or/and Solutol® HS15 at 25°C and 60°C, using a drop tensiometer. The superficial pressures were measured during 2hr-adsorption and after cooling from 60°C to 25°C. The rheological

behavior of these films was then determined using the generalized Maxwell model in order to determine the quality of the bifunctionnal polymer anchorage. This property was important to know whether the DSPE-PEG_{2000}-maleimide may bear whole OX26 MAb and Fab' fragments without desorption. Secondly, the conjugation of biomolecules on LNC was developed. Thiolation and fragmentation of MAb were performed to covalently attach antibodies and Fab' fragments on LNC surface. The influence of these chemical treatments on the recognizing activity of biomolecules has been studied by flow cytometry. The immunonanocapsules were then characterized through assessment of the ligand density and size measurements. Their ability to target cells overexpressing TfR has finally been verified by flow cytometry.

2. Materials and methods

2.1. Reagents

Lipoïd® S75-3 (soybean lecithin at 69% of phosphatidylcholine and 10% phosphatidylethanolamine) and the nonionic hydrophilic surfactant Solutol® HS15 were kind gifts from Lipoïd GmbH (Ludwigshafen, DE) and BASF (Ludwigshafen, DE), respectively. The lipophilic Labrafac® WL 1349 (caprylic-capric acid triglycerides) was generously provided by Gattefossé S.A. (Saint-Priest, FR). Due to the complex composition of these products, the brand names (Lipoïd®, Solutol® and Labrafac®) will be used in the following text. NaCl was purchased from Prolabo (Fontenay-sous-bois, FR). Deionised water was obtained from a Milli-Q plus® system (Millipore, Billerica, USA). DSPE-PEG_{2000}-maleimide was purchased from Avanti Polar Lipids (Alabaster, USA). $Na^{125}I$ and HiTrap® protein high performance column were provided by Pharmacia-Biotech (Uppsala, SE), Sepharose CL-4B,

dithiotreitol (DTT), sodium *meta*-periodate, Ellman's reagent, 2-mercaptoethylamine hydrochloride (MEA·HCl), Sephadex G-25 and G-50 were obtained from Sigma (Saint-Louis, USA). The PDPH [3-(2-pyridyldithio)propionyl hydrazide], the "ImmunoPure $F(ab')_2$ Preparation Kit" and Iodo-Gen Reagent (1,3,4,6-tetrachloro-3α-6α-diphenylglycouril) were purchased from PIERCE (Rockford, USA). The fluorescein isothiocyanate (FITC) - conjugated goat $F(ab')_2$ anti-mouse immunoglobulin (IgG) was provided by Dako (Glostrup, DK) and the mouse isotype control IgG2a were from BD Pharmingen (San Jose, USA).

2.2. Cells

The OX26 and Y3.AG.1.2.3. hybridoma cell lines were gifts of Canada Research Chair in Drug Delivery (Montreal, Canada). OX26 hybridoma was grown as a suspension culture in RPMI 1640 medium (Cambrex, Verviers, France), supplemented with 10% (v/v) fetal calf serum (FCS) and 1% (v/v) penicillin / streptomycin (Sigma, Saint-Louis, USA). Y3.AG.1.2.3. cells were cultivated in the same medium except that 1mM of sodium pyruvate (Cambrex) was added. Cells were maintained at 37°C in a humidified atmosphere containing 5% CO_2.

2.3. Interfacial properties

2.3.1. Preparation of solutions

Lipoïd® was dissolved in Labrafac® at 60°C under magnetic stirring at a concentration of 1.10^{-3} mM. Solutol® was dissolved in HEPES buffer (0.1M, pH=7.4) at room temperature under magnetic stirring at a 1.10^{-2} mM concentration. DSPE-PEG_{2000}-maleimide was

dissolved at 60°C in a HEPES buffer (0.1M, pH=7.4) under magnetic stirring at a concentration of 1mM.

2.3.2. Adsorption Kinetics

The adsorptions kinetics and rheological measurements were obtained at O/W interface by means of a rising drop tensiometer (TRACKER, ITConcept, Longessaigne, France). The oil was Labrafac® and the aqueous bulk phase was a HEPES buffer (0.1M, pH=7.4) at a volume of 5 ml. A drop was formed with an Exmire microsyringe (Prolabo, Paris, France) into an optical glass bowl (Hellma, France) containing the other phase. In our case, a rising drop of oil was formed. The axial symmetric shape (Laplacian profile) of the drop was analyzed using a video camera connected to a microcomputer.

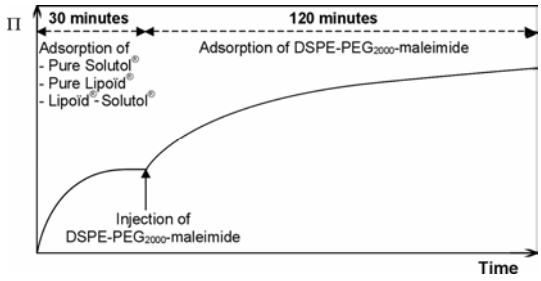

Figure 1. Protocol used to study the adsorption of DSPE-PEG_{2000}-maleimide on preformed monolayers at the O/W interface.

Solutol®, Lipoïd® and Solutol®-Lipoïd® were adsorbed at the O/W interface during 30 minutes, time necessary to reach an equilibrium surface pressure. A 50µl volume of DSPE-PEG_{2000}-maleimide solution at 1mM was then injected into the bulk phase leading to a final concentration of 1.10^{-2} mM. The bifunctional polymer was then adsorbed at 25°C and 60°C, during the same time than for the post-insertion procedure e.g., 2hrs. This protocol was described in Figure 1. In parallel, DSPE-PEG_{2000}-maleimide was adsorbed at the pure O/W interface during 2 hrs at the same temperatures. As controls, the adsorption kinetics of pure

Solutol®, pure Lipoïd® and Lipoïd®-Solutol® were performed during 2.5 hrs at the O/W interface at 25°C and 60°C. After the various adsorption kinetics at 60°C, a cooling until 25°C at a rate of 3-4 °C/min was realized and the superficial pressure was measured . The Labrafac® densities at 25°C and 60°C were 0.945 and 0.913, respectively, and the water densities were 0.999 and 0.983 at 25°C and 60°C, respectively. These values were taken into account for the calculation of surface pressures. The adsorption kinetics were performed keeping the surface area constant by using a stepping motor connected to a microcomputer to control the drop volume.

2.3.3. Rheological study

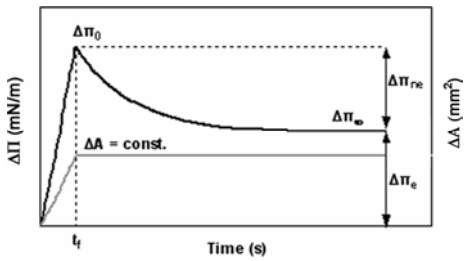

Figure 2. Fast compression and relaxation profile at constant area

The rheological behavior was studied by applying a monotonic compression of each surface layer [17]. Simultaneously, the area and the surface pressure were recorded as a function of time. Figure 2 represented the relative area variation (ΔA) and the total pressure changes (ΔΠ) during and after the compression of the interfacial film:

$$\Delta A = A(t) - A_i \quad (1)$$

$$\Delta \Pi = \Pi(t) - \Pi_i \quad (2)$$

The controlled perturbation was performed at a high constant velocity ($d/dt\ \Delta A(t)/A_i = U/A_i$ typically higher than 0.005 s^{-1}, with $\Delta\pi_{max} \leq 2.5$ mN/m) in order that the relaxation occurred only for $t > t_f$. Before the compression step, the pressure variations for each system were of $(1.0 \pm 0.8).10^{-4}$ $mN.m^{-1}.s^{-1}$ and $(6 \pm 1).10^{-4}$ $mN.m^{-1}.s^{-1}$ at 25°C and 60°C, respectively. Considering that the new equilibrium state was usually reached after 5 minutes, the pressure variations due to the adsorption of components at the O/W interface was considered as negligible during the relaxation. The equilibrium $\Delta\Pi_e$ and nonequilibrium $\Delta\Pi_{ne}$ contributions of stresses were calculated from the relaxation profile, using the following relationship:

$$\Delta\Pi_0 = \Delta\Pi_e + \Delta\Pi_{ne} \quad (3)$$

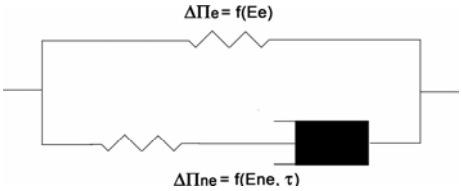

Figure 3. Mechanical model of the monolayer

$\Delta\Pi_e$ and $\Delta\Pi_{ne}$ can be described using a theorical model (generalized Maxwell) corresponding to a viscoelastic solid body (Figure 3) [18, 19]. $\Delta\Pi_e$ is related to the conservative part of the interfacial energy and depends on the equilibrium surface dilatational elasticity (E_e). This contribution is associated to the lateral interactions between the various molecules at the O/W interface. In contrast, $\Delta\Pi_{ne}$ is considered as a nonequilibrium part of the total pressure change and is in relation with both the viscoelastic part of the surface dilatational elasticity (E_{ne}) and the relaxation time of the monolayer (τ). $\Delta\Pi_{ne}$ was associated with the accumulation of energy during the compression. This accumulated energy was dissipated during the relaxation

through expulsions of molecular chains, leading to the reorganization of the monolayer [17, 20]. Some monolayers characterized in this study, exhibited features strongly elastic, not allowing the reproducible determination of τ and as a consequence, the calculations of E_e, and E_{ne}. Thus, only $\Delta\Pi_{ne}$ and $\Delta\Pi_e$ deduced from the relaxation profile, were used to characterize the rheological behavior of monolayers.

2.4. LNC preparation

The formulation of lipid nanocapsules (LNC) was based on a phase inversion process [3]. An O/W emulsion composed by Lipoid®, Labrafac® containing Solutol® and HEPES buffer (0.1M, pH 7.4) was prepared. During three cycles of progressive heating and cooling between 60 and 90°C, the O/W emulsion was inverted into W/O emulsion by passing through a phase inversion zone. At the last cycle, a fast cooling/dilution by cold HEPES buffer was performed to lead to the formation of LNC. The average hydrodynamic diameter and the polydispersity index (PI) of nanocapsules were determined by dynamic light scattering using a Malvern Autosizer 4700 (Malvern Instruments S.A., Worcestershire, UK) fitted with a 488 nm laser beam at a fixed angle of 90°. The PI was used as a measure of the size distribution. A small value of PI (< 0.1) indicates an unimodale size distribution, while a PI > 0.3 means a higher heterogeneity. The temperature of the cell was maintained at 25°C.

2.5. Post-insertion procedure to incorporate DSPE-PEG_{2000}-maleimide into LNC shell

DSPE-PEG_{2000}-maleimide was added to nanocapsule suspension in order to obtain a final concentration of 20 mM (above critical micellar concentration). LNC and

DSPE-PEG_{2000}-maleimide micelles were co-incubated 2 hrs at 60°C. The mixture was vortexed every 15 minutes and then quenched in an ice bath for 1 minute [21]. In order to study the temperature-effect on the incorporation of the DSPE-PEG_{2000}-maleimide, an incubation at 25°C was also performed. As controls, the same thermal treatments were applied to LNC suspensions without bifunctional polymer.

2.6. Assessment of DSPE-PEG_{2000}-maleimide into LNC shell

A Sepharose CL4-B column, equilibrated with HEPES buffer (pH 7.4, 0.1M), was used to separate the functionalized LNC from micelles composed of free DSPE-PEG_{2000}-maleimide. In each collected fraction, PEG concentration was determined from a colorimetric method taking advantage of the formation of a complex between PEG and iodine [22]. 50 µl of KI/I_2 solution was added to 100 µl of sample, then the turbidity of the mixture was detected spectrophotometrically at 492 nm. As blank, a second chromatography has been performed from standard LNC.

2.7. Preparation of OX26 MAb

OX26 MAb were purified from supernatant harvested from cultures of the OX26 hybridoma cell line by passage over a protein A high performance column followed by elution under acid conditions. The antibody concentration was determined from the absorbance at 280 nm (mg/ml = A_{280}/1.35) [23].

2.7.1. OX26 MAb Iodination

Iodo-Gen tubes were prepared according to manufacturer instructions and stored at -20°C. The OX26 Mab were dialyzed against HEPES (0.1M, pH 7.4) overnight at 0-4°C. A part of antibodies were mixed with 9.25 mBq of $Na^{125}I$ in Iodo-Gen tubes for 2h at room temperature. ^{125}I-OX26 was purified by passage over a Sephadex G25 gel filtration column, eluting with sodium acetate, (0.1M, pH 5.5). The radiolabeled antibodies amount in each fraction was determined by Cobra II Gamma Counter (Perkin Elmer, Boston, USA) and was added to the complete IgG solution.

2.7.2. OX26 MAb thiolation

An OX26 MAb solution at 2 mg/ml with trace amount of ^{125}I-OX26 was oxidized with sodium *meta*-periodate (15 mM) during 40 minutes in sodium acetate (0.1M, pH 5.5) [24]. This oxidation was carried out in the dark at 0 - 4°C to prevent side reactions. Excess periodate was quenched by reaction with glycerol for 15 minutes. After dialysis, the oxidized antibodies were reacted with PDPH (5 mM) [23] at room temperature under stirring for 5 h. The excess of cross-linker was isolated by Sephadex G-50 gel, equilibrated in sodium acetate (0.1 M, pH 4.5). Then, they were treated with DTT (25 mM) [25] in sodium acetate (0.1 M, pH 4.5) at room temperature for 20 minutes. The reaction mixture was applied to Sephadex G-50 column equilibrated in HEPES buffer (0.1M, pH 7.4). The protein concentration and DTT excess in each fraction were determined by absorbance at 280 nm. The fractions containing OX26 MAb were pooled together under nitrogen atmosphere.

A sulfhydryl assay was then performed to assess the number of thiol groups per protein. Ellman's reagent [26] was dissolved in a phosphate buffer (0.1M, pH 7.4) at a concentration of 4 mg/ml. Thiolated antibodies were concentrated using a nanosep 3K at

10000 g in order to exchange the HEPES buffer by the phosphate buffer. Ellman's reagent (80 µl) was added to thiolated OX26 MAb (800 µl) and allowed to incubate at room temperature for 20 minutes. Sulfhydryl levels were determined from the absorbance at 412 nm and using the following formula generated from a set of cysteine standards [27].

$$SH = \frac{1.1A_{412}}{14398C_{OX26}} \quad (1)$$

Where A_{412} is the absorbance at 412nm, C_{OX26} is the protein concentration and SH is the number of thiol equivalents.

2.8. Preparation of Fab' fragments

2.8.1. Preparation and iodination of F(ab')$_2$ fragments

F(ab')$_2$ were obtained using the "ImmunoPure F(ab')$_2$ Preparation Kit" following the instructions provided with the Kit. Briefly, a solution of OX26 MAb at 10 mg/ml in sodium acetate (0.02 M, pH 4.5) was mixed with immobilized pepsin at 37°C under magnetic stirring for 4 hrs. The F(ab')$_2$ fragments were then purified using an immobilized protein A column with a Tris-HCl buffer (0.1M, pH 8.6). A dialysis (50 K MW cut-off) was performed overnight at 4°C to remove the small Fc fragments.

The F(ab')$_2$ fragments were radiolabeled with 18.5 mBq of $Na^{125}I$ using the Iodo-Gen method as previously described. The ^{125}I-F(ab')$_2$ were purified by passage over a Sephadex G25 gel filtration column, eluting with sodium acetate (0.1M, pH 6.5).

2.8.2. Reduction of F(ab')$_2$ fragments

F(ab')$_2$ fragments were reduced using 50 mM MEA·HCl for 90 minutes at 37°C in acetate buffer (0.1M, pH 6.5). The reaction mix was passed through a Sephadex G-50 column equilibrated in HEPES (0.02M, pH 7.4) to remove the MEA excess. The collected fractions

containing Fab' fragments were determined from the absorbance at 280 nm. The fragments were then pooled together under nitrogen atmosphere.

The fragmentation was analyzed by sodium dodecyl sulfate-polyacrylamide gel electrophoresis (SDS-PAGE) under non-reducing conditions using 7.5% acrylamide/bisacrylamide.

2.9. Conjugation of thiolated OX26 MAb and Fab' fragments to LNC

Immediately after their preparation, antibodies were concentrated to obtain a final concentration comprised between 5 and 10 mg/ml. Under nitrogen atmosphere, functionalized LNC (1.2 mg) containing DSPE-PEG_{2000}-maleimide were incubated with different amounts of thiolated OX26 MAb and Fab' fragments overnight at room temperature on a rotating plate set at a low speed. Unbound biomolecules were removed by a Sepharose CL-4B column equilibrated with HEPES buffer (0.1M, pH 7.4). For each coupling procedure, an amount of functionalized LNC corresponding to the one used for the conjugation experiments was applied on the Sepharose column. A turbidimetry and a size analysis were performed for each fraction to detect the nanocapsules. They were then pooled and their concentration was assessed by turbidimetry measurement at 600 nm. This method was calibrated using a standard curve from nanocapsule suspension at different concentrations. The turbidity versus dried material concentration was linear from 0.04 to 2 mg/ml with a correlation coefficient (R^2) above 0.99. The LNC number by dried material was then estimated for each LNC preparation using the calculation developed by Minkov *et al.* [28]. Concentrations of about 3.2×10^{12} LNC/mg and 2.6×10^{12} LNC/mg were determined for nanocapsules incubated with thiolated MAb and Fab' fragments, respectively. The whole amount of particles applied to the CL-4B Sepharose column was collected after 20 ml of elution. During the chromatography,

each fraction was analyzed by gamma counting in order to evaluate the antibody and fragment amounts and by spectrophotometry at 600 nm to detect the nanocapsules. Making the ratio between the whole number of LNC collected during chromatography and the number of proteins eluted with the nanocapsules, the densities of antibodies and Fab' fragments conjugated to nanocapsules and the coupling yields were calculated. Moreover, the fractions containing immunonanocapsules were pooled and their size was analyzed by dynamic light scattering.

2.10. Flow cytometry analysis

Y3.AG.1.2.3. cells suspended in PBS containing 9% FCS and 0.02% sodium azide were incubated at 4°C for 1h with native or thiolated antibodies. A mouse IgG2a, an isotype non-specific antibody, was used as control. After washing, cells were stained with FITC-conjugated goat $F(ab')_2$ anti-mouse immunoglobulin for 30 min at 4°C. Following incubation, they were washed and fixed in 2% (v/v) formaldehyde. The same protocol was applied to $F(ab')_2$, Fab' fragments and immunonanocapsules. Stained cells were analyzed using FACScan flow cytometry with CellQuest software (Beckton-Dickinson, San Jose, USA). Fluorescence data were expressed as percentage (%) of positive cells.

3. Results and discussion

3.1. Characterization of the post-insertion of DSPE-PEG$_{2000}$-maleimide into LNC shell

To allow the conjugation of site-specific ligands, the LNC were functionalized with a maleimide sulfhydryl-reactive group using a post-insertion procedure. In order to study both the parameters playing a major role in the DSPE-PEG$_{2000}$-maleimide adsorption and the stability of polymeric coating, an interfacial model was developed by a drop rising technique.

3.1.1. Adsorption kinetics of DSPE-PEG$_{2000}$-maleimide at the O/W interface

During 2 hrs (time of the post-insertion procedure), DSPE-PEG$_{2000}$-maleimide was adsorbed at the pure O/W interface and on interfacial films composed of Solutol® or/and Lipoïd®. In this way, pure or mixed components of the LNC shell were already at the O/W interface before the DSPE-PEG$_{2000}$-maleimide adsorption. Hence, this protocol allowed to be close to the conditions of the post-insertion method. Controls were performed in the same conditions with pure Solutol®, pure Lipoïd® and Lipoïd®-Solutol®.

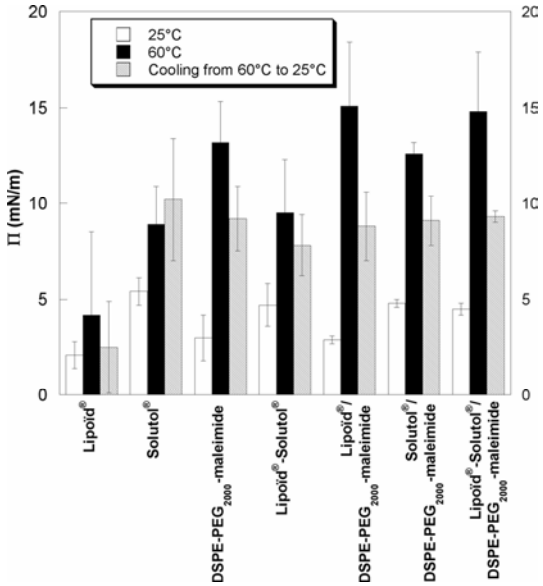

Figure 4. Superficial pressure Π of various monolayers adsorbed at the O/W interface at 25°C and 60°C. A cooling until 25°C was performed on the films formed at 60°C and the Π was then measured.

In Figure 4, a weak Π, about (3 ± 1.2) $mN.m^{-1}$, was obtained after the adsorption kinetic at 25°C of DSPE-PEG_{2000}-maleimide at the pure O/W interface. Moreover, at the same temperature, no significant change was observed after incorporation of the bifunctional polymer with the preformed interfacial films. Indeed, the Π values stayed very close to the controls performed without DSPE-PEG_{2000}-maleimide. These results suggested that, at 25°C, the bifunctional polymer was not adsorbed significantly at the O/W interface in presence of Lipoïd® and Solutol®. A superficial adsorption of this polymer on the monolayers that did not induce Π changes, could be also hypothesized.

In contrast, at 60°C, a high increase of Π was noticed after the adsorption kinetics of DSPE-PEG_{2000}-maleimide in comparison with controls. Following the incorporation of DSPE-PEG_{2000}-maleimide on the various preformed interfacial films, the Π values were in the same range than the one measured after adsorption of DSPE-PEG_{2000}-maleimide at the pure

O/W interface (13.2 ± 2.1) $mN.m^{-1}$. In order to influence the interfacial behavior of monolayers, the DSPE-PEG_{2000}-maleimide was not just adsorbed on the top of the monolayers but inserted inside of them, to be in contact with the oily phase. The polymer adsorption may also generate the desorption of Solutol® and Lipoïd® and thus, stay alone at the O/W interface. These results showed that the bifunctional polymer was strongly anchored into the interfacial film via its lipophilic part. Thus, the temperature increase from 25°C to 60°C enhanced significantly the adsorption of bifunctional polymer at the O/W interface. This phenomenon could be explained by the temperature-dependence of the PEG chain properties. Indeed, Van Hecke *et al.*[29] have shown a more lipophilic character of ethoxylated surfactant at higher temperature. Thus, at 60°C, the affinity of DSPE-PEG_{2000}-maleimide for the oil phase was improved, increasing consequently its adsorption at the O/W interface. Besides, the matter transfer between phospholipids located at the O/W interface and the bifunctional polymer into the bulk phase could not explain this incorporation. Indeed, the DSPE-PEG_{2000}-maleimide was adsorbed in a high proportion at the pure O/W interface. The presence of Solutol® did not reduce the DSPE-PEG_{2000}-maleimide incorporation. Π values in the same range were obtained after adsorption of polymer at pure O/W interface and on the Solutol® monolayer.

Π measurements were also performed at 25°C after cooling of the interfacial films formed at 60°C in order to check their stability. A Π decrease was noticed for almost all the monolayers excepted for the pure Solutol®. The DSPE-PEG_{2000}-maleimide / Solutol® and DSPE-PEG_{2000}-maleimide / Solutol®-Lipoïd® mixed monolayers were characterized by Π values in the same range as the controls performed with pure Solutol® and Solutol®-Lipoïd® as well as the monolayer of pure DSPE-PEG_{2000}-maleimide. Thus, it was not possible to determine the contributions of Solutol® and DSPE-PEG_{2000}-maleimide on the surface pressure of these mixed monolayers. Besides, both for pure DSPE-PEG_{2000}-maleimide and

Lipoïd®/DSPE-PEG_{2000}-maleimide monolayers, the values of the surface pressure were in the same range and stayed above the ones obtained after the adsorption kinetics at 25°C. These results showed that a part of bifunctional polymer was still adsorbed on pure O/W interface or on Lipoïd® monolayer after the cooling from 60°C to 25°C.

From adsorption kinetics, we may assume that the post-insertion procedure performed at 60°C promoted the incorporation of DSPE-PEG_{2000}-maleimide into the LNC. Moreover, the presence of Solutol® and Lipoïd® did not influence the insertion of bifunctional polymer. In order to study the quality and the stability of the bifunctional polymer anchorage, a rheological model has been applied to each monolayer adsorbed at the O/W interface.

3.1.2. Rheological study of DSPE-PEG_{2000}-maleimide monolayers at the O/W interface

A fast compression of monolayers was performed at the end of each adsorption kinetic. $\Delta\Pi_e$ and $\Delta\Pi_{ne}$ were then determined when the new equilibrium state was reached.

Table I. Ratio between $\Delta\Pi_{ne}$ and $\Delta\Pi_0$ for various monolayers adsorbed at the O/W interface. The interfacial films were formed at 25°C and 60°C. The rheological parameters were also determined after cooling until 25°C of monolayers obtained at 60°C.

	$\Delta\Pi_{ne}/\Delta\Pi_0$		
Monolayer	25°C	60°C	Cooling from 60°C to 25°C
Solutol®	58%	56%	51%
Lipoïd®	28%	27%	18%
DSPE-PEG_{2000}-maleimide	24%	0%	13%
Lipoïd®-Solutol®	54%	32%	36%
Lipoïd®/DSPE-PEG_{2000}-maleimide	49%	3%	14%
Solutol®/DSPE-PEG_{2000}-maleimide	56%	8%	20%
Lipoïd®-Solutol®/ DSPE-PEG_{2000}-maleimide	57%	17%	14%

Compared with controls, no change was observed at 25°C after incorporation of DSPE-PEG_{2000}-maleimide with pure Solutol® and with Solutol®-Lipoïd® films at the O/W interface (Table I). These monolayers were characterized by a viscoelastic behavior induced by the Solutol®. Indeed, their high $\Delta\Pi_{ne}$ values were very close to the one of pure Solutol® (58%). This rheological behavior of Solutol® had already been demonstrated by Heurtault *et al.* [30]. In the same conditions, the authors have shown that the nonequilibrium elasticity was higher that the equilibrium elasticity due to a fluid interface and to the expulsion of tensioactive molecules after compression. Moreover, the weak rheological contribution of bifunctional polymer on these monolayers was explained by its very low concentration at the O/W interface. These hypotheses were in agreement with the Π measurements showing that only the Solutol® influenced the Π of monolayers formed at 25°C. Besides, both DSPE-PEG_{2000}-maleimide and Lipoïd® adsorbed at the pure O/W interface were characterized by a weak $\Delta\Pi_{ne}$. In contrast, when the DSPE-PEG_{2000}-maleimide was adsorbed on the monolayer of Lipoïd®, a high increase of $\Delta\Pi_{ne}$ was observed. An additive contribution of the $\Delta\Pi_{ne}$ values obtained for the pure components could explain this behavior. Thus, neither the Lipoïd®, nor the DSPE-PEG_{2000}-maleimide governed the rheological behavior of mixed monolayers due to their too weak concentration at the O/W interface as seen through Π measurements .

After the adsorption at 60°C, the DSPE-PEG_{2000}-maleimide at the pure O/W interface, was characterized by a purely elastic behavior with a value of $\Delta\Pi_{ne}$ reaching 0. The rheological properties of preformed monolayers were strongly influenced by the presence of DSPE-PEG_{2000}-maleimide at 60°C. Indeed, compared with controls, a strong $\Delta\Pi_{ne}$ decrease was observed when the polymer was inserted into the interfacial films. The elastic feature of monolayers, generated by the bifunctional polymer insertion , may be explained according to two ways. We could hypothesize that the DSPE-PEG_{2000}-maleimide interacted with the Lipoïd® and the Solutol® located at the O/W interface, leading a strong cohesion of the mixed

monolayer (Figure 5B). The polymer may also expel the Lipoïd® and Solutol®, to finally stay alone at the O/W interface (Figure 5C).

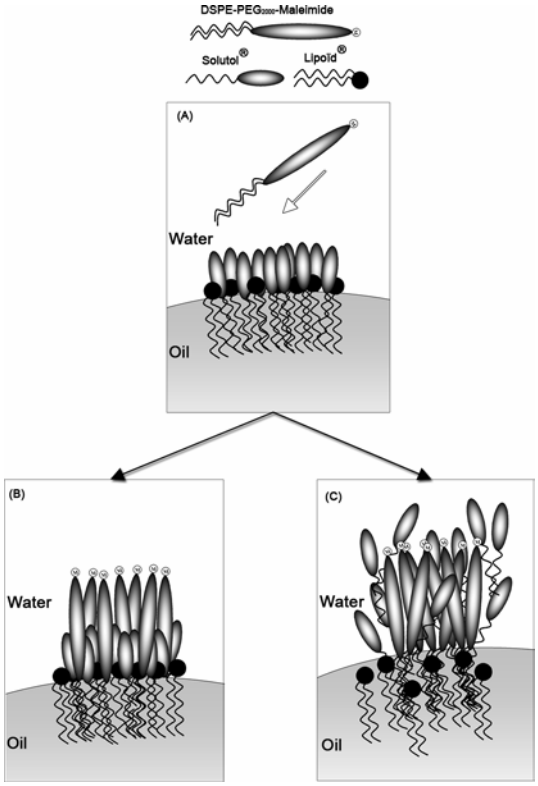

Figure 5. Schematic view of the interfacial organization of DSPE-PEG_{2000}-maleimide adsorbed at 60°C on a monolayer of Solutol®-Lipoïd® preformed at the O/W interface.
(A): Incorporation of DSPE-PEG_{2000}-maleimide after the formation of the monolayer of Solutol®-Lipoïd®. (B) Insertion of DSPE-PEG_{2000}-maleimide into the preformed monolayer and anchorage of its lipophilic part into the oil. (C) Adsorption of DSPE-PEG_{2000}-maleimide leading to the desorption of Solutol® and Lipoïd® from the interface.

After cooling of monolayers from 60°C to 25°C, the DSPE-PEG_{2000}-maleimide was always characterized by a mainly elastic rheological behavior with a $\Delta\Pi_{ne}$ value slightly increased (13%). This elastic behavior characterized also the monolayers in contact with

DSPE-PEG_{2000}-maleimide with $\Delta\Pi_{ne}$ comprised between 14% and 20%. The values of controls being higher, we assumed that the DSPE-PEG_{2000}-maleimide influenced still the rheological properties of monolayers after cooling. Thus, a high part of bifunctional polymer adsorbed at 60°C stayed strongly inserted at the O/W interface after the temperature decrease. Moreover, the elastic properties of monolayers demonstrated a strong cohesion and a stable anchorage of DSPE-PEG_{2000}-maleimide into the oil via its hydrophobic part. By extrapolation, we may assume that the polymeric coating on the LNC using the post-insertion procedure should be also characterized by elastic features. Consequently, the covalent conjugation of OX26 MAb and Fab'-fragments via the maleimide group should be possible without inducing desorption of bifunctional polymer from LNC shell.

3.1.3. Incorporation of DSPE-PEG_{2000}-maleimide into LNC shell

Post-insertion procedure was performed to incorporate DSPE-PEG_{2000}-maleimide into LNC shell. Bifunctional polymer at a concentration of 20mM, was incubated with preformed nanocapsules at 25°C and 60°C during 2 hrs and the size changes were summarized in Table II.

Table II. Size increase of LNC treated by the post-insertion procedure at 25°C and 60°C with or without DSPE-PEG_{2000}-maleimide.

DSPE-PEG_{2000}-maleimide concentration (mM)	Size increase (nm)	
	25°C	60°C
20	7.3 ± 3.8	24.9 ± 3.8
0	0.0 ± 2.7	2.9 ± 1.4

After the incubation of LNC with the bifunctional polymer, size increases of about 7.3 nm and 24.9 nm were observed at 25°C and 60°C, respectively. The evolution of the hydrodynamic diameter demonstrated the incorporation of DSPE-PEG_{2000}-maleimide into the LNC shell for each temperature. A very low size increase, of about 2.9 nm, was also observed for LNC control incubated at 60°C during 2 hrs, without bifunctional polymer. This phenomenon could be interpreted by a reorganization of the nanocapsule shell during heating. Nevertheless, it can not explain the highest size increase obtained after the thermal treatment at 60°C. The different size variations observed for each temperature, could be attributed to conformations of DSPE-PEG_{2000}-maleimide located on the LNC surface. Indeed, it has been reported in literature, that the overall length of a coiled and an extended PEG_{2000} chain was about of 5 and 10-15 nm, respectively [31]. Thus, from the size measurements, we assumed at 25°C, the DSPE-PEG_{2000}-maleimide was coiled leading to a "mushroom" conformation. In contrast, after the post-insertion at 60°C, the bifunctional polymer was more extended and organized in a structure close to the "brush" conformation. Moreover, concerning the liposomes, Uster *et al.* [16] reported that the PEG organization depended on the amount of DSPE-PEG inserted. Indeed, to reach surface density above 5 mol%, the $MPEG_{1900}$-DSPE was unfolded and consequently formed a polymeric "brush". Thus, the "brush" conformation of DSPE-PEG_{2000}-maleimide after the incubation at 60°C, was explained by a high polymer density. In contrast, the mushroom structure of DSPE-PEG_{2000}-maleimide at 25 °C, suggested a lower incorporation. These results were perfectly in agreement with interfacial model which demonstrated a higher insertion at 60°C. Besides, the brush conformation should optimise the accessibility of the maleimide reactive function.

The next experiments were realized with the LNC coated with DSPE-PEG_{2000}-maleimide using the post-insertion at 60°C.

3.1.4. Assessment of the DSPE-PEG$_{2000}$-maleimide incorporation into LNC shell

After the incubation of DSPE-PEG$_{2000}$-maleimide at 60°C, the mixture was applied to Sepharose CL-4B column in order to separate the micelles from the functionalized nanocapsules. The amount of PEG was detected by a colorimetric method with KI/I_2. In order to distinguish the free DSPE-PEG$_{2000}$-maleimide from the free Solutol® HS15 released from the LNC, native nanocapsules have been also applied to Sepharose column. The elution profiles of standard and functionalized nanocapsules were exhibited in Figures 6-A and 6-B, respectively.

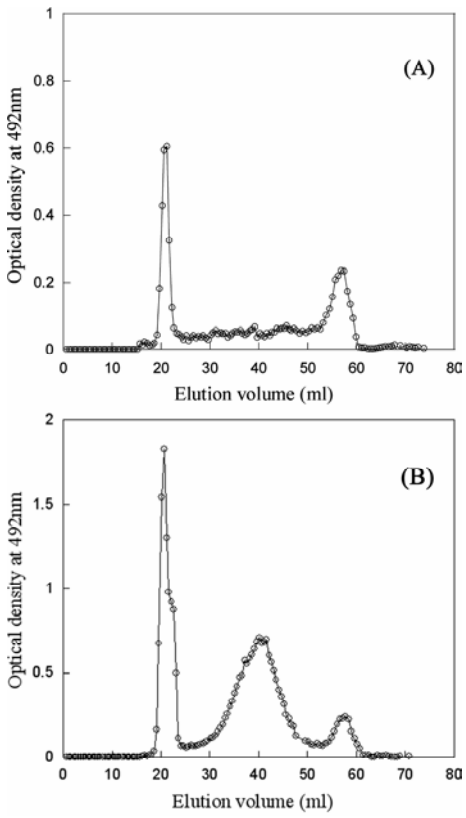

Figure 6. Elution profile of LNC obtained by Sepharose CL-4B gel filtration chromatography and quantification of the PEG release. (A) Native LNC. (B) Functionalized LNC coated with DSPE-PEG$_{2000}$-maleimide

A first peak (fractions from 19 to 24 ml) corresponding to the PEG into the nanocapsule shell was observed for each system. Nevertheless, the optical density was sharply higher for LNC treated by the post-insertion method (1.8) than for the standard ones (0.6). This difference demonstrates clearly that these nanocapsules have on their surface, a higher PEG concentration due to the DSPE-PEG_{2000}-maleimide incorporation. A second common peak was located in the last fractions (from 53 to 60 ml) corresponding to the Solutol® extracted from the nanocapsule corona. A third peak ranged from 29 to 49 ml was observed only on the elution profile of functionalized nanocapsules and could be assigned to free DSPE-PEG_{2000}-maleimide. By integrating this peak, an incorporation of less than 7% (mol/mol) versus the amount of components forming the LNC shell (Lipoïd® and Solutol®) was assessed. This value corresponds to a maximal number of 1100 maleimide groups per nanocapsule.

Post-insertion procedure performed at 60°C allowed the incorporation of DSPE-PEG_{2000}-maleimide without interference with the formulation process. Indeed, the addition of a PEG chain longer than 660 g/mol in the initial mixture would have probably increased the Phase Inversion Temperature (PIT) [32], thus preventing the nanocapsule formation from the classical formulation parameters. Furthermore, the presence of PEG_{2000} on the nanocapsule surface is supposed to enhance significantly their circulation time after intravenous administration. Indeed, this polymeric surfactant confers to nanocarriers a steric protection against plasma protein adsorption [33]. In this way, the clearance reduction should increase the probability that the conjugate will interact with the target tissue.

In order to generate a covalent link between the maleimide function anchored on the LNC surface and the OX26 MAb, sulfhydryl groups were inserted into the antibody structure.

3.2.Conjugation of OX26 MAb and Fab' fragments to functionalized nanocapsules

3.2.1. OX26 MAb thiolation

Antibody thiolation can occur through different ways. The most commonly used is the reaction between 2-iminothiolane and amine groups of antibodies [34]. Indeed, primary amines are abundantly found on exposed hydrophilic surfaces of proteins and this reaction requires only one step. However, this conjugation method can often cause partial or complete loss of recognition activity due to a modification of antigen binding site [35]. In order to prevent this effect, a thiolation procedure from the carbohydrate located within the Fc portion has been chosen. Briefly, sugar part of the OX26 MAb has been oxidized at 4°C in order to convert vicinal hydroxyls to aldehydes. Aldehydes were secondly reacted with the hydrazide group of PDPH leading to the formation of a hydrazone derivative. The 2-pyridyl-disulfide moiety of PDPH was then reduced with DTT in order to introduce sulfhydryl groups into proteins. This DTT treatment carried out at pH 4.5 during 20 minutes did not damage native disulfide bonds of the proteins [25]. The degree of thiolation was immediately estimated by reaction with Ellman's reagent. Sulfhydryl assays showed that thiolated OX26 MAb contained approximately 1 thiol equivalent.

In order to check preservation of the antigen binding site after thiolation procedure, the association of native and thiolated OX26 MAb with Y3.AG.1.2.3. cells overexpressing TfR has been studied by flow cytometry analysis. About 99% of total cells were bound to both native and thiolated antibodies (Figure 7). Moreover, fluorescence intensity of cells incubated with the thiolated OX26 MAb was close to the one obtained with native OX26. These results demonstrate clearly that the thiolation did not affect antigen specificity of the antibody.

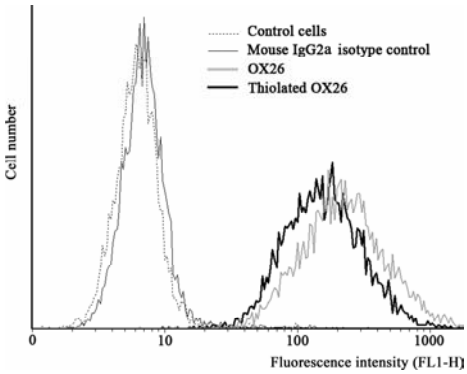

Figure 7. Cell association of the OX26 MAb after the thiolation procedure. Native and thiolated antibodies were incubated with Y3.AG.1.2.3. cells overexpressing TfR during 1 hr at 4°C. FITC-conjugated $F(ab')_2$ fragments was then added to cell suspension during 30 minutes at 4°C.

In parallel, OX26 MAb Fab' fragments were also prepared.

3.2.2. OX26 MAb fragmentation

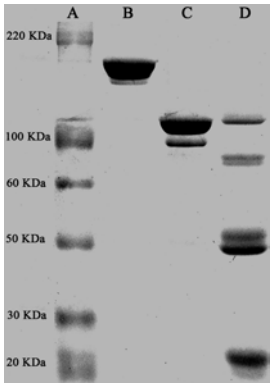

Figure 8. SDS-PAGE gel electrophoresis. (A) molecular weight marker (B) intact OX26 MAb. (C) $F(ab')_2$ fragments. (D) products obtained after reduction of $F(ab')_2$ with MEA·HCl

OX26 MAb were converted into $F(ab')_2$ fragments after 4 hrs digestion with pepsin. Fab' fragments were then generated by reduction with 50 mM MEA·HCl for 90 minutes. The

use of monovalent thiol compounds as reducing agents enables to reduce the risks of over-reduction leading to a majority of cleaved $F(ab')_2$ [36]. Fragmentation was checked by SDS-PAGE electrophoresis under non-reducing conditions (Figure 8). Intact antibodies (Figure 8B) and $F(ab')_2$ fragments (Figure 8C) were observed by single bands of apparent molecular weights of 150 KDa and 100 KDa, respectively. The Fab' fragments were observed through the band of 50 KDa molecular weight (Figure 8D). In addition, three other bands characterized by apparent molecular weights of 100 KDa, 70-80 KDa and 20-25 KDa, were noticed. The 20-25 KDa band was due to the presence of heavy chains fragments and light chains. It demonstrated a partial cleavage of disulfide bridges between the heavy and light chains, due to a prolonged exposure of $F(ab')_2$ fragments to MEA. The band at 100 KDa was explained by the unreacted $F(ab')_2$ or the formation of disulfide bonds between the Fab' fragments. Moreover, we may assume that the 70-80 KDa band revealed also an intermolecular disulfide bridge between Fab' fragments and light or heavy chains. In order to check the antigen activity of Fab' fragments, a flow cytometer analysis was performed (Figure 9). The binding degree of fragments with cells overexpressing the TfR was then studied.

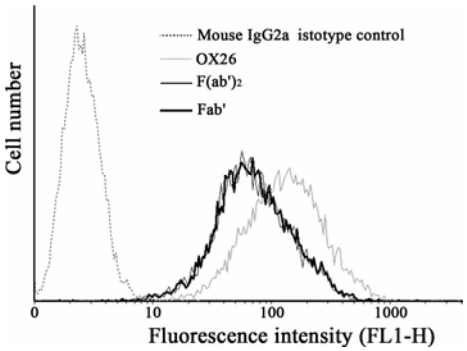

Figure 9. Cell association of whole OX26 MAb, F(ab')2 and Fab' fragments Native antibodies and fragments were incubated with Y3.AG.1.2.3. cells during 1 hr at 4°C followed by the staining with the FITC-probe during 30 min at 4°C.

As for the intact antibodies, 99% of cells incubated with F(ab')$_2$ and F(ab') were positively stained. The fluorescence level of cells labeled by these two fragment types was strictly equal. This result demonstrates both that the reduction step with MEA·HCl has preserved the antigen binding site of Fab' fragments and that the bivalent binding did not influence the cell association rate. Besides, the proportion of heavy and light chains observed by the SDS-PAGE electrophoresis was too weak to decrease significantly the association degree of Fab' fragments. Nevertheless, the cells labeled with the intact OX26 MAb were characterized by a fluorescence intensity above the other ones. This observation could be explained either by a slight alteration of the antigen binding site during the pepsin digestion or by a more intense staining of antibodies compared with fragments due to a high density of FITC probes on their Fc part.

The antigen binding sites of both thiolated antibodies and Fab' fragments were not affected, thus preserving their ability to target specifically the brain. They were then conjugated to functionalized LNC.

3.2.3. Coupling

Various amounts of thiolated [^{125}I]-labeled antibodies and [^{125}I]-labeled Fab' fragments were incubated with functionalized nanocapsules. During incubation, a reaction occurred between maleimide groups located on nanocapsule surface and thiol functions leading to formation of thioether bonds. This bond is stable in the *in vivo* conditions, in contrast with disulfide bonds, used in other conjugation procedures. Indeed, disulfide bonds are reduced in plasma, resulting in a release of antibodies from immunoliposomes [37]. The avidin/biotin technology represents also an alternative to the covalent attachment but induces an immune response [38].

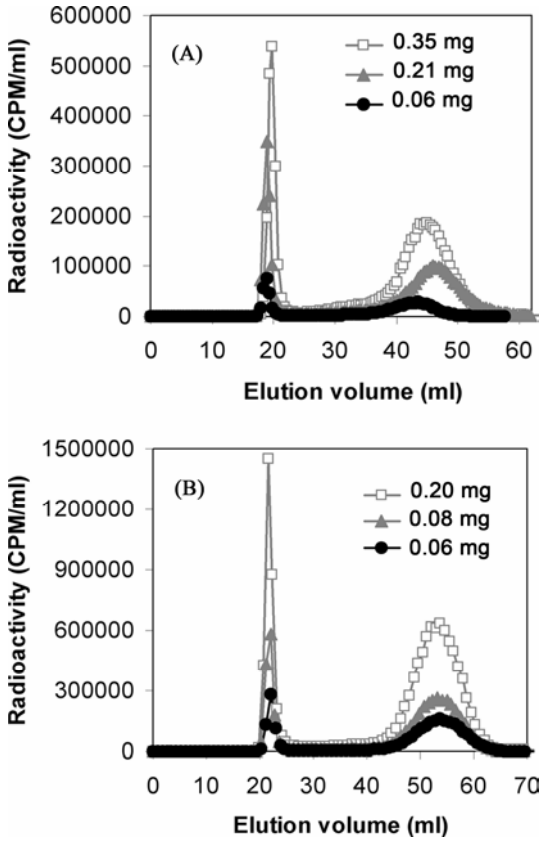

Figure 10. Elution profiles of immunonanocaspules after incubation of LNC with different amounts of ligands. (A) Separation of OX26-immunonanocapsules from unconjugated OX26 MAb. (B) Separation of Fab'-immunonanocapsules from unconjugated Fab' fragments.

After the coupling, the immunonanocapsules were separated from free [^{125}I]-OX26 and free [^{125}I]-Fab' by a Sepharose CL-4B gel filtration chromatography (Figure 10). At approximately 20 ml, the collected fractions contained both nanocapsules detected by turbidimetry at 600 nm and radiolabeled ligands, suggesting the formation of immunonanocapsules. Unconjugated antibodies were collected between 30 and 55 ml. Due to their lower size, the free fragments were eluted later, between 40 and 65 ml.

Table III. Size characterization of OX26-immunonanocapsules and Fab'-immunonanocapsules. Measurement of the immunonanocapsule size and evaluation of the ligand density for different coupling conditions. The total % of conjugated ligands was assessed after separation of immunonanocapsules from unconjugated ligands.

Coupling conditions			Immunonanocapsule characterization after chromatography				
Nanocapsule amount (mg)	Thiolated OX26 amount (mg)	Fab' amount (mg)	Hydrodynamic diameter (nm)	Polydispersity Index	Size increase (nm)	Approximate number of ligands per nanocapsule	Total % of conjugated ligands
1.2	0.06	/	149.5 ± 1	0.124 ± 0.014	12.6 ± 1.6	16	25
1.2	0.21	/	159.2 ± 0.3	0.07 ± 0.003	22.3 ± 0.9	64	29
1.2	0.35	/	167.3 ± 4.8	0.110 ± 0.021	30.4 ± 5.4	106	29
1.2	1.83	/	319.3 ± 125.2	0.941 ± 0.117	182.4 ± 125.8	183	10
1.2	/	0.06	145 ± 0.7	0.113 ± 0.014	7.2 ± 1.9	42	20
1.2	/	0.08	148.4 ± 2.8	0.090 ± 0.011	10.6 ± 4	74	25
1.2	/	0.20	157.7 ± 5.1	0.108 ± 0.001	19.9 ± 6.3	173	25

Ligand density per immunonanocapsule depended on the initial amount of whole OX26 MAb and Fab' fragments in the coupling reaction mixture. OX26-immunonanocapsules and Fab'-immunonanocapsules bore between 16 and 183 antibodies, and between 42 and 173 Fab' fragments per LNC, respectively (Table III). Coupling efficiencies of whole antibodies ranged from 10 to 29%, the 10 % value was obtained for the higher antibody concentration. Coupling yields of Fab' on the LNC were in the same range, comprised between 20 and 25 %. Despite a high number of sulfhydryl reactive maleimide group (1100) as compared to the number of site-specific ligands, coupling efficiency was far from 100%. This result has been also observed with liposomes decorated with OX26 MAb [12]. Indeed, by increasing molar ratios of phospholipids/MAb from 100/1 to 400/1, no variation of coupling efficiency was noticed, staying at around 10%. This could be explained by the steric barrier generated by PEG_{2000} as well as Solutol® located into the LNC shell.

Besides, the instability of maleimide functions [39] and the oxidation of sulfhydryl groups leading to the formation of intermolecular disulfide bonds, may also reduce the coupling efficiency. In order to check that OX26 MAb and Fab' fragments were covalently attached to the nanocapsules, incubations of functionalized nanocapsules with native antibodies or $F(ab')_2$ fragments were performed. The mixtures were then eluted in a Sepharose CL-4B column. The average percents of whole antibodies and $F(ab')_2$ fragments adsorbed onto nanocapsules were 8% and 2%, respectively. These values were lower than the ones obtained after coupling of thiolated antibodies and Fab' fragments, thus demonstrating the covalent coupling.

A size increase of LNC was noticed after the conjugation and depended on ligand density per immunonanocapsule. Except for the LNC incubated with the highest antibody amount, the hydrodynamic diameter increase of OX26-immunonanocapsules was comprised between 12 and 30 nm. These values were in accordance with apparent dimension of an antibody, in the range of 10-15 nm [40]. On the contrary, a surprising size (319.3 nm) was measured for the system in contact with a 1.83 mg antibody amount and the polydispersity index was close to 1, showing a heterogeneous distribution. This phenomenon has also been observed for a high density of antibodies grafted on liposomes [41]. This excessive size increase suggested an aggregation of immunonanocapsules, probably due to the formation of intermolecular disulfide bonds. This hypothesis explained also the weaker coupling yield obtained with this system. Concerning the Fab'-immunonanocapsules, the size increase was logically lower and comprised between 7 and 20 nm. These values were consistent with the 7 nm length of a Fab' molecule determined from X-ray crystallography data [42]. In contrast, no size increase was observed after incubation of native OX26 MAb and $F(ab')_2$, suggesting their spreading around the nanocapsule surface. Thus, size variations demonstrated clearly that the biomolecules were covalently attached at the distal end of the PEG_{2000}. Therefore,

their antigen binding sites were oriented towards the exterior medium, outside of the PEG coat. We can assume that this covalent coupling method enabled an adequate orientation of ligands for an optimal accessibility to antigen binding. However, this can also generate an enhanced exposure of the Fc region of the whole antibody, and consequently, increase recognition of OX26-immunonanocapsules by RES system. This effect should be sharply decreased with the Fab' fragments.

Adjusting the initial amount of site-specific ligands in the coupling reaction mixture, immunonanocapsules bearing between 30-40 OX26 MAb and Fab' fragments per nanocapsule were prepared for the cell association experiment. This density was considered as optimal for the brain targeting using 85 nm-immunoliposomes bearing whole antibodies [12]. Y3.AG.1.2.3. cells were incubated with immunonanocapsules labelled with a FITC-conjugated goat $F(ab')_2$ anti-mouse IgG and were then analyzed by flow cytometry. This procedure was also applied to free OX26 MAb and Fab' fragments in the same concentration range than for immunonanocapsules. In Figure 11, the staining of cells in contact with free site-specific ligands and immunonanocapsules were very close, thus suggesting the specific binding of immunonanocapsules to the transferrin receptors. Besides, no unspecific binding was observed from the controls performed with functionalized nanocapsules and IgG2a isotype.

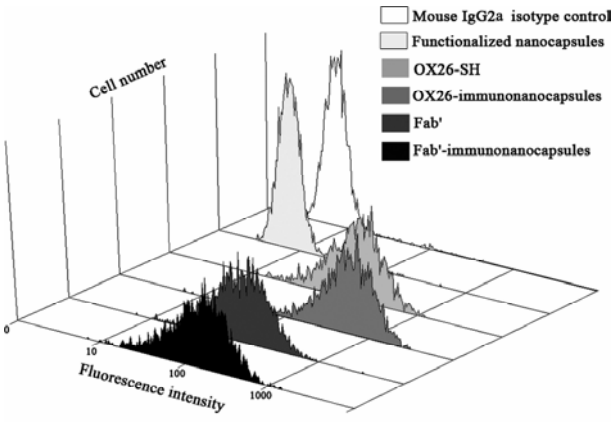

Figure 11. Fluorescent labeling of Y3.AG.1.2.3. after 1hr-incubation at 4°C with OX26-immunonanocapsules, Fab'-immunonanocapsules and free ligands.

4. Conclusions

Two novel types of immunonanocapsules have been developed by conjugation of thiolated OX26 MAb and Fab' fragments to LNC. The coupling of site-directed ligands required two steps. The first one was the incorporation of DSPE-PEG_{2000}-maleimide into LNC shell by a post-insertion procedure. An interfacial model showing the adsorption of DSPE-PEG_{2000}-maleimide at the O/W interface was used to understand the insertion mechanism and the interest of heating. The DSPE-PEG_{2000}-maleimide adsorption at the O/W interface being identical with or without Lipoïd®, the insertion was not explained by a matter exchange as in the case of liposomes but by a simple adsorption of amphiphilic polymer on the LNC. This adsorption depended on the temperature due to the lipophilic character of PEG_{2000} which increases significantly during heating. Moreover, the monolayers formed at 60°C were characterized by an elastic behavior. This interfacial property was conserved after cooling from 60°C to 25°C and demonstrated the stable anchorage of DSPE-PEG_{2000}-maleimide into the oil via its hydrophobic part. By extrapolation, we assumed that the polymeric coating on the LNC was also characterized by a strong cohesion, allowing the conjugation of site-specific ligands. The second step was the thiolation and the fragmentation of OX26 MAb followed by the reaction with maleimide functions. The modification of biomolecules did not affect their antigen binding, preserving their site-specific properties. Density of ligands per immunonanocapsule was adjusted by the proportion of OX26 MAb and Fab' fragments in the coupling reaction mixture. The size

increases observed after biomolecule conjugation demonstrated their location outside of the PEG brush, and therefore, their ideal orientation for the cell association. This hypothesis was verified by the i*n vitro* study which showed the specific binding of immunonanocapsules to TfR. Thus, this novel lipid nanovector exhibited promising features for the active transport of drugs to the brain.

Acknowledgments

We thank Myriam Moreau (Inserm U646, Angers, France) for her technical assistance. We are grateful to Dr Catherine Guillet (Service Commun de Cytométrie et d'Analyse Nucléotique, Angers, France) for skillful technical support. We thank also Professor Jean-Christophe Leroux for the gifts of OX26 and Y3.AG.1.2.3. hybridoma cell lines (Canada Research Chair in Drug Delivery, Faculty of Pharmacy, Montreal, Canada). This work was supported by the "ARC" (Association pour la Recherche sur le Cancer) and by the departmental committee of Maine-et-Loire of "La ligue contre le Cancer".

Bibliography

[1] Moghimi SM, Szebeni J. Stealth liposomes and long circulating nanoparticles: critical issues in pharmacokinetics, opsonization and protein-binding properties. Progress in Lipid Research 2003 2003/11;42(6):463-478.

[2] Maeda H, Wu J, Sawa T, Matsumura Y, Hori K. Tumor vascular permeability and the EPR effect in macromolecular therapeutics: a review. J Control Release 2000 Mar 1;65(1-2):271-284.

[3] Heurtault B, Saulnier P, Pech B, Proust J-E, Benoit J-P. A Novel Phase Inversion-Based Process for the Preparation of Lipid Nanocarriers. Pharmaceutical Research 2002 2002/06;19(6):875-880.

[4] Ballot S, Noiret N, Hindre F, Denizot B, Garin E, Rajerison H, et al. (99m)Tc/(188)Re-labelled lipid nanocapsules as promising radiotracers for imaging and therapy: formulation and biodistribution. Eur J Nucl Med Mol Imaging 2006 Feb 1:1-6.

[5] Buckingham LE, Balasubramanian M, Emanuele RM, Clodfelter KE, Coon JS. Comparison of Solutol HS 15, Cremophor EL and novel ethoxylated fatty acid sulfactants as multidrug resistance modification agents. International Journal of Cancer 1995 1995///;62(4):436-442.

[6] Coon JS, Knudson W, Clodfelter K, Lu B, Weinstein RS. Solutol HS 15, nontoxic polyoxyethylene esters of 12-hydroxystearic acid, reverses multidrug resistance. Cancer Research 1991 1991///;51(3):897-902.

[7] Lamprecht A, Benoit J-P. Etoposide nanocarriers suppress glioma cell growth by intracellular drug delivery and simultaneous P-glycoprotein inhibition. Journal of Controlled Release 2006 2006/5/15;112(2):208-213.

[8] Garcion E, Lamprecht A, Heurtault B, Paillard A, Aubert-Pouessel A, Denizot B, et al. A new generation of anticancer, drug-loaded, colloidal vectors reverses multidrug resistance in glioma and reduces tumor progression in rats. Mol Cancer Ther 2006 Jul;5(7):1710-1722.

[9] Jefferies WA, Brandon MR, Hunt SV, Williams AF, Gatter KC, Mason DY. Transferrin receptor on endothelium of brain capillaries. Nature 1984 Nov 8-14;312(5990):162-163.

[10] Friden PM, Walus LR, Musso GF, Taylor MA, Malfroy B, Starzyk RM. Anti-transferrin receptor antibody and antibody-drug conjugates cross the blood-brain barrier. Proc Natl Acad Sci U S A 1991 Jun 1;88(11):4771-4775.

[11] Philips NC, Dahman J. Immunogenicity of immunoliposomes: Reactivity against species-specific IgG and liposomal phospholipids. Immunology Letters 1995 1995///;45(3):149-152.

[12] Huwyler J, Wu D, Pardridge WM. Brain drug delivery of small molecules using immunoliposomes. Proceedings of the National Academy of Sciences of the United States of America 1996 1996///;93(24):14164-14169.

[13] Schnyder A, Krahenbuhl S, Drewe J, Huwyler J. Targeting of daunomycin using biotinylated immunoliposomes: Pharmacokinetics, tissue distribution and in vitro pharmacological effects. Journal of Drug Targeting 2005 2005///;13(5):325-335.

[14] Olivier J-C. Drug transport to brain with targeted nanoparticles. NeuroRx 2005 2005///;2(1):108-119.

[15] Aktas Y, Yemisci M, Andrieux K, Gursoy RN, Alonso MJ, Fernandez-Megia E, et al. Development and brain delivery of chitosan-PEG nanoparticles fnnctionalized with the monoclonal antibody OX26. Bioconjugate Chemistry 2005 2005///;16(6):1503-1511.

[16] Uster PS, Allen TM, Daniel BE, Mendez CJ, Newman MS, Zhu GZ. Insertion of poly(ethylene glycol) derivatized phospholipid into pre-formed liposomes results in prolonged in vivo circulation time. FEBS Letters 1996 1996/5/20;386(2-3):243-246.

[17] Saulnier P, Boury F, Malzert A, Heurtault B, Ivanova T, Cagna A, et al. Rheological model for the study of dilational properties of monolayers. Comportment of dipalmitoylphosphatidylcholine (DPPC) at the dichloromethane (DCM)/water interface under ramp type or sinusoidal perturbations. Langmuir 2001 2001///;17(26):8104-8111.

[18] Boury F, Ivanova T, Panaiotov I, Proust JE. Dilatational properties of poly(D,L-lactic acid) and bovine serum albumin monolayers spread at the air/water interface. Langmuir 1995 1995///;11(2):599-606.

[19] Boury F, Ivanova T, Panaiotov I, Proust JE. Dilatational properties of poly(D,L-lactic acid) and bovine serum albumin monolayers formed from spreading an oil-in-water emulsion at the air/water interface. Langmuir 1995 1995///;11(6):2131-2136.

[20] Raffournier C, Saulnier P, Boury F, Proust JE, Lepaul J, Erk I, et al. Oil/water "hand-bag like structures": How interfacial rheology can help to understand their formation? Journal of Drug Delivery Science and Technology 2005 2005///;15(1):3-9.

[21] Hoarau D, Delmas P, David S, Roux E, Leroux J-C. Novel long-circulating lipid nanocapsules. Pharmaceutical Research 2004 2004///;21(10):1783-1789.

[22] Sims GEC, Snope TJA. Method for the estimation of poly(ethylene glycol) in plasma protein fractions. Anal Biochem 1980;107:60-63.

[23] Ansell SM, Tardi PG, Buchkowsky SS. 3-(2-pyridyldithio)propionic acid hydrazide as a cross-linker in the formation of liposome-antibody conjugates. Bioconjug Chem 1996 Jul-Aug;7(4):490-496.

[24] Morehead HW, Talmadge KW, O'Shannessy DJ, Siebert CJ. Optimization of oxidation of glycoproteins: An assay for predicting coupling to hydrazide chromatographic supports. Journal of Chromatography A 1991 1991/12/20;587(2):171-176.

[25] Carlsson J, Drevin H, Axen R. Protein thiolation and reversible protein-protein conjugation. N-Succinimidyl 3-(2-pyridyldithio)propionate, a new heterobifunctional reagent. Biochem J 1978 Sep 1;173(3):723-737.

[26] Ellman GL. Tissue sulfhydryl groups. Arch Biochem Biophys 1959 May;82(1):70-77.

[27] Escobar NI, Morales A, Nunez G. Micromethod for quantification of SH groups generated after reduction of monoclonal antibodies. Nuclear Medicine and Biology 1996 1996/7;23(5):641-644.

[28] Minkov I, Ivanova T, Panaiotov I, Proust J, Saulnier P. Reorganization of lipid nanocapsules at air-water interface: I. Kinetics of surface film formation. Colloids and Surfaces B: Biointerfaces 2005 2005/9/25;45(1):14-23.

[29] Van Hecke E, Catte M, Poprawski J, Aubry J-M, Salager J-L. A novel criterion for studying the phase equilibria of non-ionic surfactant-triglyceride oil-water systems. Polymer International 2003 2003///;52(4):559-562.

[30] Heurtault B, Saulnier P, Pech B, Proust JE, Benoit JP. Properties of polyethylene glycol 660 12-hydroxy stearate at a triglyceride/water interface. International Journal of Pharmaceutics 2002 2002/8/21;242(1-2):167-170.

[31] Wong JY, Kuhl TL, Israelachvili JN, Mullah N, Zalipsky S. Direct measurement of a tethered ligand-receptor interaction potential. Science 1997 Feb 7;275(5301):820-822.

[32] Kunieda H, Shinoda K. Evaluation of the hydrophile-lipophile balance (HLB) of nonionic surfactants. I. Multisurfactant systems. Journal of Colloid and Interface Science 1985 1985/9;107(1):107-121.
[33] Passirani C, Benoit J. Complement activation by injectable colloidal drug carriers. In: Mahato RI, editor. Biomaterials for Delivery and Targeting of Proteins and Nucleic Acids: CRC Press, 2005. p. 187-230.
[34] Hatakeyama H, Akita H, Maruyama K, Suhara T, Harashima H. Factors governing the in vivo tissue uptake of transferrin-coupled polyethylene glycol liposomes in vivo. International Journal of Pharmaceutics 2004 2004///;281(1-2):25-33.
[35] Domen PL, Nevens JR, Mallia AK, Hermanson GT, Klenk DC. Site-directed immobilization of proteins. Journal of Chromatography 1990 1990///;510:293-302.
[36] Shahinian S, Silvius JR. A novel strategy affords high-yield coupling of antibody Fab' fragments to liposomes. Biochimica et Biophysica Acta (BBA) - Biomembranes 1995 1995/11/1;1239(2):157-167.
[37] Matzku S, Krempel H, Weckenmann HP, Schirrmacher V, Sinn H, Stricker H. Tumour targeting with antibody-coupled liposomes: failure to achieve accumulation in xenografts and spontaneous liver metastases. Cancer Immunol Immunother 1990;31(5):285-291.
[38] Phillips NC, Emili A. Immunogenicity of immunoliposomes. Immunology Letters 1991 1991/11;30(3):291-296.
[39] Xu L, Huang CC, Huang W, Tang WH, Rait A, Yin YZ, et al. Systemic tumor-targeted gene delivery by anti-transferrin receptor scFv-immunoliposomes. Molecular cancer therapeutics 2002 2002///;1(5):337-346.
[40] Schnyder A, Huwyler J. Drug transport to brain with targeted liposomes. NeuroRx 2005 2005///;2(1):99-107.
[41] Koning GA, Morselt HWM, Scherphof GL, Kamps JAAM, Gorter A, Allen TM, et al. Interaction of differently designed immunoliposomes with colon cancer cells and Kupffer cells. An in vitro comparison. Pharmaceutical Research 2003 2003///;20(8):1249-1257.
[42] Nezlin RS, Noll F. Structure and biosynthesis of antibodies. New York, 1977.

CHAPITRE III

EVALUATIONS *IN VITRO* ET *IN VIVO* DES IMMUNONANOCAPSULES

EVALUATIONS *IN VITRO* ET *IN VIVO* DES IMMUNONANOCAPSULES

La capacité des immunonanocapsules décrites dans le chapitre précédent, à reconnaître des cellules cibles a été évaluée dans cette dernière partie. En accord avec la littérature, une densité de 30 - 40 anticorps OX26 par immunonanocapsules a été choisie. Pour permettre une étude comparative, cette même densité a été fixée pour les immunonanocapsules décorées par les fragments Fab'. Leur association spécifique à des cellules surexprimant le récepteur à la transferrine a été vérifiée par cytométrie de flux. Des cellules endothéliales cérébrales de rat ont été utilisées afin de se rapprocher au mieux du modèle animal. En parallèle, les immunonanocapsules marquées par un complexe lipophile de ^{188}Re ont été injectées par la voie systémique, chez le rat sain. Leur temps de résidence vasculaire et leur accumulation au sein du cerveau ont alors été quantifiés. L'intérêt des immunonanocapsules sur le ciblage du cerveau ainsi que l'influence des fragments sur le temps de demi-vie des nanocapsules ont été décrits.

Brain targeting using novel lipid nanovectors

A. Béduneau[1], P. Saulnier[1], F. Hindre[1], A. Clavreul[1, 2], J-C. Leroux[3] and J-P. Benoit[1, 4]

[1] Inserm, U646, Angers, F-49100 France ; Université d'Angers, Angers, F-49100 France

[2]Département de Neurochirurgie CHU d'Angers, Angers, F-49033 France

[3] Canada Research Chair in Drug Delivery, Faculty of Pharmacy, C.P. 6128 Succ. Centre-ville, Montreal, QC, Canada H3C 3J7

[4] To whom correspondence should be addressed. (E-mail: jean-pierre.benoit@univ-angers.fr)

ABSTRACT

In order to improve the delivery of therapeutic agents to the brain, novel nanovectors have been developed. Lipid nanocapsules (LNC) were conjugated to whole murine anti-transferrin receptor antibodies (OX26 MAb) or Fab' fragments. The LNC included in this active targeting strategy, were characterized by a high capacity of lipophilic drug-loading and were able to inhibit the P-gp pump efflux sharply expressed on the cerebral endothelium. The specific association of immunonanocapsules to cells overexpressing the transferrin receptor such as the rat brain capillary endothelial cells, has been demonstrated. An enhanced brain uptake of immunonanocapsules was observed 24 h after their intravenous administration in rats. The weak interaction of Fab' fragments with the reticuloendothelial system (RES) allowed to prolong the vascular residence time of Fab'-immunonanocapsules. Nevertheless, their brain accumulation was lower compared with OX26-immunonanocapsules. Combining

the promising features of LNC and the site-specific property of OX26 MAb, this novel nanovector exhibits a great interest in the nanomedicine field.

MANUSCRIPT TEXT

The brain targeting of drugs is mainly limited both by the short plasmatic half-life of therapeutic molecules and by the weak permeability of the Blood Brain Barrier (BBB) separating the blood and the cerebral parenchyma.[1] In addition, BBB active drug efflux transporters of the ATP-binding cassette (ABC) restrict the delivery of a huge variety of drugs to the brain. The ABC transporter P-glycoprotein (P-gp) highly expressed on the cerebral endothelium plays a major role in this efflux mechanism.[2]

In order to enhance the accumulation of drugs into cerebral tissues, strategy of active targeting using nanocarriers has been developed. Colloidal drug carriers are conjugated to ligands, binding specifically to receptor overexpressed on BBB and triggering the receptor-mediated transcytosis.[3] The drug packaged into the colloidal carrier is protected from the host biological environment, improving its half-life and preserving its biological activity. In this way, we developed and evaluated a novel generation of targeted lipid nanocapsules for the delivery of lipophilic radionuclides and drugs to the brain. The strategy was based on the covalent coupling of murine OX26 monoclonal antibody (OX26 MAb) on lipid nanocapsules (LNC) (OX26-immunonanocapsules).

The LNC have been recently developed in our Laboratory. They exhibit promising features for the systemic drug delivery. In contrast to liposomal systems, they are produced by a solvent-free process[4] and they are physico-chemically stable (18 months at 4°C). Their size was adjustable between 20 and 100 nm by changing the component proportion during their fabrication. The Solutol® HS15 (hydroxystearate of poly(ethylene glycol), BASF,

Ludwigshafen, DEU) confined into the LNC shell confers a stealthiness and inhibits the P-gp efflux pump.[5, 6] Anti-cancer agents as well as radionuclides[7] were packaged into the oily core, with a high loading efficiency. Etoposide and paclitaxel-loaded LNC allowed to reduce significantly the growth of glioma cell lines due to the intracellular drug delivery combined with the P-gp inhibition. [8, 9]

In order to improve their distribution to the brain, murine OX26 MAb have been conjugated to LNC (OX26-immunonanocapsules). These immunoglobulins (IgG2a) bind to transferrin receptor (TfR) overexpressed on brain cerebral endothelial cells (BCECs)[10] and they trigger the receptor-mediated transcytosis across the BBB [11]. An alternative approach consisting of the conjugation of Fab' fragments instead of the whole OX26 MAb, has been also developed (Fab'-immunonanocapsules). Fragments allow to reduce significantly the reticuloendothelial system (RES) uptake via the Fc receptor-mediated mechanism, thus increasing the vascular residence time of immunonanocapsules.[12]

To allow the conjugation, LNC were functionalized by incorporating into the shell, a sulfhydryl-reactive maleimide group bound to a lipid PEG_{2000} (1,2-distearoyl-*sn*-glycero-3-phosphoethanolamine-N-[maleimide(polyethylene glycol)$_{2000}$], Avanti Polar Lipids, Alabaster, USA). In parallel, one thiol group was inserted on the OX26 MAb structure. The thiolation procedure occurred only on the carbohydrate part of the Fc portion, thus preserving its recognition activity. The fragmentation of OX26 MAb into Fab' fragments required two steps; digestion with pepsin to obtain $F(ab')_2$ fragments followed by a reduction reaction. Thiol residues were located on the intra-heavy chains of Fab' fragments. The antigen binding sites of thiolated antibodies and Fab' fragments were not affected.

The biomolecules were incubated with the functionalized LNC overnight at room temperature. The conjugation was then evaluated for different ligand concentrations. Except for the highest whole OX26 MAb concentration, the number of antibodies and Fab' fragments

per nanocapsule was directly proportional to the ligand concentration (Figure 1). For entire OX26 MAb concentration of 43 µmol/l, the relationship was not linear anymore due to the saturation of the LNC surface. Indeed, a sharp decrease of the coupling yield was observed at this concentration. The lower size of Fab' fragments enabled the conjugation of a high density of Fab' fragments (173) without inducing a saturation. Using the linear relationships, immunonanocapsules bearing between 30 and 40 ligands on their surface have been prepared for the next experiments. Indeed, in the literature, this value was considered as optimal for the targeting efficiency of 100 nm-immunoliposomes bearing whole antibodies.[13, 14] To study the influence of the Fc part, this ligand density was fixed for both OX26 and Fab'-immunonanocapsules.

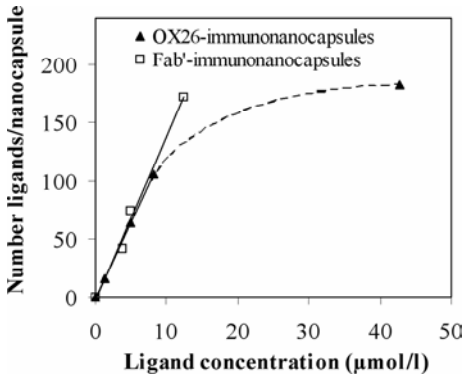

Figure 1. Relationship between the ligand concentration and the number of OX26 MAb and Fab' fragments conjugated to pegylated nanocapsules.

The specific association of immunonanocapsules with their target cells is a necessary requirement for this active targeting strategy. Y3.AG.1.2.3. cells (European Collection of Animal cell cultures, Wilshire, UK) and rat BCECs (Biopredic International, Rennes, FRA) overexpressing TfR were incubated with thiolated OX26 MAb, Fab' fragments and immunonanocapsules followed by a staining with FITC-conjugated goat F(ab')2 anti-mouse immunoglobulin (Dako, Glostrup, DNK). The cells were then analyzed by flow cytometry

(FACScan, Beckton-Dickinson, San Jose, USA). After incubation with the free antibodies, the staining of BCECs was significantly lower in comparison with Y3.AG.1.2.3 cells, suggesting a weaker TfR density on their surface (Figure 2A and 2C). This difference was also observed, in the same range, with the immunonanocapsules (Figures 2B and 2D), demonstrating clearly the binding of immunonanocapsules via the TfR. The fluorescence intensity shift between cells incubated with OX26-immunonanocapsules and Fab'-immunonanocapsules could be explained as a better cell association of the whole OX26 MAb. The Fc part of the antibody, playing the role of a spacer between the LNC surface and the recognizing site, could promote the binding to TfR. Besides, no cell was labeled after incubation with the isotype IgG2a control, demonstrating the absence of unspecific binding via the antibody. This result was in agreement with literature.[15]

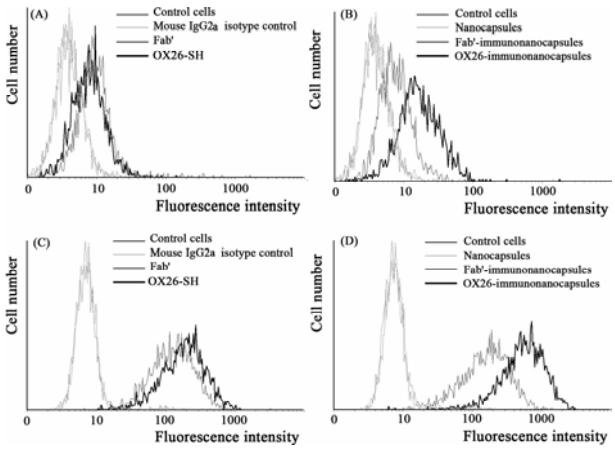

Figure 2. Fluorescent labeling of BCECs (Figures 2A and 2B) and Y3.AG.1.2.3. cells (Figures 2C and 2D) after 1hr-incubation at 4°C with OX26-immunonanocapsules, Fab'-immunonanocapsules, free OX26-SH and Fab' fragments. Ligands conjugated or unconjugated were stained with a FITC-probe. Controls were performed with IgG2a isotype or nanocapsules.

In order to study the biodistribution of immunonanocapsules in rat, LNC were labeled before the coupling, by incorporating into their oily core, a lipophilic complex: ^{188}Re $(S_3CPh)_2(S_2CPh)$ or ^{188}Re–SSS complex, prepared according to Mevellec *et al.*[16] *In vivo* studies were conducted in male Wistar rats (250g - 300g). The ^{188}Re immunonanocapsules were then injected intravenously in the penile vein under isoflurane anesthesia. Blood samples were collected intracardially at different times following injection. After 0.5hr, 1hr, 12hrs and 24hrs, animals were decapitated for removal of the brain. Blood and brain samples were weighted and counted in a gamma counter. Pharmacokinetic data were analyzed with the Kinetica 4.4.1 software (Thermo Electron Corporation, USA). The half-lives ($T_{1/2alpha}$ and $T_{1/2\ beta}$) were calculated using a bicompartmental analysis of % injected dose versus time profile. The mean residence time ($MRT_{[0-24]}$) was determined by dividing the area under the first moment curve ($AUMC_{[0-24]}$) by the area under the curve ($AUC_{[0-24]}$).

In table 1, $T_{1/2alpha}$ and $AUC_{[0-24]}$ were decreased after attachment of ligands to the nanocapsule surface, demonstrating a faster elimination of immunonanocapsules by the RES. Based on $T_{1/2alpha}$ and $AUC_{[0-24]}$ data, Fab'-immunonanocapsules were retained longer in the circulation compared with OX26-immunonanocapsules, due to the low RES uptake via the Fc receptor-mediated system of Fab' fragments. Nevertheless, the vascular residence time of OX26-immunonanocapsules seems sufficiently long to be in contact with the target tissue. Besides, very high $T_{1/2beta}$ values were obtained because of the residual concentration of LNC into the bloodstream.

Table 1. Pharmacokinetic parameters

Formulations	$T_{1/2alpha}$ (h)	$T_{1/2beta}$ (h)	$AUC_{[0-24]}$ (%dose.h)	$AUMC_{[0-24]}$ (%dose.h^2)	$MRT_{[0-24]}$ (h)
Functionalized nanocapsules	0.64 ± 0.24	19.60 ± 1.56	276 ± 46	2444 ± 328	8.8 ± 0.3
Fab'-immunonanocapsules	0.26 ± 0.01	29.99 ± 3.72	237 ± 28	2228 ± 267	9.4 ± 0.0
OX26-immunonanocapsules	0.18 ± 0.00	74.48 ± 27.21	167 ± 29	1717 ± 352	10.3 ± 0.4

The brain accumulation of immunonanocapsules and functionalized LNC was shown in Figure 3. Statistical analysis were performed using the Statview 5.0 software (SAS Institute, USA). The brain uptake of OX26-immunonanocapsules was significantly improved at each time, in comparison with the other preparations. The decrease of the injected dose observed for the short times (0.5hr and 1hr) was due to their elimination from the bloodstream. At 24 hrs, the brain uptakes of Fab'-immunonanocapsules and OX26-immunonanocapsules were, respectively, 1.5 and 2-fold higher than non-targeted nanocapsules. These results demonstrated clearly the ability of these novel nanovectors to target the brain via the TfR. Despite enhanced long-circulating properties, the brain targeting using the Fab'-immunonanocapsules was lower in comparison with OX26-immunonanocapsules. These results were in agreement with the *in vitro* study concerning the cell association of immunonanocapsules which hypothesized a better binding degree of OX26-immunonanocapsules. In contrast, Maruyama *et al.*[12] showed that the Fab' fragments allowed a higher extravasation of liposomes into solid tumor compared with whole IgG. However, the number of fragments per liposome (517) was sharply higher than for the immunonanocapsules (30-40). Based on both the *in vitro* and *in vivo* experiments, we may assume that this density value was not optimal for Fab' fragments. Thus, the increase of the fragment amount per immunonanocapsule should improve significantly the antigen binding and consequently, the brain targeting. Besides, the half-life of Fab'-immunoliposomes was

significantly higher (superior to 6 hrs) and consequently, also promoted the association with target cells.

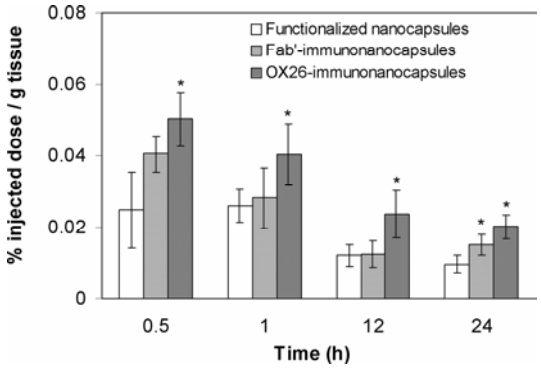

Figure 3. Brain targeting of ^{188}Re-functionalized nanocapsules and ^{188}Re-immunonanocapsules. Between 1.1 and 1.4 mg of ^{188}Re-LNC (≤ 5 µCi) was intravenously injected in the rat and the concentration of radioactivity in brain (% injected dose / g tissue) was determined at different times. Values represent means ± SEM (n = 5). * Statistical significance differences to pegylated nanocapsules (Mann-Whitney), $p<0.05$.

This study showed the profound impact of OX26 MAb and of Fab' fragments on the biodistribution of LNC. At 24 hrs-post-injection, the brain accumulation of OX26-immunonanocapsules and Fab'-immunonanocapsules was significantly enhanced compared with functionalized LNC. At the same density (30-40), the targeting of cerebral tissues with the OX26-immunonanocapsules was more efficient than with the Fab'-immunonanocapsules, despite their prolonged vascular residence time. These targeted nanocarriers represent a promising alternative to liposomal systems used in the strategy of active targeting. Besides, the coupling method could be applied to other site-specific ligands, enlarging hence the therapeutic applications of LNC.

ACKNOWLEDGMENTS

We thank Myriam Moreau (Inserm U646, Angers, France) and Pierre Legras (Animalerie Hospitalo-Universitaire, CHU, Angers, France) for their technical assistance. We are also grateful to Dr Catherine Guillet (Service Commun de Cytométrie et d'Analyse Nucléotique, Angers, France) for skillful technical support. We thank also Biopredic International (Rennes, France) for the gift of BCECs and Nathalie Rougier (Biopredic International, Rennes, France) for her advices concerning the cell culture. This work was supported by the "ARC" (Association pour la Recherche sur le Cancer) and by the departmental committee of Maine-et-Loire of "la Ligue contre le Cancer".

REFERENCES

(1) Gururangan, S.; Friedman, H. S., Innovations in design and delivery of chemotherapy for brain tumors. *Neuroimaging Clinics of North America* **2002,** *12*, (4), 583-597.

(2) Loscher, W.; Potschka, H., Blood-brain barrier active efflux transporters: ATP-binding cassette gene family. *NeuroRx* **2005,** *2*, (1), 86-98.

(3) Pardridge, W. M., Drug and gene targeting to the brain via blood-brain barrier receptor-mediated transport systems. *International Congress Series* **2005,** *1277*, 49-62.

(4) Heurtault, B.; Saulnier, P.; Pech, B.; Proust, J.-E.; Benoit, J.-P., A Novel Phase Inversion-Based Process for the Preparation of Lipid Nanocarriers. *Pharmaceutical Research* **2002,** *19*, (6), 875-880.

(5) Buckingham, L. E.; Balasubramanian, M.; Emanuele, R. M.; Clodfelter, K. E.; Coon, J. S., Comparison of Solutol HS 15, Cremophor EL and novel ethoxylated fatty acid sulfactants as multidrug resistance modification agents. *International Journal of Cancer* **1995,** *62*, (4), 436-442.

(6) Coon, J. S.; Knudson, W.; Clodfelter, K.; Lu, B.; Weinstein, R. S., Solutol HS 15, nontoxic polyoxyethylene esters of 12-hydroxystearic acid, reverses multidrug resistance. *Cancer Research* **1991,** *51*, (3), 897-902.

(7) Ballot, S.; Noiret, N.; Hindre, F.; Denizot, B.; Garin, E.; Rajerison, H.; Benoit, J. P., (99m)Tc/(188)Re-labelled lipid nanocapsules as promising radiotracers for imaging and therapy: formulation and biodistribution. *Eur J Nucl Med Mol Imaging* **2006**, 1-6.

(8) Lamprecht, A.; Benoit, J.-P., Etoposide nanocarriers suppress glioma cell growth by intracellular drug delivery and simultaneous P-glycoprotein inhibition. *Journal of Controlled Release* **2006,** *112*, (2), 208-213.

(9) Garcion, E.; Lamprecht, A.; Heurtault, B.; Paillard, A.; Aubert-Pouessel, A.; Denizot, B.; Menei, P.; Benoit, J. P., A new generation of anticancer, drug-loaded, colloidal vectors reverses multidrug resistance in glioma and reduces tumor progression in rats. *Mol Cancer Ther* **2006,** *5*, (7), 1710-22.

(10) Jefferies, W. A.; Brandon, M. R.; Hunt, S. V.; Williams, A. F.; Gatter, K. C.; Mason, D. Y., Transferrin receptor on endothelium of brain capillaries. *Nature* **1984,** *312*, (5990), 162-3.

(11) Friden, P. M.; Walus, L. R.; Musso, G. F.; Taylor, M. A.; Malfroy, B.; Starzyk, R. M., Anti-transferrin receptor antibody and antibody-drug conjugates cross the blood-brain barrier. *Proc Natl Acad Sci U S A* **1991,** *88*, (11), 4771-5.

(12) Maruyama, K.; Takahashi, N.; Tagawa, T.; Nagaike, K.; Iwatsuru, M., Immunoliposomes bearing polyethyleneglycol-coupled Fab' fragment show prolonged circulation time and high extravasation into targeted solid tumors in vivo. *FEBS Letters* **1997,** *413*, (1), 177-180.

(13) Huwyler, J.; Wu, D.; Pardridge, W. M., Brain drug delivery of small molecules using immunoliposomes. *Proceedings of the National Academy of Sciences of the United States of America* **1996,** *93*, (24), 14164-14169.

(14) Maruyama, K.; Takizawa, T.; Yuda, T.; Kennel, S. J.; Huang, L.; Iwatsuru, M., Targetability of novel immunoliposomes modified with amphipathic poly(ethylene glycol) s conjugated at their distal terminals to monoclonal antibodies. *Biochimica et Biophysica Acta (BBA) - Biomembranes* **1995,** *1234*, (1), 74-80.

(15) Schnyder, A.; Krahenbuhl, S.; Drewe, J.; Huwyler, J., Targeting of daunomycin using biotinylated immunoliposomes: Pharmacokinetics, tissue distribution and in vitro pharmacological effects. *Journal of Drug Targeting* **2005,** *13*, (5), 325-335.

(16) Mevellec, F.; Tisato, F.; Refosco, F.; Roucoux, A.; Noiret, N.; Patin, H.; Bandoli, G., Synthesis and characterization of the "sulfur-rich" bis(perthiobenzoato)(dithiobenzoato)technetium(III) heterocomplex. *Inorg Chem* **2002,** *41*, (3), 598-601.

DISCUSSION GENERALE

Les premiers vecteurs colloïdaux développés il y a plus de 40 ans pour la vectorisation de molécules actives, tels que les liposomes et les nanoparticules, étaient très rapidement pris en charge par le système immunitaire. De ce fait, ces systèmes particulaires ne pouvaient délivrer des médicaments qu'au niveau du foie et de la rate [1]. Afin de modifier leur distribution tissulaire, la surface des particules a été recouverte par des polymères hydrophiles et flexibles comme le polyéthylène glycols (PEG). Ce recouvrement hydrophile génère autour de la surface une barrière stérique, empêchant l'adsorption d'opsonines, protéines plasmatiques reconnues par des récepteurs spécifiques situés sur les macrophages, et augmentant par conséquent leur temps de résidence vasculaire. Ces nanovecteurs furtifs étaient ainsi capables de traverser les endothéliums vasculaires à perméabilité accrue comme ceux localisés au niveau des tumeurs (néovaisseaux). Cependant, leur biodistribution s'avérait aléatoire et le franchissement de certaines barrières biologiques très peu perméables comme la barrière hémato-encéphalique (BHE) était difficile à moins d'y associer un agent osmotique ou vasoactif. Ainsi, s'inscrivant dans une stratégie de ciblage actif, une troisième génération de vecteurs de médicament a été développée. Ces systèmes particulaires intelligents ont été mis au point dans le but d'administrer spécifiquement des molécules actives à des endroits précis de l'organisme. Pour ce faire, des biomolécules, reconnaissant des antigènes hautement exprimés sur la membrane de cellules cibles, ont été greffées sur la surface de liposomes et de nanoparticules furtifs.

Dans ce contexte, nous avons développé de nouveaux vecteurs particulaires dans le but d'administrer de façon spécifique des molécules actives au sein des tissus cérébraux. Ces systèmes particulaires appelés immunonanocapsules sont constitués de nanocapsules lipidiques (NCL) pégylées, décorées par des anticorps monoclonaux ou des fragments reconnaissant des récepteurs surexprimés sur les cellules endothéliales de la BHE.

I Conception de nouvelles nanocapsules lipidiques furtives

La furtivité constitue une des caractéristiques essentielles que doivent posséder les nanoparticules utilisées dans la stratégie de ciblage actif. En effet, l'augmentation du temps de résidence vasculaire favorise la reconnaissance des tissus cibles par les systèmes colloïdaux. Ballot *et. al* [2] ont montré que les NCL natives étaient caractérisées par un temps de demi-vie de 20 minutes. Cependant, ces nanocapsules sont moins furtives que les liposomes utilisés dans les stratégies de ciblage actif (demi-vie de plusieurs heures) [3, 4]. Ainsi, une nouvelle génération de NCL a été mise au point en substituant l'hydroxystéarate de PEG_{660} par le stéarate de PEG_{1500}. La chaîne polymérique est plus longue de façon à améliorer la répulsion stérique générée par le PEG, empêchant l'adsorption d'opsonines, activatrices du système immunitaire [5].

1) Formulation des nanocapsules de stéarate de PEG_{1500}

Comme pour les NCL conventionnelles, la formulation est basée sur un procédé dit de « basse énergie » nécessitant trois cycles de chauffage et refroidissement. Cette méthode utilise les propriétés thermosensibles des surfactants non-ioniques pegylés. Une variable de formulation, le DHL (Déviation Hydrophile/Lipophile) décrit l'évolution de l'affinité pour l'huile et l'eau de dérivés du PEG [6]. Le stéarate de PEG_{1500} de nature hydrophile (DHL < 0) à des températures peu élevées devient lipophile durant le chauffage (DHL > 0) en passant par une zone transitionnelle où le polymère a une affinité identique pour l'eau et l'huile (DHL = 0). Cette région appelée également « optimum de formulation » se trouve à des températures proches de la température d'inversion de phase (TIP) [7]. Généralement, le concept de BHL

(Balance Hydrophile/Lipophile) est plus utilisé que le DHL mais il ne prend pas en compte certains paramètres propres au système à savoir la température et la salinité.

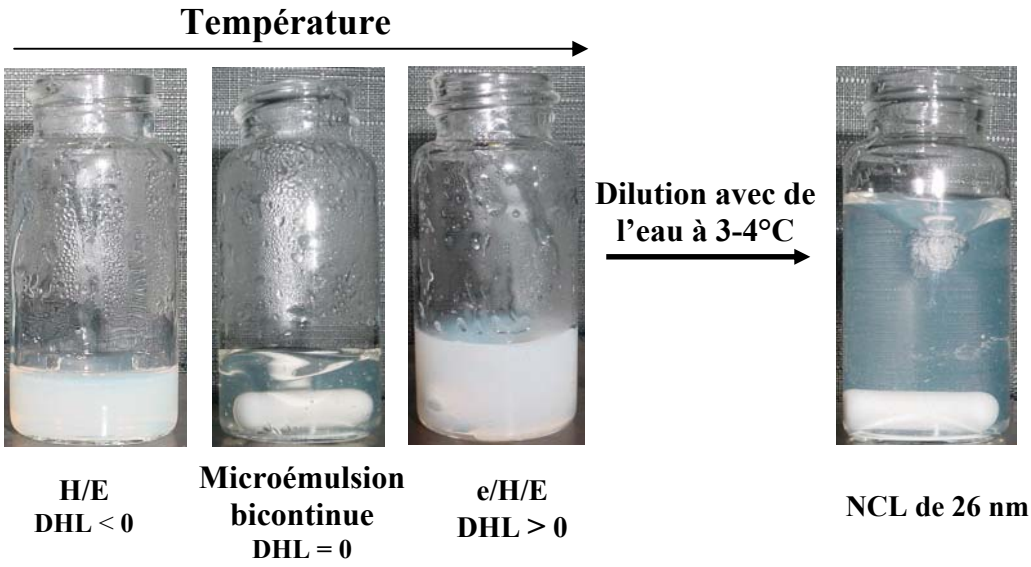

Figure 1. Observation de la préparation des NCL au cours du chauffage et après dilution

Les changements d'affinité du stéarate de PEG_{1500} avec la température engendrent une modification de la morphologie de l'émulsion. En effet, des mesures de conductivité ont montré que l'émulsion initiale H/E évoluait en une émulsion multiple e/H/E durant l'augmentation de température et inversement au cours du refroidissement. En revanche, dans le cas d'une émulsion en présence de Solutol® HS15 (NCL conventionnelles), le chauffage conduisait directement à une inversion de phase, l'émulsion initiale H/E étant inversée en émulsion E/H. Cette différence de comportement peut s'expliquer par la fraction d'eau du mélange initiale qui est beaucoup plus élevée dans le système composé de stéarate de PEG_{1500}. En effet, l'inversion de la courbure interfaciale [8] ne conduit pas à une inversion de phase car la phase aqueuse est trop conséquente pour qu'elle soit entièrement dispersée dans l'huile. Lors du dernier refroidissement, une rapide dilution avec de l'eau à 3-4°C a lieu à une

température proche de la TIP, générant la formation de NCL de 26 nm. Dans cette zone transitionnelle, le système est sous forme de microémulsion bicontinue où l'huile est entièrement solubilisée dans l'eau [9]. Ce phénomène explique l'aspect parfaitement translucide de la formulation durant la traversée de cette zone (Figure1). Par ailleurs, il est difficile de définir précisément le rôle de la dilution à froid. Est-ce le fractionnement du système ou bien la chute brutale de température qui conduit à la formation des nanocapsules lipidiques? De plus, l'effet du cyclage n'est pas encore bien compris. Cependant, au minimum 3 cycles sont nécessaires pour obtenir des NCL avec une distribution de taille monomodale.

La préparation de NCL à partir de stéarate de PEG_{4000} a également été envisagée mais les premiers essais se sont révélés infructueux. En effet, au cours des cycles de température, aucune variation significative de conductivité n'a été observée pour différents ratios huile/eau et pour différentes concentrations en surfactant. La TIP étant en relation avec le nombre d'oxydes d'éthylène, il est probable que pour de tels surfactants, elle soit très élevée et donc difficile voire impossible à atteindre. Le concept de « méthode TIP » initié par Shinoda *et al.* [10], il y a près de 40 ans, était basé sur des surfactants non-ioniques pegylés avec un nombre d'unités oxyde d'éthylène plus faible (inférieur à 10). Leur TIP était, au maximum, de 60-65°C. Les dérivés de PEG de plus haute masse moléculaire ont, en revanche, une TIP plus élevée. En effet, l'hydroxystéarate de PEG_{660} et le stéarate de PEG_{1500} portant respectivement 15 et 35 groupes ($O\text{-}CH_2\text{-}CH_2$) ont une TIP comprise entre 60 et 75°C pour l'un, et entre 80 et 90°C pour l'autre. Il est donc raisonnable de penser que cette méthode ne peut être adaptée à des surfactants portant de très longues chaînes de PEG (au delà de 1500 ou 2000 g/mol).

2) Evaluation de la furtivité

Le caractère furtif de ces nouvelles nanocapsules lipidiques a, notamment, été démontré à travers une étude *in vitro*, « le test du CH50 », évaluant l'interaction entre le vecteur colloïdal et le système du complément. Cependant, ce test ne prend en compte que la voie alterne. Deux autres voies biochimiques, à savoir la voie classique et la voie des lectines, sont également impliquées dans l'activation du système du complément [11].

Une très faible activation a été constatée puisque pour une surface totale de NCL de 5000 cm^2, la consommation d'unité CH50 atteignait seulement 20%. Ce résultat montre la capacité du PEG_{1500} à inhiber l'adsorption de protéines impliquées dans le mécanisme d'activation du complément. Cet effet peut, certes, s'expliquer par la longueur des chaînes de PEG_{1500} mais leur densité constitue aussi un paramètre important. Une distance séparant deux chaînes de PEG_{1500} de 1,7 nm a été calculée. Selon Vittaz *et al.* [12], cette valeur génère une répulsion stérique optimale du PEG.

Une étude *in vivo* a également été réalisée. Les NCL marquées au ^{99m}Tc ont été injectées chez le rat. Le stéarate de PEG_{1500} a induit une augmentation significative du temps de demi-vie des nanocapsules lipidiques, passant de 20-30 minutes pour les NCL de Solutol® HS15 à 5,5 heures pour les NCL de stéarate de PEG_{1500}. Leur comportement pharmacocinétique ($T_{1/2}$ et $AUC_{[0-24]}$) était ainsi très proche des systèmes liposomaux utilisés dans les stratégies de ciblage actif [13]. Cependant, contrairement à ces vecteurs qui ont un diamètre proche de 100-150 nm, la faible taille des NCL joue également un rôle non négligeable sur la furtivité.

Ces nouvelles nanocapsules lipidiques furtives présentent des caractéristiques intéressantes pour la vectorisation active du cerveau. Leur temps de résidence vasculaire prolongée augmente la probabilité de reconnaissance des cellules cibles et leur faible taille (26 nm) peut favoriser le mécanisme d'internalisation cellulaire. Cependant, le couplage d'anticorps sur ces nouvelles nanocapsules n'a pas pu être réalisé. La procédure de « post-insertion » permettant d'incorporer le DSPE-PEG_{2000}-maléimide n'a entraîné aucune augmentation significative de la taille, ce qui laissait supposer une insertion très faible voire inexistante de ce polymère bifonctionnel. Ce phénomène peut s'expliquer par le fort rayon de courbure de ces nanocapsules lié à leur faible taille ou bien par la répulsion stérique du stéarate de PEG_{1500}. Ainsi, nous avons choisi de transposer ce couplage aux nanocapsules lipidiques conventionnelles développées par Heurtault *et. al* [14].

II Synthèse des immunonanocapsules

1- Fonctionnalisation des NCL

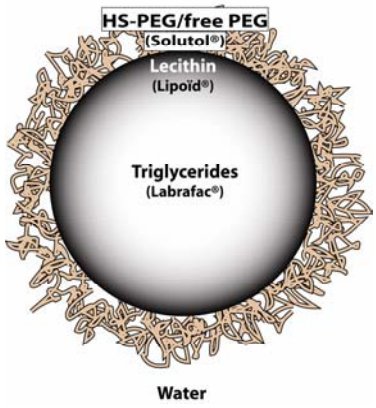

Figure 2. Représentation schématique des NCL

La préparation des NCL (Figure 2) est basée sur un procédé d'inversion de phase sans solvant organique. Ces nanocapsules sont composées d'un cœur lipophile constitué de triglycérides à chaînes moyennes (Labrafac®), d'une enveloppe interne formée par un mélange de phosphatidyléthalonamine et de phosphatidylcholine (Lipoïd®) et d'une couronne externe d'hydroxystéarate de PEG_{660} (Solutol®). Elles possèdent de nombreuses caractéristiques intéressantes qui font d'elles un vecteur potentiel de médicaments :

- Technique de fabrication basse énergie, sans solvant organique
- Non toxiques,
- Excipients biocompatibles,
- Taille modulable entre 20 et 100 nm,
- Stables en milieu aqueux,
- Encapsulation d'anticancéreux lipophiles (paclitaxel[15], étoposide[16], docétaxel[17]),

- Recouvertes d'hydroxystéarate de PEG_{660} réduisant l'opsonisation et inhibant la P-gp[18, 19],
- Faiblement activatrices du complément.

Les NCL caractérisées par un diamètre de 100 nm ont été choisies pour cette stratégie d'immunociblage. Cette taille a été préférée à une plus petite (20 ou 50 nm) afin de favoriser le couplage de macromolécules (plus faible rayon de courbure et surface plus grande par nanocapsule).

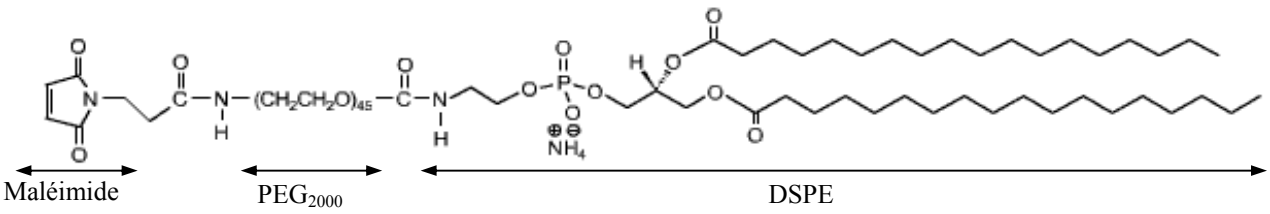

Figure 3. Structure du DSPE-PEG_{2000}-maléimide

Pour permettre la fixation covalente de ligands sur les nanocapsules, un polymère bifonctionnel (Figure 3) a été incorporé sur la surface des NCL. Ce polymère est constitué d'une chaîne de PEG_{2000} portant sur l'une de ses extrémités une partie hydrophobe (DSPE) et sur l'autre, un groupement réagissant avec la fonction sulfhydryle (maléimide). Le PEG éloigne la fonction maléimide de la surface de la particule et améliore, par conséquent, la fixation covalente du ligand. De plus, en générant une véritable barrière stérique autour de la nanoparticule, le PEG inhibe l'adsorption d'opsonines. Cependant, cet effet stérique, très dépendant de la longueur de la chaîne, peut réduire jusqu'à 50% la capacité du ligand à reconnaître les cellules cibles [20]. Ce phénomène est plus faible pour des chaînes de PEG de masse moléculaire inférieure ou égale à 2000 Da [21].

Un procédé de « post-insertion » a été utilisé pour insérer le polymère bifonctionnel sur la surface des NCL. Cette technique qui consiste à incuber les nanocapsules dans une solution micellaire de DSPE-PEG_{2000}-maléimide présente plus d'avantages que la méthode classique basée sur l'ajout du polymère bifonctionnel avant la préparation des NCL:

- Meilleure accessibilité du maléimide,
- Configuration en brosse du PEG améliorant ainsi les propriétés de furtivité des nanocapsules, [22]
- Incorporation plus importante,
- Pas de modification de la qualité de la formulation car le polymère et les constituants des nanocapsules n'interagissent pas.

Le procédé de « post-insertion » a été mis au point à partir d'un système liposomal [23] et consiste en un transfert de matière entre des liposomes constitués notamment de phosphatidylcholine de soja hydrogénée (HSPC) et des micelles de PEG couplés à des phospholipides (DSPE-PEG_{1900}). Cet échange a été réalisé à une température de 60°C, voisine de la phase de transition endothermique de l'HSPC. Bien que les NCL soient dépourvues de HSPC, une incorporation significative de DSPE-PEG_{2000} et DSPE-PEG_{5000} a été obtenue dans ces mêmes conditions, se traduisant par une augmentation du diamètre hydrodynamique des particules [22]. Une augmentation de taille (24,9 nm) a également été constatée après incubation des NCL avec une solution de DSPE-PEG_{2000}-maléimide à 20 mM. Lorsque la quantité de polymère était divisée par 2 (10 mM), un accroissement moins conséquent du diamètre des particules a été constaté (14 nm). Ces différences démontrent que la quantité de polymère inséré est en relation avec la concentration de la solution micellaire. En réalisant la post-insertion à 25 °C, l'augmentation de taille n'était plus que de 7,3 nm, montrant également le rôle important de la température. Par ailleurs, le fait que le procédé de « post-insertion »

puisse s'appliquer aussi bien pour les liposomes que pour les NCL démontre que d'autres éléments que les propriétés du HSPC expliquent cette incorporation. En outre, le polymère bifonctionnel doit être solidement ancré dans la nanocapsule pour permettre une conjugaison stable d'anticorps et de fragments c'est-à-dire sans risque de désorption.

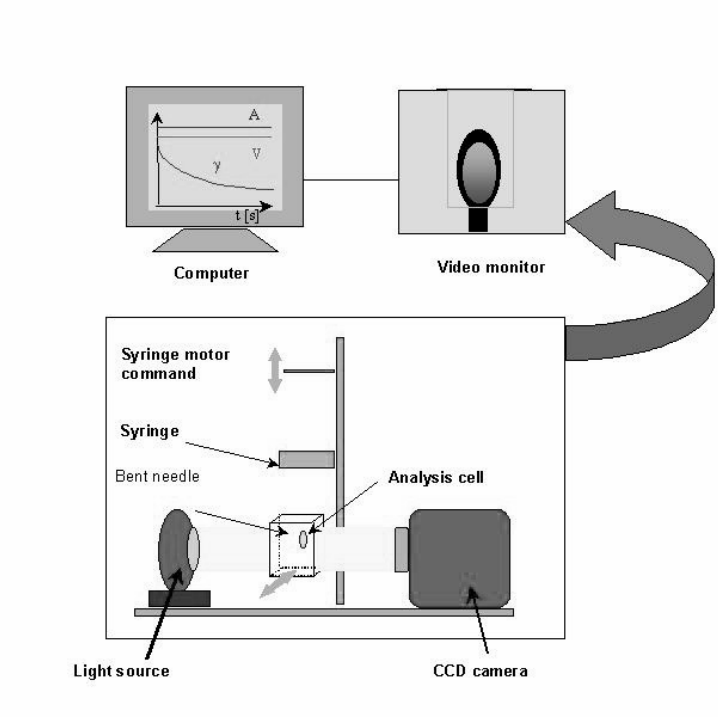

Figure 4. Représentation schématique du tensiomètre à goutte

Dans ce contexte, nous avons étudié les mécanismes régissant l'incorporation du polymère bifonctionnel et caractérisé la qualité du recouvrement. L'influence de la température a également été recherchée. Pour ce faire, une étude interfaciale a été réalisée par le biais d'un tensiomètre à goutte montante dynamique (Figure 4). Le DSPE-PEG_{2000}-maléimide a été adsorbé sur une interface H/E pure et sur des films de Solutol®, Lipoïd® et Solutol®/Lipoïd®préformés à l'interface H/E afin de se rapprocher au mieux de la structure des NCL. Les cinétiques d'adsorption effectuées à 25°C et 60°C ont duré autant de temps que

lors du procédé de « post-insertion » à savoir 2 heures. Les concentrations des différents produits qui sont élevées dans les conditions expérimentales habituelles, ont été diminuées afin d'obtenir une tension interfaciale suffisamment importante pour maintenir la goutte sur son support. L'huile utilisée était le Labrafac® et les solutions aqueuses ont été préparées avec de l'HEPES (0,1M, pH=7,4). Ce protocole a permis ainsi d'être le plus proche possible des conditions du procédé de « post-insertion ».

Cette étude a confirmé que l'adsorption du DSPE-PEG_{2000}-maléimide est significativement améliorée lorsque la température d'incubation est de 60°C. Cet effet peut s'expliquer par la propriété thermosensible du PEG_{2000} qui se traduit par une augmentation de son caractère lipophile avec la température. De plus, à 60°C, les composés présents sur la surface des NCL n'influencent pas l'insertion du DSPE-PEG_{2000}-maléimide. Au contraire, les propriétés interfaciales des monocouches mixtes sont gouvernées essentiellement par le polymère bifonctionnel, aussi bien au niveau de la pression superficielle qu'au niveau du comportement rhéologique. Ce résultat suggère que le DSPE-PEG_{2000}-maléimide est soit solidement inséré à l'interface H/E ou bien conduit à la désorption des composés déjà présents à l'interface. En revanche, ce phénomène n'a pas été observé lors des cinétiques d'adsorption effectuées à 25°C du fait d'une trop faible incorporation du polymère. Par ailleurs, le comportement élastique des films de DSPE-PEG_{2000}-maléimide observé à 60°C, a été conservé après le refroidissement à 25°C. Ce caractère élastique démontre un ancrage stable du polymère à l'interface H/E via sa partie lipophile.

En extrapolant ce modèle, nous pouvons supposer que le manteau polymérique de DSPE-PEG_{2000}-maléimide autour des NCL est également stable. Hoarau *et al.* [22] était en accord avec ces interprétations en démontrant que les NCL traitées par le procédé de « post-

insertion » restaient physiquement stables pendant 12 mois à température ambiante. De plus, le comportement élastique du film polymérique devrait permettre le couplage d'anticorps entiers ou de fragments Fab' sans entraîner d'éventuelle désorption.

2- Thiolation et fragmentation de l'anticorps monoclonal OX26

L'OX26 est un anticorps monoclonal d'origine murine se fixant sur le récepteur à la transferrine hautement exprimé sur les cellules endothéliales cérébrales de rat [24]. Sa capacité à migrer des capillaires cérébraux vers le parenchyme cérébral via un mécanisme de transcytose médiée par récepteur a été démontrée par Friden *et al.* [25]. Bien que ce mécanisme de franchissement soit contesté [26], la plupart des études pharmacocinétiques menées chez le rat ont montré une accumulation importante d'OX26 au niveau des tissus cérébraux. Cet anticorps monoclonal semble être, par conséquent, un candidat idéal pour le ciblage du cerveau.

Afin de coupler de façon covalente l'anticorps sur la nanocapsule par le biais de la fonction maléimide , des groupements sulfhydryles doivent être insérés sur la structure de l'anticorps. Pour ce faire, différentes voies sont possibles. La thiolation peut prendre place au niveau des amines primaires de la protéine par réaction avec le N-succinimidyl 3-[2-pyridyldithio]propionate) (SPDP), le (N-succinimidyl 2-mercapto-[S-acétyl]acétic acid) (SATA) ou le 2-iminothiolane (réactif de Traut). Cependant, la réaction peut avoir lieu sur le site actif de l'anticorps, altérant par conséquent son activité de reconnaissance. Afin de s'affranchir de ce problème, une autre procédure (Figure 5) n'impliquant que la modification de la partie glucidique située entre les

2 chaînes Fc [27] de la glycoprotéine a été choisie. Cette technique permet également d'orienter les régions variables de l'anticorps vers l'extérieur des NCL.

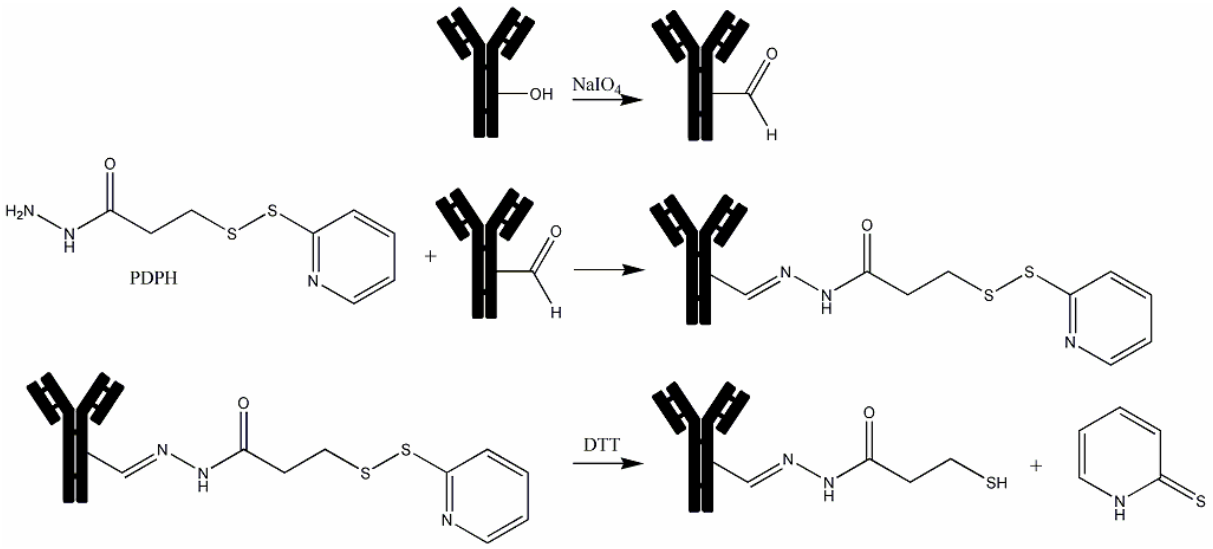

Figure 5. Thiolation de l'anticorps monoclonal OX26 à partir du 3-(2-pyridyldithio) propionyl Hydrazide (PDPH)

La présence d'anticorps sur la surface de systèmes colloïdaux peut engendrer une reconnaissance accrue du vecteur par le système réticuloendothélial et ainsi diminuer significativement son temps de résidence vasculaire. En effet, les immunoglobulines activent la voie classique du complément et sont rapidement reconnues par les macrophages qui possèdent, sur leur membrane, des récepteurs à la partie Fc. Cependant, le fait d'ancrer la partie Fc du ligand au sein du manteau polymérique de DSPE-PEG_{2000}-maléimide peut diminuer ses interactions avec le système réticuloendothélial. De plus, différentes études, reportées dans la littérature, ont montré que l'oxydation ou la déglycosylation diminue la

reconnaissance du fragment Fc, se traduisant par une plus faible activation du complément [28-30]. La modification des fonctions oligosaccharidiques, jouant un rôle important sur la structure secondaire des deux chaînes Fc, peut perturber la fonction effectrice de l'anticorps. Toutefois, en éliminant une partie des régions constantes des chaînes lourdes, la furtivité du vecteur se trouverait significativement améliorée. Ainsi, la fragmentation de l'OX26 en groupements Fab' a également été réalisée (Figure 6). Outre le fait qu'ils soient dépourvus de la fraction Fc, les fragments Fab' possèdent des groupements sulfhydryles nécessaires à leur couplage.

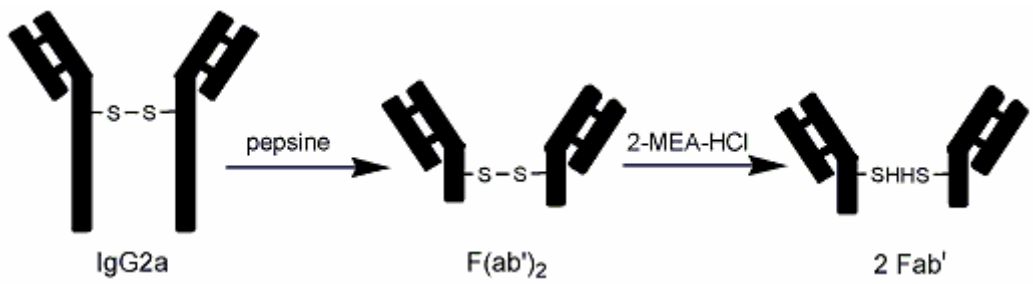

Figure 6. Fragmentation de l'anticorps monoclonal OX26 en fragments Fab'

Ces procédures de thiolation et de fragmentation n'ont entraîné qu'une très faible perte de l'activité de reconnaissance de l'anticorps. En revanche, les anticorps thiolés et les fragments Fab' sont peu stables car les fonctions SH s'oxydent très rapidement conduisant à la formation de ponts disulfures inter et intramoléculaires. Ainsi, le couplage doit être réalisé sous atmosphère inerte, immédiatement après l'insertion des fonctions thiols. Il est possible également d'ajouter des agents qui vont limiter cette oxydation comme l'EDTA.

3- Couplage des anticorps thiolés et des fragments Fab' sur les nanocapsules fonctionnalisées

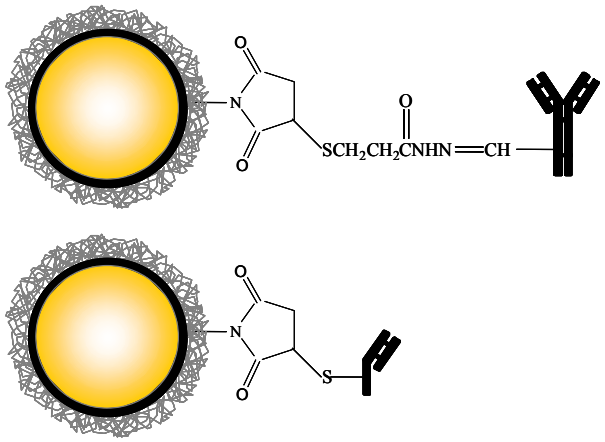

Figure 7. Représentation schématique des immunonanocapsules

Les anticorps thiolés et les fragments ont été incubés avec les nanocapsules recouvertes de DSPE-PEG_{2000}-maléimide durant près de 12 heures. Cette durée peut être réduite car la réaction entre le groupement maléimide et la fonction sulfhydryle est quasiment complète après 2 heures. La densité de ligands des immunonanocapsules schématisées dans la Figure 7 est dépendante du ratio anticorps/nanocapsules ou fragments/nanocapsules. En effet, pour une même quantité de nanocapsules, le nombre de protéines par immunonanocapsule est directement proportionnel à la concentration en immunoglobulines ou Fab'. En revanche, cette linéarité disparaît pour des concentrations en anticorps entier importantes (au-dessus de 1,2 mg/ml). En supposant raisonnablement que la surface d'un anticorps est comprise entre 100 et 225 nm^2 [21] et que les nanocapsules pegylées ont une surface de 58 000 nm^2, il est théoriquement possible de fixer entre 260 et 580 immunoglobulines par nanocapsule. Or, dans notre cas, la saturation a eu lieu à partir d'une densité comprise entre 106 et 183 OX26/nanocapsule. Le nombre de fonctions maléimide présentes sur la nanocapsule étant

supérieur à 1000, il ne peut être le facteur limitant. Il est cependant probable que le PEG_{2000} en générant une barrière stérique sur la nanocapsule empêche le couplage d'un plus grand nombre d'OX26. Dans ce sens, une étude a montré que la quantité de protéines conjuguées à des liposomes est réduite après incorporation de MePEGS-2000-DSPE dans la formulation [31]. De plus, l'incubation d'une concentration très élevée d'anticorps (6,4 mg/ml) a engendré une augmentation anormale de la taille des immunonanocapsules (diamètre multiplié par 2). Ces agrégations rencontrées également sur des immunoliposomes portant une forte densité d'immunoglobulines [32] peuvent s'expliquer par la formation de ponts disulfures intermoléculaires. Ce phénomène limiterait également le nombre d'OX26 sur les immunonanocapsules.

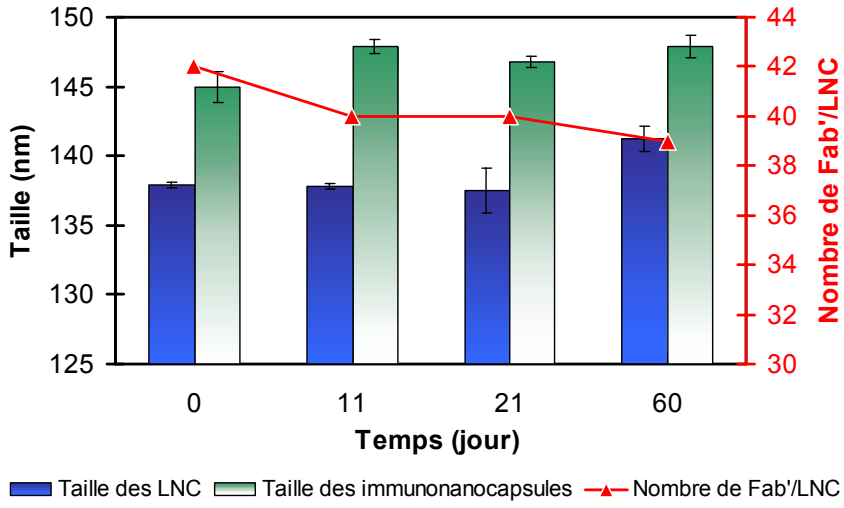

Figure 8. Etude de la stabilité du recouvrement des NCL et des immunonanocapsules

Une étude de stabilité effectuée à la fois sur les NCL recouvertes par le polymère bifonctionnel et les immunonanocapsules décorées par les fragments Fab' a été réalisée (Figure 8). Aucune variation notoire de taille n'a été constatée pour les deux systèmes après deux mois de stockage à 4°C. De plus, une diminution très peu significative du nombre de

fragments par NCL a été observée, suggérant un très fort ancrage des biomolécules sur la surface des nanocapsules. En se référant à l'étude interfaciale, la stabilité du couplage peut s'expliquer par le caractère élastique du recouvrement polymérique dû à un ancrage solide du DSPE-PEG_{2000}-maléimide sur la nanocapsule.

III Evaluation du ciblage des immunonanocapsules

1- *Ciblage in vitro*

Les OX26-immunonanocapsules utilisées pour les tests *in vitro* étaient caractérisées par une densité de ligands comprise entre 30 et 40. Divers travaux effectués sur des immunoliposomes ont en effet démontré que la reconnaissance du système particulaire est optimale aux alentours de 30-35 anticorps par particule [4, 33]. Pour permettre une étude comparative, cette même densité a été appliquée aux Fab'-immunonanocapsules.

Afin de réaliser l'évaluation *in vitro*, les ligands couplés aux nanocapsules lipidiques ont été marqués grâce à une sonde fluorescente anti-IgG-FITC. Les résultats ont montré une fixation spécifique des immunonanocapsules sur les cellules surexprimant le récepteur à la transferrine (hybridomes Y3.AG.1.2.3. et cellules endothéliales cérébrales de rat). De plus, la fluorescence des cellules incubées avec les OX26-immunonanocapsules était plus intense que celles en contact avec les Fab'-immunonanocapsules. Ce résultat peut s'expliquer par un meilleur degré de fixation des anticorps entiers. Il est également possible que la densité de sondes par anticorps soit plus importante que pour les fragments Fab'. Il aurait été plus aisé d'effectuer ces tests en marquant directement les immunonanocapsules par un fluorochrome lipophile. Cet essai a été réalisé avec du Rouge Nile, mais les nombreuses étapes que subissent les particules durant le couplage (incubation à 60°C, chromatographies) altèrent les propriétés du fluorochrome. Par conséquent l'intensité de fluorescence des nanocapsules n'était pas suffisante pour observer de façon significative la fixation spécifique des immunonanocapsules.

Le fait que ces nouveaux vecteurs particulaires se fixent de façon préférentielle sur les cellules endothéliales de cerveau de rat démontre leur intérêt potentiel pour le ciblage du cerveau. Une étude *in vivo* a donc été entreprise.

2- *Biodistribution chez le rat*

Afin de suivre les immunonanocapsules après leur administration par voie intraveineuse chez le rat, un complexe lipophile de ^{188}Re $(S_3CPh)_2(S_2CPh)$ a été encapsulé dans les NCL.

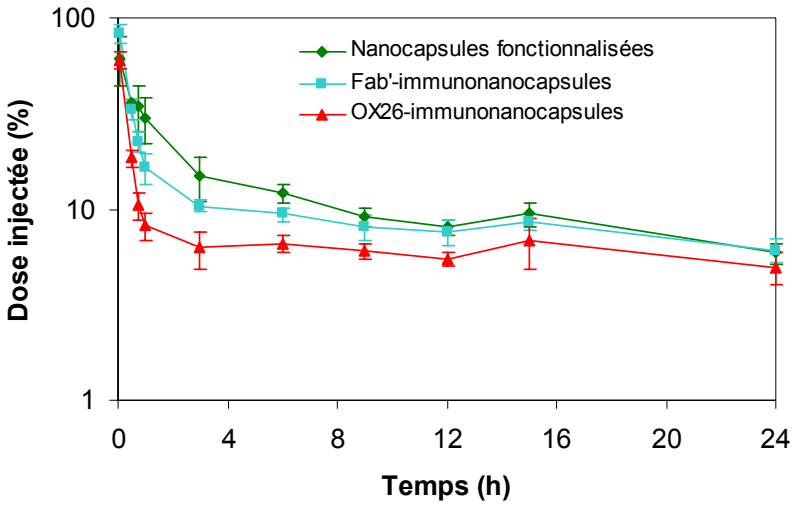

Figure 9. Profil pharmacocinétique des nanocapsules fonctionnalisées et des immunonanocapsules administrées par voie intraveineuse cher le rat.

Les cinétiques sanguines obtenues pour chaque préparation (Figure 9) ont montré une diminution du temps de résidence vasculaire des NCL couplées aux ligands de reconnaissance. Par ailleurs, conformément à la littérature, l'élimination des fragments Fab' par le système réticuloendothélial via le mécanisme médié par le récepteur Fc, est plus faible

que celle des anticorps entiers. En effet, les Fab'-immunonanocapsules restent plus longtemps dans la circulation sanguine que les OX26-immunonanocapsules.

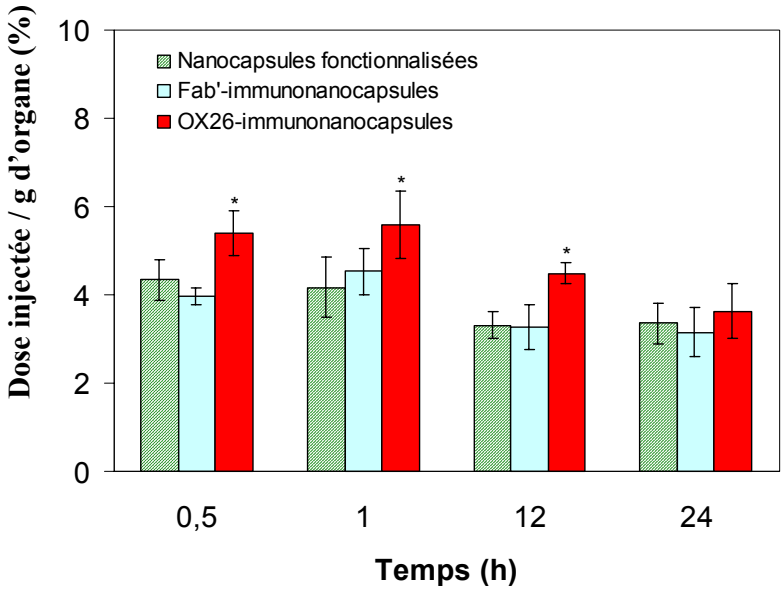

Figure 10. Accumulation hépatique des trois formulations à différents temps après leur injection par voie systémique. La significativité des différences de dose injectée par g d'organe entre les immunonanocapsules et les nanocapsules fonctionnalisées ont été calculées à partir du test de « Mann-Whitney ». (* : $p < 0,05$).

Ces résultats sont en accord avec l'étude de l'élimination hépatique des trois préparations (Figure 10). En effet, la capture par le foie est plus importante pour les OX26-immunonanocapsules. En revanche, aucune différence significative n'a été observée entre les immunonanocapsules portant des fragments Fab' et les nanocapsules fonctionnalisées, confirmant la plus faible interaction des fragments Fab' avec le système réticuloendothélial.

Nous avons également traité par une analyse bicompartimentale, les données pharmacocinétiques de nanocapsules natives de ^{188}Re (50 nm) injectées chez le rat [2]. Un

temps de demi-vie alpha ($T_{1/2\ alpha}$) de (16,8 ± 1,2) min a été calculé. Cette demi-vie, deux fois plus courte que celle des nanocapsules fonctionnalisées (38,4 ± 14,4) min, montre l'intérêt du PEG_{2000} sur les propriétés de furtivité des nanocapsules. De plus, nous comparons ici des nanocapsules de tailles très différentes puisque les NCL natives et fonctionnalisées ont un diamètre hydrodynamique respectif de 50 et 135 nm, or, le degré d'élimination des systèmes colloïdaux dépend très fortement de la taille [34]. Ainsi, il est fort probable que cette différence de demi-vie serait accrue en se référant à des nanocapsules natives de plus de 100 nm.

L'accumulation dans le cerveau des nanocapsules couplées aux anticorps entiers est supérieure aux nanocapsules fonctionnalisées à tous les temps (0,5h, 1h, 12h et 24h). En revanche, l'intérêt des Fab'-immunonanocapsules sur le ciblage du cerveau a seulement été constaté au temps t = 24h. Ces résultats montrent que, malgré un temps de résidence vasculaire moindre, les anticorps entiers sont de meilleurs ligands de reconnaissance que les fragments Fab'. Cette différence peut s'expliquer par la fraction Fc de l'anticorps qui éloigne le site de fixation antigénique de la surface de la nanocapsule, favorisant ainsi la reconnaissance des cellules cibles. Les travaux de Maruyama *et. al* [3] ne sont pas en accord avec ces résultats. Effet, ils ont démontré que l'accumulation des immunoliposomes dans des tumeurs solides était améliorée en substituant les anticorps par des fragments. Cependant, les immunoliposomes portaient une densité de fragments beaucoup plus importante que dans notre étude (517). Par conséquent, du fait de leur orientation aléatoire, nous pouvons supposer que le nombre de fragments Fab' doit être relativement élevé pour favoriser l'accumulation des immunonanocapsules dans les tissus cibles. Cette densité est plus faible pour les anticorps entiers car 30 immunoglobulines suffisent pour atteindre un degré de reconnaissance optimale [4]. Par ailleurs, le temps de résidence vasculaire des Fab'-immunoliposomes était beaucoup plus long (plusieurs heures) et largement supérieur à celui des immunoliposomes portant les

anticorps entiers. Ainsi, malgré peut-être une affinité moindre, leur temps de contact prolongé avec les cellules cibles devait également favoriser leur accumulation. Ainsi, nous pouvons supposer que dans notre cas, l'intérêt des fragments est également limité par le faible temps de demi-vie des NCL fonctionnalisées.

La méthode utilisée pour évaluer la concentration des vecteurs dans le cerveau prend en compte à la fois les particules présentes dans le tissu et celles contenues dans le sang. En considérant que le volume cérébral sanguin est de 3%,[35] la radioactivité détectée dans le cerveau ne peut correspondre uniquement aux particules présentes dans le flux sanguin. De plus, si tel était le cas, étant donné que les nanocapsules fonctionnalisées résident plus longtemps dans le sang que les deux autres formulations, leur accumulation au sein des tissus cérébraux aurait dû être plus élevée. Par conséquent, nous pouvons affirmer que les différences significatives de concentration observées au niveau du cerveau correspondent à une accumulation spécifique des immunonanoparticules au sein des tissus cérébraux.

Références

(1) Brodt, P.; Blore, J.; Phillips, N. C.; Munzer, J. S.; Rioux, J. D., Inhibition of murine hepatic tumor growth by liposomes containing a lipophilic muramyl dipeptide. *Cancer Immunology Immunotherapy* **1989,** *28*, (1), 54-58.

(2) Ballot, S.; Noiret, N.; Hindre, F.; Denizot, B.; Garin, E.; Rajerison, H.; Benoit, J. P., (99m)Tc/(188)Re-labelled lipid nanocapsules as promising radiotracers for imaging and therapy: formulation and biodistribution. *Eur J Nucl Med Mol Imaging* **2006**, 1-6.

(3) Maruyama, K.; Takahashi, N.; Tagawa, T.; Nagaike, K.; Iwatsuru, M., Immunoliposomes bearing polyethyleneglycol-coupled Fab' fragment show prolonged circulation time and high extravasation into targeted solid tumors in vivo. *FEBS Letters* **1997,** *413*, (1), 177-180.

(4) Huwyler, J.; Wu, D.; Pardridge, W. M., Brain drug delivery of small molecules using immunoliposomes. *Proceedings of the National Academy of Sciences of the United States of America* **1996,** *93*, (24), 14164-14169.

(5) Jeon, S. I.; Lee, J. H.; Andrade, J. D.; De Gennes, P. G., Protein-surface interactions in the presence of polyethylene oxide. I. Simplified theory. *Journal of Colloid and Interface Science* **1991,** *142*, (1), 149-158.

(6) Nardello, V.; Chailloux, N.; Poprawski, J.; Salager, J.-L.; Aubry, J.-M., DHL concept as a tool for the characterization of cosmetic hydrocarbon oils. *Polymer International* **2003,** *52*, (4), 602-609.

(7) Saito, H.; Shinoda, K., The stability of W/O type emulsions as a function of temperature and of the hydrophilic chain length of the emulsifier. *Journal of Colloid and Interface Science* **1970,** *32*, (4), 647-651.

(8) Bancroft, W. D., The theory of emulsification. *J. Phys. Chem.* **1913,** *17*, (501).

(9) Morales, D.; Gutiérrez, J. M.; García-Celma, M. J.; Solans, Y. C., A study of the relation between bicontinuous microemulsions and oil/water nano-emulsion formation. *Langmuir* **2003,** *19*, (18), 7196-7200.

(10) Shinoda, K.; Saito, H., The effect of temperature on the phase equilibria and the types of dispersions of the ternary system composed of water, cyclohexane, and nonionic surfactant. *Journal of Colloid and Interface Science* **1968,** *26*, (1), 70-74.

(11) Passirani, C.; Benoit, J., Complement activation by injectable colloidal drug carriers. In *Biomaterials for Delivery and Targeting of Proteins and Nucleic Acids*, Mahato, R. I., Ed. CRC Press: 2005; pp 187-230.

(12) Vittaz, M.; Bazile, D.; Spenlehauer, G.; Verrecchia, T.; Veillard, M.; Puisieux, F.; Labarre, D., Effect of PEO surface density on long-circulating PLA-PEO nanoparticles which are very low complement activators. *Biomaterials* **1996,** *17*, (16), 1575-1581.

(13) Schnyder, A.; Krahenbuhl, S.; Drewe, J.; Huwyler, J., Targeting of daunomycin using biotinylated immunoliposomes: Pharmacokinetics, tissue distribution and in vitro pharmacological effects. *Journal of Drug Targeting* **2005,** *13*, (5), 325-335.

(14) Heurtault, B.; Saulnier, P.; Pech, B.; Proust, J.-E.; Benoit, J.-P., A Novel Phase Inversion-Based Process for the Preparation of Lipid Nanocarriers. *Pharmaceutical Research* **2002,** *19*, (6), 875-880.

(15) Peltier, S.; Oger, J. M.; Lagarce, F.; Couet, W.; Benoit, J. P., Enhanced oral paclitaxel bioavailability after administration of paclitaxel-loaded lipid nanocapsules. *Pharm Res* **2006,** *in press*.

(16) Lamprecht, A.; Benoit, J.-P., Etoposide nanocarriers suppress glioma cell growth by intracellular drug delivery and simultaneous P-glycoprotein inhibition. *Journal of Controlled Release* **2006,** *112*, (2), 208-213.
(17) Khalid, M. N.; Simard, P.; Hoarau, D.; Dragomir, A.; Leroux, J.-C., Long circulating poly(ethylene glycol)-decorated lipid nanocapsules deliver docetaxel to solid tumors. *Pharmaceutical Research* **2006,** *23*, (4), 752-758.
(18) Coon, J. S.; Knudson, W.; Clodfelter, K.; Lu, B.; Weinstein, R. S., Solutol HS 15, nontoxic polyoxyethylene esters of 12-hydroxystearic acid, reverses multidrug resistance. *Cancer Research* **1991,** *51*, (3), 897-902.
(19) Buckingham, L. E.; Balasubramanian, M.; Emanuele, R. M.; Clodfelter, K. E.; Coon, J. S., Comparison of Solutol HS 15, Cremophor EL and novel ethoxylated fatty acid sulfactants as multidrug resistance modification agents. *International Journal of Cancer* **1995,** *62*, (4), 436-442.
(20) Mori, A.; Klibanov, A. L.; Torchilin, V. P.; Huang, L., Influence of the steric barrier activity of amphipathic poly(ethyleneglycol) and ganglioside GM1 on the circulation time of liposomes and on the target binding of immunoliposomes in vivo. *FEBS Letters* **1991,** *284*, (2), 263-266.
(21) Schnyder, A.; Huwyler, J., Drug transport to brain with targeted liposomes. *NeuroRx* **2005,** *2*, (1), 99-107.
(22) Hoarau, D.; Delmas, P.; David, S.; Roux, E.; Leroux, J.-C., Novel long-circulating lipid nanocapsules. *Pharmaceutical Research* **2004,** *21*, (10), 1783-1789.
(23) Uster, P. S.; Allen, T. M.; Daniel, B. E.; Mendez, C. J.; Newman, M. S.; Zhu, G. Z., Insertion of poly(ethylene glycol) derivatized phospholipid into pre-formed liposomes results in prolonged in vivo circulation time. *FEBS Letters* **1996,** *386*, (2-3), 243-246.
(24) Jefferies, W. A.; Brandon, M. R.; Hunt, S. V.; Williams, A. F.; Gatter, K. C.; Mason, D. Y., Transferrin receptor on endothelium of brain capillaries. *Nature* **1984,** *312*, (5990), 162-3.
(25) Friden, P. M.; Walus, L. R.; Musso, G. F.; Taylor, M. A.; Malfroy, B.; Starzyk, R. M., Anti-transferrin receptor antibody and antibody-drug conjugates cross the blood-brain barrier. *Proc Natl Acad Sci U S A* **1991,** *88*, (11), 4771-5.
(26) Moos, T.; Morgan, E. H., Restricted transport of anti-transferrin receptor antibody (OX26) through the blood-brain barrier in the rat. *J Neurochem* **2001,** *79*, (1), 119-129.
(27) Sutton, B. J.; Phillips, D. C., The three-dimensional structure of the carbohydrate within the Fc fragment of immunoglobulin G. *Biochemical Society Transactions* **1983,** *11 Pt 2*, 130-132.
(28) Leatherbarrow, R. J.; Rademacher, T. W.; Dwek, R. A.; Woof, J. M.; Clark, A.; Burton, D. R.; Richardson, N.; Feinstein, A., Effector functions of a monoclonal aglycosylated mouse IgG2a: Binding and activation of complement component C1 and interaction with human monocyte Fc receptor. *Molecular Immunology* **1985,** *22*, (4), 407-415.
(29) Nose, M.; Wigzell, H., Biological significance of carbohydrate chains on monoclonal antibodies. *Proceedings of the National Academy of Sciences of the United States of America* **1983,** *80*, (21 I), 6632-6636.
(30) Tao, M.-H.; Morrison, S. L., Studies of aglycosylated chimeric mouse-human IgG. Role of carbohydrate in the structure and effector functions mediated by the human IgG constant region. *Journal of Immunology* **1989,** *143*, (8), 2595-2601.
(31) Ansell, S. M.; Tardi, P. G.; Buchkowsky, S. S., 3-(2-pyridyldithio)propionic acid hydrazide as a cross-linker in the formation of liposome-antibody conjugates. *Bioconjug Chem* **1996,** *7*, (4), 490-6.

(32) Koning, G. A.; Morselt, H. t. W. M.; Gorter, A.; Allen, T. M.; Zalipsky, S.; Kamps, J. A. A. M.; Scherphof, G. L., Pharmacokinetics of Differently Designed Immunoliposome Formulations in Rats with Or Without Hepatic Colon Cancer Metastases. *Pharmaceutical Research* **2001,** *18*, (9), 1291-1298.

(33) Maruyama, K.; Takizawa, T.; Yuda, T.; Kennel, S. J.; Huang, L.; Iwatsuru, M., Targetability of novel immunoliposomes modified with amphipathic poly(ethylene glycol) s conjugated at their distal terminals to monoclonal antibodies. *Biochimica et Biophysica Acta (BBA) - Biomembranes* **1995,** *1234*, (1), 74-80.

(34) Moghimi, S. M.; Hunter, A. C.; Murray, J. C., Long-circulating and target-specific nanoparticles: Theory to practice. *Pharmacological Reviews* **2001,** *53*, (2), 283-318.

(35) Perles-Barbacaru, A. T.; Lahrech, H., A new Magnetic Resonance Imaging method for mapping the cerebral blood volume fraction: the rapid steady-state T(1) method. *J Cereb Blood Flow Metab* **2006**.

CONCLUSIONS & PERSPECTIVES

Ce projet de thèse a porté sur la conception et l'évaluation d'un vecteur particulaire de troisième génération, capable après son administration par voie intraveineuse, de reconnaître spécifiquement les tissus cérébraux. Pour ce faire, des anticorps monoclonaux OX26 et des fragments issus de ce même anticorps, dirigés contre le récepteur à la transferrine de rat, ont été greffés de façon covalente sur la surface des NCL (immunonanocapsules).

La première partie de ce travail a consisté à mettre au point et à caractériser les immunonanocapsules. Entre 16 et 183 anticorps entiers OX26 et entre 42 et 173 fragments Fab' ont été greffés sur la surface des NCL. La densité de ligands par NCL était ajustable en modifiant le ratio ligand/NCL durant le couplage. Dans la seconde partie, l'affinité de ces nouveaux vecteurs colloïdaux, pour les cellules surexprimant le récepteur à la transferrine, a été évaluée. Les études *in vitro* ont montré que les immunonanocapsules s'associaient spécifiquement aux cellules endothéliales cérébrales de rat. 24 heures après leur administration chez le rat, une accumulation significative des immunonanocapsules était détectée au niveau des tissus cérébraux. En effet, la concentration dans le cerveau des OX26-immunonanocapsules et des Fab'-immunonanocapsules était 2 et 1,5 fois plus élevée comparé aux NCL non ciblées. A des densités égales (30 - 40), les anticorps entiers se sont révélés être des vecteurs plus efficaces que les fragments Fab', malgré leur forte interaction avec le système réticuloendothélial.

Les prochains travaux s'axeront sur l'amélioration du temps de résidence vasculaire des immunonanocapsules. L'incorporation de DSPE-PEG_{2000}-maléimide a, certes, prolongé le temps de demi-vie systémique des NCL mais il reste très nettement inférieur à ceux des liposomes pegylés utilisés dans les stratégies de ciblage actif (plusieurs heures). Le rayon de

courbure des particules jouant un rôle prépondérant sur les mécanismes d'élimination, notamment l'opsonisation [1], l'utilisation de nanocapsules ayant un diamètre hydrodynamique inférieur à 100 nm est à envisager. Cependant, cette même caractéristique peut limiter aussi la post-insertion du DSPE-PEG_{2000}-maléimide. En effet, l'insertion n'a pu être réalisée sur les nanocapsules de stéarate de PEG_{1500} de diamètre égale à 26 nm. Par conséquent, les NCL de 50 nm seront préférées à celles de 20 nm pour les prochains tests. Leur surface devrait être suffisamment importante pour y greffer au moins 30 anticorps. En plus de prolonger le temps de résidence vasculaire, cette taille de 50 nm pourrait favoriser les mécanismes d'internalisation cellulaire.

L'utilisation d'un modèle in vitro de BHE permettrait d'évaluer le franchissement de la BHE par ces nanovecteurs lipidiques. L'influence de la taille ou bien de la densité d'anticorps et de fragments pourrait alors être étudiée dans le but d'optimiser les caractéristiques des immunonanocapsules.

Par ailleurs, afin d'étudier leur potentiel thérapeutique, une étude chez le rat portant un modèle de gliome murin, devrait être envisagée. Même si en l'état actuel, la quantité d'immunonanocapsules dans le cerveau de rat sain semble insuffisante pour une application thérapeutique, nous pouvons supposer que, chez l'animal porteur d'un gliome, la concentration des particules dans le parenchyme cérébral devrait être accrue. En effet, les effets engendrés par les tumeurs cérébrales à savoir la rupture locale et partielle de la BHE, l'augmentation de sa perméabilité et le phénomène de néoangiogénèse augmentant l'interface tumeur/sang [2] devrait favoriser l'accumulation des nanovecteurs dans le cerveau. De plus, la lyophilisation qui a déjà été réalisée sur les nanocapsules lipidiques [3], permettrait d'augmenter considérablement la quantité d'immunonanocapsules injectée.

La technologie développée dans cette étude pour coupler l'OX26 aux NCL peut s'appliquer à une grande variété d'anticorps monoclonaux ou de peptides possédant une cysteine. Le ligand doit répondre à deux exigences : reconnaître des antigènes surexprimés sur les cellules cibles et être endocyté après fixation. Dans le cas du ciblage cérébral, cette endocytose doit être suivie d'une exocytose afin que le vecteur puisse traverser la BHE et atteindre le parenchyme cérébral. Ces conditions peuvent être réunies en conjuguant à la même particule, différents types de biomolécules ayant des propriétés complémentaires. Ainsi, dans le cas des tumeurs cérébrales, des ligands induisant la transcytose médiée par récepteur, peuvent être combinés à des peptides ou des anticorps monoclonaux reconnaissant les sites antigéniques des cellules cancéreuses. De nombreux antigènes des tumeurs cérébrales ont été répertoriés dans la littérature [4]. L'un des récepteurs à l'interleukine 13 (IL13Rα2), la forme variante III du récepteur au facteur de croissance épidermique (EGFRvIII) [5] ainsi que la protéine transmembranaire HER2 [6], sont très fortement exprimés sur les gliomes de haut grade, notamment le glioblastome multiforme. Du fait de leur faible niveau d'expression sur les tissus sains, ces systèmes semblent intéressants pour le ciblage spécifique des tumeurs cérébrales.

Ainsi, le développement de systèmes particulaires caractérisés par une biodistribution et un trafic intracellulaire contrôlés, constitue une stratégie prometteuse pour le transport systémique de médicaments. La première étape dite « de preuve du concept » a ainsi été réalisée avec succès à partir des nanocapsules lipidiques. Elle ouvre la voie à la vectorisation de molécules actives dans le SNC pour le traitement des tumeurs cérébrales ou des maladies neurodégénératives.

Références

(1) Passirani, C.; Benoit, J., Complement activation by injectable colloidal drug carriers. In *Biomaterials for Delivery and Targeting of Proteins and Nucleic Acids*, Mahato, R. I., Ed. CRC Press: **2005**; pp 187-230.

(2) Gururangan, S.; Friedman, H. S., Innovations in design and delivery of chemotherapy for brain tumors. *Neuroimaging Clinics of North America* **2002,** *12*, (4), 583-597.

(3) Dulieu, C.; Bazile, D., Influence of lipid nanocapsules composition on their aptness to freeze-drying. *Pharm Res* **2005,** *22*, (2), 285-92.

(4) Boskovitz, A.; Wikstrand, C. J.; Kuan, C. T.; Zalutsky, M. R.; Reardon, D. A.; Bigner, D. D., Monoclonal antibodies for brain tumour treatment. *Expert Opin Biol Ther* **2004,** *4*, (9), 1453-71.

(5) Saikali, S.; Avril, T.; Collet, B.; Hamlat, A.; Bansard, J.-Y.; Drenou, B.; Guegan, Y.; Quillien, V., Expression of nine tumour antigens in a series of human glioblastoma multiforme: Interest of EGFRvIII, IL-13Ra2, gp100 and TRP-2 for immunotherapy. *Journal of Neuro-Oncology* **2007,** *81*, (2), 139-148.

(6) Mineo, J.-F.; Bordron, A.; Quintin-Roue, I.; Maurage, C.-A.; Buhe, V.; Loisel, S.; Dubois, F.; Blond, S.; Berthou, C., Increasing of HER2 membranar density in human glioblastoma U251MG cell line established in a new Nude mice model. *Journal of Neuro-Oncology* **2006,** *76*, (3), 249-255.

ANNEXE

Pharmaceutical Research, Vol. 23, No. 9, September 2006 (© 2006)
DOI: 10.1007/s11095-006-9061-y

Research Paper

Pegylated Nanocapsules Produced by an Organic Solvent-Free Method: Evaluation of their Stealth Properties

Arnaud Béduneau,[1] Patrick Saulnier,[1,3] Nicolas Anton,[1] François Hindré,[1] Catherine Passirani,[1] Holisoa Rajerison,[2] Nicolas Noiret,[2] and Jean-Pierre Benoit[1]

Received February 24, 2006; accepted May 10, 2006; published online August 9, 2006

Purpose. To develop from an original process, a novel generation of stealth lipidic nanocapsules in order to improve the lipophilic drug delivery in accessible sites.
Materials and Methods. Nanocapsules covered by PEG_{1500} stearate were obtained by a low energy emulsification method. Conductivity measurements and ternary diagram were performed to describe the formulation mechanism. Hemolytic dosage CH50 and pharmacokinetic study in rats have been achieved in order to study the stealth properties of nanocapsules.
Results. Transition from an O/W emulsion to a w/O/W emulsion was necessary to produce PEG_{1500} stearate nanocapsules. Interestingly nanocapsules with a size around 26 nm and a polydispersity index inferior to 0.1 were obtained. The CH50 test has revealed a very weak complement consumption in the presence of such nanocapsules. Moreover, after intravenous injection into rats, PEG_{1500} stearate nanocapsules exhibited long circulating properties. The experimental data support the concept of steric repulsion of the surface towards proteins, displayed by nanocapsules covered with PEG_{1500} stearate. These *in vivo* results were in agreement with the PEG_{1500} density calculated at the nanocarrier surface.
Conclusions. Injectable drug carriers have been developed. Their long-circulating properties could confer them a strong potential for lipophilic drug targeting.

KEY WORDS: lipidic nanocapsules; PEG chain density; polyethylene glycol; "stealth" colloids; transitional inversion.

INTRODUCTION

For 40 years, drug carriers in the nanometer range have been in development. Most of them are used in the field of cancer therapy and diagnosis. Indeed, these submicronic systems, after intravenous administration, are expected to improve the targeting and release of the encapsulated drug. Liposomes and more recently, nanocapsules represent an important part of these carriers. They are composed of nonionic surfactants, macromolecules and / or phospholipids.

Unfortunately, following intravenous injection, these nanocarriers are rapidly cleared from the blood. Macrophages of the mononuclear phagocytic system, particularly Kuppfer cells in the liver, recognized and removed them from the bloodstream. The adsorption of plasma proteins at the surface of these particles (opsonization process) seems to be responsible of the short lifetime in the bloodstream because of their interaction with specific plasma membrane receptors on monocytes and various subsets of tissue macrophages (1). Therefore, to increase the circulating half-time of nanocarriers, some studies have shown the impact of grafting polyethylene-glycol (PEG) derivatives at their surface (2). Indeed, the presence of such polymers reduces the protein adsorption by ensuring an efficient steric stabilization. The PEG density, corona thickness and PEG chain length are important parameters to consider to avoid opsonization (3).

In this context, lipid nanocarriers covered with PEG_{660} hydroxystearate have been developed by Heurtault *et al.* (4) over the last five years. These standard nanocapsules were prepared according to an organic solvent-free process using the Phase Inversion Temperature (PIT) method (5). When an oil-in-water (O/W) emulsion prepared with a nonionic surfactant of the ethylene oxide type is heated to a critical temperature (PIT), the emulsion inverts to a water-in-oil emulsion (W/O) (6). During a rapid cooling at PIT, the system crosses a point of zero spontaneous curvature promoting the formation of submicron-scale particles. Despite of the presence of PEG, these lipid nanocapsules exhibit an early disappearance half-time of 21 min after injection in the bloodstream (7). In order to extend the disappearance half-time, a novel long-circulating particle with longer PEG chain (PEG_{1500} stearate) based on low-energy emulsification method, without phase inversion, was developed.

In this study, the formulation process of these nanocarriers was investigated. The nanocapsule structure was then explored by cryo-transmission electron microscopy (Cryo-TEM). The influence of the PEG length on the electrokinetic properties of the particles was compared to the standard nanocapsules developed by Heurtault *et al.* (8). The ability of the PEG_{1500}

[1] Inserm U646, Université d'Angers, Angers F-49100, France.
[2] UMR-CNRS 6052, ENSC, Rennes F-35700, France.
[3] To whom correspondence should be addressed. (e-mail: patrick.saulnier@univ-angers.fr)

stearate (density and length) to inhibit the *in vitro* activation of the complement system and to prolong the lifetime of the nanocapsules after intravenous injection in rats was also evaluated in comparison with PEG_{660} hydroxystearate nanocapsules.

MATERIALS AND METHODS

Lipoïd® S75-3 (soybean lecithin at 69% of phosphatidylcholine and 10% phosphatidylethanolamine) and DUB SPEG 30S® (PEG_{1500} stearate) were kind gifts from Lipoïd GmbH (Ludwigshafen, Germany) and Stearinerie Dubois (Citron, France), respectively. Due to its complex composition, the brand name of soybean lecithin will be used in the following. The lipophilic Labrafac® WL 1349 (caprylic-capric acid triglycerides) was generously provided by Gattefossé S.A. (Saint-Priest, France). NaCl was purchased from Prolabo (Fontenay-sous-bois, France). Deionised water was obtained from a Milli-Q plus® system (Millipore, Paris, France).

Formulation of Stearate PEG_{1500} Nanocapsules

An aqueous phase containing deionised water, NaCl, and hydrophilic non-ionic surfactant (DUB SPEG 30S®) was added to the oil phase (Labrafac®) and lecithin (Lipoïd®) (Table I under magnetic stirring at an agitation speed of 200 rpm. As for the preparation of standard nanocapsules, at least three temperature cycles alternating from 60 to 95°C at a rate of 4°C/min were realized to obtain stable nanocapsules (9). During the last cooling, the formulation reaching 80°C, was rapidly diluted (1:3.5) with 12.5 ml cold water to form particles, and then continuously stirred for 30 min.

Conductivity Measurement

The conductivity of the bulk phase was measured using a conductimeter LF 325B (WTW, Weilheim, Germany) with two platinum plate attachments. Conductivity was determined during heating, between 60 and 100°C, under magnetic stirring at an agitation speed of 200 rpm. The conductivimeter mode used was the nonlinear temperature compensation (nLF). Four different compositions corresponding to high, low and intermediate water fraction F_w (0.85, 0.66, 0.5 and 0.33) have been studied with F_w described as:

$$F_w = \frac{V_{water}}{(V_{water+} V_{oil})} \quad (1)$$

Where V_{water} and V_{oil} were the volumes of water and oil, respectively, in the nanocapsule suspension before dilution. Moreover, concentration of PEG_{1500} stearate was fixed at 30% w/w. The conductivity measurements were performed in triplicate indicating an accuracy around 1.5%.

Table I. Composition of PEG_{1500} Stearate Nanocapsules A

PEG_{1500} stearate nanocapsules (26 nm)	
Constituents	Quantity (g)
PEG_{1500} stearate	1.403
Lipoïd®	0.075
NaCl	0.250
Labrafac®	0.468
Deionized water	2.805
Deonized water at 0°C	12.50

Feasibility Domain

In order to optimize constituent proportions, a ternary diagram was built. For each plot, the preparation process was unchanged but the proportions of water, oil and PEG_{1500} stearate were modified. The sum of the amounts of these three components was considered to be 100% (w/w). Concentrations of Lipoïd® S75-3 and NaCl in water were fixed at 1.5% (w/w) and 5% (w/w), respectively. The feasibility domain was defined as an area that allowed the formation of nanocapsules. After dilution, the hydrodynamic diameter range and the polydispersity index of each formulation were characterized by dynamic light scattering spectroscopy.

Particle Characterization

Size Measurements

The average hydrodynamic diameter and the polydispersity index (PI) of nanocapsules were determined by dynamic light scattering using a Malvern Autosizer 4700 (Malvern Instruments S.A., Worcestershire, United Kingdom) fitted with a 488 nm laser beam at a fixed angle of 90°. The polydispersity index was used as a measurement of the size distribution. A small value of PI (< 0.1) indicates an unimodale size distribution, while a PI > 0.3 indicates a higher heterogeneity. The temperature of the cell was maintained at 25°C. Nanocapsules were diluted 1:100 (v/v) in deionised water in order to assure a convenient scattered intensity on the detector.

Cryo Transmission Electron Microscopy (Cryo-TEM)

Cryo-TEM observations were performed at −170°C on a Philips CM120 electron microscope operating at −120 kV following the method previously developed by Lambert *et al.* (10).

Determination of the Proportion of Free PEG_{1500} Stearate in the Nanocapsule Suspension

We assumed that the whole quantity of Labrafac® and Lipoïd® used in the preparation was confined into spherical particles. On the contrary, a release of the PEG_{1500} stearate from the nanocapsule shell has been noticed. So, an assessment of PEG_{1500} stearate amount in the external phase of the suspension was performed. The free hydrophilic polymer was separated from the nanocapsules by steric exclusion chromatography. Nanocapsule suspension was deposited on 1.5 × 40 cm Sepharose CL-4B column and was eluted with distilled water. About 200 fractions of 400 µl were successively collected and the PEG concentration was determined from a colorimetric method taking advantage of the formation of a complex between PEG and iodine (11). 50 µl of KI/I_2 solution was added to 100 µl of sample diluted at 1:4 (v/v) and the turbidity of the medium was then detected spectrophotometrically at 492 nm. Three measurements by fraction were performed to evaluate the PEG concentration indicating a 1% accuracy. After chromatography, the amount of PEG_{1500} stearate adsorbed on the Sepharose gel was determined according to the same method.

Measurement of the Electrophoretic Mobility

Electrophoretic mobility measurements of nanocapsules were carried out using a Zetasizer 2000, (Malvern Instruments S.A.) based on the laser Doppler effect. Measurements were made in water at pH 7.4 with cell voltage 150 V. The nanocarriers were diluted in water at 1:10 (w/w) and seven NaCl concentrations were chosen: 1, 2, 10,15, 25, 50 and 100 mM. The electrophoretic mobility measurements were carried out in triplicate. All the values were measured with a relative accuracy of 1%.

From these experimental electrophoretic mobilities, a soft particle analysis theory (12) was applied. It aimed at characterizing the surface electric properties of PEG_{1500} stearate nanocapsules (13). Two physical constants ZN and $1/\lambda$ were then determined: ZN ($C.m^3$) represented spatial charge density in the polyelectrolyte region and λ^{-1} (m) was the depth of the layer accessible by counterions like Na^+.

Complement Consumption Studies

Complement consumption was assessed in human serum (HS) by measuring the residual hemolytic capacity of the complement system after contact with nanocapsules. Various amounts of the nanocapsule suspension (50,100, 125, 150, 200, 250 µl) were diluted with VBS^{2+} (Veronal Buffer Saline) in order to obtain a total volume of 300 µl for each sample. After addition of 100 µl of HS, the suspensions were incubated at 37°C for 60 min, under gentle agitation. Simultaneously, sheep erythrocytes were sensitized with hemolysine diluted at 1:1,600 (v/v) in VBS^{2+} and suspended to a final concentration of 1.10^8 cells/ml. After incubation, nanocapsules in HS were diluted to 1:24 (v/v) and different amounts of the mixture nanocapsules/serum (0.2, 0.25, 0.3, 0.35, 0.4, 0.6 ml) were diluted with VBS^{2+} to reach a total volume of 0.8 ml. The sensitized sheep erythrocytes (0.2 ml) were also added and the sample were incubated at 37°C for 45 min. After addition of 2 ml of NaCl, unlysed erythrocytes were separated by centrifugation. The lysis of cells measured at 405 nm allowed to determine the level of residual active complement in HS previously exposed to nanocapsules. Zymosan particles, a strong complement activator (14), were used as a positive control. Results were expressed as CH50 units consumption (15). The CH50 units represent the concentration of serum of hemolytic complement units per ml of serum able to cause 50% hemolysis of a fixed volume of these sheep red cells.

***In Vivo* Studies**

Preparation of Radiolabeled Nanocapsules

Nanocapsules were labeled by incorporating in their oily core a lipophilic complex: ^{99m}Tc $(S_3CPh)_2(S_2CPh)$ or ^{99m}Tc-SSS complex, prepared according to Mevellec *et al.* (16). ^{99m}Tc was obtained from a $^{99}Mo/^{99m}Tc$ generator purchased from CIS bio International/Schering (Gif sur Yvette, France). 1 ml of deionised water was added to a vial containing 7.5 mg sodium gluconate and 0.075 mg $SnCl_2.2H_2O$ in a freeze-dried form. Pertechnetate (370 Mbq, 0.5 ml) was mixed with this solution at room temperature for 10 min. 4 mg of a sodium dithiobenzoate and trithiobenzoate mixture in 0.5 ml of deionised water were finally added and heated for 30 min at 100°C. The radiochemical purity of the lipophilic complex was determined by thin layer chromatography and the migration was evaluated using a phospho-imager apparatus (Packard, Cyclone™ storage phosphor system). The chromatography was carried out on silica/alumina 60 F_{254} gel plates (Merck), using a solution of petroleum (6/4) as eluant (Rf 0.7). PEG_{1500} stearate nanocapsules were prepared in adding ^{99m}Tc-SSS complex to the raw materials. Its volume was deduced of the total amount of deionised water before dilution. The rest of the preparation process previously described remained then unchanged. The nanocapsules were finally dialyzed against distilled water (2 l), at room temperature during 2 h.

Animal Experimentation

Animal studies were carried out in accordance with the French regulation (law 0189.4 of January 24, 1990) on male Wistar rats (400–450 g). The ^{99m}Tc nanocapsules (500 µl, 0.2 MBq) were injected intravenously in the penile vein under gaseous isoflurane anesthesia. Blood samples (0.5 ml) were withdrawn on four animals intracardially at 15, 45, 90 min, 2, 4, 6, 16, 24, 41 and 48 h after injection. They were then introduced into vials, weighted and counted in a gamma counter (Packard Auto-Gamma 5000 series) for activity. Nanocapsule concentrations in blood at the various time points were calculated based on the assumption that blood represents 7% of rat body weight and were expressed as percent of the injected dose.

Data Analysis

The pharmacokinetic data were analyzed by a non-compartmental analysis. The time corresponding to the disappearance of 50% of the total injected dose was determined by linear interpolation. The $AUC_{[0-24]}$ and $AUC_{[0-48]}$ calculations were performed by the trapezoidal method during the experimental period.

RESULTS AND DISCUSSION

Conductivity Measurements

The conductivity study was performed on four formulations containing a constant PEG_{1500} stearate concentration (30% w/w) and different F_w. The conductivity evolutions were determined under magnetic stirring while the temperature was increased. Two different behaviors were observed for systems with high and low water proportions. In order to describe these profiles, two representative preparations (Table II) among the four were chosen: the formulation A ($F_w = 0.85$) and the formulation B ($F_w = 0.5$).

The conductivity of the system A as a function of the temperature was exhibited in Fig. 1A. A constant conductivity around 33 mS/cm corresponding to a O/W emulsion was observed until 76°C. Then, the conductivity exhibited a variation zone between 76 and 90°C to attain afterwards a threshold value of 29 mS/cm. This significant conductivity above 90°C denoted an aqueous external phase. So, this behavior was not suggestive of a phase inversion but of a transition from a O/W emulsion to a w/O/W emulsion (17) by

Table II. Composition of Preparations Used for Conductivity Studies

Quantity (g)	Formulation A	Formulation B
PEG_{1500} stearate	28.05	28.05
Lipoïd®	1.5	1.5
NaCl	5	2.92
Labrafac®	9.35	32.73
Deionized water	56.1	32.73

The water fractions (F_w) for formulations A and B were 0.85 and 0.5, respectively. For each preparation, the NaCl concentration in aqueous phase was constant (89 g/l).

passing through a transitional zone characterized by conductivity changes (in gray on the graph). The proportion of inner water ($F_{w_{in}}$) contained in the multiple emulsion was calculated from the difference between the experimental conductivity and the expected one predicted by Bruggeman's law described below:

$$\kappa = \kappa_w \times F_W^{3/2} \quad (2)$$

Where κ was the emulsion conductivity and κ_w, the aqueous phase conductivity with the same NaCl concentration. For temperatures below 76°C corresponding to a O/W emulsion, this equation was applied. The experimental conductivity was around 33 mS/cm and the conductivity calculated from Bruggeman's law was 33.7 mS/cm with κ_w = 43 mS/cm. On the contrary, after the transitional zone, the conductivity measured (29 mS/cm) was lower than the one determined from Bruggeman's law suggesting the presence of water within the oil drops. The inner water amount was determined from these conductivity differences to be about 8% (w/w) and the total internal phase of the w/O/W emulsion was around 25% (w/w).

The conductivity of the composition B containing equal amount of oil and water (F_w = 0.5) is illustrated in Fig. 1B. As in the case of the system A, the conductivity stayed constant (i.e., 8.5 mS/cm) for temperatures below 75°C. This conductivity value was in agreement with the one determined with the Bruggeman's equation (i.e., 8.1 mS/cm with κ_w = 23 mS/cm). Between 75 and 95°C, a rapid conductivity decrease was observed until 0 mS/cm corresponding to an external phase inversion. Indeed, during the temperature increase, the inner oil phase moved to the external phase in crossing a transitional zone and the O/W emulsion became a W/O emulsion. This behavior is representative of classical PIT method used by Heurtault *et al.* (9).

The conductivity changes observed for each formulation occurred at the same range of temperature, between 75 and 90°C into a transitional zone corresponding to the gray region in Fig. 2. For emulsions composed of 30 to 65% of water, the interfacial curvature was inverted with temperature increase according to the Bancroft's rules (18) while crossing the transitional zone. Phase inversion was not possible for systems with higher water fraction because the oil amount is too small, and their interfacial curvature is opposite to the one naturally induced by the non-ionic surfactant leading to multiple emulsion w/O/W (19). During the temperature cycles, these morphology changes were due to the variation of surfactant affinity for aqueous and oily phases defined by an empirical formulation variable so-called the hydrophilic–lipophilic deviation (HLD). HLD > 0 and HLD < 0 correspond to surfactant affinity for oil and for water, respectively (20). A HLD value equal to 0 represents an optimum formulation where an uniform repartition of surfactant between the two phases occurs. A formulation-composition map introduced 20 years ago described the variations of the emulsion morphology according to the water fraction F_w and the HLD (21). Thus, making a correlation between this map and the Fig. 2, we hypothesized that the transitional zone corresponds to the optimum formulation of system with a HLD value close to 0. In this narrow domain, the spontaneous curvature of the PEG_{1500} stearate is near zero leading to the disappearance of droplets (22). Then, a bicontinuous microemulsion phase with excess water and/or oil takes place (23).

After three temperature cycles, the preparations A and B were diluted with cold water and were analyzed by photon correlation spectroscopy (PCS). Some nanocapsules exhibiting a small hydrodynamic diameter (26 nm) and a monomodal distribution (PI < 0.1) were produced from the composition A. On the contrary, despite of the inversion phase observed during the temperature increase, no structure

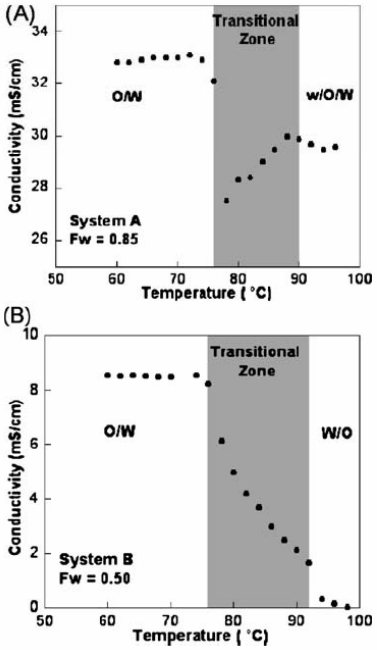

Fig. 1. Evolution of the conductivity as the temperature increases. The PEG_{1500} stearate concentration was 30% (w/w). The conductivity variations occurred in the transitional zone represented in gray on the graphics. (A) For the system A composed of a water fraction (F_w) of 0.85, the crossing of the *gray zone* corresponded to a transition from a O/W emulsion to a multiple w/O/W emulsion. (B) For system with a lower water fraction (F_w = 0.5), the conductivity when temperature increased, sharply decreased up to 0 mS/cm denoting a phase inversion.

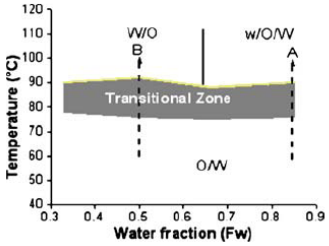

Fig. 2. Morphology evolutions as a function of temperature for four systems containing 30% (w/w) of PEG_{1500} stearate and different water fractions: F_w = 0.33; 0.5; 0.66; 0.85. Transitional zone (*in gray on the graphic*) represented conductivity variations denoting a morphology change. For preparations composed of high water fractions (F_w > 0.6), temperature increase led to a transition from a O/W emulsion to a multiple w/O/W emulsion. For systems with lower water proportions, phase inversion took place in the transitional zone.

was obtained for the formulation B. These results could be correlated with the work of Wadle *et al.* (24) who had demonstrated that the occurrence of phase inversion was not a guaranty of the nanocapsule formation. Moreover, according to Morales *et al.* (25), the preparation of nano-emulsion implies a complete solubilization of the oil phase in a bicontinuous microemulsion, at PIT. Thus, we could suppose that for low F_w inducing phase inversion during temperature cycles, the oil is not entirely soluble. Concerning the standard nanocapsules developed by Heurtault *et al.*, their preparation required the crossing of a phase inversion zone between 70 and 85°C (9). These formulations composed of PEG_{660} hydroxystearate were characterized by lower water fractions leading to phase changes (8). Hence, for these systems, a significant oil solubilization occurs within the bicontinuous microemulsion.

Feasibility Domain

A ternary diagram was established to define the constituents proportions of salted water, Labrafac® and PEG_{1500} stearate allowing the formation of submicron particles with a monodisperse size distribution. The formulation process, previously described, was applied for each point of the diagram (Fig. 3). Particle size and distribution were then determined for each formulation. A feasibility domain, in gray on the graphic, corresponding to the formation of nanocapsules with a size comprised between 20 and 150 nm and an polydispersity index inferior to 0.3 was revealed. It is described as a parallelogram whose relative proportions are comprised between 20 and 40% (w/w) of non-ionic surfactant, 40 and 75% (w/w) of salted water and 5 and 20% of Labrafac®. Furthermore, as in the case of system A, we noticed that the particle formation occurred only at F_w above 0.65. Thus, we could suppose that for all the systems within the feasibility domain, the process of particle formation is similar to the one occurring during the preparation of A: no phase inversion but a transition from a W/O emulsion to a w/O/W emulsion by passing through a zone corresponding to a bicontinuous phase allowing the formation of nanocapsules.

In conclusion, the complete process leading to the nanocapsule formation is illustrated in Fig. 4, where the morphology changes of systems occurring during the temperature cycle is exhibited. A transition from a O/W emulsion into a w/O/W is induced when the temperature is increased to 95°C and vice-versa. Three temperature cycles were applied and a rapid cooling was performed inside the transitional zone.

The previously mentioned system (A) was subjected to Cryo-TEM observation (Fig. 5). The capsules analyzed by using electron beam at different angles (results not shown) were spherical. The size observed was around 25 nm, similarly to the hydrodynamic diameter determined by PCS (26 nm). The narrow size distribution characterized by both Cryo-TEM and PCS (PI < 0.1) contributed to improve the stability of the suspension by reducing the Ostwald ripening (6). This hypothesis was confirmed by macroscopic observations at 4 and 37°C and at different pH (6, 7.4 and 8) showing a stability of the suspension over three months.

The next studies have been carried out on the system A which exhibited a monomodal granulometric distribution and an interesting size (26 nm) for drug delivery. Each experiment was performed immediately after the preparation of nanocapsules.

Influence of the PEG_{1500} Stearate on the Stealthiness of Nanocapsules

The capacity of PEG_{1500} stearate into the nanocapsule shell to reduce complement consumption has been exhibited in Fig. 6. The results were then compared to a previous study of Vonarbourg *et al.* (26) concerning the evaluation of the complement activation by 50 nm PEG_{660} hydroxystearate nanocapsules. Complement activation expressed as CH50 units consumption was evaluated as the residual lytic capacity of the serum after contact with nanocapsules. A strong complement activation occurred in the presence of very small amount of Zymosan particles. On the contrary, nanocapsules did not induce any response of the complement

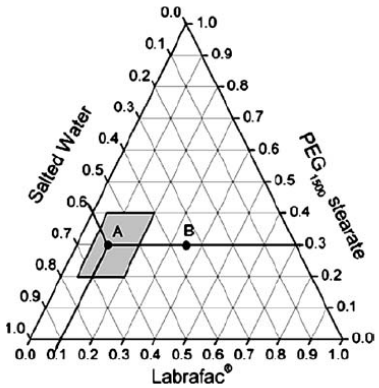

Fig. 3. Ternary diagram allowing the determination of feasibility domain comprising nanocapsules with a size smaller than 150 nm and a polydispersity index inferior to 0.3. The composition A characterized by a water fraction F_w = 0.85, led to the formation of nanocapsules with a size around 26 nm and a monomodal distribution. On the contrary, the formulation B composed of a lower water amount (F_w = 0.5) was located outside of the feasibility domain.

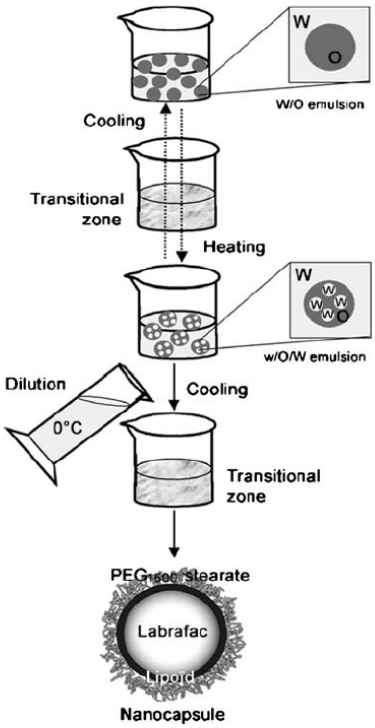

Fig. 4. Formulation process of lipid nanocapsules composed of a high water fraction and description of morphology changes during the temperature cycles.

system for a surface area lower than 1,000 cm^2. For higher surface area, between 2,000 and 5,000 cm^2, the complement consumption took place reaching a maximum of 20% and 15% for PEG_{1500} stearate and PEG_{660} hydroxystearate nanocapsules, respectively. This very weak complement activation observed for each type of nanocapsules was mainly due to the synergistic effect between the nanocapsule size and PEG layer. Indeed, the complement cascade involving a chain reaction of several complement components requires a certain local area on the nanocapsule surface. Ishida *et al.* (27) reported that the surface area of liposomes recognized by complement surface (SRC) was proportional to their diameter. Thus, the small size of nanocapsules limits the recognition of complement system (28). In addition to the size, the PEG layer surrounding the particle plays a major role in the weak complement activation observed in this study. The steric repulsion exerted by the PEG reduces adsorption of complement fragments (29). This protein-resistant effect was dependent on both polymer chain length and polymer surface density (1). However, Jeon *et al.* (30) demonstrated that the PEG surface density had a greater effect than length on steric repulsion.

In this context, the stearate PEG_{1500} density at the surface of nanocapsules has been assessed. The method used

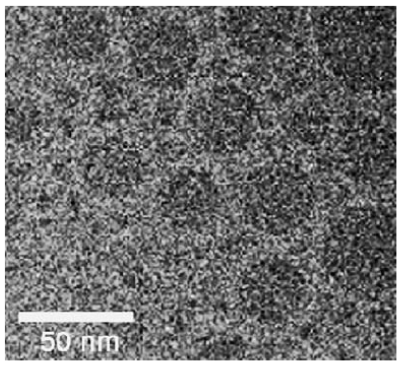

Fig. 5. Cryo-TEM image of nanocapsules A.

to evaluate the number of nanocapsules by volume unit (N_{caps}) has been developed by Minkov *et al.* (31) and was applied to PEG_{660} hydroxystearate nanocapsules. The authors hypothesized that the thickness of the particle shell was mainly influenced by the Lipoid® and corresponded to a 4.5 nm bilayer membrane. As a consequence, the shell thickness of 26 nm nanocapsules was estimated to about 4.5 nm and the diameter of the Labrafac® core (d) to about 17 nm. Moreover, the free PEG_{1500} stearate contained in suspension was separated by Sepharose CL-4B column chromatography. Its assessment was performed by a colorimetric method. Two peaks were observed from the chromatogram in Fig. 7, the nanocapsules were first eluted, their diameter analyzed by dynamic light scattering was about 30 nm. The free PEG_{1500} stearate corresponding to the second peak was composed of 43% (w/w) of the total amount of PEG contained in the nanoparticle suspension. Moreover, a negligible amount of PEG_{1500} adsorbed on the Sepharose gel was determined after chromatography. Thus, we could consider that the nanocapsule shell contained 57% (w/w) of the total PEG_{1500} stearate amount incorporated in the formulation. From this value ($P_{st\ PEG1500} = 0.57$) and the other approximations, the surface of one PEG_{1500} stearate molecule confined into the nanocapsule corona ($S_{st\ PEG1500}$) was calculated by the following equation:

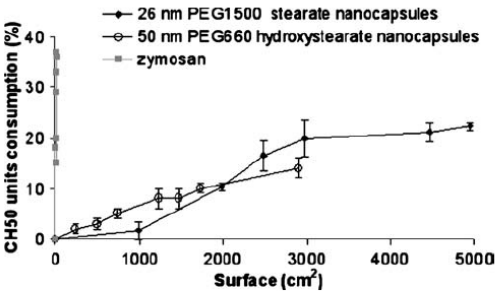

Fig. 6. Consumption of CH 50 units in the presence of 26 nm PEG_{1500} stearate nanocapsules A , 50 nm PEG_{660} hydroxystearate nanocapsules and Zymosan particles as function of surface area.

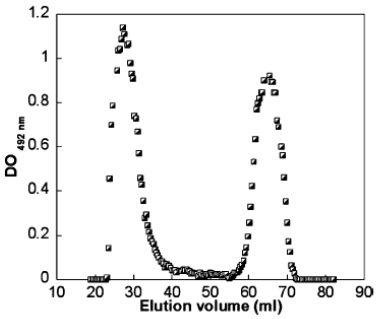

Fig. 7. Elution profile of PEG_{1500} stearate nanocapsules A obtained by Sepharose CL-4B gel filtration chromatography. The first peak corresponded to nanocapsules and the second one to free PEG_{1500} stearate.

$$S_{\text{st PEG1500}} = \frac{(N_{\text{caps}} \times S_{\text{caps}})}{(N_{\text{st PEG1500}} \times P_{\text{st PEG1500}})} \quad (3)$$

Where $N_{\text{st PEG1500}}$ was the total number of PEG_{1500} stearate molecules per unit volume in the preparation, $P_{\text{st PEG1500}}$ was the proportion of surfactant molecules in the nanocapsule shell, S_{caps} was the surface area of one nanocapsule and N_{caps} was the number of nanocapsules per unit volume, N_{caps} was given by:

$$N_{\text{caps}} = \frac{N_{\text{lab}}}{n_{\text{lab}}} \quad (4)$$

Where N_{lab} was the total number of Labrafac® molecules per unit volume and n_{lab} was the number of Labrafac® molecules confined in the nanocapsule core, n_{lab} was given by:

$$n_{\text{lab}} = \frac{V_{\text{core}}}{V_{\text{lab}}} \quad (5)$$

Where V_{core} was the volume of the Labrafac® core and V_{lab} (32,33) was the volume of one Labrafac® molecule. The numerical data used:

$P_{\text{st PEG1500}} = 0.57$
$N_{\text{st PEG1500}} = 2.7 \times 10^{19}$
$S_{\text{caps}} = 2124\ \text{nm}^2$
$N_{\text{lab}} = 3.4 \times 10^{19}$
$V_{\text{core}} = 2572\ \text{nm}^3$
$V_{\text{lab}} = 1.54\ \text{nm}^3$

The surface covered by one molecule of PEG_{1500} stearate was then estimated to about 2.8 nm^2, corresponding to a distance D between two PEG chains of about 1.7 nm. From previous studies about interactions between protein adsorption and PEG density, the polymer surface density is believed to be sufficient to prevent the opsonization process. Indeed, Jeon *et al.* (30) demonstrated that D = 1 nm and D = 1.5 nm were the optimal distances to prevent the adsorption of small and large proteins, respectively. Furthermore, Gref *et al.* (3) have shown that nanospheres made from copolymer block PEG-PLA allowed a maximum protein repelling when D = 1.4 nm. A weak complement consumption has been obtained for nanocapsules possessing on their surface some PEG chains separated by a distance D of about 2 nm (34). Therefore, these results are in agreement with previous assessments of the complement consumption. Indeed, the complement system was weakly activated by the nanocapsules because of the optimal PEG_{1500} stearate density surface which prevented the adsorption of complement protein fragments. The presence of such a surfactant strongly reduced Van Der Vaals forces and increased steric repulsion between particles and proteins. Concerning the standard nanocapsules, the PEG density has not been assessed. However, Vonarbourg *et al.* (35) showed that PEG_{660} hydroxystearate was organized in brush conformation suggesting a high PEG density on the particle surface.

The electrokinetic properties of the PEG_{1500} stearate nanocapsules have also been assessed from a soft particle electrophoresis analysis (12). The electrophoretic mobilities of nanocapsules as a function of the salt concentration were observed in Fig. 8. The best fit between experimental points and those corresponding to the theoretical model was obtained when ZN = -1.12×10^6 C.m^{-3} and $\lambda^{-1} = 1.0 \times 10^{-9}$ m with $R^2 = 0.97$. ZN corresponded to spatial charge density and λ^{-1} represented the depth of the layer accessible to the counterions. The correlation coefficient > 0.95 proved that nanocapsules verified the theory of soft particle. These results have been compared to the values obtained for standard lipid nanocapsules (LNC) with PEG_{660} hydroxystearate and the same Lipoïd® amount (Table III). We noticed that the charge density of PEG_{1500} stearate nanocapsules was three-fold higher than LNC. Vonarbourg *et al.* (35) demonstrated that PEG chains own negative dipolar charges playing a major role in the particle electrokinetic properties. So, this important ZN value could explain a higher PEG_{1500} stearate density into the nanocapsule shell. Furthermore, in spite of the longer PEG chain, the thickness of the accessible layer to Na^+ ions was thinner for PEG_{1500} nanocapsules than for LNC. We could hypothesize that λ^{-1} was weaker because of the short distance between two polymer chains, preventing the penetration of counterions into the accessible layer. In consequence, both ZN and λ^{-1} suggest, as the previous study, a high PEG_{1500} stearate density at the nanocapsule surface.

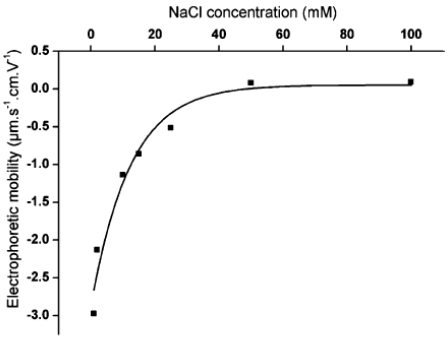

Fig. 8. Evolution of the electrophoretic mobility as a function of NaCl concentration for PEG_{1500} stearate nanocapsules A.

In a last part, the PEG_{1500} stearate nanocapsule pharmacokinetics were investigated in healthy rats in order to study the correlation between the low complement consumption by the particles and their circulation time in the bloodstream. The nanocapsule concentration in the bloodstream was determined *versus* time (Fig. 9). The results were compared to a pharmacokinetic study realized on standard ^{99m}Tc-labelled nanocapsules (7). The free ^{99m}Tc-SSS complex in the suspension was previously removed by dialysis. The half disappearance time of PEG1500 stearate nanocapsules was observed around 5.5 h. Moreover, 20% of the dose was still present in the blood 24 h after injection. These pharmacokinetic characteristics are more advantageous in comparison with standard LNC. Indeed, Ballot *et al.* demonstrated the rapid clearance from blood of nanocarriers composed of PEG_{660} hydroxystearate with a $t_{1/2}$ of 21 min. Although these capsules activate very weakly the complement system, they are rapidly recognized by the reticulo-endothelial system (RES) organs. These results could be explained by the change of physicochemical properties of standard nanocapsules after their intravenous administration. Indeed, we could hypothesize a possible leakage of PEG_{660} hydroxystearate from shell and / or a modification of the surfactant organization after injection in the blood. Moreover, by grafting DSPE-PEG_{2000} and DSPE-PEG_{5000} on the surface of these nanocapsules, Hoarau *et al.* (2) showed a significant improvement of their circulation time. This pharmacokinetic behavior was due to the length of PEG chains which reduced protein adsorption (36). Gref *et al.* (37) reported that the blood circulation time for nanospheres composed of PLA-PEG copolymers was significantly improved with increasing of molecular weight of PEG chains. Nevertheless, although the nanocapsules modified by Hoarau *et al.* were composed of PEG chains with a molecular weight superior to 1,500 g/mol, their $AUC_{[0-24]\ blood}$ (796%dose.h) corresponded to only 75% of that of PEG_{1500} stearate nanocapsules (1,053% dose.h). So, this difference suggested that the protein-resistant effect of the PEG density was greater than the length of the polymer chain. Moreover, this experiment allowed to correlate the low complement activation by the nanocapsules with their long-circulating properties. Indeed, by reducing the complement proteins consumption, the injected nanocapsules were not rapidly recognized by macrophages, increasing their residence time in the bloodstream (38,39). Thus, decreasing the recognition by complement system, the PEG density and the size of colloids represent essential parameters to confer stealth properties to particles. Nevertheless, an other parameter, the lecithin presence, could be taken into account. Mosqueira *et al.* (40) has compared nanocapsules composed of PLA-$PEG_{20\ 000}$ copolymers and of lecithin with nanospheres without phospholipids and characterized by a higher

Table III. ZN and $1/\lambda$ Parameters for Classic Lipid Nanocapsules Prepared with PEG_{660} Hydroxystearate and Novel Nanocapsules A Composed of PEG_{1500} Stearate

Type of LNC	ZN (10^6 c.m^{-3})	$1/\lambda$ (10^{-9} m)	R^2
PEG_{660} nanocapsules 20 nm	−0.32 ± 0.08	2.5 ± 0.5	0.99
PEG_{1500} nanocapsules 26 nm	−1.12 ± 0.08	1 ± 0.5	0.97

R^2 corresponded to the correlation coefficient obtained from the fitting.

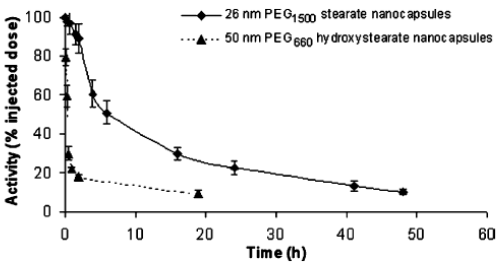

Fig. 9. Blood concentration-time profile for PEG_{1500} stearate nanocapsule A. Formulation was intravenously injected at a dose of 500 µl nanocapsules/rat and evolution of blood activity was expressed in percentage of injected dose. The results were compared to 50 nm PEG_{660} hydroxystearate nanocapsules.

PLA-$PEG_{20\ 000}$ density. The results showed that liver association of nanocapsules was 2- to 3-fold lower for nanocapsules in spite of their low PEG density. The authors have explained this phenomenon by the presence of lecithin that confers hydrophilic properties to the nanocapsule surface. Indeed, hydrophilic coating is known to decrease the opsonization process (41). However, their $AUC_{[0-24]\ blood}$ was sharply lower in comparison with PEG_{1500} nanocapsules (190%dose.h) probably due to their larger size (197 nm). Consequently, the Lipoïd® inside the PEG_{1500} stearate shell could contribute to long-circulating properties. Furthermore, the lipidic nanocapsules show an other advantage for lipophilic drug delivery in comparison with submicron lipid emulsions. Lundberg *et al.* (42) reported that the rapid clearance of 44 nm nanoemulsion composed of triolein (TO), dipalmitoyl phosphatidylcholine (DPPC) and polyethylene glycol modified phosphatidylethalonamine (PEG-PEG) was mainly due to the lypolis of the TO and not by uptake of whole emulsion droplets. In our case, the enzymatic degradation of nanocapsules was prevented by the polymeric shell protecting the oily core.

CONCLUSIONS

In this study, we have developed a new generation of nanocapsules composed of an oily core surrounded by a PEG_{1500} stearate layer with phospholipids and where no coating was necessary to make them stealthy. Their preparation did not allow the crossing of an inversion zone as in the case of the PIT method, but a transition from a O/W emulsion into a w/O/W multiple emulsion. *In vitro* and *in vivo* studies have revealed the long-circulating properties of these novel nanocapsules. Indeed, the complement system playing a major role in phagocytosis of colloidal drug carriers was only slightly activated in the presence of nanocapsules. This *in vitro* behavior also corroborated *in vivo* results. When nanocarriers were injected intravenously to rats, 20% of the total dose was still in the bloodstream 24 h after administration. Hence, we could suppose that these capsules prevented the opsonization process, consequently reducing their uptake by the mononuclear phagocytic system. The optimal protein-resistant effect of PEG_{1500} stearate on nanocapsule surfaces was considered to be dependent on both chain length and surface density. The PEG_{1500} stearate density calculated on

the nanocapsule surface was consistent with the literature findings. Indeed, the distance of 1.7 m between each PEG chain corresponded to a threshold value for optimal protein resistance. Moreover, the small size (26 nm) and the presence of lecithin on the nanocapsule surface contribute also to their stealth properties.

So, these PEG_{1500} stearate nanocapsules characterized by long-circulating properties allowed a potential application for delivery of lipophilic drugs to solid tumors. Indeed, contrary to the standard colloidal carriers that were rapidly recognized by macrophages, the stealth properties of these nanocapsules could lead to an important accumulation of drugs in accessible sites.

ACKNOWLEDGMENTS

The authors thank O. Lambert for Cryo-TEM studies (UMR-CNRS 5471, Bordeaux, F−33405 France; Université de Bordeaux 1, Bordeaux, F-33405 France). We also want to thank Andréanne Bouchard (University of Technology, Delft, NL-2600 AA The Netherlands) for her valuable comments and suggestions. This work was supported by the departmental committee of Maine-et-Loire of "Ligue contre le cancer."

REFERENCES

1. C. Passirani and J. Benoit. Complement activation by injectable colloidal drug carriers. In R. I. Mahato (ed.), *Biomaterials for Delivery and Targeting of Proteins and Nucleic Acids*, CRC, 2005, pp. 187–230.
2. D. Hoarau, P. Delmas, S. x. E. p. David, E. Roux, and J.-C. Leroux. Novel long-circulating lipid nanocapsules. *Pharm. Res.* **21**:1783–1789 (2004).
3. R. Gref, M. Luck, P. Quellec, M. Marchand, E. Dellacherie, S. Harnisch, T. Blunk, and R. H. Muller. 'Stealth' corona-core nanoparticles surface modified by polyethylene glycol (PEG): influences of the corona (PEG chain length and surface density) and of the core composition on phagocytic uptake and plasma protein adsorption. *Colloids Surf., B Biointerfaces* **18**:301–313 (2000).
4. B. Heurtault, P. Saulnier, B. Pech, J. E. Proust, and J. P. Benoit. Properties of polyethylene glycol 660 12-hydroxy stearate at a triglyceride/water interface. *Int. J. Pharm.* **242**:167–170 (2002).
5. K. Shinoda. The stability of O/W Type Emulsions as Functions of Temperature and the HLB of Emulsifiers: The Emulsification by PIT-Method. *J. Colloid Interface Sci.* **30**:258–263 (1969).
6. T. Tadros, P. Izquierdo, J. Esquena, and C. Solans. Formation and stability of nano-emulsions. *Adv. Colloid Interface Sci.* **108–109**:303–318 (2004).
7. S. Ballot, N. Noiret, F. Hindre, B. Denizot, E. Garin, H. Rajerison, and J. P. Benoit. (99m)Tc/(188)Re-labelled lipid nanocapsules as promising radiotracers for imaging and therapy: formulation and biodistribution. *Eur. J. Nucl. Med. Mol. Imaging* 1–6 (2006).
8. B. Heurtault, P. Saulnier, B. Pech, M.-C. Venier-Julienne, J.-E. Proust, R. Phan-Tan-Luu, and J.-P. Benoit. The influence of lipid nanocapsule composition on their size distribution. *Eur. J. Pharm. Sci.* **18**:55–61 (2003).
9. B.a. Heurtault, P. Saulnier, B. Pech, J.-E. Proust, and J.-P. Benoit. A novel phase inversion-based process for the preparation of lipid nanocarriers. *Pharm. Res.* **19**:875–880 (2002).
10. O. Lambert, N. Cavusoglu, J. Gallay, M. Vincent, J. L. Rigaud, J. P. Henry, and J. Ayala-Sanmartin. Novel organization and properties of annexin 2-membrane complexes. *J. Biol. Chem.* **279**:10872–10882 (2004).
11. G. E. C. Sims and T. J. A. Snope. Method for the estimation of poly(ethylene glycol) in plasma protein fractions. *Anal. Biochem.* **107**:60–63 (1980).
12. H. Ohshima. Dynamic electrophoretic mobility of a soft particle. *J. Colloid Interface Sci.* **233**:142–152 (2001).
13. V. Ducel, P. Saulnier, J. Richard, and F. Boury. Plant protein-polysaccharide interactions in solutions: application of soft particle analysis and light scattering measurements. *Colloids Surf., B Biointerfaces* **41**:95–102 (2005).
14. W. Wang, K. Okamoto, J. Rounds, E. Chambers, and D. O. Jacobs. *In vitro* complement activation favoring soluble C5b-9 complex formation alters myocellular sodium homeostasis. *Surgery* **129**:209–219 (2001).
15. M. T. Peracchia, C. Vauthier, C. Passirani, P. Couvreur, and D. Labarre. Complement consumption by poly(ethylene glycol) in different conformations chemically coupled to poly(isobutyl 2-cyanoacrylate) nanoparticles. *Life Sci.* **61**:749–761 (1997).
16. F. Mevellec, F. Tisato, F. Refosco, A. Roucoux, N. Noiret, H. Patin, and G. Bandoli. Synthesis and characterization of the "sulfur-rich" bis(perthiobenzoato)(dithiobenzoato)technetium(III) heterocomplex. *Inorg. Chem.* **41**:598–601 (2002).
17. J. Allouche, E. Tyrode, V. Sadtler, L. Choplin, and J. L. Salager. Simultaneous conductivity and viscosity measurements as a technique to track emulsion inversion by the phase-inversion-temperature method. *Langmuir* **20**:2134–2140 (2004).
18. W. D. Bancroft. The theory of emulsification. *J. Phys. Chem.***17**: (1913).
19. J. Allouche, E. Tyrode, V. Sadtler, L. Choplin, and J. L. Salager. Single and two steps emulsification to prepare a persistent multiple emulsion with a surfactant-polymer mixture. *Ind. Eng. Chem. Res.* **42**:3982–3988 (2003).
20. S. Marfisi, M. P. Rodriguez, G. Alvarez, M.-T. Celis, A. Forgiarini, J. Lachaise, and J.-L. Salager. Complex emulsion inversion pattern associated with the partitioning of nonionic surfactant mixtures in the presence of alcohol cosurfactant. *Langmuir* **21**:6712–6716 (2005).
21. J. L. Salager, M. Minana-Perez, M. Perez-Sanchez, M. Ramirez-Gouveia, and C. I. Rojas. Surfactant-oil-water systems near the affinity inversion. Part III. The two kinds of emulsion inversion. *J. Dispers. Sci. Technol.* **4**:313–329 (1983).
22. M. C. E. Van Hecke, J. Poprawski, J.-M. Aubry, and J.-L. Salager. A novel criterion for studying the phase equilibria of non-ionic surfactant-triglyceride oil-water systems. *Polym. Int.* **52**:559–562 (2003).
23. J. Poprawski, M. Catte, L. Marquez, M.-J. Marti, J.-L. Salager, and J.-M. Aubry. Application of hydrophilic–lipophilic deviation formulation concept to microemulsions containing pine oil and nonionic surfactant. *Polym. Int.* **52**:629–632 (2003).
24. A. Wadle, T. Forster, and W. Rybinskivon. Influence of the microemulsion phase structure on the phase inversion temperature emulsification of polar oils. *Colloids Surf., A Physicochem. Eng. Asp.* **76**:51–57 (1993).
25. D. Morales, J. M. Gutiérrez, M. J. García-Celma, and Y. C. Solans. A study of the relation between bicontinuous micro-emulsions and oil/water nano-emulsion formation. *Langmuir* **19**:7196–7200 (2003).
26. A. Vonarbourg, C. Passirani, P. Saulnier, and J. P. Benoit. Evaluation of pegylated lipid nanocapsules *versus* complement system activation and macrophage uptake. *J. Biomed. Mater. Res. A* In Press: (2006).
27. T. Ishida, H. Harashima, and H. Kiwada. Liposome clearance. *Bios. Rep.* **22**:197–224 (2002).
28. H. Harashima, K. Sakata, K. Funato, and H. Kiwada. Enhanced hepatic uptake of liposomes through complement activation depending on the size of liposomes. *Pharm. Res.* **11**:402–406 (1994).
29. S. M. Moghimi and J. Szebeni. Stealth liposomes and long circulating nanoparticles: critical issues in pharmacokinetics, opsonization and protein-binding properties. *Prog. Lipid Res.* **42**:463–478 (2003).
30. S. I. Jeon, J. H. Lee, J. D. Andrade, and P. G. De Gennes. Protein-surface interactions in the presence of polyethylene oxide. I. Simplified theory. *J. Colloid Interface Sci.* **142**:149–158 (1991).

31. I. Minkov, T. Ivanova, I. Panaiotov, J. Proust, and P. Saulnier. Reorganization of lipid nanocapsules at air-water interface. I. Kinetics of surface film formation. *Colloids Surf., B Biointerfaces* **45**:14–23 (2005).
32. V. G. Ivkov and G. N. Berestovskii. Conformation of hydrocarbon chains in a lipid bilayer. *Biofizika* **24**:633–636 (1979).
33. J. M. Smaby, W. J. Baumann, and H. L. Brockman. Lipid structure and the behavior of cholesteryl esters in monolayer and bulk phases. *J. Lipid Res.* **20**:784–788 (1979).
34. M. Vittaz, D. Bazile, G. Spenlehauer, T. Verrecchia, M. Veillard, F. Puisieux, and D. Labarre. Effect of PEO surface density on long-circulating PLA-PEO nanoparticles which are very low complement activators. *Biomaterials* **17**:1575–1581 (1996).
35. A. Vonarbourg, P. Saulnier, C. Passirani, and J. P. Benoit. Electrokinetic properties of noncharged lipid nanocapsules: influence of the dipolar distribution at the interface. *Electrophoresis* **26**:2066–2075 (2005).
36. A. Mori, A. L. Klibanov, V. P. Torchilin, and L. Huang. Influence of the steric barrier activity of amphipathic poly (ethyleneglycol) and ganglioside GM1 on the circulation time of liposomes and on the target binding of immunoliposomes *in vivo*. *FEBS Lett.* **284**:263–266 (1991).
37. R. Gref, Y. Minamitake, M. T. Peracchia, V. Trubetskoy, V. Torchilin, and R. Langer. Biodegradable long-circulating polymeric nanospheres. *Science* **263**:1600–1603 (1994).
38. J.-C. Leroux, E. Allemann, F. De Jaeghere, E. Doelker, and R. Gurny. Biodegradable nanoparticles—from sustained release formulations to improved site specific drug delivery. *J. Control. Release* **39**:339–350 (1996).
39. J.-C. Leroux, F. De Jaeghere, B. Anner, E. Doelker, and R. Gurny. An investigation on the role of plasma and serum opsonins on the internalization of biodegradable poly(D,L-lactic acid) nanoparticles by human monocytes. *Life Sciences* **57**:695–703 (1995).
40. V. C. F. Mosqueira, P. Legrand, J.-L. Morgat, M. Vert, E. Mysiakine, R. Gref, J.-P. Devissaguet, and G. Barratt. Biodistribution of long-circulating PEG-grafted nanocapsules in mice: effects of PEG chain length and density. *Pharm. Res.* **18**:1411–1419 (2001).
41. S. I. Jeon, J. H. Lee, J. D. Andrade, and P. G. De Gennes. Protein-surface interactions in the presence of polyethylene oxide. I. Simplified theory. *J. Colloid Interface Sci.* **142**:149–158 (1991).
42. B. B. Lundberg, B.-C. Mortimer, and T. G. Redgrave. Submicron lipid emulsions containing amphipathic polyethylene glycol for use as drug-carriers with prolonged circulation time. *Int. J. Pharm.* **134**:119–127 (1996).

Résumé

Cette thèse porte sur l'élaboration d'un vecteur particulaire lipidique reconnaissant activement les tissus cérébraux après son administration par voie intraveineuse. Ce système devrait favoriser l'accumulation au sein du cerveau, de molécules thérapeutiques dans le cadre du traitement des maladies cérébrales comme les gliomes malins. La première partie de notre travail consistait à greffer sur la surface de nanocapsules lipidiques (LNC) des anticorps monoclonaux d'origine murine (OX26) ou des fragments Fab' dirigés contre le récepteur à la transferrine de rat, surexprimé sur l'endothélium cérébral. Des immunonanocapsules portant entre 16 et 183 anticorps entiers et entre 42 et 173 fragments Fab' ont été obtenues. Leur capacité à s'associer aux cellules endothéliales cérébrales de rat a ensuite été vérifiée. De plus, 24 h après leur administration chez le rat, la concentration dans le cerveau des OX26-immunonanocapsules et des Fab'-immunonanocapsules était respectivement 2 et 1,5 fois plus élevée que celle des LNC dépourvues de ligands.

Mots clés

Immunonanocapsules, ciblage actif, anticorps monoclonal OX26, fragment Fab', récepteur à la transferrine, PEG, cerveau.

Abstract

This thesis concerns the development of a lipidic nanovector recognizing actively the cerebral tissues after its intravenous administration. This system should promote the accumulation into the brain, of therapeutic molecules for the treatment of cerebral diseases such as the malignant gliomas. The first part of our work consisted to attach on the surface of lipid nanocapsules, murine monoclonal antibodies (OX26) or Fab' fragments directed against the rat transferrin receptor, overexpressed on the cerebral endothelium. Immunonanocapsules bearing between 16 and 183 whole antibodies and between 42 and 173 Fab' fragments were achieved. Their capacity to associate to rat cerebral endothelial cells has then been checked. Moreover, 24 after their intravenous administration in rats, the concentration of OX26-immunonanocapsules and Fab'-immunonanocapsules was 2 and 1.5-fold higher than non-targeted nanocapsules.

Keywords

Immunonanocapsules, active targeting, OX26 monoclonal antibody, Fab' fragment, transferrin receptor, PEG, brain.

Laboratoire d'accueil
INSERM U646
« Ingénierie de la Vectorisation Particulaire »
Bâtiment IBT
10 rue André Boquel
49100 Angers
FRANCE